A POLARIMETER FOR INFRARED ASTRONOMY

by

David Leon Rosen M.A.

A thesis submitted for the degree
of
Doctor of Philosophy of the University of London
and
for the Diploma of Imperial College.

Astronomy Group
Blackett Laboratory
Imperial College
London S.W.7.

October 1982

Abstract

Infrared polarimetry is a natural progression from infrared photometry, which is becoming a routine astronomical technique. The extra information provided by polarimetric measurements is useful for the investigation of magnetic fields, the composition, alignment and distribution of dust grains, and emission mechanisms. To date, very few infrared polarimetric measurements have been made at wavelengths longer than 5μ.

A new type of polarimeter has been designed and constructed for infrared astronomy. It incorporates a slowly-rotating wire-grid analyser and is completely helium-cooled in order to minimize thermal emission from the analyser. The drive is produced by a magnetic coupling across the dewar wall which eliminates heat leak and maintains vacuum integrity. Spatial chopping at $\sim$ 20 Hz is performed by a helium-cooled self-resonant tuning-fork chopper, mounted at the focal plane in front of a Fabry lens. The entire polarimeter and photometer assembly is situated inside a standard helium dewar which can be mounted at the Cassegrain focus of a telescope. The instrument was designed to be used with the Imperial College 41" balloon-borne telescope for far-infrared astronomy.

Fluctuations of the chopper amplitude can cause an increase in the noise, but by use of a novel electronic bucking system, it is shown that the polarimeter can be detector noise-limited. A complete data processing system has been assembled, permitting photometry and polarimetry to be simultaneously carried out in real time using an on-line mini-computer.

The polarimeter has been used at the 1.5 metre flux collector at Izaña, Tenerife to make measurements of some bright stars at 10μ.

The polarization of α Ori was confirmed and polarizations of 3.3±0.8% in α Sco and 4.4±2.1% in R Crt were found. Upper limits were set on the polarizations of W Hya and VY CMa.

to Miriam

Acknowledgements

It is with pleasure that I acknowledge the help and support of the following people in this work.

Jim Allen for much help and practical advice with electrical and mechanical aspects.

Bob Joseph, my supervisor, for inspiring this work and directing my studies.

Martin Kessler, my contemporary, for keeping me cheerful over the last five years, and for much practical help at Tenerife when 'fighting' the on-site equipment.

Peter Meikle for continual advice, help and encouragement with every aspect of this work.

Steve Morris for much help on the last observing trip to Tenerife.

Miriam Rosen, my wife, for much tolerance, support and financial assistance.

Monty and Rosemary Rosen, my parents, for their encouragement and financial support for the last 29 years.

The Science Research Council for its financial support during my four year studentship.

Finally, my sincere thanks to Yvonne Masson who was responsible for the typing of this manuscript.

Contents

List of Tables

List of Figures

Chapter 1 Introduction

1-1 Infrared Astronomy

Over the last 20 years, infrared astronomy has developed into a major science, yielding vital information about the universe. The infrared region is of great interest to astronomers because:

a) It spans a large central portion of the electromagnetic spectrum

b) Cool objects (10K to 1000K) will emit most of their energy in the infrared. Such objects include some powerful extragalactic sources, as well as dusty stars, protostars and molecular clouds.

c) Extinction decreases with wavelength, so that objects such as the galactic centre, with $\sim$ 30 magnitudes of visual extinction, may be observed in the infrared.

d) The vibrational and rotational lines of important atoms and molecules lie in this wavelength region.

The infrared part of the electromagnetic spectrum lies between the optical and the radio regions. It is usually considered to span three decades, 1 to 1000μ (microns). The shorter wavelength region, up to about 5μ, is referred to as the 'Near Infrared', the part between 5 and 20μ is the 'Middle Infrared', the remainder being the 'Far Infrared'. These terms are very subjective, and an optical astronomer might refer to 1μ as the far infrared.

The main obstacle for infrared astronomy is the atmosphere. H_2O, and to a lesser extent CO_2, O_3 and other molecules, have strong and wide absorption bands in the infrared, which render the atmosphere almost opaque for sea-level astronomers. At high altitudes, the number and size of the atmospheric windows increases (Fig.1-1) but to make observations in the far infrared, it is usually necessary to use an airborne

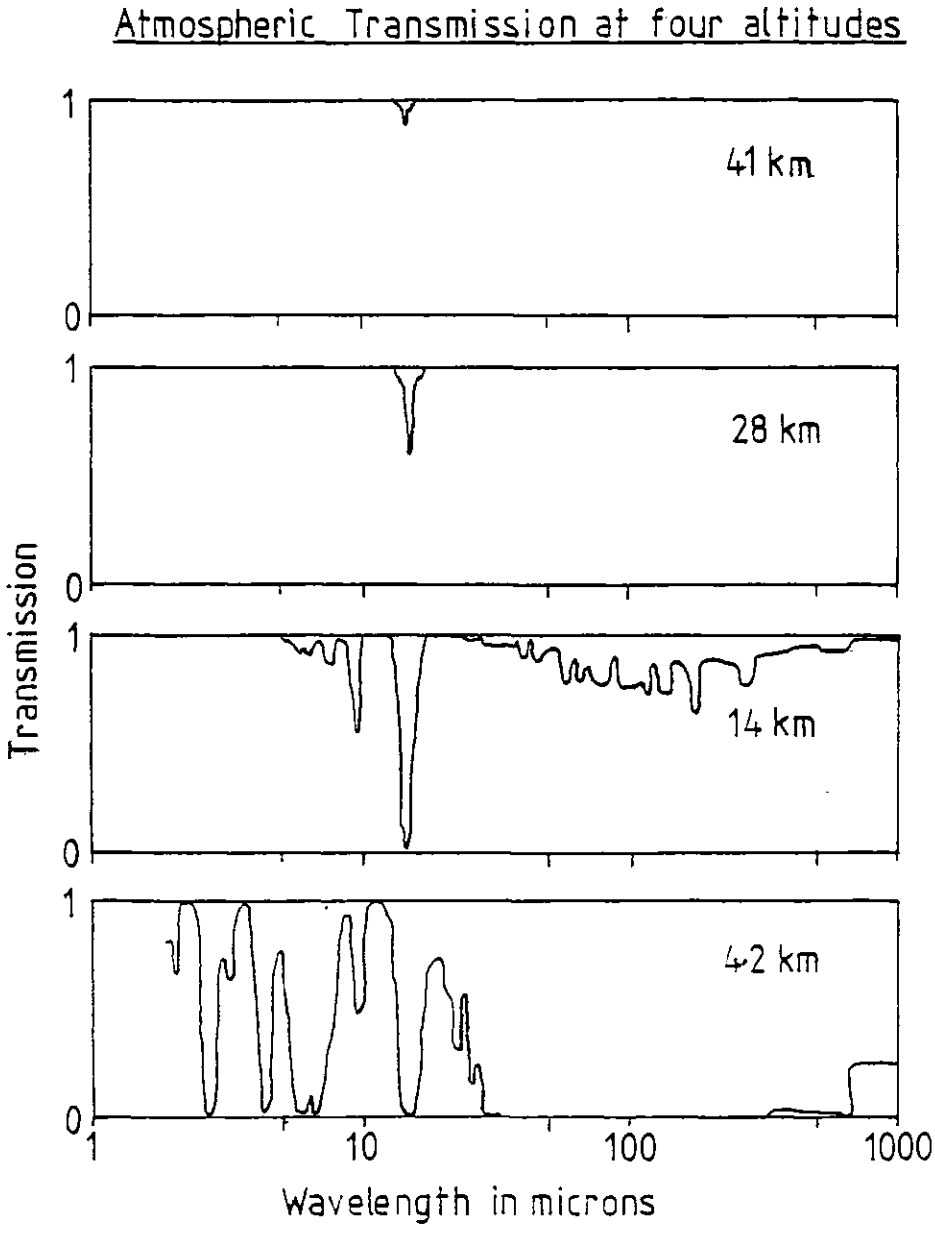
Atmospheric Transmission at four altitudes
Transmission
1
0
41 km
28 km
14 km
4·2 km
1
10
100
1000
Wavelength in microns

Fig 1-1

or space telescope.

As well as absorbing infrared radiation, the molecules of the atmosphere emit strongly in the infrared, roughly as a 270K black body. This has the peak of its emission around 10μ and so the sky is very bright at infrared wavelengths. One can justifiably equate 10μ astronomy with optical astronomy attempted during the daytime. To make observations in the infrared, one is looking for small fluxes in the presence of a very large background (typically one part in 10^6) and sophisticated techniques are needed to extract the signal.

It is not surprising that infrared astronomy has a rather short history. It was only at the end of the eighteenth century that Sir William Herschel discovered the presence of 'calorific rays' beyond the red portion of the sun's spectrum. In 1856, the Scottish Astronomer Royal, Piazzi Smyth, was just able to detect the moon in the infrared from Tenerife, but the lack of really sensitive detectors delayed the progress of infrared astronomy for another century. In the 1950's, lead sulphide detectors were used for the near infrared region - up to about 5μ, and in the 1960's the development of the doped-germanium bolometer, cooled with liquid helium, opened up the entire infrared.

Infrared astronomers initially concentrated on photometry, and one of the major achievements of the 1960's was the two-micron sky survey catalogue (IRC) produced by Neugebauer and Leighton (1969). This contains 5621 sources north of declination -33° and is thought to be complete to magnitude 3.0 at 2.2μ. It revealed several unusual objects such as NML Cyg and NML Tau. The AFCRL survey catalogue (Walker and Price 1975) and the AFGL survey catalogue (Price and Walker 1976) are based on rocket-borne observations using cooled telescopes. The AFGL catalogue extends the infrared sky survey data out to 27μ, but no similar all-sky far-infrared survey has yet been published.

As photometric techniques have become established for the various

parts of the infrared spectrum, astronomers have gone on to develop more specialised and sophisticated instruments, such as spectrometers and polarimeters, to permit more detailed studies to be made of individual sources.

This thesis deals with the construction and use of an infrared polarimeter, and observations made with it at 10μ using the 1.5m infrared telescope in Tenerife.

1-2 Infrared Emission Mechanisms

Before the development of infrared astronomy over the last 15 years, it was assumed that most astronomical objects would be very weak emitters in the infrared. Stars are generally rather hot objects, with the peak of their black-body spectra in the visible, and the emission was expected to drop off along the Rayleigh-Jeans tail. Thus it was a surprise when many stars were found to have infrared fluxes considerably above that expected from their temperatures and an extrapolation of their black-body spectra. It was said that such objects had an 'infrared excess'. A number of objects have also been discovered which were previously undetected at other wavelengths (e.g. the Becklin-Neugebauer source in Orion) but these can generally be explained by a model involving stars heavily obscured by dust.

The following processes constitute the principal infrared emission mechanisms.

1-2.1 Thermal radiation

A perfectly-absorbing object in thermodynamic equilibrium at a temperature T(K) has an emission spectrum

$$B_\nu(T) = 2h\frac{\nu^3}{c^2}\left[\exp\left[\frac{h\nu}{kT}\right] - 1\right]^{-1}$$

$$\text{watts m}^{-2}\text{ster}^{-1}\text{Hz}^{-1}$$

where h is the Planck constant, k is the Boltzmann constant, and c is the velocity of light.

This spectrum peaks at $\lambda_{max} \simeq \frac{5100}{T(K)}\mu$, and thus cool objects (5-500K) have the peak of their emission between 1mm and 10μ. The total black-body emission (obtained by integrating $B_\nu(T)$ over all wavelengths) is σT^4 watts m^{-2}, where σ is the Stefan-Boltzmann constant. The object may not be perfectly absorbing, in which case its emission will be modified by its emissivity, and this will generally be wavelength-dependent.

1-2.2 Free-Free Emission By A Plasma

In a partially-ionized gas, free electrons will experience acceleration as they pass close to ions and will emit photons. Eventually, any electron will lose so much energy in this fashion that it will recombine with an ion. Therefore, to keep the gas partially ionized, an ionizing source such as a nearby hot star must be present.

An electromagnetic wave passing through the ionized gas will do work by accelerating free electrons, but this energy will be dissipated by electron-ion collisions. Hence the wave will lose energy, and the absorption coefficient, $K(\nu)$, in an optically-thin HII region will be

$$K(\nu) = \frac{8}{3\sqrt{2\pi}} \frac{e^6 n^2}{c(mkT)^{3/2}\nu^2} \log_e \left[\frac{1.32(kT)^{3/2}}{2\pi e^2 m^{\frac{1}{2}} \nu} \right]$$

(p230 Harwit 1973)

where e is the electron charge, m is the electron mass, n is the electron density and T is the gas temperature. Thus the free-free emission spectrum from the plasma will be of the form $I_\nu = K(\nu)B_\nu(T)$. The frequency dependence of the logarithmic term in $K(\nu)$ is relatively weak, so the brightness should be roughly independent of frequency since $K \propto \nu^{-2}$ and the intensity of black-body radiation, in the Rayleigh-Jeans

part of the spectrum, is proportional to ν^2. At lower frequencies, where the cloud becomes optically thick, the spectrum will revert to the ν^2 dependence of the Rayleigh-Jeans spectrum.

1-2.3 Synchrotron Radiation

Any charged particle that is accelerated will emit radiation, and in the particular case of relativistic electrons accelerated by a magnetic field, this emission is called synchrotron radiation. The relativistic velocities, v, of the electrons restrict the emitted radiation to a narrow cone of half-angle $\theta \sim \sqrt{1-\frac{v^2}{c^2}}$ about the forward direction of motion, so the observer sees radiation, not at the gyrofrequency $\omega_c = \frac{eB}{m_o c}$, but at the frequency $\omega_m \sim \omega_c\left(1-\frac{v^2}{c^2}\right)^{-1}$. Ginzberg and Syrovatskii (1965) show that if the electrons have an energy spectrum $n(\varepsilon) \propto \varepsilon^{-\gamma}$, then the intensity of the radiation $I_\nu \propto B^{\alpha+1}\nu^{-\alpha}$ where the spectral index, $\alpha = \frac{\gamma-1}{2}$. The intensity of synchrotron radiation is dependent on both the strength of the magnetic field and the energy of the electrons, and from a strong source such as the Crab Nebula, synchrotron radiation is detected across the entire electromagnetic spectrum.

Some large and intense synchrotron sources (e.g. 3C 147) have a turnover in their spectrum. This is interpreted as self-absorption - at low frequencies the source becomes optically thick to its own radiation.

1-2.4 Line Emission

Many atoms and molecules have strong emission lines in the infrared and these may be less obscured by dust than lines in the optical. The measurement of the intensity and shape of these lines yields information about the abundance of the elements and molecules, and the velocities of sources and components within them (e.g. the motion of clouds within an HII region).

In the near infrared, the dominant lines are the hydrogen recombina-

tion lines, while in the 10μ window the transitions of ArIII, SIV and NeII occur. The field of far-infrared spectroscopy has only recently been opened up. The first detections were of the OIII fine structure line at 88μ (Ward et al., 1975) in M17 and since then the field has expanded rapidly.

1-3 Infrared Sources

Virtually all astronomical objects emit a proportion of their radiation in the infrared. However, one of the achievements of infrared astronomy has been to demonstrate that for many objects, the major portion of their bolometric luminosities is emitted in this region.

The following is a brief outline of some important types of infrared sources. A more detailed review is given by Beckman & Moorwood (1979).

1-3.1 Stars

Most of the strong near-infrared sources are found to be cool late-type stars. For many of these, their temperatures of several thousand degrees give a peak emission at or around 1μ, and their fluxes fall off along the Rayleigh-Jeans slope at longer wavelengths. However, some of the brightest 10μ objects, such as IRC+10216, VY Cma, NML Tau and NML Cyg, have a peak emission much further into the infrared, with either the spectrum of a black-body at a few hundred degrees K, or a spectrum that can only be explained by the synthesis of black-body spectra of two different temperatures.

One explanation for these infrared 'excesses' is the presence of circumstellar dust, which has either condensed out of material ejected by the star, or is the remnant of the protostellar dust and gas cloud. If this dust is optically thick, it will absorb all the short wavelength flux from a star and re-radiate the energy at longer wavelengths with a Planck spectrum corresponding to the dust temperature. The temperature

T of a dust grain in the vicinity of a star will be determined by the energy balance between the short wavelength absorbed radiation and the longer wavelength emitted radiation. If the star has luminosity $L_\nu d\nu$ at frequency ν, and the dust grain has absorption efficiency $Q_{abs}(\nu)$, radius a and lies at a distance R from the star, then

$$\int_0^\infty \frac{L_\nu}{4\pi R^2} \pi a^2 Q_{abs}(\nu) d\nu = \int_0^\infty 4\pi a^2 Q_{abs}(\nu) B_\nu(T) d\nu$$

Absorbed energy Emitted energy

Some early-type stars such as Be stars are also found to have infrared excesses. This is interpreted as free-free emission from gas in the stellar atmosphere which is ionized by the very hot star.

1-3.2 Molecular Clouds and Planetary Nebulae

Strong infrared sources have been detected in several nebulae, notable examples being the Becklin-Neugebauer source in the Orion nebula, and the IRS-5 source in W3. These are good candidates for very young stars in the process of condensing out of collapsing gas-dust complexes. The clouds themselves are also found to be diffuse far-infrared sources due to the black-body continuum radiation from the large quantities of dust which are present.

A young hot star, in or near a hydrogen cloud, will ionize the gas to produce an HII region. Free-free emission will dominate the radio spectrum, but at shorter wavelengths, black-body radiation from surrounding dust, heated by ultra-violet radiation from the star, may exceed the free-free by several orders of magnitude. Such sources seem to be the dominant feature of the far-infrared sky.

Planetary nebulae are thought to represent a relatively short period ($\sim 10^4$ years) in stellar evolution before the white dwarf phase.

The mass loss increases at this time, producing a spherical shell which is ionized by the hot central star. The observed emission is then similar to that from an HII region, with the thermal dust emission dominant in the infrared.

1-3.3 The Galactic Centre

The Galactic centre has received a great deal of attention from infrared astronomers. Since there are an estimated 27 magnitudes of visual extinction at the Galactic centre, infrared, X-ray, and radio observations provide essentially all of the currently-available data. The infrared maps are fairly complex, with a number of discrete sources present, as well as large extended sources. Becklin and Neugebauer (1975) found ten point sources in their 10μ map of Sgr A, which has 2.5" resolution. The far-infrared emission extends 6.5^{o} along and 2^{o} across the galactic plane and the total luminosity is $\sim 10^{9} L_{\odot}$. It is thought possible to explain this luminosity by invoking the presence of a large number of obscured stars, although a more exotic explanation (e.g. accretion onto a black hole) is not ruled out.

1-3.4 Extragalactic Objects

Certain galaxies are found to have infrared excesses, indicating that their bolometric luminosities are far greater than would be inferred from optical measurements. Whilst about one hundred galaxies have been detected at 10μ, barely ten have been detected at 100μ (Rieke and Lebofsky 1979). In particular, NGC 1068, M82, NGC 253 have been extensively studied, and their peak emission appears to be at about 100μ.

The energy source and emission mechanism for these galaxies is still debated. Telesco and Harper (1980) suggest that the far-infrared emission results from the heating of dust by early-type stars, and Rieke *et al.* (1980) calculate that the large infrared fluxes from the nuclei

of such galaxies require a recent burst of star formation to account for the fluxes by thermal means.

Quasars and BL Lac objects exhibit steadily-rising near-infrared spectra towards longer wavelength, rapid variability, large polarization and massive fluxes if redshift is proportional to distance. It is very difficult to account for these unless a non-thermal source such as a black hole is invoked. However, by its nature, such an emission mechanism is more difficult to confirm (or rule out) than a stellar source.

1-3.5 The Cosmic Background Radiation

The cosmic background has the characteristics of a 2.7 K black body. The exact shape of its spectrum, its polarization and its isotropy are of central interest to cosmological theory. The peak of this radiation occurs at $\sim$ 1mm wavelength and the flux falls rapidly at shorter wavelengths along the Wien tail. The cosmic background is difficult to observe because of the problem of discriminating against both instrumental emission and sky background, and it is generally necessary to use a cooled telescope.

1-4 The Development of Astronomical Polarimetry

In 1669, Bartholinus in Denmark discovered the phenomenon of double refraction in Iceland spar. However, it is thought that polarization effects were employed long before that by the Vikings, who used dichroic crystals as a navigational aid to locate the sun when it was obscured by clouds (p448 Crawford 1968). The credit (or blame) for the use of the term 'Polarization' is given to Sir Isaac Newton (p43 Gehrels 1974).

It was not until the 19th century that a quantitative description of polarized light was made when, in 1808, Malus formulated his cosine^2 law. Chapter II of this thesis deals with modern mathematical representations of polarized radiation.

The birth of astronomical polarimetry can be attributed to Arago who, in the early nineteenth century, observed the polarization of two comets and the moon. The absence of a convenient compact optical polarizer delayed progress until 1928 when Land invented his sheet polarizer, and HR-sheet polarizers were later developed to cover wavelengths up to about 3μ. Lyot's thesis of 1929 marks the beginning of high precision polarimetry, previous work having been primarily qualitative.

The large amount of polarization data now assembled has revealed much information about the composition of the interstellar medium, interstellar magnetic fields, the magnetic fields of stars and non-thermal-emission processes. In 1949, Hall and Hiltner discovered interstellar polarization and subsequently published catalogues of polarized starlight. One of the most-often-quoted results is the plot in galactic co-ordinates of the polarization of 1800 stars by Mathewson and Ford (1970) which clearly indicates the Galactic magnetic field.

Radio astronomers are able to obtain polarization data quite simply because linearly polarized fields (such as dipoles) are often used. At these wavelengths, Faraday rotation becomes important and measurements of the wavelength dependence of position angle permit the determination of magnetic field strengths. In this way, polarization observations of pulsars have been used to measure the local Galactic magnetic field. Radio sources are often found to be polarized, and this is generally attributed to a non-thermal emission mechanism. Although some extragalactic sources, such as 3C 273, have only moderate polarization, fluctuations in flux are sometimes found to be correlated with changes in the polarization, indicating that the variable part of the flux is strongly polarized.

X-ray polarization measurements are still relatively sparse. The first non-solar polarization measurement was of the Crab Nebula, which is found to be $\sim$ 15% polarized.

1-5 Infrared Astronomical Polarimetry

The first polarization measurements in the infrared are attributed (Duverney and Vergnoux 1957) to Bérard, who was investigating the properties of the infrared end of the solar spectrum in about 1810. He showed that "...la chaleur était capable de subir la double réfraction et la polarisation."

Infrared polarimetry of fainter celestial objects could not seriously be contemplated until the development of more sensitive detectors. By the time modern infrared astronomy got underway in the 1960's, there were several good polarizers available, including the HR-sheet polarizer and the wire grid.

Forbes (1967) appears to have been the first astronomer to construct and use an infrared polarimeter in modern times, and he found the polarization of NML Cyg to be 4.9% at 1.6μ and 4.2% at 2.2μ. Since then, at least ten other astronomers have developed their own infrared polarimeters and these are discussed in section 4-7. The particular problems that face infrared astronomers attempting polarimetry, particularly the instrumental polarization introduced by off-axis choppers, are dealt with in the earlier sections of chapter 4.

Dust is associated with most infrared sources, and it is thought to be the polarizing agent in the majority of galactic sources where infrared polarization has been observed. Polarization is either produced by asymmetrical scattering off a dust cloud, or by dichroic absorption or emission by magnetically-aligned asymmetric grains. Non-thermal emission processes such as synchrotron emission can produce polarized radiation, and such processes may be responsible for the infrared polarization found in extragalactic sources such as BL Lac objects. These, and other processes that can polarize or depolarize infrared radiation, are discussed in sections 3-1 and 3-2.

Infrared astronomical polarimetry is at least 13 years old, and yet relatively few measurements have been made, particularly at far-infrared wavelengths. Those that have been reported are listed in section 3-3. The error bars are generally several tenths of a percent, contrasting with optical polarimetry where sensitivities of 10^{-3} per cent are now achieved (p15 Gehrels 1974). Chapter 4 discusses the techniques used for infrared astronomical polarimetry.

I have designed, built and used a new type of infrared polarimeter and this is the subject of chapters 5 to 7. In chapter 8 the results are discussed, particularly with reference to scattering mechanisms, and then in chapter 9 suggestions are made about the way that further work should proceed.

Chapter 2. Mathematical Treatment of Polarized Radiation

2-1 Introduction

There are many different methods and notations for describing polarized radiation. This can be confusing when the results of two or more papers are to be compared. A brief but fairly comprehensive account is given below, concentrating on the methods and notations which are most useful for astronomical polarimetry.

2-2 Electromagnetic Radiation

Electromagnetic radiation is a transverse wave motion, the waves travelling at the velocity of light. The electric and magnetic vectors of the radiation lie in a plane perpendicular to the direction of propagation of the wave, and the two vectors are mutually perpendicular. The strengths and directions of the vectors of the electric and magnetic fields are connected by Maxwell's equations, and therefore it is only necessary to consider the variation of one of these two vectors. In the theory of polarization, it is conventional to consider the electric vector.

The electric field at a time t, of a quasi-monochromatic electromagnetic wave, may be considered to be the sum of two components along perpendicular axes, x and y, which together with the axis in the direction of propagation make a right-hand-orthogonal set. The magnitude of the two components E_x and E_y, is given by the two equations

$$E_x = E_{x_o} \cos(\omega t+\delta_x) \qquad (2\text{-}1)$$

$$E_y = E_{y_o} \cos(\omega t+\delta_y), \qquad (2\text{-}2)$$

where E_{x_o} and E_{y_o} are the amplitudes of the x and y vibrations, ω is the angular frequency ($\omega=2\pi\nu$) and δ_x and δ_y are the phases of the x and y

vibrations.

2-3 Elliptical Polarization

To determine the motion of the electric vector, one can eliminate t between equations (2-1) and (2-2) to obtain

$$\frac{E_x^2}{E_{x_o}^2} - \frac{2E_xE_y}{E_{x_o}E_{y_o}}\cos\delta + \frac{E_y^2}{E_{y_o}^2} = \sin^2\delta, \qquad (2\text{-}3)$$

where $\delta = \delta_x - \delta_y$.

This is a standard equation of the form

$ax^2+2hxy+by^2+c = 0$, the equation of a conic.

Since $ab-h^2 = \frac{1}{E_{x_o}^2E_{y_o}^2} - \frac{\cos^2\delta}{E_{x_o}^2E_{y_o}^2}$

$$= \frac{\sin^2\delta}{E_{x_o}^2E_{y_o}^2} \geqslant 0 ,$$

equation (2-3) represents an ellipse. It is called the polarization ellipse of the radiation.

2-4 A Description Of A General Beam of Radiation

The above description is valid for a totally polarized beam of radiation, but radiation from astronomical sources is usually only partially polarized. We can split any general quasi-monochromatic beam of radiation into two parts, a totally unpolarized part having r.m.s. amplitude E, and a totally polarized part having components E_x and E_y as in equations 2-1 and 2-2. The unpolarized part is characterised by the property that if one considers the amplitudes of any two perpendicular

components of the electric vector, E_1 and E_2, then $\langle E_1 \rangle = \langle E_2 \rangle$ (where "$\langle\ \rangle$" indicates the time average taken over a time that is long compared with the period of vibration $\frac{1}{\nu}$), and the relative phase of E_1 and E_2 changes rapidly and randomly so that there is no fixed phase relationship between them.

A beam of quasi-monochromatic radiation can thus be characterized by the five parameters E, E_{x_o}, E_{y_o}, δ_x and δ_y, where E is the r.m.s. amplitude of the electric vector of the unpolarized part of the radiation, E_{x_o} is the amplitude of the electric vector of the completely polarized part of the radiation in the x direction, having phase δ_x, and E_{y_o} is the amplitude of the electric vector of the completely polarized part of the radiation in the y direction, having phase δ_y.

2-5 Stokes Parameters

It is convenient to group these parameters together in the following way to form the Stokes parameters (Stokes 1852) which we shall label I, Q, U and V following Walker (1954). Other labels for the same parameters are (A,B,C,D), (I,M,C,S), (S_0,S_1,S_2,S_3) etc.

$$I = E^2 + \frac{E_{x_o}^2 + E_{y_o}^2}{2} \tag{2-4}$$

$$Q = \tfrac{1}{2}\left[E_{x_o}^2 - E_{y_o}^2\right] \tag{2-5}$$

$$U = E_{x_o} E_{y_o} \cos\delta \tag{2-6}$$

$$V = E_{x_o} E_{y_o} \sin\delta. \tag{2-7}$$

For completely polarized radiation (i.e. E=0), $I^2 = Q^2+U^2+V^2$. Equations (2-6) and (2-7), and the second, third and fourth equations of expression (2-8) below, show that Q, U and V are orthogonal and thus are sufficient to handle completely polarized radiation.

The four parameters are usually expressed as a column vector, and the effect of any optical element can be represented by a 4x4 matrix, known as a Mueller matrix. The premultiplication of the Stokes vector of radiation entering the optical element by the appropriate Mueller matrix gives the Stokes vector for the resulting radiation. However, before discussing Mueller matrices, there are several points to note concerning the Stokes vector.

Firstly, although the relative phase information is retained in the Stokes vector, as δ, the absolute phase information is lost. Therefore, Stokes vectors are unsuitable for handling the combination of coherent beams. A different vector, the Jones vector (Jones 1941) complements the Stokes vector. The "Full Jones vector" is $\begin{bmatrix} E_{x_o} e^{i\delta x} \\ E_{y_o} e^{i\delta y} \end{bmatrix}$ and for optical components there is an associated 2x2 Jones matrix. The Jones vector retains the absolute phase information but does not include information on the unpolarized part of the beam. This formulation cannot therefore handle partially polarized radiation, depolarization effects, or the combination of incoherent beams. These constraints make it simpler to use the Stokes vector for astronomical polarimetry, where beams are often only partially polarized and one is not usually concerned with recombining split beams.

The Stokes vector is often expressed differently from equations (2-4) to (2-7), using alternative parameters, and these formulations may sometimes be more convenient. Some common expressions are:

$$\begin{aligned} I &= I \\ Q &= I p \cos 2\theta \\ U &= I p \sin 2\theta \\ V &= I q \ , \end{aligned} \qquad (2\text{-}8)$$

or $I = I$

$Q = IP\cos 2\varepsilon\cos 2\theta$

$U = IP\cos 2\varepsilon\sin 2\theta$

$V = IP\sin 2\varepsilon,$ (2-9)

or $I = \langle E_{x_i}^2 \rangle + \langle E_{y_i}^2 \rangle$

$Q = \langle E_{x_i}^2 \rangle - \langle E_{y_i}^2 \rangle$

$U = \langle 2E_{x_i}E_{y_i}\cos\delta \rangle$

$V = \langle 2E_{x_i}E_{y_i}\sin\delta \rangle$, (2-10)

where I = the intensity of the whole beam,

p = the degree of linear polarization,

q = the degree of circular polarization,

θ = the angle of linear polarization — which is the angle between the major axis of the polarization ellipse, and the x-axis,

P = the degree of total polarization,

and $\varepsilon = \tan^{-1}\frac{b}{a}, \frac{-\pi}{4} \leq \varepsilon \leq \frac{\pi}{4}$, where a and b are the semi-major and semi-minor axes of the polarization ellipse.

The four expressions for the Stokes Parameters are equivalent, as may be shown by the application of straightforward trigonometry. This equivalence is proved in Appendix I. Expression (2-8) is often most convenient as it explicitly includes the degrees of linear and circular polarization, p and q.

2-6 Mueller Matrices For A Partial Polarizer

It is now necessary to determine the Mueller matrices for the various optical components that I shall be using.

For completely linearly polarized radiation, there will be a unique axis of the partial polarizer such that maximum radiation is transmitted

when this axis is parallel to the direction of linear polarization. Let this maximum transmittance be T_{MAX}. There will be a perpendicular axis such that minimum radiation is transmitted when this axis is parallel to the direction of linear polarization. Let this minimum transmittance be T_{MIN}. T_{MAX} and T_{MIN}, along with ϕ, the angle of the axis of maximum transmittance compared to the x-axis, characterise the partial polarizer. T_{MAX} and T_{MIN} will almost certainly be wavelength-dependent, but in what follows, it will be assumed that the radiation is sufficiently monochromatic for this not to matter.

It is necessary, as a preliminary, to determine the Stokes parameters for a beam referred to new axes at an angle η to the original x and y axes. This enables us to determine the rotation matrix $R(\eta)$. I and V (=Iq) will be invariant under this rotation, whilst

$$Q = Ip\cos 2\theta \rightarrow Ip\cos 2(\theta-\eta)$$

and $$U = Ip\sin 2\theta \rightarrow Ip\sin 2(\theta-\eta).$$

Now $$Ip\cos 2(\theta-\eta) = Ip(\cos 2\theta\cos 2\eta+\sin 2\theta\sin 2\eta)$$
$$= Q\cos 2\eta + U\sin 2\eta$$

$$Ip\sin 2(\theta-\eta) = Ip(\sin 2\theta\cos 2\eta-\cos 2\theta\sin 2\eta)$$
$$= U\cos 2\eta - Q\sin 2\eta$$

and so $$R(\eta) = \begin{bmatrix} 1 & 0 & 0 & 0 \\ 0 & \cos 2\eta & \sin 2\eta & 0 \\ 0 & -\sin 2\eta & \cos 2\eta & 0 \\ 0 & 0 & 0 & 1 \end{bmatrix}.$$

This is a rotation of 2η in the Q-U plane.

Consider a partial polarizer with parameters $T_{MAX} = t_x^2$ and $T_{MIN} = t_y^2$, aligned so that the axis of maximum transmission is parallel to the x-axis. Let the outgoing radiation have Stokes parameters

$$I' = \langle E'^2_{x_i} \rangle + \langle E'^2_{y_i} \rangle$$

$$Q' = \langle E'^2_{x_i} \rangle - \langle E'^2_{y_i} \rangle$$

$$U' = \langle 2E'_{x_i} E'_{y_i} \cos\delta \rangle$$

$$V' = \langle 2E'_{x_i} E'_{y_i} \sin\delta \rangle .$$

The phase, δ, is unprimed because the partial polarizer we are considering is not a retarder and thus the phase difference in the x and y components is unchanged.

Then $$E'_{x_i} = t_x E_{x_i}$$

$$E'_{y_i} = t_y E_{y_i} .$$

So $$I' = \tfrac{1}{2}(t_x^2 + t_y^2) I + \tfrac{1}{2}(t_x^2 - t_y^2) Q$$

$$Q' = \tfrac{1}{2}(t_x^2 - t_y^2) I + \tfrac{1}{2}(t_x^2 + t_y^2) Q$$

$$U' = t_x t_y U$$

$$V' = t_x t_y V .$$

Thus the Mueller matrix for a partial polarizer is

$$M = \tfrac{1}{2} \begin{bmatrix} t_x^2 + t_y^2 & t_x^2 - t_y^2 & 0 & 0 \\ t_x^2 - t_y^2 & t_x^2 + t_y^2 & 0 & 0 \\ 0 & 0 & 2t_x t_y & 0 \\ 0 & 0 & 0 & 2t_x t_y \end{bmatrix}$$

To find the Mueller matrix $M(\phi)$ for a partial polarizer inclined at an angle ϕ to the x-axis, we must first rotate the co-ordinate axes through ϕ, then apply the above Mueller matrix, and finally rotate the axes through $-\phi$. Therefore,

$$M(\phi) = R(-\phi)\, M\, R(\phi)$$

$$= \tfrac{1}{2}\begin{bmatrix} t_x^2+t_y^2 & (t_x^2-t_y^2)\cos 2\phi & (t_x^2-t_y^2)\sin 2\phi & 0 \\ (t_x^2-t_y^2)\cos 2\phi & (t_x-t_y)\cos^2 2\phi+2t_xt_y & \tfrac{1}{2}(t_x-t_y)^2\sin 4\phi & 0 \\ (t_x^2-t_y^2)\sin 2\phi & \tfrac{1}{2}(t_x-t_y)^2\sin 4\phi & (t_x-t_y)^2\sin^2 2\phi+2t_xt_y & 0 \\ 0 & 0 & 0 & 2t_xt_y \end{bmatrix}. \qquad (2\text{-}11)$$

For a perfect polarizer with $T_{MAX} = t_x^2 = 1$ and $T_{MIN} = t_y^2 = 0$, (2-11) reduces to

$$\tfrac{1}{2}\begin{bmatrix} 1 & \cos 2\phi & \sin 2\phi & 0 \\ \cos 2\phi & \cos^2 2\phi & \tfrac{1}{2}\sin 4\phi & 0 \\ \sin 2\phi & \tfrac{1}{2}\sin 4\phi & \sin^2 2\phi & 0 \\ 0 & 0 & 0 & 0 \end{bmatrix}.$$

If the incident radiation on a perfect polarizer is totally linearly polarized, the emergent radiation has the Stokes vector

$$\tfrac{1}{2}\begin{bmatrix} 1 & \cos 2\phi & \sin 2\phi & 0 \\ \cos 2\phi & \cos^2 2\phi & \tfrac{1}{2}\sin 4\phi & 0 \\ \sin 2\phi & \tfrac{1}{2}\sin 4\phi & \sin^2 2\phi & 0 \\ 0 & 0 & 0 & 0 \end{bmatrix}\begin{bmatrix} I \\ I\cos 2\theta \\ I\sin 2\theta \\ 0 \end{bmatrix}$$

and thus the intensity is $I' = \tfrac{1}{2}I(1+\cos 2\phi\cos 2\theta+\sin 2\phi\sin 2\theta)$

$$= I\cos^2(\theta-\phi)\ ,$$

which is Malus' law.

If the partial polarizer is a wire-grid analyser with the grid aligned at an angle ψ and principal transmittances $T_\perp$ and T_{11} for radia-

tion polarized perpendicular and parallel to the wires, then $T_{MAX} = T_\perp$, $T_{MIN} = T_{11}$ and $\phi = 90^\circ+\psi$, since $T_\perp > T_{11}$. The Mueller matrix for a wire-grid analyser is therefore

$$\tfrac{1}{2}\begin{bmatrix} T_\perp+T_{11} & -(T_\perp-T_{11})\cos 2\psi & -(T_\perp-T_{11})\sin 2\psi & 0 \\ -(T_\perp-T_{11})\cos 2\psi & (\sqrt{T_\perp}-\sqrt{T_{11}})^2\cos^2 2\psi+2\sqrt{T_\perp T_{11}} & \tfrac{1}{2}(\sqrt{T_\perp}-\sqrt{T_{11}})^2\sin 4\psi & 0 \\ -(T_\perp-T_{11})\sin 2\psi & \tfrac{1}{2}(\sqrt{T_\perp}-\sqrt{T_{11}})^2\sin 4\psi & (\sqrt{T_\perp}-\sqrt{T_{11}})^2\sin^2 2\psi+2\sqrt{T_\perp T_{11}} & 0 \\ 0 & 0 & 0 & 2\sqrt{T_\perp T_{11}} \end{bmatrix}. \qquad (2\text{-}12)$$

2-7 Instrumental Polarization

Any non-retarding optical system can be regarded as a partial linear polarizer. Often it is said that an optical system has an instrumental polarization i at an angle ϕ. Suppose the transmission of the instrument for unpolarized radiation is T_r. Then if ϕ is as above, and

$$T_r = \tfrac{1}{2}(T_{MAX}+T_{MIN}), \quad i = \frac{T_{MAX}-T_{MIN}}{T_{MAX}+T_{MIN}},$$

and so $T_{MAX} = T_r(1+i)$ and $T_{MIN} = T_r(1-i)$.

Substituting these into (2-11), the Mueller matrix becomes

$$T_r\begin{bmatrix} 1 & i\cos 2\phi & i\sin 2\phi & 0 \\ i\cos 2\phi & (1-\sqrt{1-i^2})\cos^2 2\phi+\sqrt{1-i^2} & \tfrac{1}{2}(1-\sqrt{1-i^2})\sin 4\phi & 0 \\ i\sin 2\phi & \tfrac{1}{2}((1-\sqrt{1-i^2})\sin 4\phi & (1-\sqrt{1-i^2})\sin^2 2\phi+\sqrt{1-i^2} & 0 \\ 0 & 0 & 0 & \sqrt{1-i^2} \end{bmatrix}. \qquad (2\text{-}13)$$

For small instrumental polarizations, this can be slightly simplified.

If $i \ll 1$,

$$(1+i)^{\frac{1}{2}} \simeq 1+\tfrac{1}{2}i \text{ and } (1-i)^{\frac{1}{2}} \simeq 1-\tfrac{1}{2}i$$

and the matrix becomes

$$T_r \begin{bmatrix} 1 & i\cos 2\phi & i\sin 2\phi & 0 \\ i\cos 2\phi & 1 & 0 & 0 \\ i\sin 2\phi & 0 & 1 & 0 \\ 0 & 0 & 0 & 1 \end{bmatrix} .$$

Suppose there is an optical element (e.g. a telescope) before the polarimeter with instrumental polarization i at an angle ϕ. Then the polarization measured by the polarimeter will be the polarization of the source, modified by the optical element. If the optical element is represented by the Mueller matrix M, the polarimeter measurements will yield the Stokes vector I', Q', U', V' when the Stokes vector of the source is I,Q,U,V, where

$$M \begin{bmatrix} I \\ Q \\ U \\ V \end{bmatrix} = \begin{bmatrix} I' \\ Q' \\ U' \\ V' \end{bmatrix} ,$$

and

$$\begin{bmatrix} I \\ Q \\ U \\ V \end{bmatrix} = M^{-1} \begin{bmatrix} I' \\ Q' \\ U' \\ V' \end{bmatrix} .$$

Therefore if M has an inverse (i.e. if $\det M \neq 0$), the polarization of the

source can be determined. The determinant of the matrix (2-13) (setting $T_r=1$) is just $(1-i^2)^2$ which is non-zero for all $i < 1$. Thus it is possible, in general, to determine the source polarization, despite instrumental polarization. It should be noted that the retardance of the instrument has not been included in (2-13), and this could introduce linear-to-circular conversion. If it were felt that this was significant, retardance could be included in the Mueller matrix for the instrument.

2-8 The Mueller Matrix For A Pure Retarder

It will also be useful to derive the matrix for a pure retarder. This is an optical element that changes the relative phase (but not the relative amplitude) of orthogonal components of the radiation.

Suppose the retarder is aligned with its 'fast' axis along the x axis and its 'slow' axis along the y axis, and vibrations along the y axis are delayed by τ. Then if the incident radiation has Stokes parameters as in (2-4) to (2-7), and primed variables represent the emergent radiation,

$$I' = E^2 + \underline{E_{x_o}^2 + E_{y_o}^2}$$

$$Q' = \tfrac{1}{2}\left[E_{x_o}^2 - E_{y_o}^2\right]$$

$$U' = E_{x_o}E_{y_o}\cos(\delta-\tau) = E_{x_o}E_{y_o}\cos\delta\cos\tau + E_{x_o}E_{y_o}\sin\delta\sin\tau$$
$$= U\cos\tau + V\sin\tau$$

$$V' = E_{x_o}E_{y_o}\sin(\delta-\tau) = E_{x_o}E_{y_o}\sin\delta\cos\tau - E_{x_o}E_{y_o}\cos\delta\sin\tau$$
$$= -U\sin\tau + V\cos\tau.$$

The matrix of this retarder is then

$$\begin{bmatrix} 1 & 0 & 0 & 0 \\ 0 & 1 & 0 & 0 \\ 0 & 0 & \cos\tau & \sin\tau \\ 0 & 0 & -\sin\tau & \cos\tau \end{bmatrix},$$

a rotation of τ in the U-V plane.

Employing the rotation matrix $R(\eta)$ as before, the matrix of a retarder with retardance τ and fast axis at an angle ψ

$$= R(-\psi) \begin{bmatrix} 1 & 0 & 0 & 0 \\ 0 & 1 & 0 & 0 \\ 0 & 0 & \cos\tau & \sin\tau \\ 0 & 0 & -\sin\tau & \cos\tau \end{bmatrix} R(\psi)$$

$$= \begin{bmatrix} 1 & 0 & 0 & 0 \\ 0 & \cos^2 2\psi+\cos\tau\sin^2 2\psi & \tfrac{1}{2}\sin 4\psi(1-\cos\tau) & -\sin\tau\sin 2\psi \\ 0 & \tfrac{1}{2}\sin 4\psi(1-\cos\tau) & \sin^2 2\psi+\cos\tau\cos^2 2\psi & \sin\tau\cos 2\psi \\ 0 & \sin\tau\sin 2\psi & -\sin\tau\cos 2\psi & \cos\tau \end{bmatrix}.$$

Chapter 3. Astrophysics of Infrared Polarimetry

3-1 Polarizing Processes

In this section the principal processes by which infrared radiation from an astronomical source may become polarized are considered. Such processes may be a feature of the emission mechanism in an infrared source, they may occur in the immediate vicinity of the source, e.g. in a local dust cloud, or they may operate along the line-of-sight in the interstellar or intergalactic medium. There are also many depolarization effects which may reduce the amount of polarization one measures at the detector, and these are discussed in section 3-2.

3-1.1 Synchrotron Radiation

Relativistic electrons spiralling in a magnetic field have constant velocity in the direction of the field lines and only experience accelerations perpendicular to the field lines. Synchrotron radiation will therefore be linearly polarized perpendicular to the field lines, and Ginzberg and Syrovatskii (1965) show that the polarization of a synchrotron source is wavelength-independent and equal to $p = \frac{\gamma+1}{\gamma+7/3}$ (3-1)

where γ is the spectral index of the electron energy distribution as in section 1-2.3. Since γ is typically 2 or 3, $p \sim 70\%$. Therefore, in principle, synchrotron radiation can produce very highly polarized radiation. Equation 3-1 applies only to an optically-thin source, and when synchrotron self-absorption occurs, the radiation will be depolarized, for in the same way that different intensities of radiation are emitted perpendicular and parallel to the magnetic field, differential absorption will take place. Ginzberg and Syrovatskii (1969) show that in this case, the polarization is $p = \frac{3}{6\gamma+13}$, which is $\sim 10\%$ for typical values of γ.

It has been the high degree of linear polarization in many extragalactic radio sources which, along with their non-thermal spectra, pro-

vided convincing evidence that synchrotron radiation is the dominant emission mechanism in these objects.

3-1.2 Scattering

Radiation will be scattered if it is incident on a cloud of particles, which may consist of dust, molecules, ions or electrons. Theoretical calculations may be carried out using Mie theory for spherical particles, or one of its extensions for more complex shapes, and these show (p656 Born and Wolf 1975) that radiation scattered through an angle Θ will have a degree of linear polarization given by

$$P = \frac{\sin^2\Theta}{1+\cos^2\Theta} \qquad (3\text{-}2)$$

Thus radiation scattered at 90^o to the incident rays may be 100% linearly polarized.

Scattering is the process that produces the very large polarizations measured in some reflection nebulae e.g. CRL2688 - the Egg Nebula (Section 3-3.5). It is also thought to be the mechanism that polarizes radiation in stars with circumstellar shells. Dyck and Beichmann (1974) have pointed out that polarization due to scattering can be identified, since the polarization in a scattering source should be inversely correlated with any absorption bands. The scattered radiation will be more heavily absorbed having traversed a greater distance within the source than the unpolarized component which reaches the observer more directly.

3-1.3 Polarization By Dichroic Grains

Dust grains are thought to be responsible for most of the observed optical and infrared polarization that astronomers have observed. Scattering is the mechanism operating in many polarized sources (such as dust rings or reflection nebulae), but for others, the asymmetrical distribution of grains, required for scattering, may not be present. If

scattering or reflection were occurring in a large dust cloud, one would expect to see variations in the polarization direction across the cloud.

In the visible Hall (1949) and Hiltner (1949) found that the light from distant stars is partially linearly polarized, and that the percentage polarization is roughly correlated with colour excess. The larger polarizations tend to be found in the galactic plane where the dust extinction is greatest. These observations strongly suggest that the polarization is mainly caused by the dust in the interstellar medium, rather than being intrinsic to the stars. Whilst the maximum polarization value P_{MAX}, and the wavelength at which this occurs λ_{MAX}, vary from star to star, Serkowski, Mathewson and Ford (1975) found empirically that for all stars showing interstellar polarization at visible wavelengths

$$P_\lambda/P_{MAX} = \exp\left[-1.15\log_e{}^2(\lambda/\lambda_{MAX})\right]$$

where P_λ is the polarization at wavelength λ. Dyck and Jones (1978) found that at near-infrared wavelengths, this expression underestimates the polarization. Serkowski's formula at visible wavelengths does provide, however, a good test for theoretical models of interstellar grains.

Absorption by dust decreases with increased wavelength and therefore normal interstellar polarization is expected to become insignificant in the infrared. However, very heavily obscured objects with no optical counterparts, such as the BN source in Orion and the Galactic centre, are found to be highly polarized in the infrared (cf. Section 3-3). A random distribution of grains cannot produce polarized radiation except, as outlined in Section 3-1.2, by off-axis scattering. However, if the grains themselves have, on average, some sort of overall anisotropy, it is possible for polarized radiation to result from differential absorption (dichroism) or thermal emission. This anisotropy cannot be produced by a homogeneous cloud of spherical grains, and it is necessary to assume

that the grains are both elongated and aligned.

Dust grains are thought to be present in the majority of infrared sources and thus their properties are fundamental to infrared astronomy. However, the number of free parameters involved is very large and only an outline discussion of the properties most relevant to polarimetry can be attempted here. Amongst the parameters are the size, shape, composition and temperature of the grains, the size, density and geometry of the dust cloud, the type and strength of the alignment mechanism, any randomising effects, and the characteristics of the surrounding gas and of the emitting source.

A number of theories for the alignment mechanism for interstellar grains have been proposed, and they are reviewed by Aannestad and Purcell (1973). One basic property of elongated grains is that they will be rapidly spinning, due to random collisions with atoms and molecules, and therefore alignment in this case means that there will be a preferred direction for the angular momentum vector of the grains. The most generally accepted theory of grain alignment is the Davis-Greenstein mechanism (Davis and Greenstein 1951), which suggests that paramagnetic relaxation is the damping process that acts to align the spin axis of the grain parallel to a magnetic field. Radiation polarized parallel to the long axis of the grain (and thus perpendicularly to the magnetic field) will be preferentially absorbed, resulting in polarization parallel to the magnetic field. It can be noted that if this explanation is the correct one, then the plot in galactic co-ordinates of interstellar polarization by Mathewson and Ford (1970) shows that the galactic magnetic field lies mainly along the galactic plane. One quantitative difficulty which is encountered by the Davis-Greenstein mechanism is that rather large magnetic fields, $\sim 10^{-3}$gauss, seem to be required. The interstellar magnetic field derived from pulsar measurements is only $\sim 3\times10^{-6}$gauss. However, Spitzer (p189, 1978) concludes that other non-magnetic orient-

ation schemes are not sufficiently effective, and that paramagnetic relaxation is acceptable if either the complex magnetic susceptibility is enhanced by a clumpy distribution of iron atoms, making the grains 'superparamagnetic', or if the "spin-up" is long lived, i.e. if the randomizing processes are small. One possible mechanism for creating strong magnetic fields is the contraction of a dust cloud with the interstellar magnetic field 'frozen-in'.

It is not immediately apparent why the grains should be elongated. Hall and Serkowski (1962) note that the growth of dust grains which are not monocrystals seems to be a symmetrical process, and thus roughly spherical grains would be expected. However, significant elongation or flattening of the grains is required to explain the observed polarizations.

The size of interstellar grains is generally taken to be in the range 0.1μ - 1μ. This is based on the fact that there is an approximately linear relation between extinction by dust and reciprocal wavelength, and such a relation is expected from Mie theory when the circumference of the grains is of the order of the wavelength ($2\pi a/\lambda \sim 1$). That the wavelength of maximum interstellar polarization is typically $\sim 0.5\mu$ further confirms this inference.

The composition of the interstellar grains is the subject of considerable debate. The principal features in a plot of interstellar extinction versus wavelength (e.g. Savage and Mathis 1979) are broad absorption bands at 2175Å, 3.07μ and 9.7μ. No single substance appears to have these features, and they are usually associated with graphite, H_2O and silicate respectively. A further band at $\sim 18\mu$ is also attributed to silicates. The 9.7μ feature is correlated with increased polarization in some objects (e.g. the BN source), indicating that the silicates can be aligned.

In order to calculate the polarization due to aligned, elongated,

absorbing grains, we define (following Dyck and Beichman 1974)

G = geometrical cross-section of a grain,

L = path length in the medium,

N_a = number density of totally aligned particles,

N_r = number density of particles which are randomly oriented in the plane perpendicular to the line of sight,

$N = N_a + N_r$ = total number density of grains,

f = fraction of totally aligned grains $= \frac{N_a}{N}$,

and $Q_{11,\perp}$ are the grain extinction efficiencies for radiation polarized parallel and perpendicularly to the grain axis of symmetry. Then the optical depths in the two directions x and y, parallel and perpendicular to the grain alignment direction, are

$$\tau_{x,y} = [N_a Q_{11,\perp} + \tfrac{1}{2}(Q_{11}+Q_{\perp})N_r]\, GL$$

$$= \tfrac{1}{2}[(1+f)Q_{11,\perp}+(1-f)Q_{\perp,11}]\, GNL$$

and the polarization is

$$P_a = \frac{\exp(-\tau_y) - \exp(-\tau_x)}{\exp(-\tau_y) + \exp(-\tau_x)} .$$

A second way that aligned, elongated dust grains may produce polarized radiation is by their own thermal emission. An important feature of this radiation is that it should be polarized perpendicularly to the direction of polarization for radiation which has been differentially absorbed by the grains.

In this case, the polarization is

$$P_e = \frac{[1-\exp(-\tau_x)] - [1-\exp(-\tau_y)]}{[1-\exp(-\tau_x)] + [1-\exp(-\tau_y)]}$$

$$= \frac{\exp(-\tau_y) - \exp(-\tau_x)}{2 - \exp(-\tau_y) + \exp(-\tau_x)}$$

Using this model, Dennison (1977) finds that the far-infrared polarization by emission in the KL nebula in Orion is expected to be $\sim$ 5%. The presence of far-infrared polarization, perpendicular to the near-infrared polarization, would be a key distinguishing feature of aligned grains (as opposed to an asymmetrical scattering dust cloud).

Although a considerable amount of effort has been expended on attempts to understand the observational evidence on interstellar grains, progress has been slow due to the large number of parameters involved. In addition, the manufacture of sub-micron size particles for laboratory experiments is found to be very difficult, and theoretical calculations are at present restricted to simple particle shapes such as spheres or infinite cylinders.

3-1.4 Cosmic Masers

In the radio region the emission mechanism for certain very intense compact sources has been attributed to maser action. In this process stimulated emission produces intense coherent radiation which will be totally linearly polarized. No such sources have yet been identified in the infrared although Harwit (1974) suggests that compact dust clouds could possibly give rise to stimulated far-infrared emission.

3-1.5 Circular Polarization

Circular polarization measurements have not yet been reported in

the infrared at 10μ or longer wavelengths. This is due to the need for slightly more complicated observational techniques, since a retarder (such as a quarter-wave plate) is required, in addition to a linear polarizer. Also, only very small amounts of circular polarization are generally expected from astronomical sources.

Circular polarization may result from several astrophysical processes. Spectral lines which have been split by the Zeeman effect of a strong magnetic field will be circularly polarized in opposite directions for the two components. Circular polarization is also expected to be a second-order effect of synchrotron emission. A cloud of aligned dust grains will be weakly birefringent and thus will cause some linear-to-circular conversion. The amount of interstellar circular polarization expected from this effect will be only $\sim$ 0.01% (Martin 1978). Martin finds that the peak of the linear polarization should coincide with a change in sign of the circular polarization, provided the grains are made of a dielectric material.

3-2 Depolarization Effects

When an astrophysical process produces radiation with a certain degree of polarization, it is likely that this radiation, when analysed by an astronomical polarimeter, will be found to have a considerably reduced polarization due to the action of one or more depolarization effects. It is important to take these into account when deducing the astrophysics of the source of polarized radiation. Infrared astronomy is particularly affected by observational effects, such as large fields of view, wide bandpasses and long integration times, which are often used to achieve sufficient signal-to-noise.

3-2.1 Observational Effects

In the infrared, one cannot, at present, analyse radiation photon-

by-photon, so it must be recognized that an infrared polarimeter may smear out the polarization.

3-2.1a Spatial Depolarization. The detector has a finite field of view on the sky, which may be chosen to maximise the scientific value of the observations, or simply to accommodate the "seeing" disc, the diffraction disc, or telescope pointing or tracking precision. It is possible that within the field of view, there may be several sources, each with a distinct percentage and angle of polarization. For example, the magnetic field responsible for synchrotron radiation may not be uniform on the scale of the field of view. Alternatively, the radiation may pass through a magnetoionic medium which produces Faraday rotation, and if the magnetic field is not uniform on the scale of the field of view, depolarization will result.

To analyse the result of such effects, we can suppose that there are n sources in the field of view, each with polarization p, intensity I and random position angles θ_i ($0 \leq \theta_i \leq \pi$, $i = 1$ to n). Then the Stokes parameters for each source will be $[I, Ip\cos 2\theta_i, Ip\sin 2\theta_i, 0]$ if we ignore any circular polarization. The Stokes parameters for the total radiation in the field of view are $\left[nI, Ip \sum_{i=1}^{n} \cos 2\theta_i, Ip \sum_{i=1}^{n} \sin 2\theta_i, 0\right]$. The mean value of $|\cos 2\theta|$ $0 \leq \theta \leq \pi$ is $\frac{2}{\pi}$. The term $\sum_{i=1}^{n} \cos 2\theta_i$ is like a random walk from zero with step size $\frac{2}{\pi}$. After n steps, the r.m.s. value is $\sqrt{n}\frac{2}{\pi}$ and the same result is obtained for $\sum_{i=1}^{n} \sin 2\theta_i$. Thus the polarization, p_{TOTAL}, of the whole beam will have the r.m.s. value

$$p_{TOTAL} = \frac{\sqrt{(Ip\sqrt{n}\frac{2}{\pi})^2 + (Ip\sqrt{n}\frac{2}{\pi})^2}}{nI}$$

$$= \frac{2\sqrt{2}\,p}{\pi\sqrt{n}}$$

$$\simeq 0.9\,\frac{p}{\sqrt{n}} \quad .$$

3-2.1b Spectral Depolarization. The detector and filters determine the wavelengths over which the instrument is sensitive. The radiation may be polarized in particular lines or wavelength regions, but these effects will be diluted over the whole spectral window of the instrument. Also, Faraday rotation is proportional to the square of wavelength since $\Omega = 8.1\times10^{5}\lambda^{2}\int_{o}^{L} N_e H\cos\psi d\ell$ where ψ is the rotation in radians, λ is the wavelength in metres, N_e is the electron density in cm^{-3}, H is the magnetic field in gauss, ψ is the angle between the magnetic field and the line of sight, and L is in parsecs (p57, Lang 1974). Therefore, radiation, having suffered Faraday rotation, will be reduced in polarization when analysed over a finite wavelength interval. Faraday rotation is far less important in the infrared than in the radio, due to the λ^2 dependence. For example, the Crab Nebula, which has a rotation measure of $-25 rad\ m^{-2}$, exhibits a rotation of polarization position-angle of $\sim 30^{o}$ at 20cm wavelength, compared to its zero-wavelength position angle. However, at 20μ, the Faraday rotation will be reduced by a factor of 10^{8}, and hence will not be observable.

3-2.1c Temporal Depolarization. Certain infrared sources such as quasars and BL Lac objects have polarizations which vary with time. If this variation is on a time-scale comparable with the observation time, the measured polarization may be diluted.

3-2.2 Masking

Extragalactic infrared sources (e.g. NGC 1068) often seem to have a quasi-thermal spectrum. This may be interpreted as indicating a dust shroud round the source which re-radiates the radiation it has absorbed from an underlying energy source. This thermal radiation will certainly not have the polarization characteristics of the enshrouded source.

3-2.3 Dichroic Media

The passage of polarized radiation through a dichroic medium (e.g.

aligned dust grains) may alter the degree of polarization. It is possible that the polarization may be reduced or enhanced, depending on the relative orientation of the grains and the original polarization angle of the radiation.

Synchrotron self-absorption can be considered to be an example of this effect, whereby the polarization is reduced from $\sim$ 70% to $\sim$ 10% (cf. Section 3-1.1).

3-3 Infrared Polarization Measurements

In this section the astronomical measurements made to date, with infrared polarimeters, are considered. The relatively large number of observations that have been made at very short infrared wavelengths (<5μ) are discussed in general terms, whilst for measurements made at longer wavelengths, a fairly complete list is given.

3-3.1 Stars

A number of stars (mainly late-type) are strong near-infrared sources and some of these are found to have large infrared polarizations. These characteristics are attributed to dust clouds around the stars. Examples of such stars are VY CMa, NML Cyg, IRC+10216, and these have all been measured polarimetrically in the near-infrared.

The first reported measurement of the infrared polarization of a star was by Forbes (1967). He found polarization of about 4% at 1.6μ and 2.2μ in NML Cyg. Further observations of reddened stars at near-infrared wavelengths are reported by Hashimoto *et al.* (1970), Forbes (1971b), Dyck, Forbes and Shawl (1971), Forbes (1972), Maihara, Okuda and Sato (1972) and Cox *et al.* (1976). These observations indicate that whilst the majority of stars have only small polarizations, certain stars, such as those mentioned above, stand out by virtue of polarizations of 4% or more.

Capps and Dyck (1972) extended the measurements on 10 stars with circumstellar shells out to 10μ. None of these showed polarizations of more than 2%, and Capps and Dyck were only able to measure significant (>2σ) polarizations for α Ori (1.3±0.3%), IRC+10216 (1.3±0.4%) and α Her (1.2±0.4%). Capps and Knacke (1976a) remeasured IRC+10216 and found polarizations of 1.83±0.18% at 11μ, and 1.75±0.27% at 12.6μ. The only other reported infrared polarization measurements at wavelengths of 10μ or more (other than of M42, NGC 1068 or the galactic centre) are by Landau (1974). He measured 7 stars at 10.6μ and reports significant polarizations for α Sco (5±1%), and IRC+10216 (4±2%). However, his instrumental polarization appears to have been rather large (several percent) and these results may be questionable.

The simplest interpretation of these stellar polarizations is that stellar radiation is scattered off an asymmetrical dust shell and the polarization is diluted at longer wavelengths by thermal grain emission. The presence of a dust shell is indicated by an infrared excess, and Dyck et al. (1971) show that intrinsic visible polarization is correlated with infrared excess. Zellner and Serkowski (1972) discuss the polarization mechanisms for stars with circumstellar dust. For pure Rayleigh scattering off particles smaller than the wavelength, the percentage polarization of the scattered radiation is independent of wavelength. However, the scattered intensity, and hence the overall polarization, decreases with wavelength as λ^{-4}. This is in general agreement with most of the above measurements which show a decrease in polarization towards the infrared. Zellner and Serkowski report an interesting sinusoidal time variation in the percentage polarization of IRC+10216 at 1μ. It is 180° out of phase with its intensity variations, and they attribute this to rotation of an anisotropic light source.

Be stars are early-type stars which have an infrared excess due to their characteristic extended atmospheres. Jones (1979) finds that at

1.25μ and 2.2μ, some Be stars are intrinsically polarized and this is attributed to an equatorial scattering disk.

3-3.2 HII Regions and Molecular Clouds

Dyck and Capps (1978) examined 15 compact infrared sources associated with HII regions and molecular clouds. Seven of these are found to have large (> 10%) polarization at 2.2 or 3.8μ and a good correlation between polarization and compactness was found. One of the sources was the BN object itself, and Dyck and Capps infer that this and the other highly polarized sources (W3/IRS5, W33A, CRL 2591, S140, NGC 7538/IRS1, NGC 7538E) are sites of star formation.

Capps, Gillett and Knacke (1978) made further measurements of W33A and found that the polarization reaches a maximum of 23% at 2.4μ and falls to ∿ 11% at 4μ. In general, more polarization measurements at other wavelengths (especially far-infrared) are required to determine whether the high polarizations are due to scattering or dichroic absorption. Capps et al. note that aligned grains in W33A would indicate a local magnetic field strength of a few milligauss.

Measurements of molecular cloud sources by Lonsdale et al. (1980) revealed large circular polarizations (∿ 0.5-1.5%), the largest values being for BN and W33A. These findings are consistent with birefringent aligned grains.

3-3.3 The Orion Nebula

The Orion nebula is a cloud of gas and dust containing some very strong infrared sources. It contains a compact infrared nebula, the K-L nebula (Kleinmann and Low 1967), and a very strong point source, the B-N object (Becklin and Neugebauer 1967). Rieke, Low and Kleinmann (1973) mapped the region of the K-L nebula at 5.21μ and found four distinct sources in addition to the B-N object. At far-infrared wavelengths, the whole nebula is a strong extended source (Werner et al. 1976).

Large polarizations of the B-N object have been consistently detected by a number of observers. Breger and Hardorp (1973) reported 25±3% polarization at 1.6μ and 14±1% at 2.2μ, and Loer, Allen and Dyck (1973) extended this to 7±1% at 3.4μ. Dyck et al. (1973) measured substantial polarization out to 11μ with a peak of 15% coincident with the silicate absorption feature at 10μ. Dyck and Beichmann (1974) measured the polarization at 11.1μ with 9" resolution for several regions of the K-L nebula and found a roughly uniform polarization angle across the entire nebula. Capps, Gillett and Knacke (1978) report a detailed polarization spectrum of BN showing a steady decline from 30% at 1.6μ to 9% at 2.8μ followed by a peak at 3.1μ of 15% coincident with the 3μ 'ice' absorption band. Knacke and Capps (1979) made additional polarization measurements of BN and KL at 11.1μ and 19.6μ, finding a polarization for BN of 6.8% at 19.6μ.

Dyck and Beichmann (1974) considered the possible polarization mechanisms and concluded that the uniform polarization angle across the nebula, and the correlation of polarization with absorption bands, suggest absorption by aligned grains, rather than scattering. Using the Davis-Greenstein alignment mechanism, they deduce grain temperatures of $\sim 6^{\circ}K$, but such low temperatures do not fit the observed far-infrared fluxes. A magnetic field of strength 7×10^{-3} gauss is indicated. Dennison (1977) assumes a larger optical depth which allows more reasonable (higher) grain temperatures. He also points out that effects such as superparamagnetism could allow a weaker magnetic field. The increased polarization across the 3 and 10μ absorption bands points to an ice-silicate mixture for the grains. Knacke and Capps (1979) conclude that the consistency of the polarization angle with wavelength excludes polarized grain emission out to 19.6μ and that the polarization is due to absorption by a cold cloud of aligned grains overlying BN and KL. They reject the analysis of Elsässer and Staude (1978) (at least for BN at

wavelengths longer than 4μ) who proposed that the infrared polarization is due to asymmetrical scattering off interstellar dust and electrons.

Circular polarization of 0.86% at 3.45μ of the BN object was measured by Serkowski and Rieke (1973) and subsequently by Lonsdale et al. (1980) who found ∿ 1.5% circular polarization at 2.2μ.

Dennison et al. (1977), Gull et al. (1978 and 1980) have attempted to measure the far-infrared polarization of the KL Nebula from airborne observatories. The instruments had beams of 6' and 1' and instrumental polarizations of ∿ 5% and ∿ 8% respectively. No positive results were obtained.

3-3.4 The Galactic Centre

The centre of our galaxy appears as a rather complex region at 10μ, with at least 10 distinct sources in a 40" field (Becklin and Neugebauer 1975). The region is highly obscured in the visible with an extinction of ∿ 30 magnitudes (Becklin and Neugebauer 1968). Infrared radiation suffers far less extinction, and thus observations in this wavelength region are very important.

Early polarization measurements by Low et al. (1969) used a 25" beam at 10μ, and Maihara et al. (1972) used a 30" beam at 2.2μ. Low et al. were only able to put a 3σ upper limit of about 6% on the polarization, whilst Maihara et al. obtained 5.3±1.3%. Dyck, Capps and Beichmann (1974) used an 11" beam and obtained polarizations of 8±2% at 3.4μ and 2.4±0.4% at 11μ.

A much more detailed polarimetric study is reported by Capps and Knacke (1976b) and Knacke and Capps (1977) at wavelengths from 2.2μ up to 11.5μ. They confirm the discovery by Dyck, Capps and Beichmann (1974) of a large rotation of position angle between 2.2μ and 11.5μ, indicating that a different polarization mechanism is dominant at the two wavelengths. The percentage polarization varies from source to source with a

maximum of 6%. At shorter wavelengths, the polarizations are roughly parallel to the galactic plane, as is the optical polarization as measured by Mathewson and Ford (1970), whilst the 11.5μ polarization is roughly perpendicular to the galactic plane. Knacke and Capps (1977) conclude that the 2.2μ polarization is due to differential absorption by aligned dust grains along the line-of-sight, whilst the 11.5μ polarization is due to aligned silicate grains in or near the infrared sources.

Later observations by Maihara et al. (1977), Adams and Hough (1977) and Hough et al. (1978) at 1.7μ and 2.2μ, are consistent with the previous measurements.

3-3.5 CRL 2688 (The Egg Nebula) - A Bipolar Reflection Nebula

This object was first discovered to be a strong infrared source during the AFCRL rocket survey, and in the visible it is seen as an elliptical nebulosity with two components separated by $\sim 8''$. Ney et al. (1975) suggest that the object consists of a central star obscured by a dust toroid, and that the two visible components are dust clouds illuminated by the obscured star. The infrared source lies between the two visible components and has a diameter of $\sim 1''$. Michalsky et al. (1976) measured very high linear polarizations from the reflection nebulae (41% to 58%) in the visible and these are confirmed by Shawl and Tarenghi (1976). Near-infrared polarization measurements of the northern optical component made by Jones and Dyck (1978) show that the degree of polarization peaks at 50% near 1μ, and drops off in the infrared to 31% at 2.2μ. Ney et al. (1975) report that Becklin and Neugebauer observed less than 1% polarization from the infrared source at 10μ.

The very high values of the polarization indicate a scattering angle of close to 90°. Shawl and Tarenghi (1976) find that the wavelength dependence of both the polarization and reddening data suggests that scattering grains are composed of graphite rather than silicate. Jones

and Dyck (1978) ascribe the drop-off in polarization at longer wavelengths to the existence of an unpolarized source of thermal radiation in the dust cloud which dilutes the scattered highly polarized radiation above 1μ.

Two other objects have been identified which are probably reflection nebulae similar to CRL 2688. Jones and Dyck (1978) found 16% polarization at 2.2μ in NGC 2261, and Kobayashi et al. (1978) measured 30% polarization at 2.2μ in OH 0739-14. It is probable that both these objects are reflection nebulae similar to CRL 2688.

3-3.6 NGC 1068 - A Seyfert Galaxy

NGC 1068 is the brightest Seyfert galaxy at infrared wavelengths. The emission mechanism that gives rise to this large flux is not yet agreed, and polarization measurements impose useful constraints.

Knacke and Capps (1974) measured polarizations of 3.2±0.4% at 3.5μ and 2.3±0.5% at 10.2μ and Lebofsky, Rieke and Kemp (1978) made more measurements between 1.25μ and 3.45μ which showed a peak polarization of $\sim$ 4% at 2.2μ. The position angle increases from 99±7° at 1.25μ to 125±2° at 3.45μ. Lebofsky, Rieke and Kemp (1978) suggest that the near-infrared spectrum and polarization arise from a heavily obscured non-thermal source, whilst at longer wavelengths, the dust emission dominates. However, the existence of the non-thermal source is by no means certain, and further polarimetric measurements would help confirm or contradict this.

Kemp et al. (1977) made polarimetric observations of four other extra-galactic infrared sources, NGC 1275, NGC 4151, MRK 231 and 3C 273. All of these were thought to contain strong non-thermal emitters. However the measured polarizations were all below 1% at 2.2μ, suggesting that if non-thermal mechanisms are responsible for the infrared radiation, they must be unpolarized or there are large depolarization effects.

3-3.7 BL Lac Objects and Quasars

The origin of the radiation from BL Lac objects and quasars has been an open question since their discovery. However, polarization measurements can help to resolve the issue, for synchrotron radiation should be polarized, and the polarization should be roughly independent of wavelength. If dust grains are involved, polarization is possible, but both the percentage polarization and the position angle should change with wavelength.

Knacke, Capps and Johns (1976) observed BL Lac itself at 0.44, 2.2 and 3.5μ. They found roughly 10% polarization with a fairly constant position angle at all three wavelengths, and suggest that this is indicative of a synchrotron source. Puschell and Stein (1980) found that the polarization of BL Lac varies on a time-scale of days, and that it is sometimes strongly wavelength-dependent, although this wavelength dependence could be a result of very rapid variability on a time-scale of hours. A number of near-infrared polarimetric studies (e.g. Rieke et al. 1977, Capps and Knacke 1978, Puschell and Stein 1980) of other BL Lac objects show a common pattern of high polarizations which vary rapidly and are usually not strongly wavelength-dependent.

The quasar 3C 273 has been measured polarimetrically in the infrared by Kemp et al. (1977) and by Knacke, Capps and Johns (1979) and both found very little polarization ($\sim$ 0.5%) at 2.2μ. However, the highly variable quasar 3C 345 was found by Knacke, Capps and Johns to have a very large polarization (up to 32%) at 2.2μ. This considerably exceeds the optical polarization of $\sim$ 4%.

The common factors of large polarizations, rapid variability and non-thermal spectra are strong indications that these objects contain synchrotron radiation sources.

3-3.8 Planets

Forbes (1971a) measured the infrared polarization of Venus between 1.25 and 3.6μ. He found a 90° change in polarization angle at ∿ 2μ and increasing polarization with wavelength reaching nearly 9% at 3.6μ. The use of single-particle Mie theory indicates that Venus' atmosphere contains particles ∿ 1μ in size.

Kemp et al. (1978) made studies of Saturn and Jupiter and also discovered a 90° rotation of the polarization angle at ∿ 2μ, particularly on the poles. The maximum polarization was 2% at 3.5μ from Saturn's rings. Like Forbes, they infer a particle size of ∿ 1μ.

3-3.9 The Cosmic Background Radiation

Rees (1968) has suggested that anisotropies present in the early cosmological expansion could induce partial polarization of the cosmic background radiation. In the "HII case" (re-ionization of the pregalactic gas, which then stays fully ionized until a redshift of $z \sim 8$), the polarization could be of the same order as the large-scale anisotropy $\Delta T/T$. Anile and Breuer (1977) and Caderni et al. (1978a) show that such polarizations could survive intact to the present epoch, and so the measurement of the polarization could be a very sensitive measure of the isotropy.

Caderni et al. (1978b) flew a far-infrared (500μ-3mm) polarimeter to measure the linear polarization of the background radiation. They report a 1σ upper limit of 8×10^{-4} at an angular scale of 40° for the polarization.

Chapter 4. Techniques of Infrared Polarimetry

4-1 Types of Analyser

Every polarimeter must incorporate some element which has different properties for radiation polarized parallel and perpendicular to some axis of the element. Such an element is called an analyser or polarizer and the following is a description of those that are suitable for the infrared.

4-1.1 Dichroic Polarizers

In the optical and near-infrared, sheet polaroid is readily available. The molecules in such materials are aligned by uni-axial stretching with the result that the material has different transmittances for radiation polarized parallel and perpendicular to the direction of stretching. Such analysers can be very efficient, with $\frac{T_{11}-T_{\perp}}{T_{11}+T_{\perp}}$ close to unity. HR sheet is the material used for near-infrared work, and is useful out to 2.7μ. Various other materials having a directional crystal or molecular structure can be used in the infrared, but they often have drawbacks. For example, pyrolitic graphite can be used over the range 5-500μ (Rupprecht, Ginsberg and Leslie 1962) but its brittleness restricts the size of analyser. Many substances are ruled out because of deep absorption bands in the infrared.

4-1.2 Brewster Angle Polarizers

The reflectivity of a dielectric surface, for radiation polarized with its electric vector in the plane of incidence, is a function of the angle of incidence, and tends to zero at the Brewster Angle. By passing a beam of radiation through a 'pile of plates' of a suitable dielectric, tilted at the Brewster angle, one may obtain a transmitted beam which is very highly polarized. It is possible to largely compensate for the lateral shift in the beam, but at the expense of compactness. In the

infrared, mylar or polythene can be used as a dielectric (Mitsuishi et al. 1960).

There are several disadvantages of such analysers. a) They can only cope with a narrow range of angles of incidence. b) They tend to be bulky. c) There is often a lateral shift in the beam. d) There may be interference effects between the plates. e) Transmission may be low because the beam must pass through a large number of layers (typically 5 to 15).

4-1.3 Grid Polarizers

A beam of radiation passing through a grid of parallel wires will tend to set up induced currents in the wires. However, since the currents can only flow along the wires, it is only radiation that has its electric vector parallel to the wires that can set up such currents. These currents produce radiation in the forward and backward directions. However, radiation in the forward direction interferes destructively with the indicent wave so that for radiation polarized parallel to the wires, the grid acts as a partial reflector.

If the wire spacings are of the order of the wavelength of the radiation, then almost 100% linearly polarized radiation is transmitted. In the microwave region, such wire grid polarizers are easy to make, but for most of the infrared, the wires would have to be too thin to be free-standing. Therefore, grids for the infrared are made by photographically depositing metallic strips on a transmitting substrate - often polythene for the far-infrared and KRS-5 for the 1-10μ region. Grid polarizers for the infrared are now readily available and appear to be the most convenient for use as an analyser. The techniques of making such finely spaced grids are described by Auton (1967) and Auton and Hutley (1972). Further detail about polarization by grids is given in Section 4-2.

4-1.4 Photoelastic Analysers

Strain in certain transmitting materials can cause them to become birefringent, and this phenomenon can be exploited to construct an infrared analyser. By imposing the appropriate stress on a suitable thickness of such material, one can create a quarter wave plate. This will convert circularly polarized radiation to linearly polarized radiation, will convert linearly polarized radiation to elliptically polarized radiation, and will not change unpolarized radiation. By vibrating the material, it is possible to switch the retardance between $\pm\frac{\lambda}{4}$ to produce an A.C. signal at the detector. Very little power is necessary if frequencies near the natural frequency of the material are used. Piezoelectric transducers are often employed to provide the oscillation.

To measure linear polarization, one can employ a three-element system consisting of a $\frac{\lambda}{4}$ wave plate, an oscillating $\pm\frac{\lambda}{4}$ element aligned with the wave plate, and a linear polarizer at 45° to the slow and fast axes of the $\frac{\lambda}{4}$ elements. The system then oscillates between the Mueller matrices

$$\tfrac{1}{2}\begin{bmatrix}1&0&1&0\\0&0&0&0\\1&0&1&0\\0&0&0&0\end{bmatrix}\begin{bmatrix}1&0&0&0\\0&1&0&0\\0&0&0&1\\0&0&-1&0\end{bmatrix}\begin{bmatrix}1&0&0&0\\0&1&0&0\\0&0&0&1\\0&0&-1&0\end{bmatrix}=\tfrac{1}{2}\begin{bmatrix}1&0&-1&0\\0&0&0&0\\1&0&-1&0\\0&0&0&0\end{bmatrix} \quad -A$$

Linear polarizer at 45° | $+\frac{\lambda}{4}$ element | $\frac{\lambda}{4}$ waveplate

and $$\tfrac{1}{2}\begin{bmatrix}1&0&1&0\\0&0&0&0\\1&0&1&0\\0&0&0&0\end{bmatrix}\begin{bmatrix}1&0&0&0\\0&1&0&0\\0&0&0&-1\\0&0&1&0\end{bmatrix}\begin{bmatrix}1&0&0&0\\0&1&0&0\\0&0&0&1\\0&0&-1&0\end{bmatrix}=\tfrac{1}{2}\begin{bmatrix}1&0&1&0\\0&0&0&0\\1&0&1&0\\0&0&0&0\end{bmatrix} \quad -B$$

Linear polarizer at 45° | $-\frac{\lambda}{4}$ element | $\frac{\lambda}{4}$ waveplate

The effect of matrix A on a general beam of radiation $\begin{bmatrix} I \\ Ipcos2\theta \\ Ipsin2\theta \\ Iq \end{bmatrix}$

is to give the transmitted beam $\frac{1}{2}\begin{bmatrix} I-Ipsin2\theta \\ 0 \\ I-Ipsin2\theta \\ 0 \end{bmatrix}$

whereas the effect of matrix B is to give the transmitted beam $\frac{1}{2}\begin{bmatrix} I+Ipsin2\theta \\ 0 \\ I+Ipsin2\theta \\ 0 \end{bmatrix}$

By phase-sensitively detecting the resulting infrared detector signal at the oscillation frequency, one obtains the difference of these two, i.e. the intensity Ipsin2θ. To eliminate offset, the linear polarizer can be regularly switched through 90^{o} to produce a square wave from the PSD. Alternatively, the phase of the oscillation could be changed by 180^{o} to give the same effect. The other Stokes parameter, Ipcos2θ, is obtained by rotating the whole polarimeter through 45^{o} and repeating the measurements.

Kemp et al. (1977) describe in outline the use of a similar instrument. They overcome the problem of the very high frequencies (∿ 50KHz) at which such modulators operate by beating the CaF_2 modulators to produce a 15-20Hz beat frequency suitable for conventional infrared detectors.

Since the photoelastic modulator is a quarter-wave plate, it is much more straightforward to measure the circular polarization with such a device than with conventional polarimeters employing a rotating analyser.

4-2 Polarization by Grids

The polarizing property of a grid of wires has been known for a long time, and Hertz used such a grid in 1888 when investigating radio

waves.

The theory of wire grids is usually dealt with using a transmission line model, and for a given grid width and spacing, the transmission can be calculated. Auton (1967) does this and concludes that in general, a grid interval, d, equal to twice the width of the wires, a, is most suitable if the wavelength is about 5 times the grid spacing, i.e. $\frac{a}{d} = 0.5$ when $\frac{\lambda}{d} \sim 5$ where λ is wavelength (see Fig.4-1). At longer wavelengths, the ratio $\frac{a}{d}$ is less important. Given two identical polarizers, the evaluation of their transmittances $T_{\perp}$ and T_{11} is quite straightforward using the method given by Rupprecht, Ginsberg and Leslie (1962). Four measurements are made using an unpolarized radiation source and a radiation detector which is not required to be free of instrumental polarization.

1. I_o = Total power transmitted with no polarizers in the beam.

2. I_H = Total power transmitted through a single grid polarizer with its wires horizontal.

3. I_V = Total power transmitted through a single grid polarizer with its wires vertical.

4. $I_{\perp}$ = Total power transmitted through a pair of polarizers, one with wires vertical and the other with wires horizontal.

Then, if the transmittances for the optical system alone are denoted by t_h and t_v for radiation polarized horizontally and vertically respectively, and if I is the power output from the source,

$$I_o = \tfrac{1}{2}I(t_h+t_v) \ ,$$

$$I_H = \tfrac{1}{2}I(t_h T_{11}+t_v T_{\perp}) \ ,$$

$$I_V = \tfrac{1}{2}I(t_h T_{\perp}+t_v T_{11}) \ ,$$

$$\text{and} \quad I_{\perp} = \tfrac{1}{2}I(t_h T_{\perp} T_{11}+t_v T_{\perp} T_{11}) = \tfrac{1}{2}I T_{\perp} T_{11}(t_h+t_v) \ ,$$

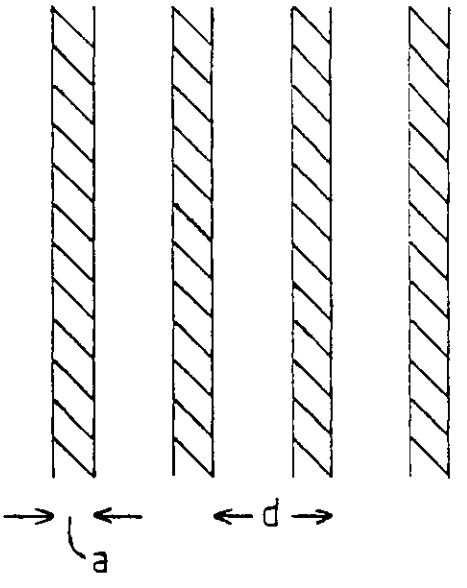

Wire Grid Polarizer

Fig 4-1

Eliminating I, t_h and t_v gives

$$T_{\perp} = \tfrac{1}{2}\frac{I_H+I_V}{I_o}\left[1+\sqrt{1-\frac{4I_{\perp}I_o}{(I_H+I_V)^2}}\right]$$

$$T_{11} = \tfrac{1}{2}\frac{I_H+T_V}{I_o}\left[1-\sqrt{1-\frac{4I_{\perp}I_o}{(I_H+I_V)^2}}\right] .$$

For any useful pair of polarizers, $I_{\perp}$ will be small, and we can write

$$\sqrt{1-\frac{4I_{\perp}I_o}{(I_H+I_V)^2}} \simeq 1-\frac{2I_{\perp}I_o}{(I_H+I_V)^2}$$

$$T_{\perp} \simeq \frac{I_H+I_V}{I_o} - \frac{I_{\perp}}{I_H+I_V}$$

$$T_{11} \simeq \frac{I_{\perp}}{I_H+I_V} .$$

The polarization efficiency of an analyser is usually given as the percentage polarization of an initially unpolarized beam that had passed through the analyser. Thus polarization efficiency $= \dfrac{T_{\perp}-T_{11}}{T_{\perp}+T_{11}}$

$$= 1-\frac{4I_{\perp}I_o}{(I_H+I_V)^2}$$

$$\simeq 1-\frac{2I_{\perp}I_o}{(I_H+I_V)^2} \quad \text{for } I_{\perp} \text{ small} .$$

If one has available two non-identical analysers, an extra five measurements must be made in order to determine the 4 transmittances. The computations are given by Young, Graham and Peterson (1965).

4-3 Chopping

At infrared wavelengths longer than about 5μ, the use of a spatial chopper becomes essential for the infrared astronomer. The background from the warm sky and telescope becomes a significant fraction of, and more usually, several orders of magnitude greater than, the infrared flux from the source to be observed. This background can vary on timescales down to a few seconds due to temperature drifts in the telescope, movement of air across the field of view, and the changing air mass as the altitude of the object varies. A cooled telescope in space may not experience this problem, but for balloon-borne or ground-based telescopes a chopper is required so that the detector alternately sees sky and then sky plus source. The signal from the source is obtained using an A.C. filter to subtract off the sky component and measured using some sort of phase-sensitive detector.

For infrared polarimetry, it can be feasible to avoid the use of a spatial chopper, given a moderate background which can be relied upon to be unpolarized. Simply rotating an analyser in front of a detector will give an a.c. signal at twice the rotation frequency if the source is polarized. This a.c. signal can be measured with a phase-sensitive detector to give the polarized flux from the source. The degree of polarization is not immediately given and can either be calculated using prior knowledge of the source's total flux, or the total flux can be quickly obtained by placing a second analyser in a fixed position in the beam.

The requirement of a moderate unpolarized background makes this method useless for wavelengths of 10μ or longer where the background radiation may be 10^6 times greater than the flux from the source. If the background were only 10^{-6}% polarized, a spurious signal equal to that from a 1% polarized source would arise. Thus one must resort to some form of spatial chopping to subtract off the background radiation.

However, the use of a spatial chopper can create fundamental difficulties when carrying out polarimetry. Many choppers employ reflections from one or more off-axis mirrors. But when radiation is reflected at anything other than normal incidence, the components of the radiation polarized perpendicular and parallel to the plane of incidence will suffer different reflection losses. Thus previously unpolarized light will be partially polarized by the chopper mirror and the chopper will be a source of instrumental polarization. The precise amount of polarization caused by a single reflection is difficult to predict as it is often strongly dependent on the microscopic qualities of the surface, e.g. the asymmetry of aluminization of a mirror (Gehrels 1974). However, a discussion of reflection at a metal surface is given in Appendix II. The difficulties experienced by Landau (1974) and Gull et al. (1978) clearly indicate that off-axis reflections should be avoided unless careful compensation techniques are used.

There are various types of spatial choppers in use for infrared astronomy. Their suitability for polarimetry will be considered below.

4-3.1 Primary Chopping

Here the primary mirror of the telescope is wobbled to alternately image the source and an adjacent patch of sky on the detector. This introduces no extra reflections, but the use of this technique is confined to small telescopes due to the mechanical problems associated with wobbling a large and heavy mirror.

4-3.2 Secondary Chopping

This is probably the most satisfactory method of chopping. As with primary chopping, no polarization problems arise, though on very large telescopes even the secondary mirror can be heavy enough to give some mechanical problems. In general, primary or secondary chopping are not techniques over which the user of an infrared polarimeter has control -

either the telescope is equipped with such a facility or it is not.

4-3.3 Tertiary Chopping

Here a third mirror is wobbled to throw the beam. It is inevitable that this mirror will be off-axis (usually at 45^{o} to the beam) and so the radiation may become spuriously polarized. Cox (1976) has shown, however, that a fourth 45^{o} mirror can be inserted in such a way as to compensate completely for the first mirror, given good enough alignment.

It should be pointed out that placing the analyser in advance of the tertiary mirror makes little difference to the detrimental effects of the mirror unless a depolarizer is employed. The radiation emerging from the analyser will be almost 100% linearly polarized and therefore the reflected beam will vary in intensity according to the relative directions of the polarization angle and the mirror's plane of incidence. A perfect depolarizer placed after the analyser would eliminate the problem, but good depolarizers are not available for the infrared.

4-3.4 A Tuning-Fork Focal-Plane Chopper

This method involves moving a small aperture in front of the detector so that the detector alternately sees sky and sky plus star through the aperture. An instrument equipped with such a chopper is independent of the chopping facilities (or lack of them) available on the telescope. Of course the detector and chopper need to be very close together so that either the detector and the chopper are both in the focal plane, or the chopper and the Fabry lens are both in the focal plane. In either case there would be an unacceptable radiation load on the detector if the moving plate with the aperture were not cooled.

This chopping technique is described further in Section 5-5, and it is believed that such a chopper has not been used before for infrared astronomy. It was developed by us specifically for use with the polarimeter, in order to avoid off-axis reflections which are a feature of most

tertiary choppers.

4-3.5 Nodding

For completeness, it should be pointed out that it is possible to chop by moving the whole telescope. On large telescopes, this cannot be achieved in less than several seconds, and it may be difficult to achieve the required accuracy of movement. If the background radiation is relatively stable with no variations on timescales of less than a minute, it is possible to nod the telescope regularly to subtract the background radiation. However, it is generally desirable to chop at the highest frequency that the detector response time will allow, in order to reduce $^{1}/_{f}$ detector noise. At infrared wavelengths, the technique of nodding the telescope is frequently used in addition to chopping, to subtract chopper offset.

4-4 Guiding

Guiding may be a problem in infrared polarimetry. The usual method of guiding with an infrared telescope is to insert a 45° beamsplitter into the beam, which reflects the infrared radiation, but transmits some of the optical rays to a guide eyepiece. However, as with any 45° reflection, this will introduce instrumental polarization. The converse method involving a beamsplitter which passes infrared radiation but reflects optical radiation must also be rejected, as in practice some small portion of the incident radiation will still be reflected. This reflected portion will preferentially include radiation polarized perpendicularly to the plane of incidence.

Amongst the possible guiding methods are:

4-4.1 Flip-in Mirror. A mirror which throws the beam into a guide eyepiece can be arranged to flip into position only when it is felt that the telescope is drifting off the star, and for setting up on new

objects. For the period whilst infrared measurements are made, the mirror remains out of the beam. Clearly, the telescope must have a pointing stability better than the beam size for this method to be feasible.

4-4.2 Mirror With a Central Hole. The main beam can be passed through a 45^{o} mirror with central hole. The optics must be carefully arranged to ensure that the detector cannot see the edges of the hole. One can then point a guide eyepiece at the mirror and offset guide on stars (if there are any) around the perimeter of the telescope field of view.

4-4.3 Guide Telescope. Frequently a large telescope has a smaller finder/guider telescope clamped to the side of it. Given sufficient magnification, one can guide through this smaller telescope. However there may be problems arising from movement and flexure of the guide telescope relative to the main telescope.

4-4.4 Automatic Guiding

Some modern large telescopes e.g. the Anglo-Australian Telescope, have a "blind" pointing accuracy of a few arc seconds so that guiding by eye is unnecessary.

4-5 Detection Limits

Infrared polarimetry is still in its infancy, and whilst measurements to an accuracy 0.1% are desirable, measurements with only 1% accuracy are still useful. Thus a signal must be measured which is 1% of the photometric signal. Since signal-to-noise increases only as the square root of the observing time, to obtain, say, a 3σ measurement of the polarization to 1%, one must observe for 10^{4} times longer than one would require to establish its photometric intensity at the 3σ level. Polarimetry is therefore limited to bright sources, with concomitant selection effects in its astronomical results.

Given the signal-to-noise ratio of photometry carried out in conjunction with polarimetry, it is possible to set an upper limit on the accuracy of the polarization measurements.

Let the photometric signal-to-noise ratio measured through the polarimeter be $\left(S/N\right)_{phot}$. Assuming the use of an analyser which is 100% efficient (i.e. for a grid polarizer, $T_{11}=0$), then it should be possible to measure simultaneously a polarization of $\frac{100}{(S/N)_{phot}}$ % at the 1σ level.

Alternatively, given that a source is p% polarized, the signal-to-noise ratio that should be achieved in the measurement of this polarization, $\left(S/N\right)_{pol}$, is given by

$$\left(S/N\right)_{pol} = \frac{p}{100} \left(S/N\right)_{phot} .$$

Thus, to achieve a 3σ measurement of 1% polarization, a signal-to-noise ratio of 300 in the photometry is required.

It will be useful to be able to estimate the flux of the faintest source for which polarimetry is possible. Suppose one has a telescope of area Am^2 with optics of overall transmission t_r and a passband of $\Delta\nu$ Hz. Then the flux from a source of J Janskys reaching the detector will be $Jx10^{-26}At_r\Delta\nu$ W. If the detector has a responsivity of R VW^{-1} and there is a detector noise of N $VHz^{-\frac{1}{2}}$, then in an integration time of t seconds, the signal-to-noise ratio in the photometry will be $\frac{Jx10^{-26}At_r\Delta\nu Rt^{\frac{1}{2}}}{N}$

If a 3σ measurement of 1% polarization is required, then

$$J \geq \frac{300N}{10^{-26}At_r\Delta\nu Rt^{\frac{1}{2}}} \qquad (4\text{-}1)$$

This expression can be used to estimate the flux of the faintest source for which polarimetry is possible with a 100cm balloon-borne far-infrared telescope. One might hope to achieve a detector noise of $40nV\,Hz^{-\frac{1}{2}}$, a responsivity of 10^6V/W and an overall transmission of 0.2.

Then in the 40 - 300μ passband ($\Delta\nu = 6.5 \times 10^{12}$Hz) and integrating for (say) half an hour (t = 1800secs), expression 4-1 indicates that the faintest measurable source would have a flux of $\sim$ 30Jy.

4-6 Instrumental Polarization

Instrumental polarization is the polarization recorded by a polarimeter when measuring an unpolarized source. This spurious polarization may be an effect of the polarimeter, the telescope, the atmosphere, or all three.

Instrumental polarization can arise in the following ways. Firstly, the radiation from the source may be spuriously polarized by some optical elements of the instrument. Secondly, unpolarized background emission may be spuriously polarized by the optical elements mentioned above. Thirdly, some of the background radiation may itself be intrinsically polarized. For example, scattered atmospheric radiation may be polarized, as may thermal emission from an off-axis mirror or a grid filter. Lastly, there may be effects of the data analysis which will produce a positive result when in fact the source is unpolarized. An example of this is the (random) polarization that arises from the noise on the signal. Wardle and Kronberg (1974) show that the measured signal-to-noise ratio for polarization deviates from the true signal-to-noise ratio at small signal-to-noise ratios. When the true ratio is 0, the measured ratio is 1. Thus a measurement of p±p% must be interpreted as being consistent with zero polarization.

It is preferable to minimise or eliminate instrumental polarization in order to avoid the need for extra calibration and data analysis, and the increased uncertainties that this may produce. The use of a spatial chopper, preferably close to the detector, will eliminate the effects arising from background radiation (whether or not it is instrinsically polarized). Alternatively, it may be possible to work at a wavelength at

which background radiation is negligible. The avoidance of optical elements such as off-axis mirrors (cf. Section 4-3), grid filters and polarization-sensitive detectors should minimize spurious polarization arising from the polarimeter or telescope. Such elements will introduce instrumental polarization even if they are placed after the analyser (unless a depolarizer is placed after the analyser).

In theory, it might be possible to determine the Mueller matrix of the instrument by calculating the dichroism, retardance and emissivities of every optical element. In practice, it is safer and easier to do it experimentally. Either a source that is known to be unpolarized can be measured, or an average may be taken of a large number of sources which are thought to have low and random polarizations. Such measurements, however, run the risk of confusing polarized background radiation with effects arising from the instrument. A further method would be to rotate the instrument with respect to a source. Then, any rotation of position angle is due to polarization from the instrument.

Having determined the Mueller matrix for the instrument, the matrix can be used (cf. Sections 2-7 and 7-7) to correct the measured Stokes parameters of the source. If necessary, the polarization from background radiation can then be subtracted off the Stokes parameters to give the polarization of the source.

4-7 Other Infrared Polarimeters

In this section, a brief survey is made of the infrared polarimeters that have been reported in the astronomical literature.

4-7.1 Forbes' Polarimeter

Forbes (1967) reported significant polarization of NML Cyg measured with a simple infrared polarimeter. The apparatus consisted of a rotating (0.67 Hz) HR sheet polarizer or wire grid analyser placed between a

PbS nitrogen-cooled detector and a spatial-chopping mirror as shown in Fig.4-2. Dyck, Forbes and Shawl (1971) compare it with Dyck and Shawl's polarimeter.

The advantages of placing the analyser between the chopper and the detector are:

a) The detector always sees the same portion of the analyser, reducing the effect of any non-uniformity in the analyser.

b) The analyser can be very close to the detector, reducing the effects of beam wander caused by non-parallelism of the analyser faces and allowing a small analyser to be used.

However, the 45° reflection at the chopper is likely to be a source of instrumental polarization and indeed, Dyck, Forbes and Shawl quote the instrumental polarization as 0.94% at 1.2μ, 0.82% at 1.6μ, 0.56% at 2.2μ, and 0.82% at 3.5μ.

Forbes (1967) used a 2-channel tape recorder to record the amplified detector signal and the phasing signal, and the detector signal was later played back into an oscilloscope, triggered by the phase signal. The polarization information could then be measured directly from photographs of the display. Later, Forbes (1971a) describes the use of a 400-channel pulse height analyser to do real time averaging. A least-squares fit is made to a $\cos 2\theta$ curve, after correction for instrumental polarization.

4-7.2 Low's Polarimeter

Low et al. (1969) used a wire grid polarizer placed outside a helium dewar to make polarization measurements at 10μ of the galactic centre. No further details are given except the instrumental polarization (0.2±0.2%) and the remark "No special problems have been encountered in making polarization measurements at these wavelengths." Despite this, the 10μ measurements of the galactic centre - 1.7±2.1% and 0.9±1.6% - were hardly conclusive.

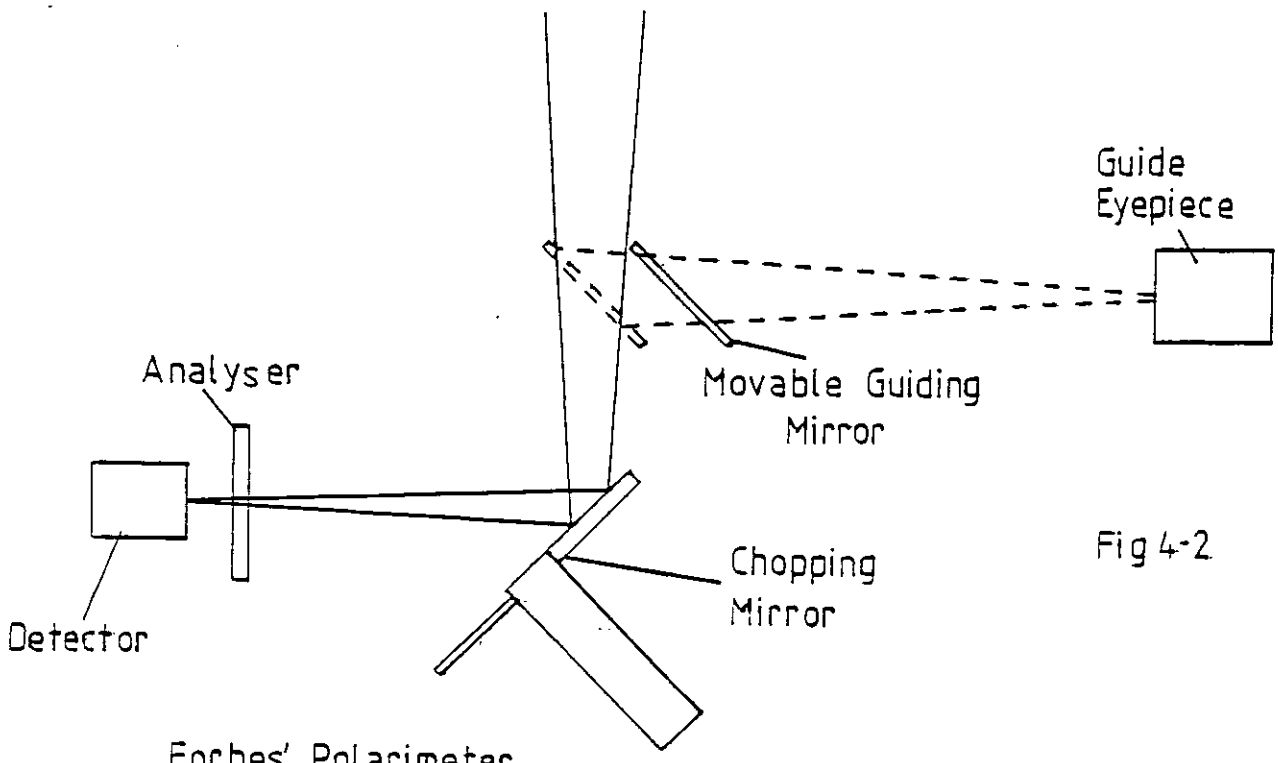

Fig 4-2

Forbes' Polarimeter

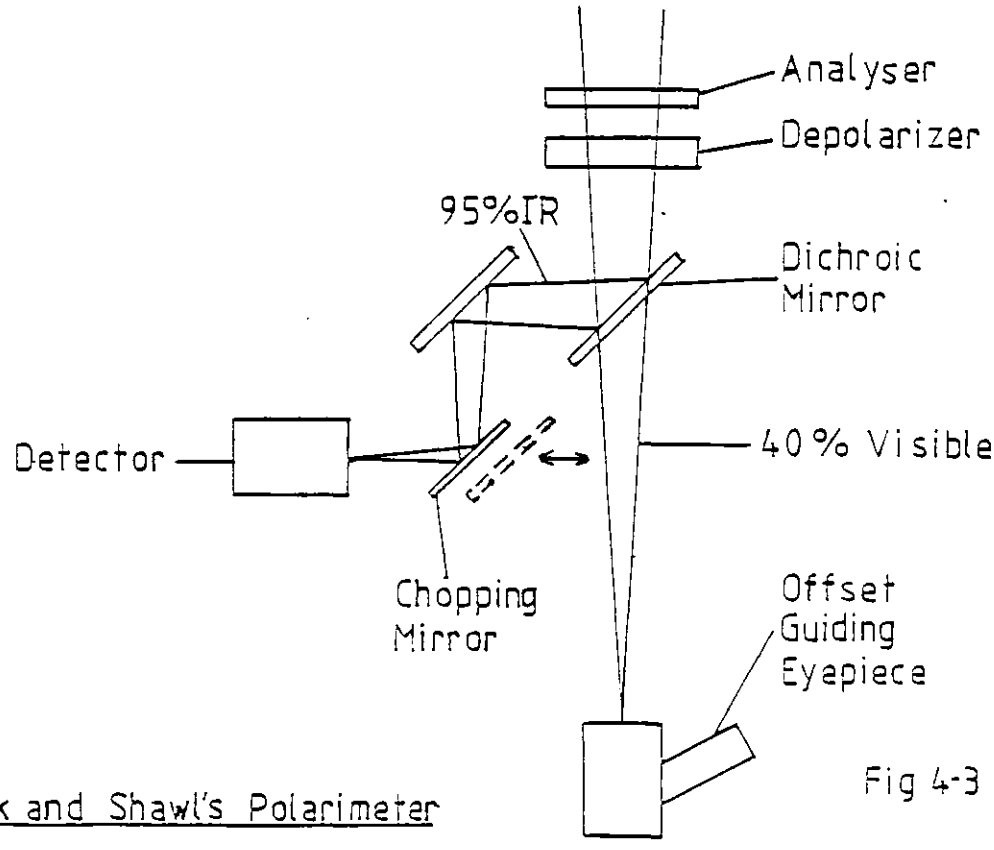

Fig 4-3

Dyck and Shawl's Polarimeter

4-7.3 Dyck and Shawl's Polarimeter

A diagram of the early version (Dyck, Forbes and Shawl 1971) of this polarimeter is shown in Figure 4-3. The analyser was an HR sheet and a PbS detector was used. The positioning of the analyser before the chopper requires the analyser to have nearly 1 inch of clear aperture. They report that beam wander was a problem. However, the use of the depolarizer means that instrumental polarization is substantially reduced and that the polarization from the two 45° mirrors does not matter. The instrumental polarization was measured as 0.12% at 1.05μ, 0.22% at 1.6μ and 0.43% at 2.2μ. Data reduction is effected by fitting a cos2θ curve to the data by least squares, after correcting for instrumental polarization.

Capps and Dyck (1972) used the same instrument at 8-14μ with a wire grid analyser and a Ga:Ge bolometer. They found that they had an instrumental polarization of between 5 and 7 percent. An attempt was made to correct for this in the data analysis, and they claim to have measured the polarization of two stars (α Ori and VY CMa) to a 1σ accuracy of 0.3%.

Dyck et al. (1973) used the instrument at the Kitt Peak National Observatory on the 50" telescope, equipped with a chopping secondary. They report that the instrumental polarization was less than 2% at wavelengths from 3.6μ up to 11.1μ. Dyck, Capps and Beichmann (1974), using the same telescope, placed the analyser just in front of the dewar, behind two compensating 45° mirrors. Later, Knacke and Capps (1974) report that they managed to reduce an instrumental polarization at 10.2μ of 2.1%, to 0.5% by carefully selecting a polarizer for the parallelism of its faces and by moving the polarizer close to the detector. The 3.5μ and 18.4μ instrumental polarizations were then 0.8% and 7% respectively, though they suggest that the high figure at 18.4μ may be due to an interference filter.

The details of the observing procedure are described by Dyck and Beichmann (1974). The polarizer can be rotated to eight positions at equally-spaced 45° intervals. One observation consists of eight, 10-second integrations at each position of the analyser, plus a further eight, 10-second integrations with the telescope nodded to put the star in the other beam.

A further modification to the polarimeter is noted by Capps and Knacke (1976b) and Knacke and Capps (1977). This involved the use of a Bi:Si photoconductive detector system, operated at 10K, which could be mounted at the Cassegrain focus so as to eliminate the need for any off-axis reflections. A wire grid polarizer is mounted just in front of the detector on the optic axis. Knacke, Capps and Johns (1979) give the sensitivity of the system as roughly capable of measuring, to an accuracy of 1% polarization, a source with 2.2μ magnitude 11 in one hour of integration time at the KPNO 4m telescope. They also give the instrumental polarizations as 0.42% at 1.25μ, 0.38% at 1.6μ and 0.12% at 2.2μ. The correction for this was made by subtracting the appropriate Stokes parameters - a rather dubious procedure, since it ignores the instrumental effects on the polarized part of the source's radiation. A reference is made to a forthcoming paper by Capps and Knacke which will describe the polarimeter.

A very similar polarimeter to that described above is in use at the Mauna Kea 2.2m telescope on Hawaii. It has been used only at short wavelengths (up to 3.8μ) and is described by Jones and Dyck (1978), Dyck and Jones (1978) and Jones (1979). The early version of the instrument rotated the analyser in 45° steps, but later a continuously rotating (0.5Hz) analyser was used.

4-7.4 Maihara, Okuda and Sato's Polarimeter

This is a PbS photometer with either an HR sheet polarizer or a wire-grid polarizer rotating at about 1 revolution per minute. The original

system is outlined by Maihara, Okuda and Sato (1972) when it included a rotating chopper. Subsequently (Kobayashi 1978) a secondary mirror chopper was used. The instrumental polarization was less than 1%.

4-7.5 The Hatfield Polarimeter

This instrument is described in some detail by Cox, Hough and McCall (1978). It is an in-line system with no off-axis reflections and incorporates a rotating HR sheet or wire grid analyser mounted immediately over the window of an upward-looking nitrogen dewar. The polarimeter is shown in Fig.4-4. No sky chopping is performed. Instead, the analyser is rotated at 45Hz to produce a 90Hz signal if the source is polarized. A calibration polarizer can also be inserted in the beam to completely polarize the radiation and thus to give a measure of the total flux from the source. This restricts the use of the instrument to short wavelengths ($\lesssim$ 2.2μ) as a large varying radiation background cannot be tolerated.

The instrument has been used at Tenerife on the 1.5m flux collector, where the NOVA mini-computer was used for instrument control and data processing. Instrumental polarization at Tenerife was 0.05% at 1.25μ, 0.09% at 1.6μ, and 0.03% at 2.2μ, and Cox, Hough and McCall conclude that they are limited by the instrumental polarization of the telescope. They also find that the surface quality of the Fabry lens is a critical factor. This is because any movement of the image at the Fabry lens (due to the rotating analyser or seeing) will cause modulation of the signal at the detector if the Fabry lens is imperfect or unclean.

A similar polarimeter was also used to make 2.2μ measurements using the 1m South African Astronomical Observatory at Sutherland (Adams and Hough 1977).

4-7.6 Kemp's Photoelastic Polarimeter

This polarimeter is the most unconventional one in use. It does not

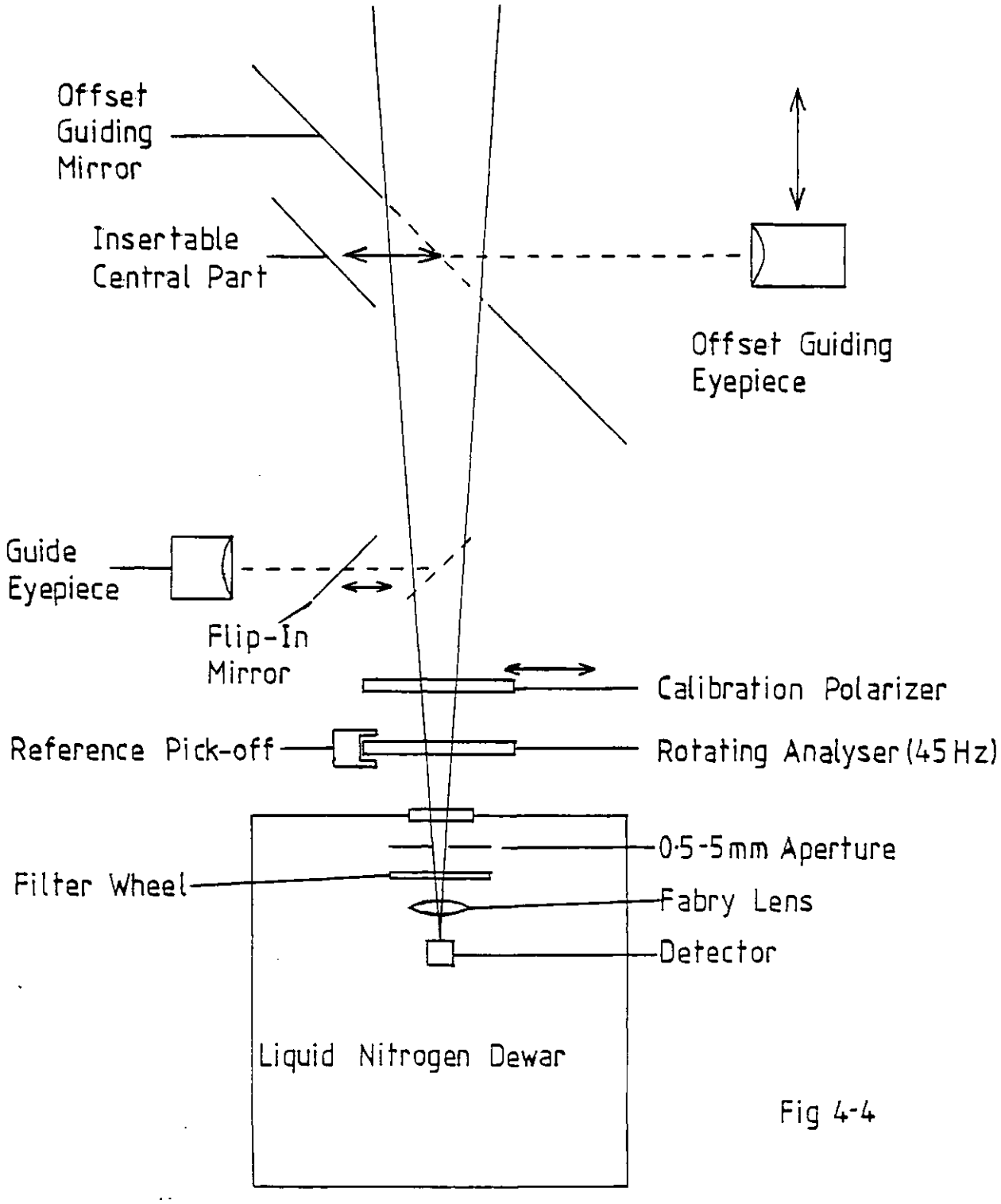

Fig 4-4

The Hatfield Polarimeter

use a rotating analyser, but incorporates two photoelastic modulators. These are blocks of Calcium Fluoride which become waveplates when strain is applied through piezo-electric transducers. The modulators operate at frequencies of about 50KHz, but Kemp et al. (1977) use two modulators beating with one another to produce a signal at 15-20Hz, suitable for an InSb detector. Instrumental polarization is estimated as 0.01±0.03% at 1.6μ and 0.03±0.04% at 2.2μ. Sky chopping is not performed, and any polarization of the thermal background is removed after making separate calibration measurements looking at blank sky.

4-7.7 The Caltech Polarimeter

Loer, Allen and Dyck (1973) used a polarimeter developed at the California Institute of Technology. The instrument was used at 2.2μ, and they report that compared with the Kitt Peak polarimeter, values of polarization ∿ 25% smaller are found. No further details of the instrument are given.

4-7.8 The Berkeley Polarimeter

Landau (1974) describes a polarimeter designed for the wavelength range 2-11μ. The original version had two 45° reflections between the telescope and the wire grid polarizer which was slowly rotated (10 revolutions per minute) in front of a helium dewar containing a germanium bolometer. One of the 45° mirrors was a 12.5Hz chopper. The instrumental polarization was 25% at 2μ, dropping to 10% at 11μ, but replacement of the beamsplitter (the second 45° reflection) by a mirror reduced the instrumental polarization to a few percent.

Each observation is composed of 6 analyser revolutions with the star in one beam, and six revolutions with the telescope nodded to put the star in the other beam. Data analysis is carried out with a PDP8/I Computer.

4-7.9 The Italian Balloon-Borne Polarimeter

Dall'Oglio et al. (1973) describe a balloon-borne polarimeter which was flown in 1971. The system is shown in Fig.4-5 and consists of a 25cm Cassegrain telescope, a rotating wire grid analyser and a helium-cooled bolometer. No chopping was employed and the filter bandwidth spanned the range 100μ - 2mm. These two features mean that it is difficult to separate source polarization from background polarization, and an estimate of percentage polarization cannot be made without knowledge of the size of the unpolarized signal and of the wavelength dependence of the polarization. A strong polarization effect was observed in radiation from the Sun.

The instrument has also been used by Caderni et al. (1978b) to set an upper limit to the polarization of the cosmic background radiation.

4-7.10 Far-Infrared Polarimeter used with the NASA Lear Jet 30cm Telescope

A rotating wire grid analyser was mounted between a helium dewar containing a Ge:Ga photoconductive detector, and the NASA 30cm telescope carried in a Lear jet aircraft. The bandpass was 60 - 130μ and 30Hz chopping was performed with a wobbling secondary mirror. Despite the absence of off-axis reflections, Dennison et al. (1977) report an instrumental polarization of about 5%. They also note an instrumental effect caused by a slightly wedge-shaped analyser which produced movement of the image in the focal plane. The analyser was rotated in 80° steps and the data was subsequently folded. To subtract offset, the telescope is also pointed $15'$ away from the source, in a direction perpendicular to the chopper throw, and a set of rotations is made in this position.

4-7.11 Far-Infrared Polarimeter used with the NASA C-141 91cm Telescope

The system used by Gull et al. (1978) is shown in Fig.4-6. Four filters could be used covering the wavelengths 16-26μ, 28-48μ, 44-72μ and

The Italian Balloon-Borne Polarimeter

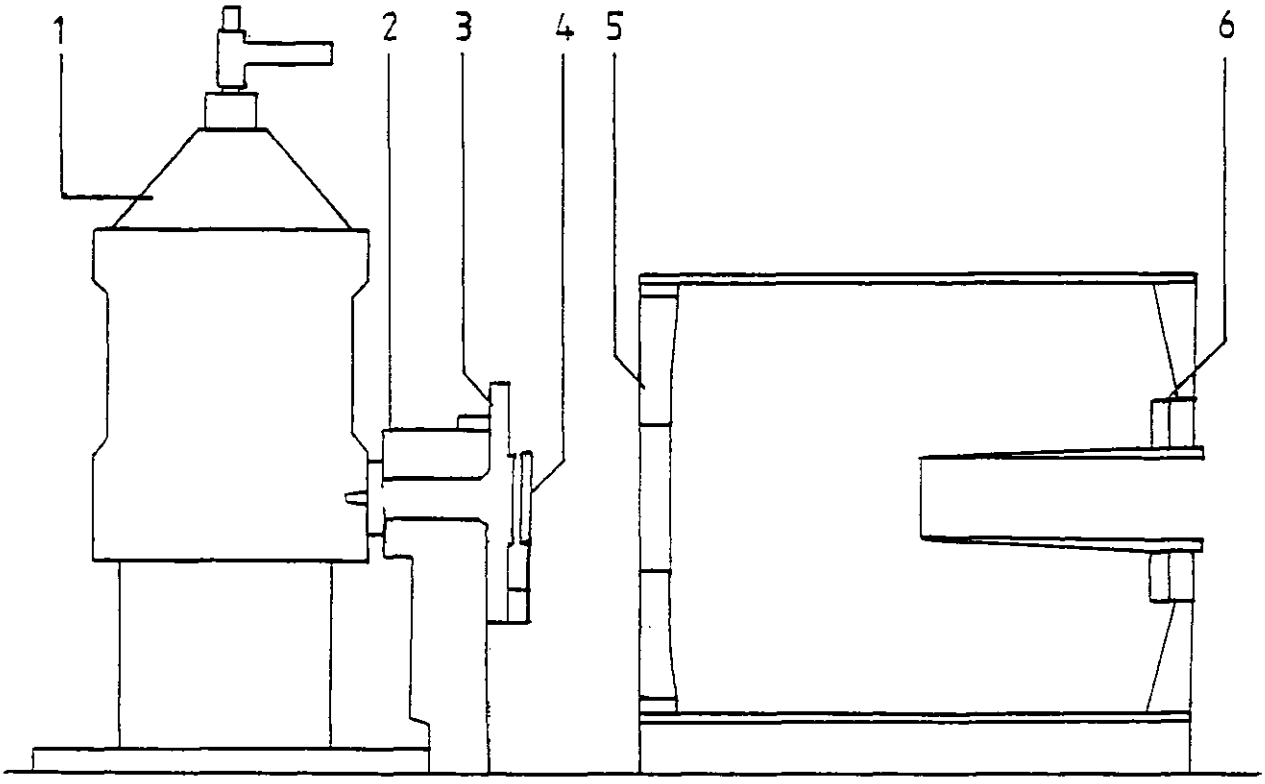

1. Liquid-helium dewar.
2. Diaphragm defining the field of view.
3. Rotating analyzer assembly.
4. Calibration source.
5. Primary mirror, 25cm, f/4
6. Secondary mirror, flat.

Fig 4-5

Fig 4-6

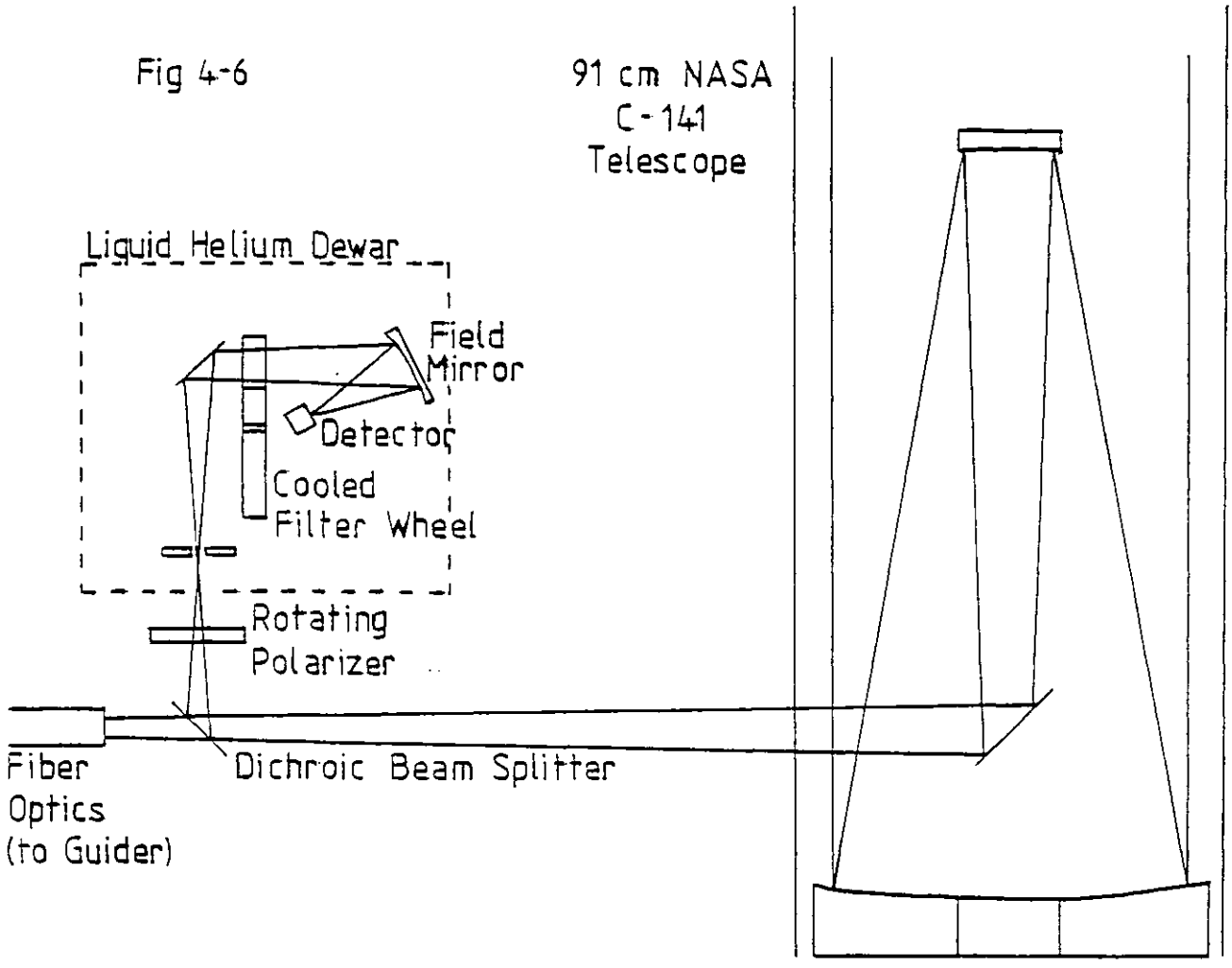

The Polarimeter on the Kuiper Airborne Observatory

71-115μ. The system contains four off-axis reflections and hence it is not surprising that large instrumental polarizations were found. Measurements of Jupiter seemed to indicate an instrumental polarization of about 3% at the longer wavelengths rising to about 8% at 28-48μ. Uncorrected polarization measurements of Orion in this latter waveband are scattered in the range 7-9%. This scatter is attributed to long-term drifts, possibly in atmospheric transmission or in chopper stability.

4-7.12 Summary

Since Low's attempted measurement of 10μ polarization from the galactic centre, at least a dozen different infrared polarimeters have been constructed. At near-infrared wavelengths, Dyck and Shawl's polarimeter, incorporating a rotating analyser, is capable of better than 0.5% accuracy. At 2.2μ and below, it is surpassed by Kemp's photoelastic polarimeter which is capable of $\sim$ 0.05% accuracy. In the far-infrared, both the polarimeters that have been flown on NASA aircraft appear to suffer from very large ($\sim$ 5%) instrumental polarizations, whilst Dall' Oglio's instrument has not been successfully used for stellar observations.

Instrumental polarization is only one of the limiting factors when making polarization measurements. Often, a more critical factor is observing time, in that it is inconvenient to observe a single object for periods exceeding an hour or so. Therefore, it would be interesting to compare the instrumental efficiencies or detection limits (as in Section 4-5) for the polarimeters mentioned. Unfortunately, the variety of methods and details given in the published papers is so great that it is not possible to derive sufficient information to be able to make worthwhile or valid comparisons.

Chapter 5. The Design and Construction of the Polarimeter

5-1 Design Considerations

The polarimeter was originally designed for use with the Imperial College 41" balloon-borne far-infrared telescope. This is mounted on the Science Research Council's Stabilised Balloon Platform (SBP) which provides target acquisition and tracking to arc-minute accuracy. The ICST telescope, and the associated instrumentation, were first flown in November and December 1976 and it was expected that further flights would be made annually. Unfortunately, problems with the SBP delayed further flights until December 1979.

A detailed description of the Imperial College telescope is given by Joseph et al. (1977). It is of f/7 Cassegrain design incorporating aluminium optics and structure, and the helium dewar containing the detectors is mounted immediately behind the primary mirror.

The polarimeter was designed with the following considerations in mind.

1. It must be capable of operating at temperatures down to $-50^{o}C$ and pressures down to 8 torr.

2. It should fit onto the telescope without the need for any off-axis reflections.

3. It must be capable of remote control from the ground.

4. It must be rugged and reliable.

5. The hold time of the LHe dewar should be sufficient for a flight lasting about 12 hours.

As the ballooning programme slipped, it was decided to test and use the polarimeter at shorter wavelengths from the ground. The sections that follow discuss the implementation of the above considerations in the polarimeter itself and the associated instrumentation and hardware.

5-2 Hot versus Cold Operation

All the instruments described in 4-7 operate at the ambient temperature and therefore constitute a source of large thermal background on the detector. A LHe-cooled instrument will eliminate this. The polarimeter had to be designed to operate at the balloon float altitude of about 40Km where temperatures of about $-50^{\circ}C$ and pressures of a few millimetres are encountered. This clearly prompted consideration of whether it would be significantly more difficult to design an instrument that would operate inside the helium dewar.

These considerations are set out below.

Advantages of Cold ($1.7^{\circ}K$) Operation

a) The instrument could be installed inside the helium dewar containing the detector, making a compact polarimeter/photometer.

b) The polarimeter is in a completely stable environment. Once it is operating satisfactorily on the ground, it should continue to do so in flight. A polarimeter exposed to ambient conditions would undergo a transition from $+20^{\circ}C$ and 1 atmosphere pressure on the ground to $-50^{\circ}C$ and $\frac{1}{100}$ atmospheric pressure at float altitude. Differential thermal contractions and the possibility of ice forming on the instrument would be potential problems.

c) The detector sees only the minimum number of ambient temperature components - the dewar window and the two telescope mirrors. Hence the radiation load on the detector will be minimised, permitting maximum detector sensitivity to be achieved. An ambient temperature analyser would only increase the thermal load on the detector by a factor of ~ 2, as the dewar window will emit a similar amount of black-body radiation. However, the key point is that the analyser will be rotating, and hence will almost certainly give rise to a fluctuating detector signal (cf. point e).

d) The analyser could be very close to the detector so that only a small area of analyser is required. Also, any problems of beam wander arising from non-parallelism of the analyser faces would be minimised.

e) Imperfections of the analyser, and temperature gradients across the analyser, will give rise to spurious signals in-phase with the analyser rotation. Imperfections giving rise to an emissivity difference $\delta\varepsilon$ may produce a signal proportional to $T^4\delta\varepsilon$ if the peak of the black-body radiation from the analyser (at temperature T) lies in the pass-band of the filters. Similarly, temperature gradients with temperature differences δT may give signals proportional to $T^3\delta T$. Such signals can, in principle, be eliminated by nodding the telescope. Nevertheless, the best design strategy is to eliminate them altogether by cooling the analyser, and thus be certain to avoid problems of saturation and additional noise.

From the above 5 points, it is clear that the ideal polarimeter would be cooled, but there are a large number of practical difficulties. The most important of these are listed below.

a) A cooled polarimeter is very inaccessible, making development of the instrument a time-consuming affair. A large amount of the testing must be done with the instrument at helium temperature and therefore inside a helium dewar. Usually, one cannot see into a helium dewar by eye, so the cause of any problems with the instrument may be quite difficult and time-consuming to locate. At the very least, one must warm the polarimeter up, dismantle the dewar, try to find the source of the problem (and it may be one that only occurs at low temperatures), reassemble the dewar having made modifications, and finally make a helium run to see if the problem has been eliminated. Such a procedure consumes a minimum of a day's work.

b) The volume available inside a helium dewar is necessarily rather limited, if the dewar is to be of moderate size and have a useable hold

time. A cooled polarimeter will therefore have to be a very compact device and access to it may be restricted.

c) The large mass of extra metal in the dewar, and the presence of moving parts (which may be in poor thermal contact with the cold surface) will extend the LHe transfer time. Each extra 100g of copper requires an extra 200cc of LHe to cool it to $4^{o}K$.

d) The problems of rotating an analyser at LHe temperature have to be overcome. These problems result from differential contractions, scarcity of good lubricants for moving parts, and the necessity to transmit power into the dewar with minimal conductive heat leak while maintaining vacuum integrity.

e) The proximity of moving parts to the detector may result in pick-up appearing in the detector signal, either as excess noise or a periodic signal, caused by vibrations or capacitance effects.

Quantification of many of the above points was difficult. However the elimination of a warm moving object in the field-of-view, and the placing of the polarimeter in a stable environment, were felt to be important and worthwhile advantages of a cooled polarimeter, deserving an attempt to overcome the problems.

5-3 Detector

The detector used for the polarimeter was a LHe-cooled gallium-doped germanium bolometer of the type developed by Low (1961). Such detectors are suitable for use throughout the infrared and m.m.-wave spectral region. Their sensitivity may approach fundamental thermodynamic limits, which is Johnson noise at LHe temperature for low background conditions.

The bolometer element consists of a 2mmx2mm gallium-doped germanium crystal suspended by two metal leads in an integrating cavity. These leads provide the mechanical support, the electrical connections and the

heat sinking for the crystal. Being a semiconductor, the resistance of the bolometer has a negative temperature coefficient and at its operating temperature of 1.7°K, the bolometer resistance reaches about 1.2MΩ under low background conditions. This temperature is achieved by mounting the detector inside a liquid helium dewar and pumping on the helium vapour to reduce the boiling point from 4.2°K at 1 atmosphere to 1.7°K at 8 torr. (With a balloon experiment, a pump is not required - the helium can is simply vented to the atmosphere.) The bolometer is connected in series with a 7MΩ load resistor as shown in Fig.5-1, and biased by a battery.

A Low bolometer has an extremely high temperature coefficient of resistance,

$$\alpha = \frac{1}{R}\frac{dR}{dT} \sim -0.7\,K^{-1} .$$

If the time-varying radiant heat input to the bolometer δQ produces a temperature rise δT, then

$$C\frac{d\delta T}{dt} + G(T+\delta T-T_o) = P_B + \delta Q$$

where C is the heat capacity of the bolometer element which is at temperature T, G is the thermal conductance of the leads, T_o is the helium bath temperature and P_B is the steady-state heat input to the bolometer. However, in the steady-state

$$G(T-T_o) = P_B ,$$

so

$$C\frac{d\delta T}{dt} + G\delta T = \delta Q \qquad (5\text{-}1)$$

and this has homogeneous solution $\delta T = e^{-\frac{t}{\tau}}$ where $\tau = \frac{C}{G}$ is the time constant of the bolometer. When the temperature of the bolometer changes

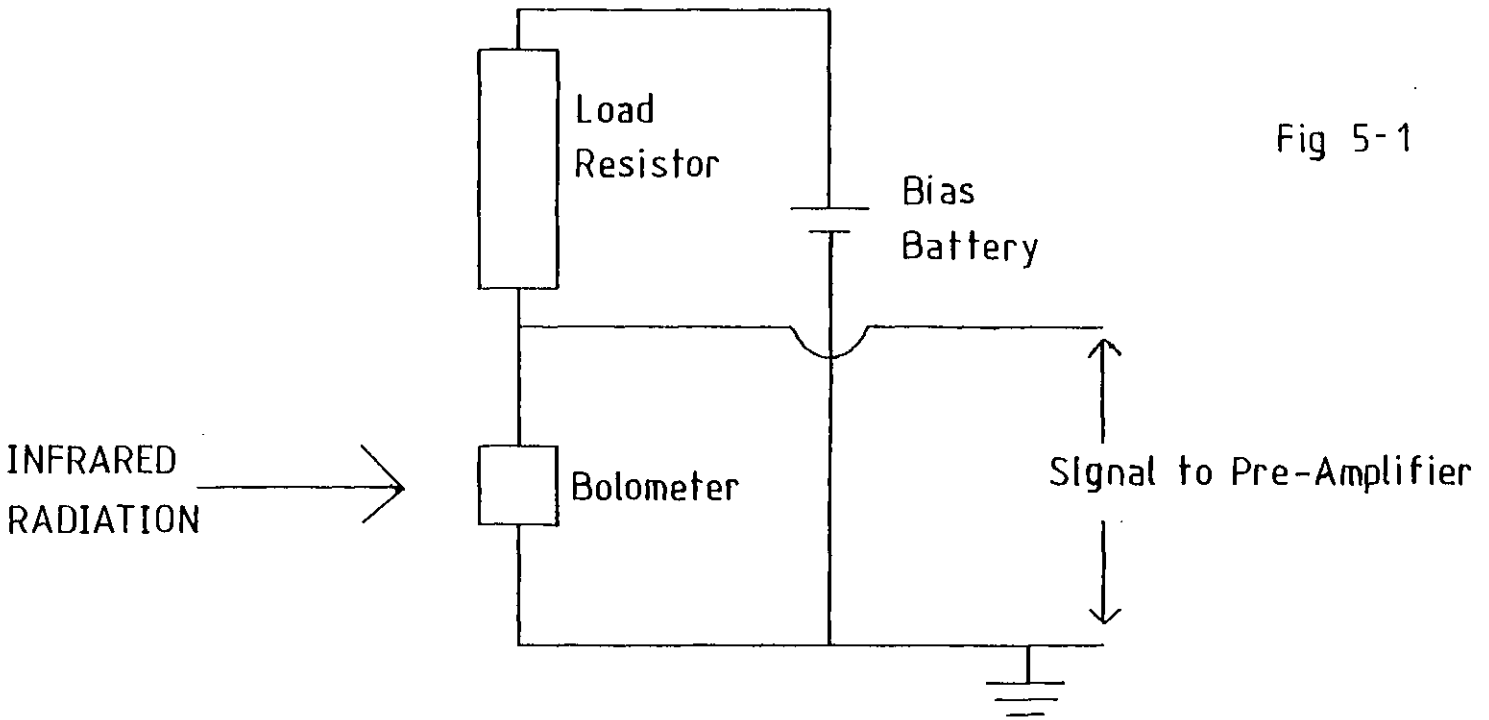

Fig 5-1

Bolometer Connections

by δT, the resistance changes by $\delta R = \alpha R \delta T$ and thus the joule heating changes by $\alpha P \delta T$ where P is the bias power dissipated in the bolometer when it has resistance R.

Thus eqn.(5-1) becomes

$$C \frac{d\delta T}{dt} + (G-\alpha P)\delta T = \delta Q$$

The bias voltage change induced by δQ will be $\delta V = I\delta R$ where I is the current through the bolometer. But $\delta R = \alpha R \delta T$, so

$$\delta V = \alpha I R \delta T$$

$$= \alpha V \delta T$$

$$= \frac{\alpha V \delta Q}{(G-\alpha P)}$$

Thus the responsivity of the bolometer is

$$R = \frac{\delta V}{\delta Q} = \frac{\alpha V}{G-\alpha P} \quad .$$

An alternative expression for responsivity, $R = \frac{Z-R}{2V}$ where Z is the dynamic resistance, $\frac{dV}{dI}$, is useful for determining R from purely electrical quantities derived from a load curve. If R is plotted for different values of the bias voltage (see Fig.5-2), the optimum bias voltage may be determined. It was found that a suitable bias voltage of 1.5V gave a zero-frequency electrical responsivity of $\sim 0.5 \times 10^6$ Volts/Watt for the bolometer used.

5-3.1 Bolometer Noise

There are three principal contributions to the total bolometer noise. These are Johnson noise, Phonon noise and Photon noise, and their magni-

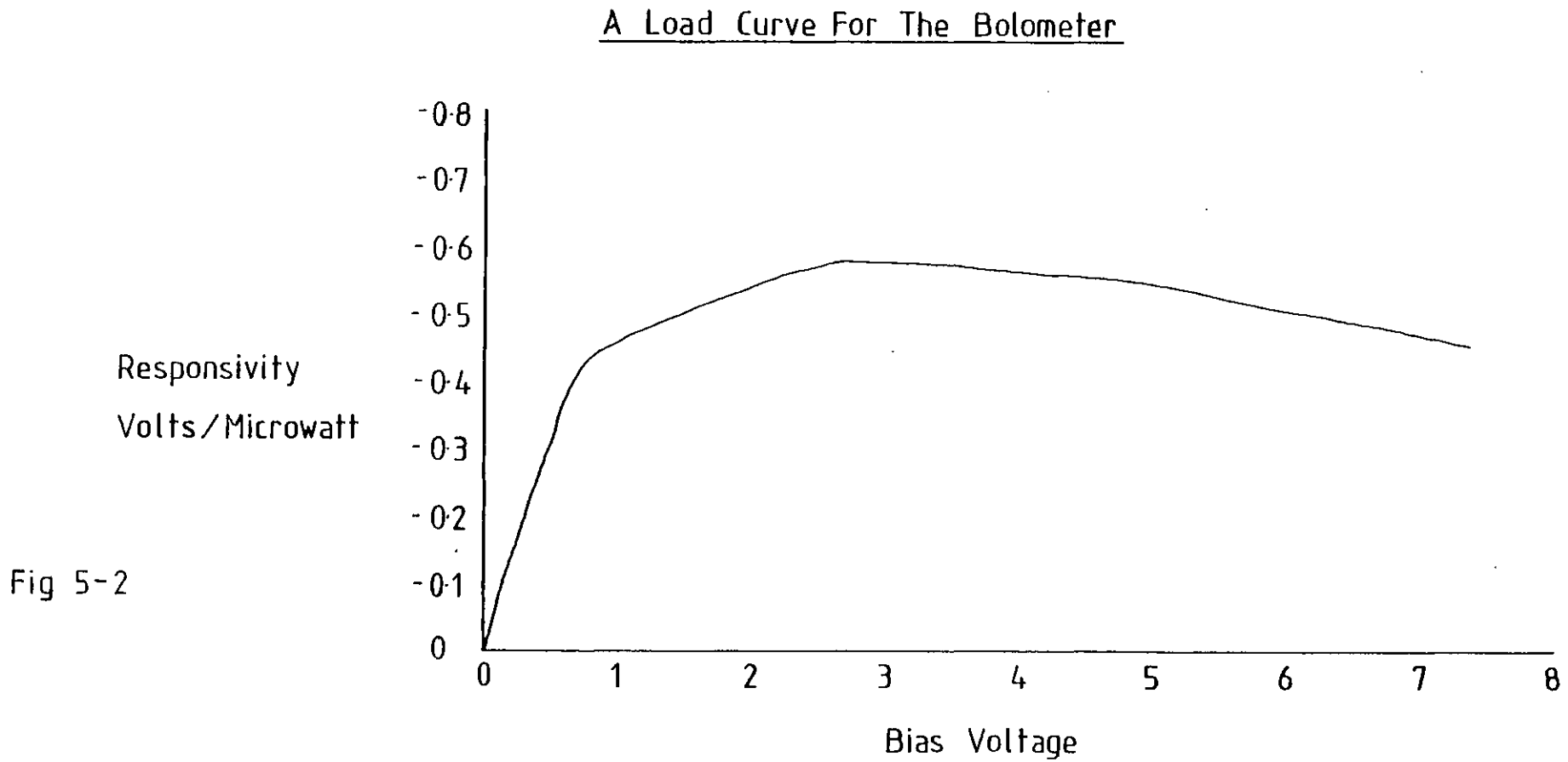
A Load Curve For The Bolometer
Responsivity
Volts/Microwatt
0·8
0·7
0·6
0·5
0·4
0·3
0·2
0·1
0
0
1
2
3
4
5
6
7
8
Bias Voltage

Fig 5-2

tudes are estimated below.

a) Johnson Noise = $\sqrt{4kTR\Delta\nu}$ volts (Nyquist 1928) where k is Boltzmann's constant, T is the bolometer temperature, R is the bolometer resistance and $\Delta\nu$ is the bandwidth. With $T = 1.7^{o}K$ and $R = 1.2M\Omega$, the Johnson noise of the bolometer = $10.6nVHz^{-\frac{1}{2}}$.

b) Phonon Noise. This is thermal noise arising from variations in heat flow along the leads which act as heat sinks from the detector to the helium bath.

Phonon Noise = $\sqrt{4kT^{2}G\Delta\nu}$ x R volts (p213 Smith, Jones and Chasmar 1968) where G is the thermal conductivity of the leads and R is the responsivity of the detector.

Typically, $G = 2x10^{-7}W^{o}K^{-1}$ and $R = 10^{6}V/_{W}$ so Phonon Noise of bolometer = $5.6nVHz^{-\frac{1}{2}}$.

c) Photon Noise. This noise arises from the statistical variations of the photon flux incident on the detector.

From each source irradiating the bolometer, the mean square fluctuation $\overline{\Delta F^{2}}$ of the total flux is

$$\overline{\Delta F^{2}} = 2\int_{\nu_1}^{\nu_2} \frac{tF(\nu)h\nu\exp(h\nu/kT)d\nu}{\exp(h\nu/kT)-1} \; W^{2}Hz^{-1}m^{-2}$$

(p216 Smith, Jones and Chasmar 1968) where $F(\nu)d\nu$ is the flux of radiant energy in an interval $d\nu$, T is the source temperature (ν_1,ν_2) is the passband of the optics with transmission t.

For a thermal source of emissivity ε, subtending a solid angle Ω at the focal plane aperture of area A,

$$\overline{\Delta F^{2}} = 4\frac{h^{2}}{c^{2}} A\Omega \int_{\nu_1}^{\nu_2} \frac{\varepsilon t\nu^{4}\exp(h\nu/kT)d\nu}{(\exp(h\nu/kT)-1)^{2}} \; W^{2}Hz^{-1}$$

If ε and t are assumed to be frequency-independent for (ν_1,ν_2), then

writing $x = \frac{h\nu}{kT}$,

$$\overline{\Delta F^2} = 4 \frac{k^5 T^5}{c^2 h^3} A\Omega\varepsilon t \int_{x_1}^{x_2} \frac{x^4 e^x}{(e^x-1)^2} dx W^2 Hz^{-1}$$

In standard infrared photometry, the largest thermal radiation source is usually the dewar window, since its emissivity is large. The noise contribution from a dewar window of emissivity 0.25 is calculated for two cases, the near-infrared using the IRFC at Tenerife, and the far-infrared using the ICST 41" balloon-borne telescope. The parameters are given in Table 5-1. A transmission, t, of 0.5 is used in both cases. The integral was evaluated using Simpson's rule.

For the near-infrared case the noise is $1.9 \times 10^{-14} WHz^{-\frac{1}{2}}$, whilst for the far-infrared case the noise is $8.0 \times 10^{-14} WHz^{-\frac{1}{2}}$. Assuming a value for the detector responsivity of $10^6 V/W$, the detector noise arising from this source is $19nVHz^{-\frac{1}{2}}$ at 10-13μ and $80nVHz^{-\frac{1}{2}}$ at 30-300μ.

Table 5-1

	T	A	Ω	ν_1 ν_2
IRFC at Tenerife	293K	$8 \times 10^{-7} m^2$	$4 \times 10^{-3}_{sr.}$ (f/13.8)	$2.3 \times 10^{13} Hz$ $3 \times 10^{13} Hz$ (10 - 13μ)
ICST 41" Balloon-Borne Telescope	223K	$2.8 \times 10^{-5} m^2$	$1.6 \times 10^{-2}_{sr.}$ (f/7)	$1 \times 10^{12} Hz$ $1 \times 10^{13} Hz$ (30 - 300μ)

Parameters for calculating Photon Noise.

A 'warm' analyser with $\varepsilon \sim 0.75$ would increase this noise by a factor of approximately 3.

The total theoretical bolometer noise is the sum in quadrature of

the three noise sources, i.e.

At 10-13μ, the bolometer noise is

$$(10.6^2+5.6^2+19^2)^{\frac{1}{2}} \text{ nV Hz}^{-\frac{1}{2}}$$

$$= 22 \text{ nV Hz}^{-\frac{1}{2}}$$

At 30-300μ, the bolometer noise is

$$(10.6^2+5.6^2+80^2)^{\frac{1}{2}} \text{ nV VHz}^{-\frac{1}{2}}$$

$$= 81 \text{ nV Hz}^{-\frac{1}{2}}$$

At the IRFC in Tenerife, the actual bolometer noise was $\sim 40 \text{ nV Hz}^{-\frac{1}{2}}$, a little larger than the theoretical value. This excess can probably be accounted for by microphonics, $\frac{1}{f}$ noise or noisy junctions on the bolometer. Compared with the noise that arose in the observations from chopper fluctuations and guiding, this excess was not very signiciant.

In the above calculations, it has been assumed that the optical efficiency of the detector is unity, so that the optical responsivity is the same as the electrical responsivity determined from a load curve. In practice, the optical efficiency will be considerably less than unity due to the roll-off of the detector response at the chopping frequency (about 75% of the d.c. value at 20Hz) and the non-perfect absorption efficiency of the detector. Whilst this will reduce the signal received from an astronomical source, it will also have the beneficial effect of reducing the photon noise from the values calculated above.

5-3.2 Optimum Chop Frequency

The time constant of the bolometer, τ, is C/G when its thermal capacity is C and G is the thermal conductivity of its supporting leads. The bolometer had a time constant of ~ 12 mS (derived from manufacturer's test data) so the chop frequency was chosen to trade off the reduced sensitivity at high frequencies against the increased $\frac{1}{f}$ noise, which

rises steeply at frequencies below 15 Hz. At chopper frequencies of $\sim$ 20 Hz, the sensitivity is $\sim$ 25% below the d.c. response, which is acceptable.

5-4 Dewar

A telescope suspended beneath a balloon imposes a slightly different set of constraints on the LHe dewar, to those that would hold for a ground-based telescope. In particular, the Imperial College telescope sits on a platform which is centrally suspended from the balloon. The platform has 360° of rotational freedom in azimuth and the telescope can never point at, or pass through, the zenith. The stow position is near horizontal. This contrasts with a normal ground-based telescope where the "stowed" position of the telescope is vertical and the telescope will often move through the vertical position.

With balloon work in mind, the dewar was designed with a side-entry window, so that the dewar would be vertical when the telescope is horizontal, and the telescope beam therefore passes straight through the central hole in the primary mirror and into the dewar without any off-axis reflection.

For ground-based work, a side-entry dewar is a disadvantage. If the dewar is mounted so that the beam passes into the window directly from the hole in the primary, the cryogenic liquids will start to spill out as the telescope nears the vertical. However, the ground-based observations were primarily considered as tests for the polarimeter before carrying out balloon-borne observations, and so the restrictions imposed by a side entry dewar were accepted.

The standard configuration for ICST ground-based infrared photometry is to use a bottom entry dewar, the beam descending through the central hole in the primary and turned through 180° by two 45° mirrors to enter

the LHe dewar from below. Of course, any reflections would be most undesirable for polarimetric work. For a ground-based telescope, an upward-looking dewar would be the ideal.

The dewar that was used for the polarimeter was manufactured by Oxford Instruments and is a modified model MD800. The capacities of the helium and nitrogen vessels are 1.7 litres and 1.4 litres respectively. A cross-sectional view is shown in Fig.5-3. The dewar had a LHe hold time of $\sim$ 100 hours before any modifications were made to it to hold detectors and the polarimeter, indicating a radiative and conductive heat leak of $\sim$ 11 mW.

5-5 Chopper

A sky-chopper is essential for wavelengths longer than about 5 microns in order to discriminate against the large thermal background emitted by the optics and the atmosphere. Since neither the Imperial College 41" telescope nor the 60" Tenerife telescope had secondary choppers when the polarimeter was designed, a focal plane tuning-fork type chopper was used. This is manufactured by Bulova and incorporates two rectangular vanes at the ends of a tuning fork. It is shown in Fig.5-4. The chopper is driven resonantly with two coils, one acting as the drive and the other as a pick-up. The drive circuit, which also provides a reference signal for the Lock-in amplifier, is shown in Fig.5-5.

The telescope forms an image of the sky at the focal plane. By drilling a hole in one of the vanes and mounting the chopper so that this vane covers the Fabry lens, the detector field of view is determined by the hole in the vane. Thus spatial chopping can be performed if the hole alternately coincides with the image of a star, and the image of an adjacent patch of sky. The hole diameter of 1mm was chosen to be larger than the stellar images, which may be up to $\sim$ 5" in diameter (equivalent

The Helium Dewar

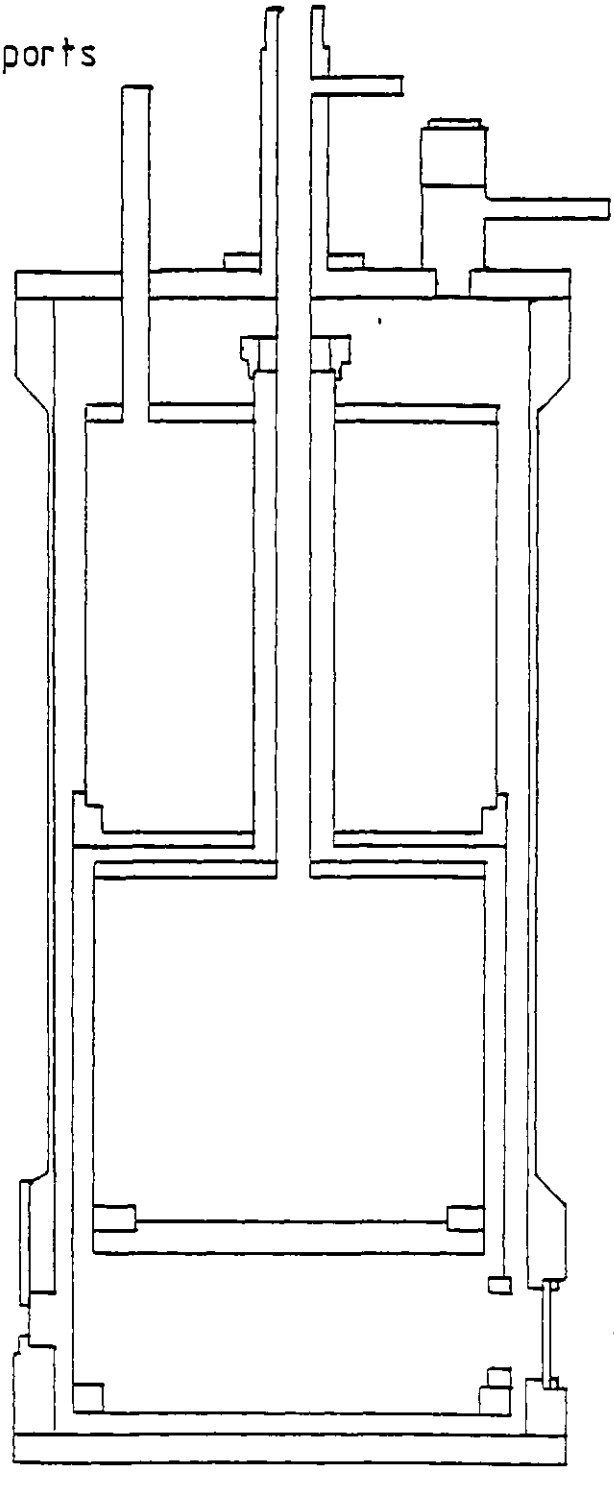

Fig 5-3

Tuning-Fork Focal-Plane Chopper

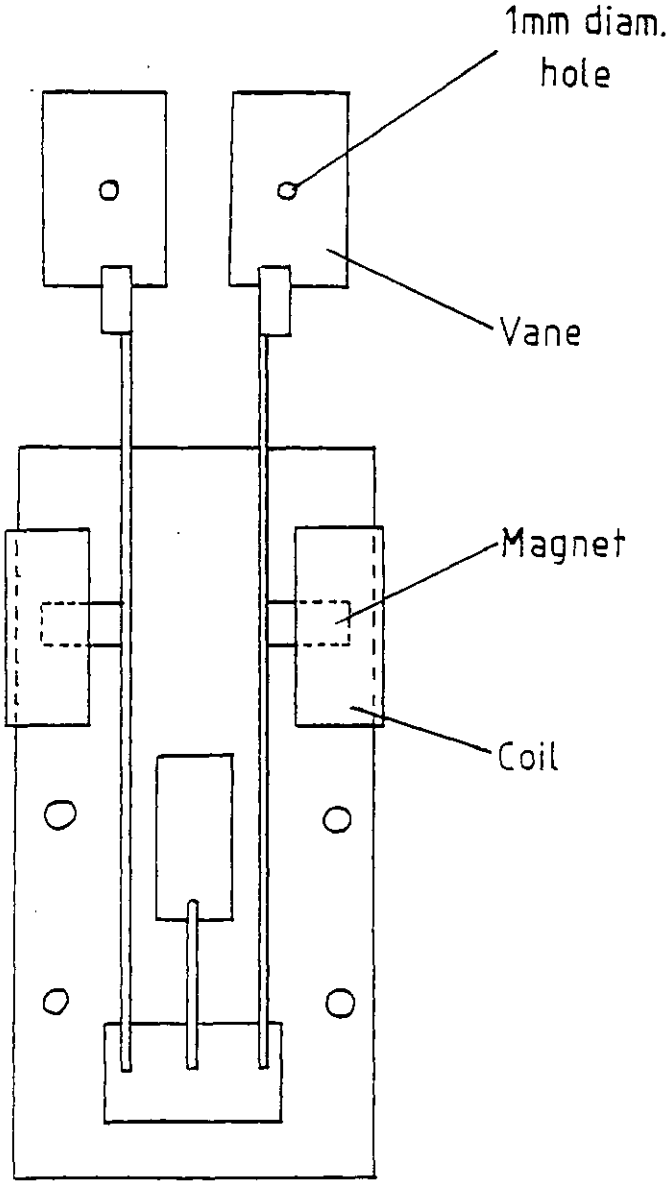

Scale: 2×Actual Size

Fig 5-4

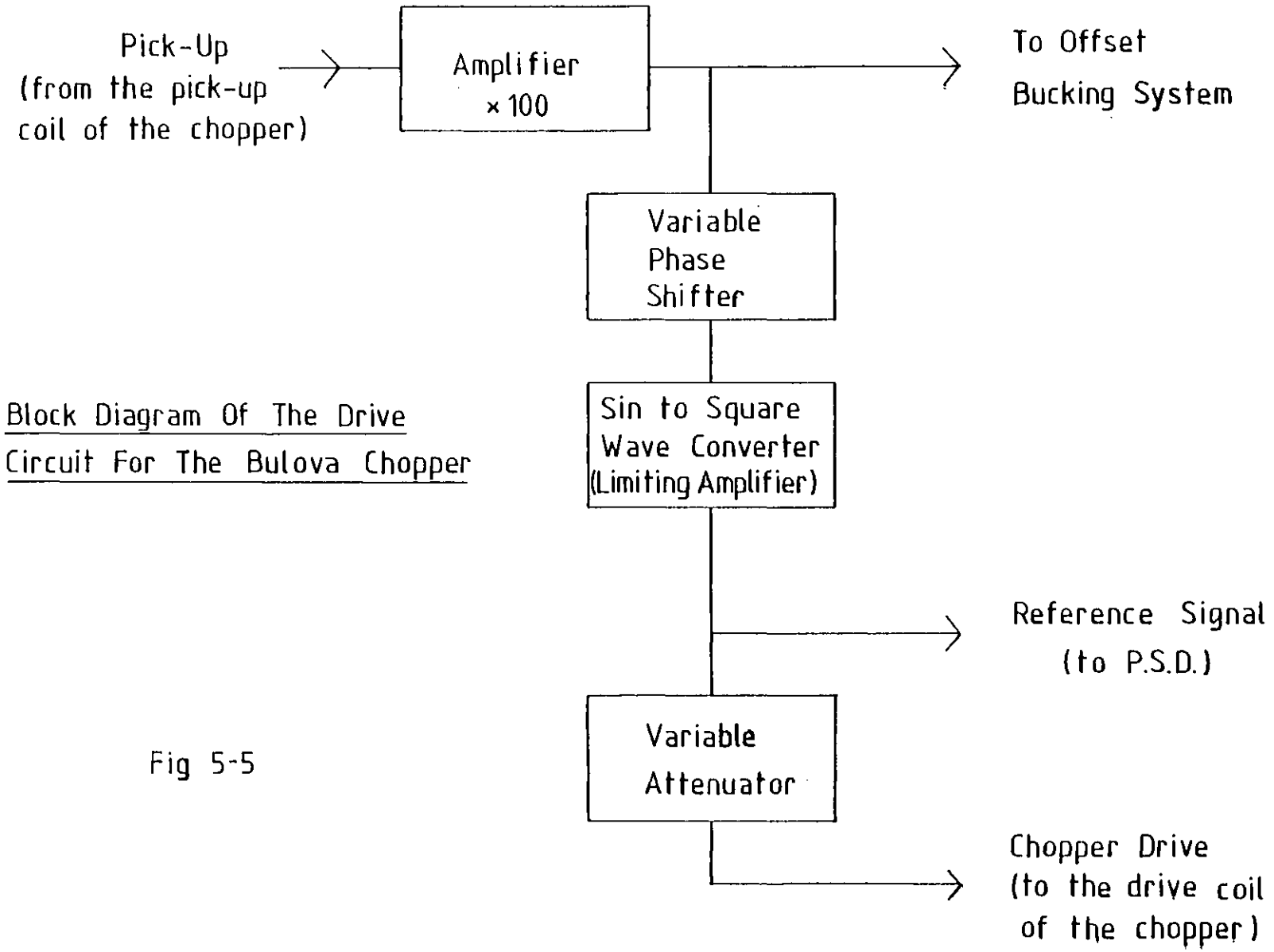

Block Diagram Of The Drive Circuit For The Bulova Chopper

Fig 5-5

to 0.5mm in the focal plane in Tenerife).

The frequency of the chopper depends on the mass of the vanes and the stiffness of the arms. At room temperature, the chopper vibrates at 19.5 Hz, but at liquid helium temperatures, this increases to 21.3 Hz because the metal becomes less flexible.

It was found that the chopper amplitude undergoes small vibration-induced fluctuations which can cause excess noise at the detector. This effect was eliminated by the use of an offset bucking system which is described in 5-13.

5-6 Analyser

The analyser was a type IGP225 obtained from Cambridge Physical Sciences. It consists of an aluminium grid of about 0.4μ period deposited by photolithography on a 25mm diameter KRS-5 substrate of 2mm thickness. The transmission properties are shown in Fig.5-6 and its efficiency, defined as $\frac{T_{\perp}-T_{\parallel}}{T_{\perp}+T_{\parallel}}$, is very near to 100% at 10μ.

5-7 Rotation of the Analyser

The key problem of rotating the analyser inside the helium dewar was a severe one. Firstly, space is extremely limited. The helium cold surface has a diameter of only 12cm and the lid of the nitrogen can limits the height to 7½cm (although the dewar could have been extended if necessary). This volume has to contain a detector, load resistors, a tuning-fork chopper, the filters and Fabry lens, and the analyser rotation unit and reference system. Considerable ingenuity was necessary to fit all these components in, and the separation between the helium temperature heat shield, and the nitrogen can, is only a millimetre or two in several places. Certain components are only accessible by dismantling the whole unit - a time-consuming operation, and assembly from scratch takes ∿ 1 day's work.

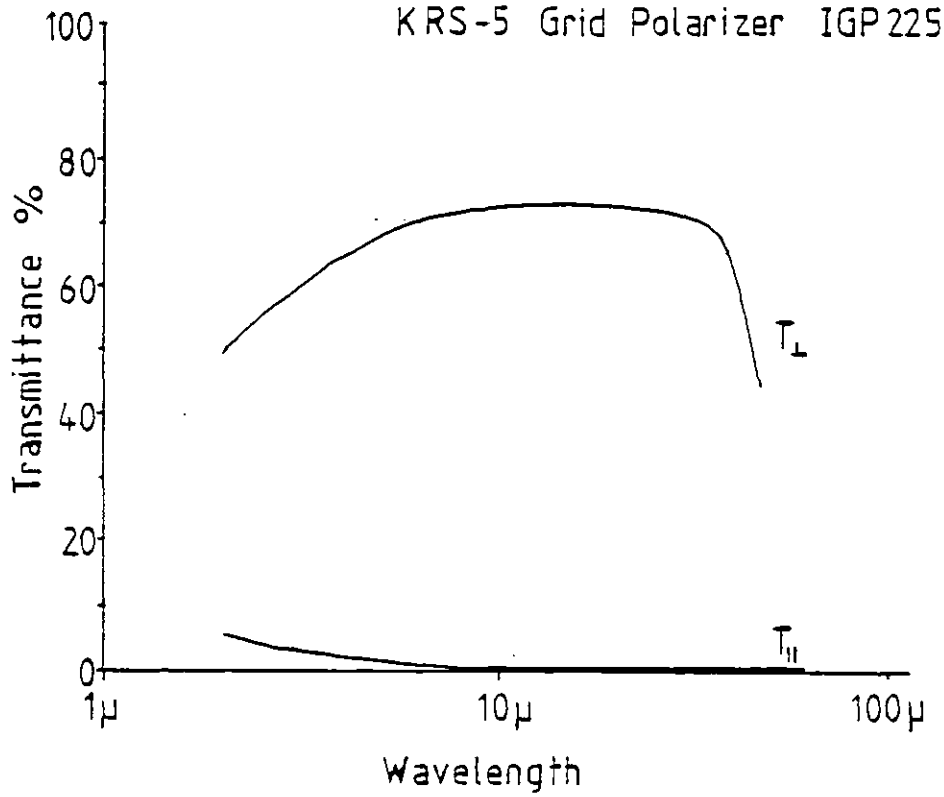
KRS-5 Grid Polarizer IGP225
100
80
60
40
20
0
Transmittance %
$T_\perp$
$T_{||}$
1μ
10μ
100μ
Wavelength

Fig 5-6

Secondly, the environment is a hostile one for rotating components. The temperature at the helium-cold surface is 1.7°K, and the analyser and the other components inside the dewar should be as near as possible to that temperature. The vacuum is higher than 10^{-6}torr - the dewar is pumped out to 10^{-6}torr with a diffusion pump, and the liquid helium cryopumps the dewar further. The dewar holds 1.7 litres of helium which has a latent heat of evaporation of 4.08 kJ (compared with 274 kJ for the same volume of liquid nitrogen). Thus to achieve a hold time of (say) 12 hours, the heat reaching the helium must be less than $\sim$0.1 watts. A copper wire connecting the helium and nitrogen cans, a centimetre long and only $\frac{1}{5}$ mm thick, would create a heat leak of this magnitude.

A motor is necessary to provide the drive power and a choice must be made to situate it either inside or outside the dewar. Although, at balloon altitudes, the pressure drops to 8mm and the temperature drops to $\sim$ -55°C, it is not difficult to find motors which will operate in this environment. However, it is much more difficult to operate a motor inside a dewar, for it would have to be completely degreased and this may lead to considerable problems at low temperatures (presumably due to differential contractions). Of course, wherever the motor is placed, any drive shaft will be a possible heat path to the helium although it may be possible to use a very good insulator for the shaft material to minimise this. A further problem, with any form of drive shaft if an external motor is used, is to pass the shaft through the dewar wall while maintaining the vacuum. A Wilson seal is often used to achieve this, but usually for intermittent rotation. This approach was rejected for two reasons; firstly it was felt that continuous rotation could cause wear of the seal and hence a leak; secondly at the low temperatures at balloon altitudes, the seal could freeze up and either stop the rotation or create a leak.

The method finally adopted to rotate the analyser was to use an

external motor and to transmit the drive across the dewar wall with a magnetic coupling. Such a method has been used by Robson (1973). This involves attaching a large magnet to the motor and placing a follower magnet inside the dewar. The magnets and motor are shown in Fig.5-7. Thus there is no problem with maintaining vacuum integrity or with heat transfer to the helium. The new problem becomes one of the relative weakness of this coupling and the associated necessity of having a reference system to monitor the analyser position. If a direct drive using a shaft is used, the analyser position can be monitored by measuring the position of the portion of shaft external to the dewar. However, with a magnetic coupling, it is possible for the external magnet to be smoothly rotating whilst the internal magnet is either stationary or rotating in jerks. The reference system used is described in 5-8.

The major design features of the analyser rotation unit are detailed below. The unit is shown in Fig.5-7.

a) The telescope beam passes through a tube with the analyser mounted at one end so that the beam always passes through the same portion of analyser.

b) The drive is bent through a right angle using ratio level gears. The motor can thus be kept out of the rotation axis of the analyser, which is also the telescope beam. The 4:1 gear ratio helps to overcome any friction.

c) The nitrogen can was modified to incorporate an extension, and the dewar wall was drilled out, to minimise the separation of the two magnets and hence increase the transmitted torque.

d) The bearings for the drive shaft and the rotating tube were a major problem. Normally bearings are liberally lubricated. However, any oil or grease freezes at helium temperatures and also may outgas and degrade the high vacuum. Thus, the bearings must be run dry and self-

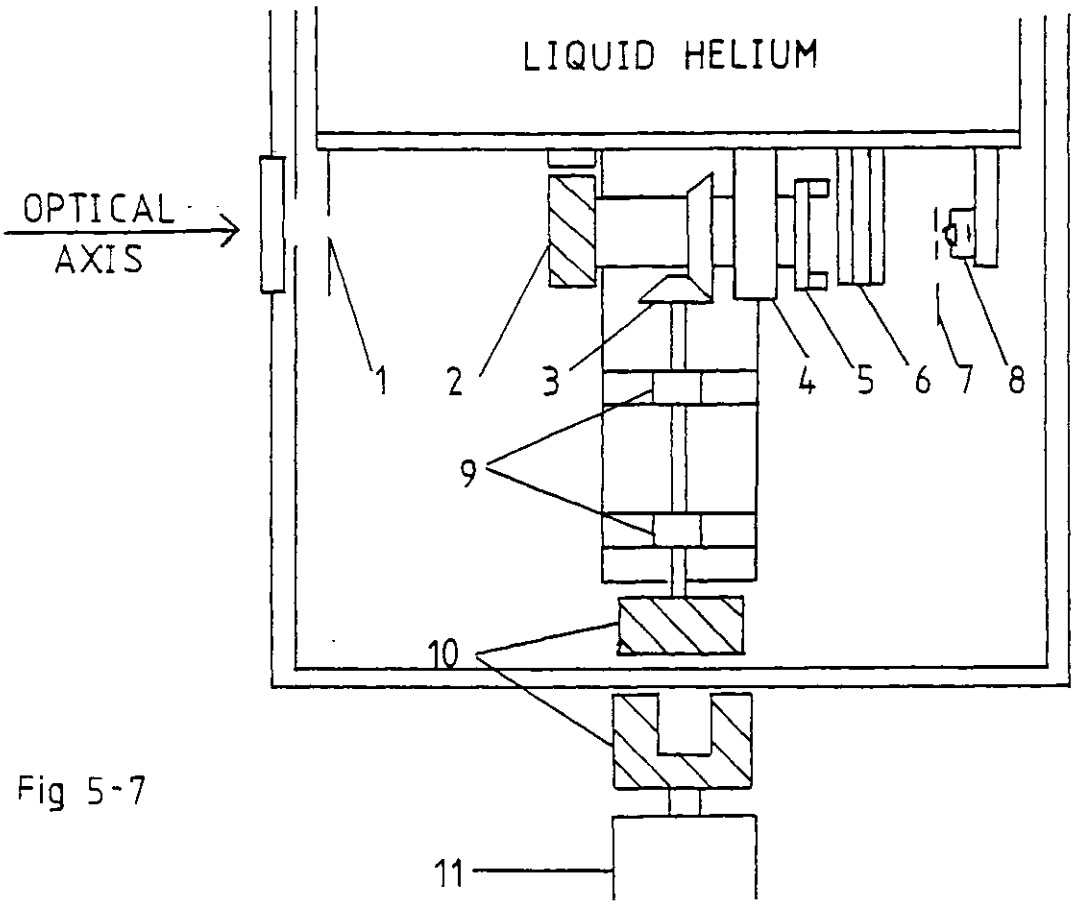

Fig 5-7

THE POLARIMETER

(1) Cold Aperture Stop

(2) Circular Magnet Below Magneto-Resistive Device

(3) Ratio Bevel Gears

(4) Bearing

(5) Wire Grid Analyser

(6) Infrared Filters

(7) Chopper

(8) Detector

(9) Bearings

(10) Magnets

(11) Motor

lubricating bearings using oil-impregnated materials are ruled out.

A simple bearing such as a metal shaft passing through a hole in PTFE was considered, but was rejected as it was felt that friction could be considerable at helium temperature and the bearing could become worn. Following Robson's (1973) successful use of a ball bearing inside a dewar, it was decided to use miniature ball bearings. Three were used - two $\frac{1}{8}$" internal diameter bearings supported the vertical shaft from the drive magnet to the small bevel gear, and a $\frac{5}{8}$" internal diameter bearing supported the $\frac{1}{2}$" internal diameter tube with the analyser at one end and the large bevel gear and reference magnet at the other end. The bearings were thoroughly degreased before use, and a very light dusting of molybdenum disulphide applied as a dry lubricant. The $\frac{3}{8}$" ball bearings seemed to work much better at low temperatures than the $\frac{5}{8}$" bearing, which ran very roughly when degreased. This was thought to be due to the presence of a cage in the ball race of the large bearing which keeps the balls separated, but also creates extra points of contact. It was found that by filing down the ball cage to minimum thickness, and removing two-thirds of the balls, the $\frac{5}{8}$" bearing ran more smoothly.

e) The standard method of mounting ball bearings is to push-fit them into a block. However, upon cooling, the aluminium blocks will contract down onto the steel bearings causing the bearings to seize up. The bearing holders were enlarged to allow for the differential contractions which amounted to 0.03mm (0.012") for the $\frac{1}{8}$" bearings and 0.09mm (0.035") for the $\frac{5}{8}$" bearings. A thin slivver of phosphor-bronze was put round each bearing to act as a spring to keep the bearing in place.

Testing of the bearings was generally done by plunging them into liquid nitrogen (77^{o}K), as it was felt that this is sufficiently near to liquid helium temperature for any potential problems to show up. It is important to use fairly clean nitrogen - one batch contaminated with

water ice had to be filtered before use, as it was noticed that the ice crystals cling to any metal object and were blocking up the bearings.

f) A small electric motor was mounted on the dewar lid with a large conventional magnet attached to the shaft. The motor is a Faulhafer-type, operating from a 6 volt d.c. supply, and incorporates a 1734:1 gearbox. The temperature specification is $-50^{\circ}C$ to $+75^{\circ}C$. The maximum torque is 1000 gcm when it consumes $\sim$ 0.4 Watts. However, in normal use, the power consumption was only $\sim$ 0.1 Watts.

g) The follower magnet was ceramic, diametrically magnetised, as was the reference magnet (cf. 5-8). They were kindly donated by Darwins Magnets International Limited, Sheffield. Despite misgivings from various magnet manufacturers about possible loss of strength at very low temperatures, these magnets retained their fairly strong fields at low temperature, and after a large number of thermal cycles.

An extension was made to the nitrogen shield, and the dewar base was drilled out to minimum thickness, which permitted the external magnet and the follower magnet to be separated by only $\sim$ 6mm.

5-8 Analyser Reference

It is essential to know the position of the analyser at all times. For successful polarimetry, it is necessary to be sure that the analyser is rotating smoothly and regularly and to be able to sample at the correct points in the rotation cycle. Therefore, information must be obtained from inside the dewar; knowledge of the motion of the external drive-magnet is not sufficient. It is also important to have a continuous monitor - a signal once or twice per revolution is inadequate.

Various optical methods were considered. The most promising involved the use of a fixed light-emitting diode (LED) shining through two pieces of optical polaroid onto a photo-transistor. One piece of polaroid

would be fixed, the other attached to the rotating tube so that the light detected by the photo-transistor would vary with the rotation angle as a $\cos^2$ wave. The LED shone brightly, at least at 77°K, but the photo-transistor lost all sensitivity at low temperatures. Further drawbacks to this idea included the considerable power dissipated in the dewar by an LED ($\sim$ 20mW) and the danger of scattered light reaching the detector.

The method eventually chosen was to use a magneto-resistive device (MRD) to sense the position of a circular magnet. The MRD consists of two magneto-resistors. By arranging them in a wheatstone bridge with two other resistors (see Fig.5-8) the two magneto-resistors can be compared, any change in their relative resistance indicating a change in the magnetic field in which they lie. The MRD is virtually noise-free - the dominant noise is Johnson noise - so very small currents can be used and hence very low power dissipation can be achieved. A current of $\sim$ 2mA was used, giving a power dissipation inside the dewar of $\sim$ 1 mW.

A diametrically-magnetised circular magnet was attached to the rotating tube and the MRD sited on the copper baseplate immediately below, so that one rotation of the tube produces one complete sine wave at the output of the MRD circuit.

To attach the ceramic magnet to a holder which would fit onto the tube, a variety of glues including Evostick, Bostick, Araldite, low-temperature Araldite, Superglue and Stycast were tried. All seemed promising when tested by immersing the magnet and its holder into liquid nitrogen. However, all these adhesives eventually failed after cycling down to liquid helium temperatures, some only after a considerable number of cycles. It is believed that this was due to the differential contractions of the ceramic magnet, the glue, and the aluminium holder. The extreme hardness of the ceramic magnet makes it difficult to drill, although the central hole was successfully enlarged with a diamond-tipped cutter. Eventually, two small holes were made in the magnet with an

Bridge Circuit for the MRD

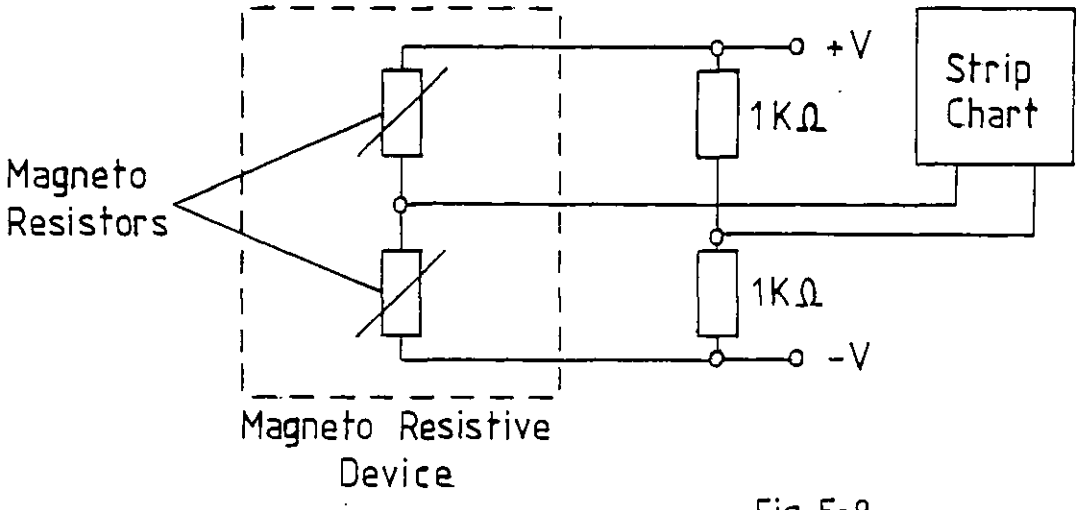

Fig 5-8

ultra-sonic drill, and by this means it was securely attached to the holder with nuts and bolts. The magnetic field was slightly affected by these holes so that the MRD output gave a sine wave with two small 'bumps', but these were not big enough to affect its use (see Figs.5-9 and 5-10).

5-9 Filters

Filters are used to define the spectrum of radiation reaching the detector. The ideal passband will be the result of several trade-offs. The polarimeter uses only a single detector, so there must be a compromise between covering a wide region of the spectrum, and obtaining a measurement of polarization at a particular wavelength. For a ground-based instrument, the filters should at least eliminate radiation from outside the atmospheric windows. Further narrowing of the pass-band will reduce the background radiation on the detector, thus reducing the photon noise and maintaining the bolometer element as close as possible to the helium bath temperature. However, it will also reduce the signal at the detector, and hence may increase the integration time required to reach a particular signal-to-noise ratio. One particular consideration for polarimetry is that if the polarization is high only at a particular wavelength, or if the polarization angle changes with wavelength, then a wide band-pass will smear out the polarization.

For Tenerife, it was decided to use the whole of the 10-12μ window. There are effectively 4 filters used,

i) The Dewar window. This is a 25mm diameter, 3mm thick piece of polished KRS-5 (thallium bromoiodide, Tl(Br,I)). The transmission curve is shown in Fig.5-11.

ii) The Analyser. This is an alumium grid deposited on a 25mm diameter, 2mm thick piece of KRS-5. The transmission properties are shown in Fig.5-6.

Output Of MRD Showing Analyser Rotation

Fig 5-9

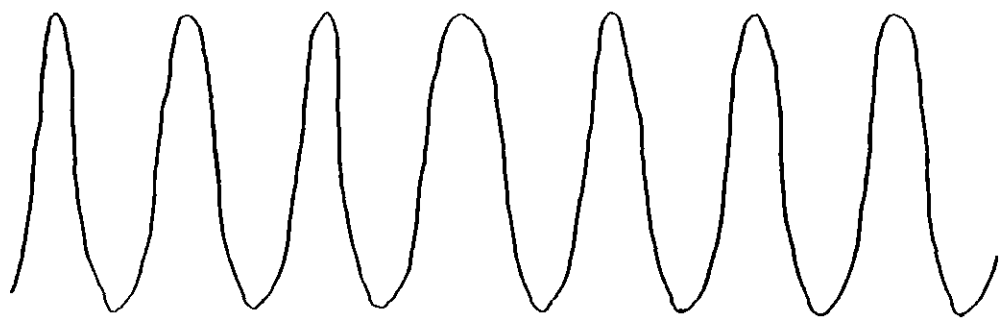

The apparent variation in the period is due to a slightly irregular paper drive on the chart recorder.

Fig 5-10

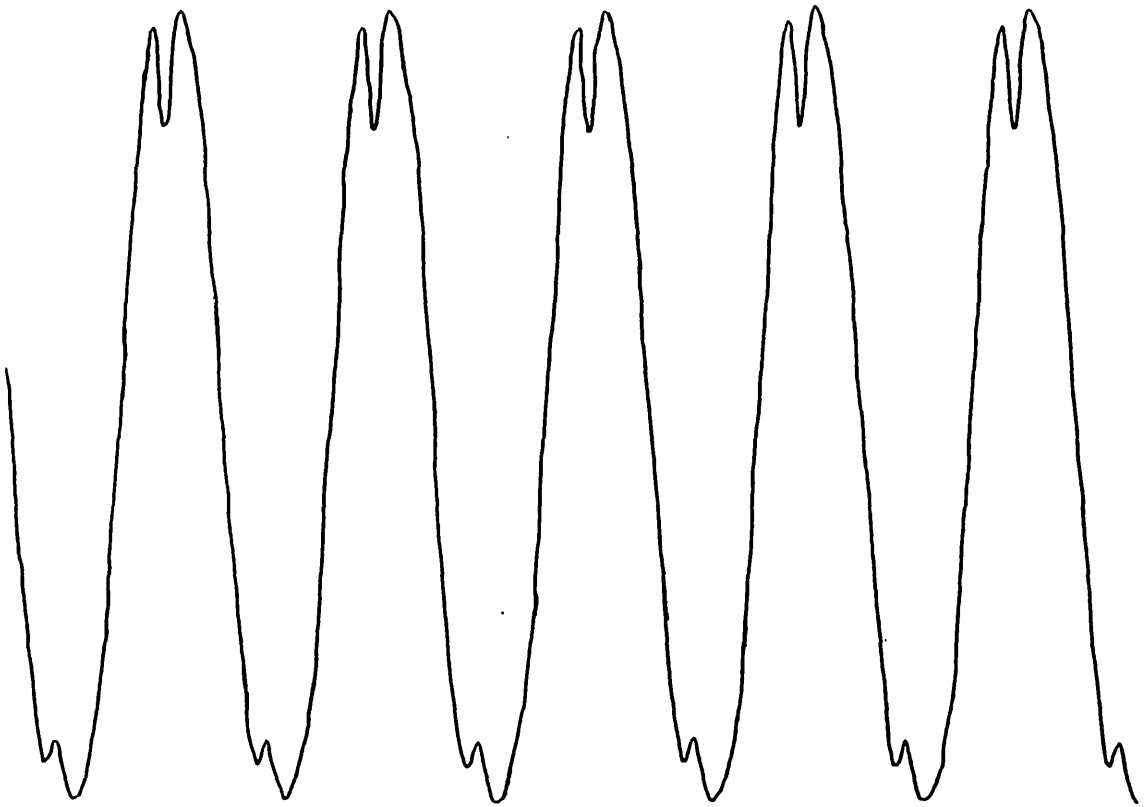

MRD Output After Holes Had Been Drilled In The Magnet

Transmission of KRS-5 (thallium bromoiodide)

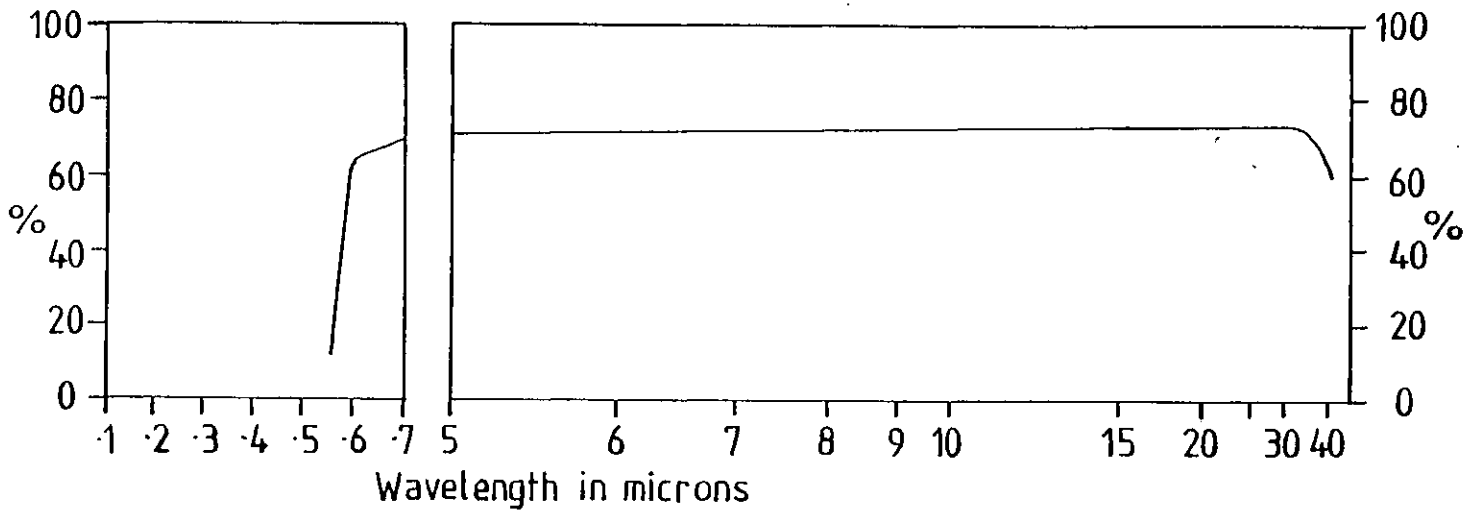

Fig 5-11

iii) The Fabry lens. This is a 12mm focal length plano-convex lens made of BaF_2. Its transmission curve is shown in Fig.5-12.

iv) A narrow-band interference filter (OCLI). This filter is designed for the 10-12μ window. Its transmission curve is shown in Fig.5-13.

The filters (except for the dewar window) are all inside the dewar at liquid helium teperature to minimise their black-body radiation. The Fabry lens and the OCLI narrow-band filter are kept in good thermal contact with the filter holder by small spring washers made of phosphor-bronze.

5-10 Optical Lay-out and Transmission

Fig.5-7 shows the positions of the optical components inside the dewar. The polarimeter is designed to accommodate the whole of the f/13.8 beam at the Cassegrain focus of the Tenerife 1.5m telescope. The aperture stop restricts the field of view of the detector, so that it only receives radiation from the sky and components along the optical axis. To minimise the thermal background, it is important that the detector cannot "see" any warm objects such as the instrument cage or the rear of the primary mirror.

The overall transmission, t_r, of the optical system for unpolarized radiation is the product of the absorption efficiency of the bolometer, the transmissions of the Fabry lens, OCLI filter, analyser, and dewar window, and the reflectivities of the secondary mirror and of the primary mirror. The absorption efficiency of the bolometer is difficult to estimate - in the absence of further information it will be assumed to be one, and this is probably reasonable at wavelengths short compared with the detector thickness ($\sim$ 0.2mm). Thus an estimate for the transmission is

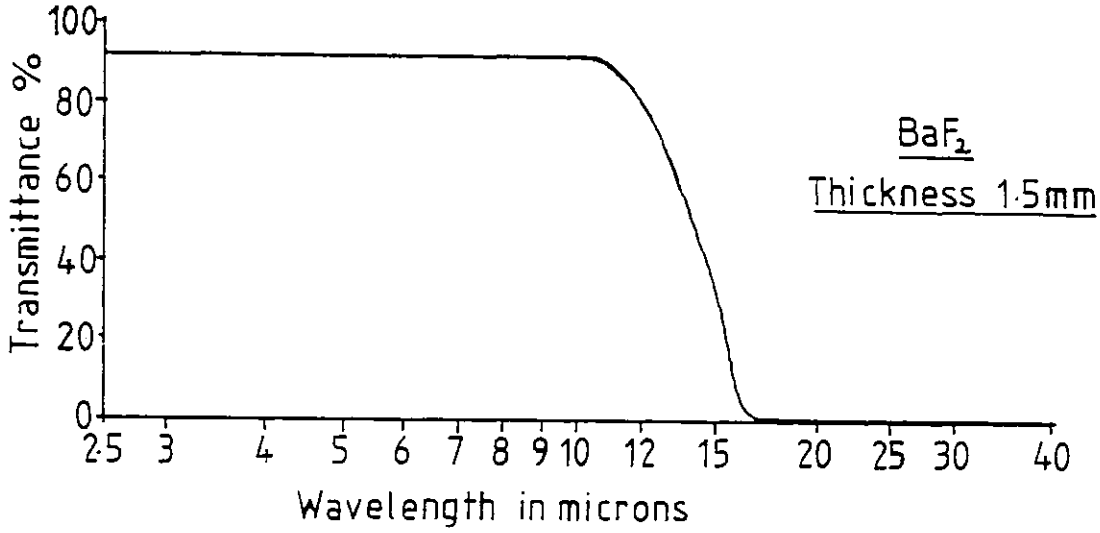
100
80
60
40
20
0
Transmittance %
2·5
3
4
5
6
7
8
9
10
12
15
20
25
30
40
Wavelength in microns
BaF2
Thickness 1·5mm

Fig 5-12

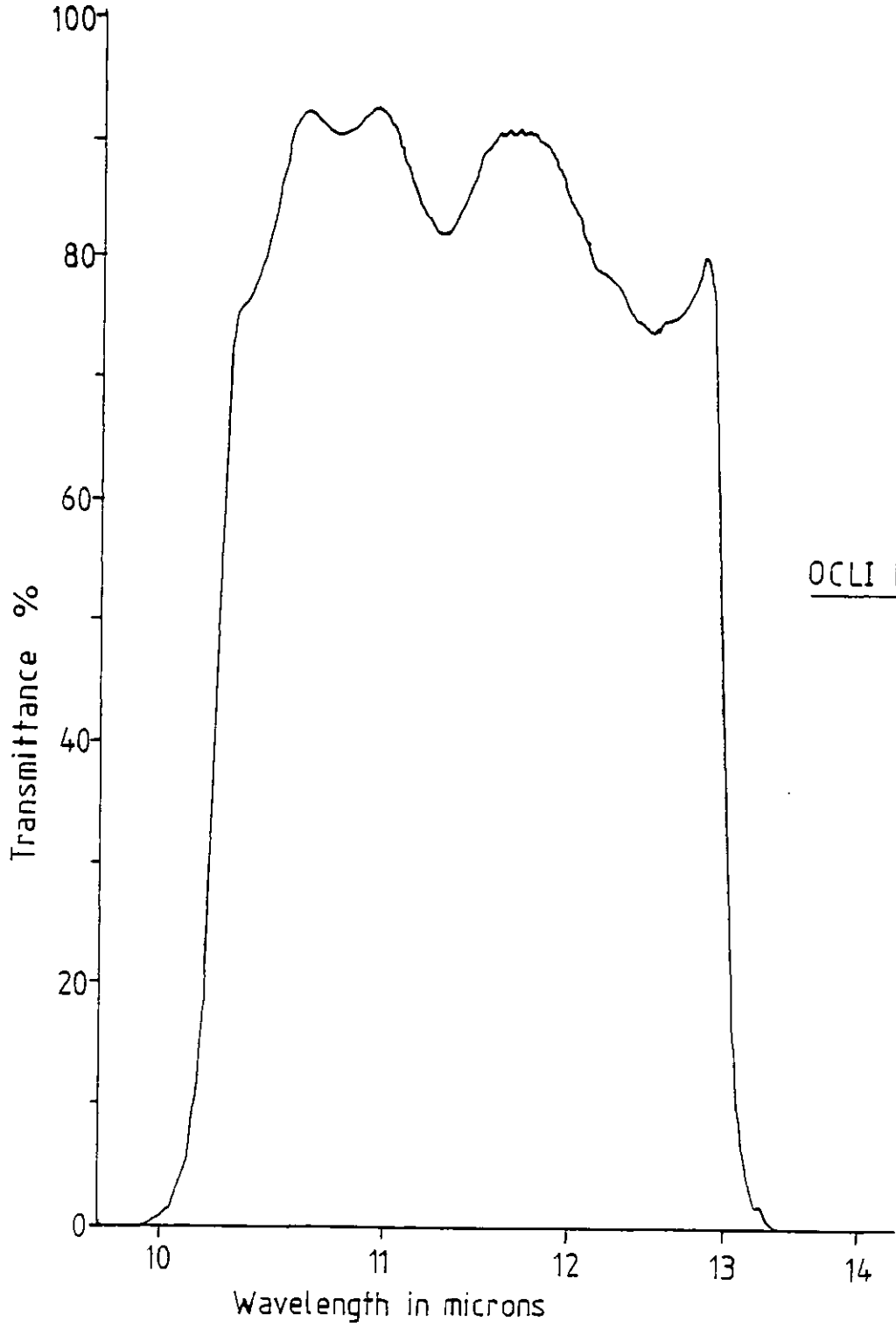

OCLI Bandpass Filter

Fig 5-13

$$t_r = 1 \times 0.9 \times 0.85 \times 0.35 \times 0.7 \times 0.95 \times 0.95$$

$$= 0.17 .$$

In section 7-7.5, this is compared with the measured transmission obtained by observing a star of known flux.

5-11 Dewar Mount at Tenerife

On ground-based telescopes, it is conventional to use a bottom-entry dewar, and this can be mounted in a vertical position in a cage beneath the telescope's instrument mounting flange. However, the use of a side-entry dewar, and the requirement that there should be no off-axis reflections, necessitated the design of a new dewar mount to hold the polarimeter. This mount was designed and constructed to cater for the following requirements.

a) The mount should be sufficiently rigid that the dewar does not move significantly with respect to the telescope beam as the telescope tracks across the sky.

b) It is necessary to be able to move the dewar slightly to align it.

We can define 3 perpendicular axes A, B and C, as shown in Fig.5-14, giving 3 rotational and 3 linear movements about and along the axes. Axis A lies along the optical axis of the telescope, axis B is parallel to the baseplate of the cage and parallel with the dewar fill-tubes, and axis C is parallel to the baseplate, but perpendicular to the dewar fill-tubes. All three axes should pass through the centre of the focal-plane field stop.

Rotation about A is unnecessary - this merely rotates the star on

Fig 5-14

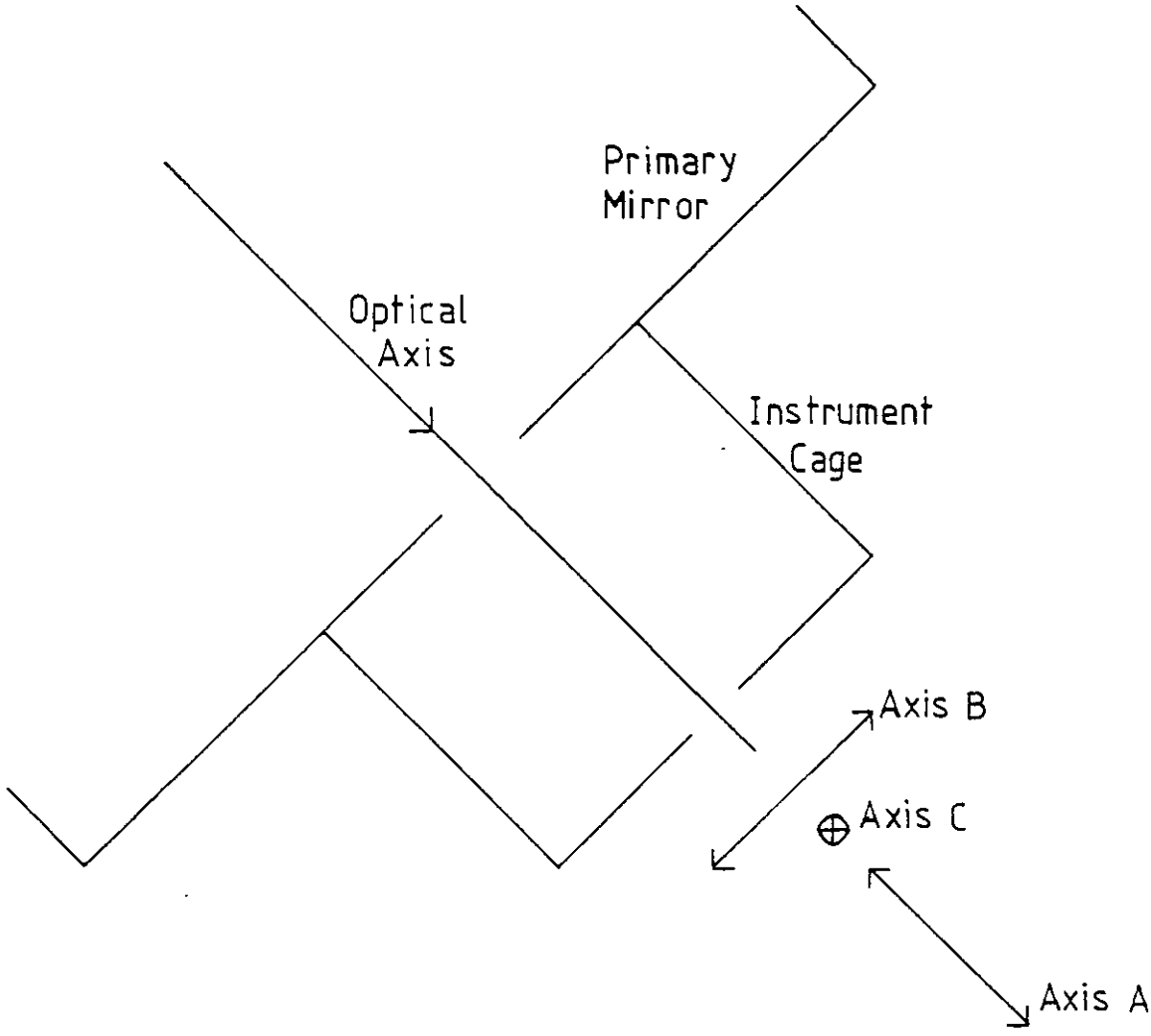

Axes For Dewar Movement

the detector. Also movement along A is unnecessary as focussing is carried out by a motor which moves the secondary mirror. This leaves 4 movements which the dewar mount must permit:

1 and 2. Rotations about B and C respectively, so that the optical axis of the dewar can be made parallel with the optical axis of the telescope.

3 and 4. Movement along B and C respectively, so that the optical axes, once parallel, can be moved to coincide.

These 4 movements were achieved with the mount shown in Fig.5-15.

Movements 1 and 3 are achieved by loosening the Allen screws on the split rings and twisting or pushing the dewar.

Movement 2 is achieved by moving the nuts on the three pieces of studding passing through the baseplate.

Movement 4 is achieved by adjusting the Allen screws passing through the extensions on the large split ring.

Once the dewar has been aligned on the Tenerife telescope, the split rings are tightened up and remain attached to the dewar when it is lifted off for refilling. The dewar should then be accurately lined up when it is replaced, without need for readjustment.

5-12 Guiding

The Tenerife telescope was built for a remarkably small expenditure using lightweight materials and fairly simple instrumentation. It is rather subject to buffeting by wind, backlash in the gears, drifts etc. Thus constant manual guiding is necessary. There is no auto-guider and infrared observers generally incorporate some sort of guide eyepiece into their photometry system. This may utilize a 45° beamsplitter which reflects infrared radiation but transmits a proportion of optical

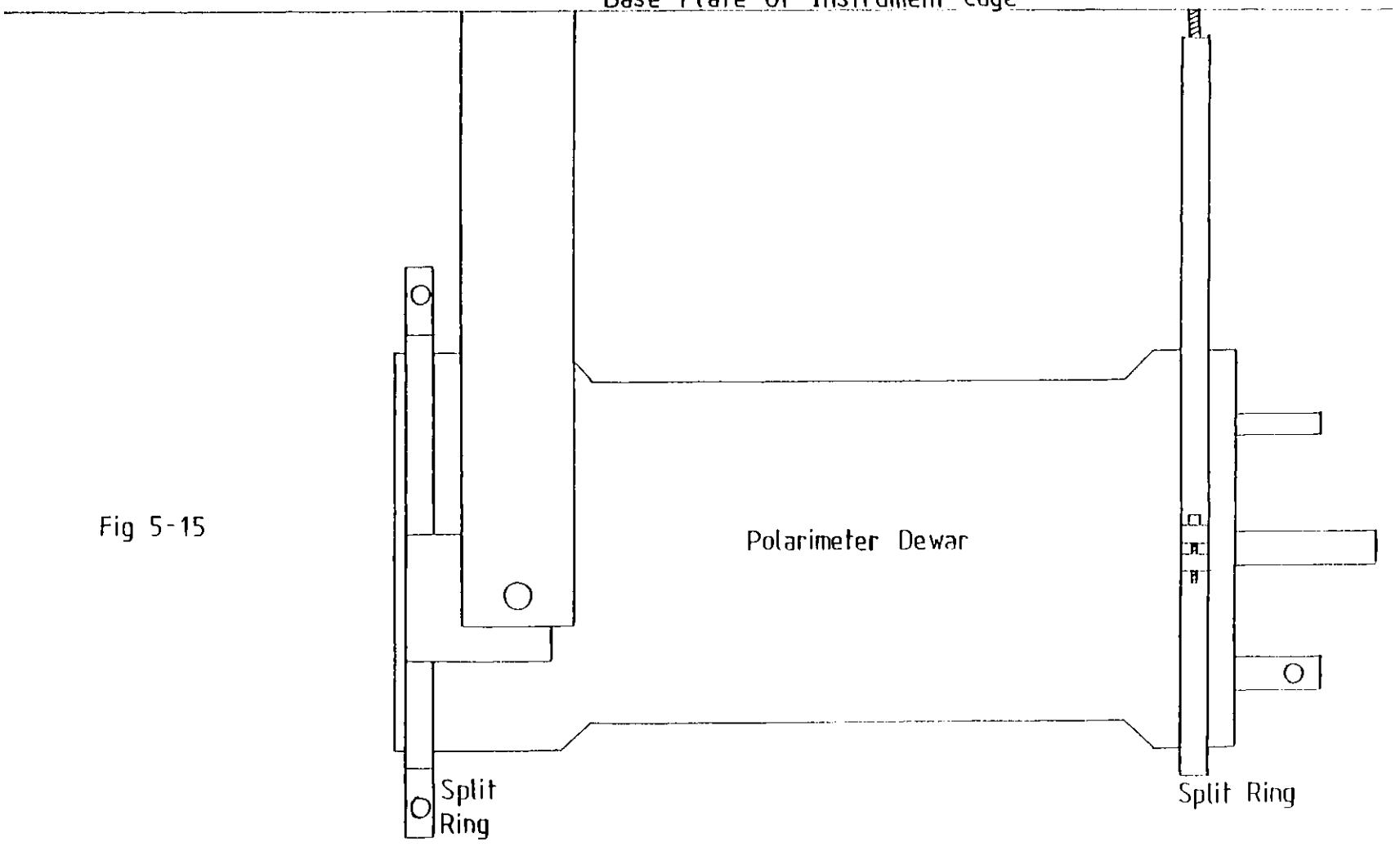

Fig 5-15

The Dewar Mount

radiation. For polarimetry, such a mirror is unacceptable, and a flip-in mirror is ruled out by the necessity for continual manual guiding.

One solution attempted was to use a 45° mirror with a central hole in it. However, a rather large hole is needed to be certain that the detector cannot see the edges of the mirror and this leaves only a rather small area of sky in the guide eyepiece, which does not include the infrared source. There is not always another object in the field of view to use for guiding, and so this method was found to be unsuitable.

The guiding method finally adopted made use of the 10" guide telescope that is fixed to the side of the main telescope. Despite a degree of differential flexure between the two telescopes, the method was useable and realignment of the infrared and optical beams was only necessary when setting up on a new object which was some distance from the previous one.

The 10" guide telescope was modified by fitting a new Kelner eyepiece and graticule. The parameters of the 10" telescope are given in Table 5-2.

Table 5-2

	Effective Focal Length	F-number	Plate Scale	Eyepiece Focal Length	Eyepiece Field of View	Magnification	Telescope Field of View
Before modification	523 cm	20.6	39.4"/mm	26.5mm	50°	200	$\frac{1}{4}$°
After modification	523 cm	20.6	39.4"/mm	9mm	40°	580	4'

Parameters of the 10" Guide Telescope Before and After Modification

The original graticule consisted only of two sets of parallel lines, which is insufficient for guiding. A new graticule was made forming a

complete matrix as shown in Fig.5-16.

The finest fibres were obtained from 'lacing' cord. They are made of rayon and have diameters of $\sim 25\mu$ (1 thou). Double thicknesses were made by putting two fibres together.

The graticule was illuminated by four red miniature light-emitting diodes.

Despite the new graticule and the large field of view, guiding was probably the largest noise source. The best images were rarely better than 3", and bright sources tend to flare to much greater sizes. Faint objects are particularly difficult to guide on if the seeing is bad. In general, guiding error was least on the moderately bright stars (magnitudes 3 or 4) which were clearly visible but not bright enough to flare.

The modifications to the 10" guide telescope were successful and produced a workable solution to the problem of guiding.

5-13 The Offset Bucking System

When the chopper vibrates, a large signal is obtained, despite the fact that the telescope may be pointed at blank sky. This 'chopper offset' is a characteristic of most chopping systems operating with large infrared backgrounds, and arises from slight misalignments of the optics and small differences in the temperature or emissivities of objects in the two fields of view.

If this offset is small, it will merely produce a small offset on the PSD which will be cancelled out by the technique of "nodding". However, a large offset may saturate the pre-amplifier or the PSD, restricting the amplification available. Also, it is shown below that a large offset increases the effect of chopper amplitude variations with a corresponding increase in signal noise.

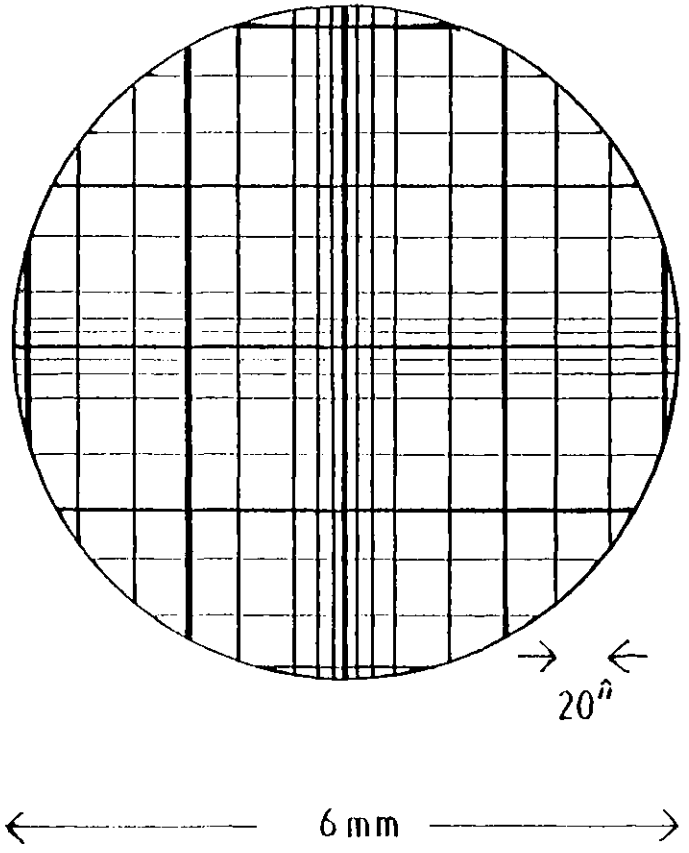

The Graticule For The Eyepiece Of The 10" Guide Telescope

Fig 5-16

A method of bucking out the chopper offset was implemented using the signal from the pick-up coil of the chopper. This is at exactly the same frequency as the detector signal, though its phase and amplitude are different. Therefore, by suitably amplifying and phase-shifting the pick-up signal, it is possible to add it to the detector signal to completely null out the fundamental frequency in the chopper offset. A similar system was used in the electronics of the Imperial College 41" Far-Infrared Telescope to overcome the restricted dynamic range resulting from the presence of a large chopper offset (Joseph et al. 1977). A diagram for the offset bucking system is shown in Fig.5-17.

5-13.1 Theoretical Analysis of The Offset Bucking System

The bolometer signal amplitude is roughly a linear function of the chopper displacement, with small higher order terms. This is clear because the roughly sinusoidal movement of the chopper produces a roughly sinusoidal response from the bolometer. However, at large chop amplitudes (peak-to-peak > 1mm), the bolometer response becomes more distorted as the higher order effects become more significant (see Figs.5-18 and 5-19).

We can describe the bolometer offset signal of amplitude T by the expression

$$T = a_0 + a_1 x + a_2 x^2 + a_3 x^3 + \ldots , \qquad (5\text{-}2)$$

where x is the chopper displacement and the sizes of the coefficients a_i depend on the chopper amplitude. The signal T is amplified by the pre-amplifier (which has a wide band-pass, 0.1 - 300 Hz), and then is processed by the PSD (referenced by the chopper) which completely eliminates D.C. and Fourier components that are even multiples of the chopper frequency. Table 5-3 gives a list of the harmonics and shows that the relative contribution of higher order harmonics is reduced by

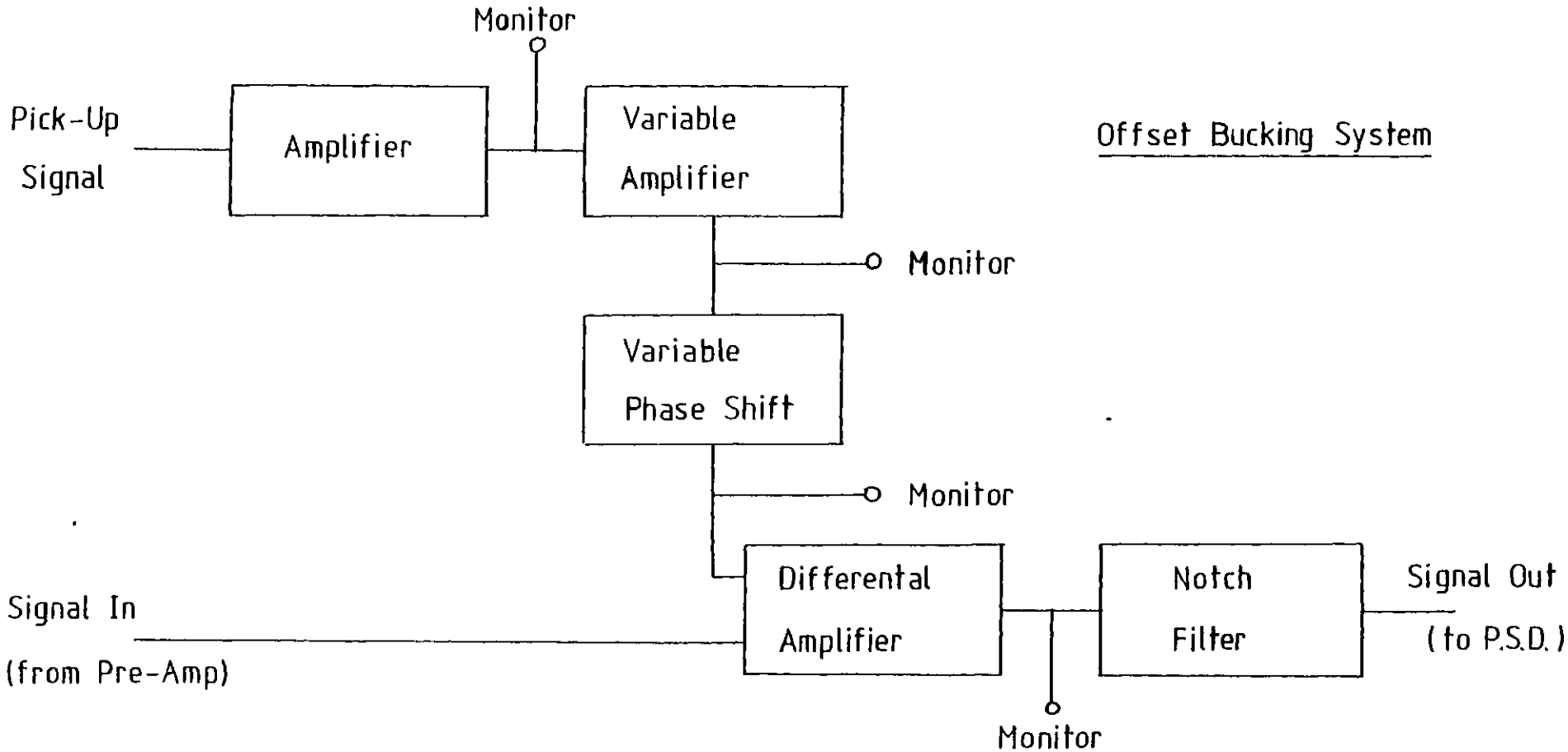
Monitor
Pick-Up
Signal
Amplifier
Variable
Amplifier
Offset Bucking System
Monitor
Variable
Phase Shift
Monitor
Differental
Amplifier
Notch
Filter
Signal Out
(to P.S.D.)
Signal In
(from Pre-Amp)
Monitor

Fig 5-17

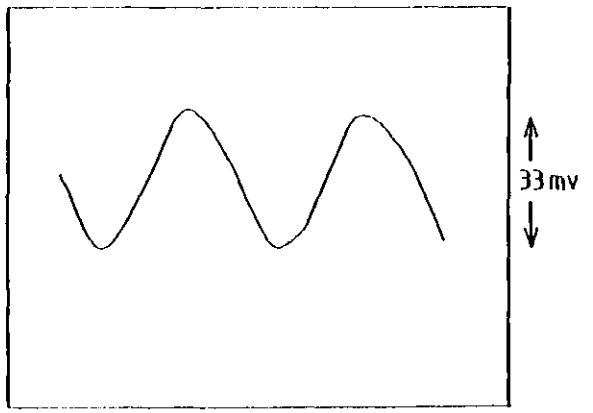

Instrumental Signal

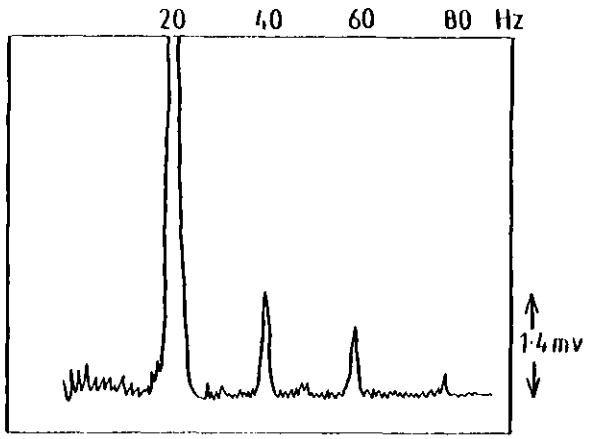

Spectral Analysis Of Signal

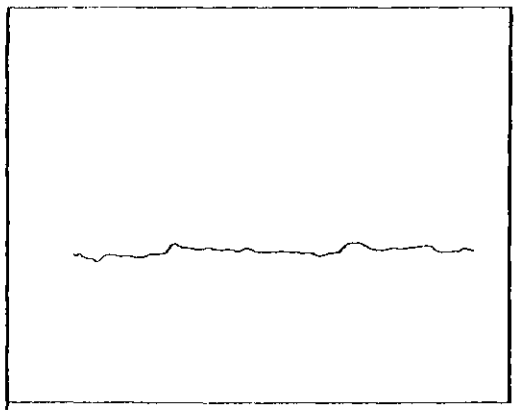

Bucked Instrumental Signal

(Same scale as above)

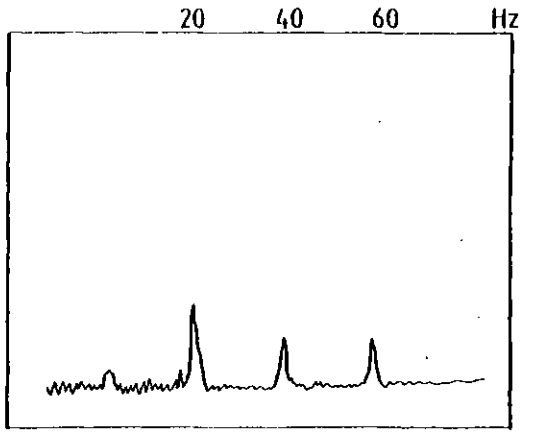

Spectral Analysis Of Bucked Signal

(Same scale as above)

Spectral Analysis And Bucking Of Normal Chopped Signal Fig 5-18

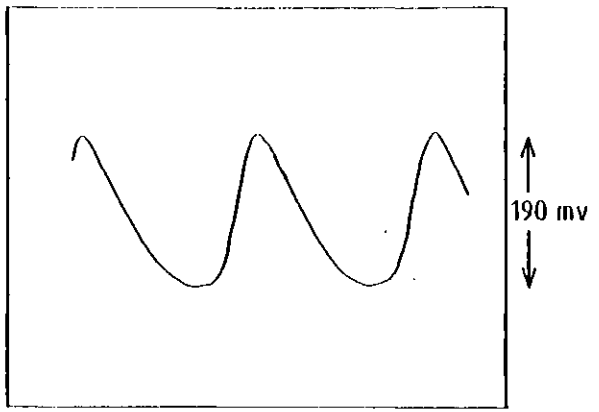

Instrumental Signal for very large chop

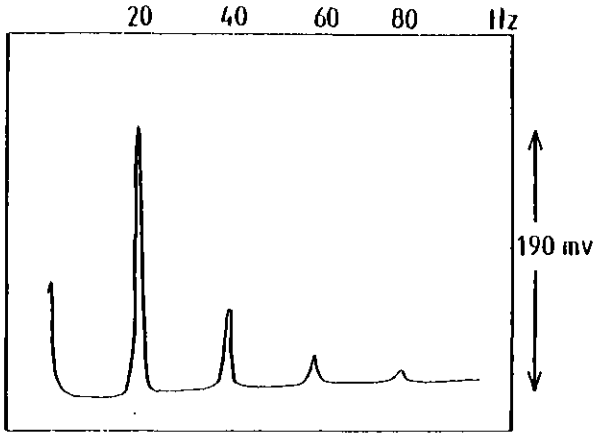

Spectral Analysis Of Signal

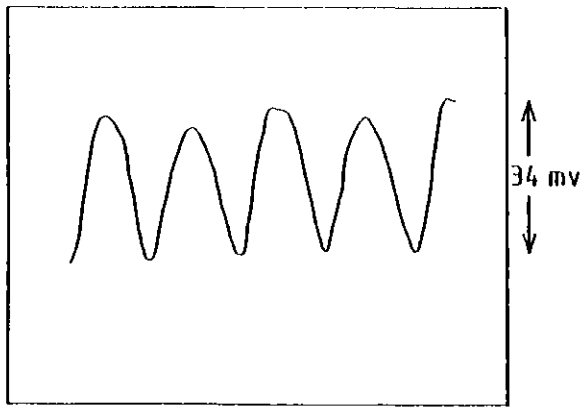

Bucked Instrumental Signal

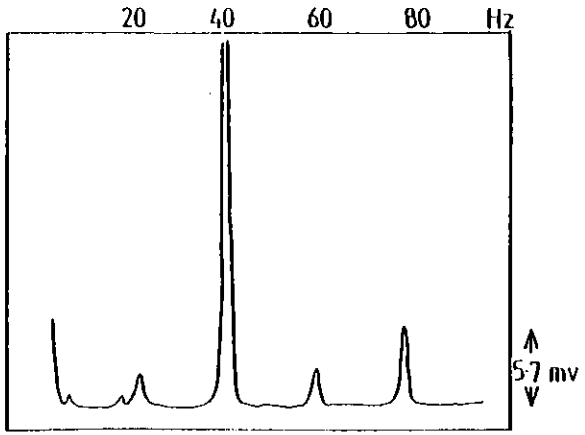

Spectral Analysis Of Bucked Signal

Spectral Analysis And Bucking Of Signal With Very Large Chopper Amplitude

Fig 5-19

Table 5-3

Effect of the PSD on signals at harmonics of the reference frequency f

Input Signal Frequency	Relative Output Amplitude
D.C.	0
f	Ø
2f	0
3f	Ø/3
4f	0
5f	Ø/5
6f	0
7f	Ø/7
8f	0
9f	Ø/9
10f	0

Ø is a factor between 0 and 1 depending on the relative phase of the reference and the signal. The output signal will be further attenuated by the variable filter which is controlled by the time constant setting on the PSD.

the PSD.

Chopper displacement is monitored by the pick-up coil, and when this signal was Fourier analysed by a spectrum analyser, was found to be a fairly pure sine wave - the 40 Hz 1st harmonic was less than 2% of the 20 Hz fundamental. (This also suggests that the pick-up coil has a reasonably linear response.) We can therefore describe the chopper motion sufficiently accurately by

$$x = b \sin \omega t$$

where b is the maximum chopper displacement from its rest position and $\omega = 2\pi$ x chopper frequency.

Substituting into (5-2) we obtain

$$T = a_o + a_1 b \sin\omega t + a_2 b^2 \sin^2 \omega t + a_3 b^3 \sin^3 \omega t + \ldots$$

which can be rearranged as

$$T = \left[a_1 b + \frac{3a_3 b^3}{4} \right] \sin\omega t - \frac{a_3 b^3}{4} \sin 3\omega t \qquad (5\text{-}3)$$

+ a D.C. term, even harmonics, and terms with coefficients $a_i : i \geq 5$.

The D.C. term and the even harmonics are eliminated by the PSD, and since the detector signal is a fairly pure sine wave for chop amplitudes of $\sim$ 1mm p-p, the higher order coefficients will be very small. Thus the only significant contributions to the PSD are contained in Equation 5-3.

We buck out the fundamental by phase shifting and amplifying the chopper pick-up signal and adding it in anti-phase to the bolometer signal, i.e. we subtract a signal $\left[a_1 + \frac{3a_3 b^2}{4} \right] (1\text{-}c)\, b \sin\omega t$ where c is a measure of the bucking accuracy. For perfect bucking $c = 0$. If there is no bucking $c = 1$. Otherwise $0 < c < 1$.

After bucking, the signal becomes

$$T = \left[a_1 + \frac{3a_3b^2}{4} \right] cb\sin\omega t - \frac{a_3b^3}{4} \sin 3\omega t ,$$

ignoring the remaining terms which do not affect the post-PSD noise.

Fluctuations of the chopper amplitude can produce noise in the signal, so we investigate the noise dT produced by the fluctuation db.

$$dT = \left[a_1 + \frac{9a_3b^2}{4} \right] c\sin\omega t \, db - \frac{3a_3b^2}{4} \sin 3\omega t \, db \qquad (5\text{-}4)$$

It is not necessary for the bucking to be precise. It is sufficient if noise due to chopper fluctuations is below the detector noise, N.

So we require $$\left[a_1 b + \frac{9a_3b^3}{4} \right] \frac{db}{b} c < N$$

and $$\frac{a_3b^3}{4} \frac{db}{b} < N$$

(The factor 3 cancels with the factor $\frac{1}{3}$ due to the action of the PSD on the 2nd harmonic,)

It should be noted that c, the measure of bucking precision, does not depend entirely on the experimenter's ability to make two signals equal in size and phase. The size of the chopper offset varies with the analyser position, giving a distinctive analyser rotation signal from the PSD. This puts a lower limit on c, for even if the bucking is perfect at certain analyser positions, it will not be perfect at others.

The 2nd harmonic term could, in theory, be removed by a second bucking system which tripled the chopper pick-up frequency before adding it in antiphase to the bolometer signal. However, the simpler solution of using a notch filter was adopted. This was tuned to three times the

chopper frequency ($\sim$ 60 Hz) and is sufficiently narrow to leave the fundamental unaffected.

5-13.2 Use of the Bucking System

The bolometer offset signal, T, can be investigated using a spectrum analyser to obtain the sizes of the fundamental and harmonics of the signal h_1 h_2 h_3 ... Then a theoretical calculation of the noise can be made using equation (5-3) in which $h_1 = a_1 b + \frac{3a_3 b^3}{4}$ and $h_3 = \frac{a_3 b^3}{4}$.

Hence, $$a_1 b + \frac{9a_3 b^3}{4} = h_1 + 6h_3 \text{ and } \frac{a_3 b^3}{4} = h_3 \qquad (5\text{-}5)$$

The ratio $\frac{db}{b}$ measures the chopper amplitude fluctuation and is obtained by spectral analyses of the chopper pick-up signal.

Laboratory tests were carried out with the chopper at a moderate and at an extreme chop amplitude, and the sizes of the fundamental and first two harmonics of the detector signal are given in Table 5-4. Also shown are the sizes of the chopper fluctuations and the peak-to-peak variation in h_1 due to the analyser rotation.

Chop amplitude	h_1	h_2	h_3	$\frac{db}{b}$	Peak-to-peak variation in h_1
1mm	20μV	0.8μV	0.6μV	$1.25 \times 10^{-2} Hz^{-\frac{1}{2}}$	600nV
5mm	100μV	30.5μV	13μV	$6 \times 10^{-3} Hz^{-\frac{1}{2}}$	3μV

Sizes of the fundamental and first two harmonics of the chopper signal

Table 5-4

Clearly, at 5mm chop amplitude the detector signal is very distorted. Nevertheless, the bucking system was able to reduce the noise to acceptable levels.

Using the values of Table 5-4 and equations 5-4 and 5-5 a theoretical value for the excess noise can be calculated and a theoretical estimate of the excess noise after bucking can be made. This can be combined with the fundamental detector noise ($\sim 40\ n\,V\,Hz^{-\frac{1}{2}}$) to give the total noise, and these figures are shown in Table 5-5. The bucking accuracy, c, is obtained by summing the limit imposed by the peak-to-peak variation in h_1 from Table 5-4, and the accuracy to which it was found possible to buck out the fundamental signal, h , with the analyser motionless.

Chop amplitude	Bucking accuracy(c)	Calculated excess noise before bucking	Theoretical excess noise after bucking	Total theoretical noise after bucking (i.e. including $40\ n\,V\,Hz^{-\frac{1}{2}}$ detector noise)
1mm	0.07	$295\ n\,V\,Hz^{-\frac{1}{2}}$	$21\ n\,V\,Hz^{-\frac{1}{2}}$	$45\ n\,V\,Hz^{-\frac{1}{2}}$
5mm	0.045	$1070\ n\,V\,Hz^{-\frac{1}{2}}$	$48\ n\,V\,Hz^{-\frac{1}{2}}$	$62\ n\,V\,Hz^{-\frac{1}{2}}$

Theoretical Noise After Bucking

Table 5-5

In Table 5-5, the noise arising from the second harmonic has not been included in the theoretical excess noise after bucking. This is because the notch filter was found to reduce the noise from this source to a negligible level ($\sim 10\ n\,V\,Hz^{-\frac{1}{2}}$ with a 5mm chop amplitude).

In Table 5-6, the theoretical values are compared with values obtained in laboratory tests, and it can be seen that there is good agreement.

Chop Amplitude	Noise before bucking ($n\,V\,Hz^{-\frac{1}{2}}$)		Noise after bucking ($n\,V\,Hz^{-\frac{1}{2}}$)	
	Theoretical	Laboratory	Theoretical	Laboratory
1mm	295	200	45	40
5mm	1070	1000	62	100

Comparison of Theoretical Bucking Figures with Laboratory Values

Table 5-6

In conclusion, the bucking system can make a very significant reduction in the noise due to fluctuations in chopper amplitude, as well as reducing chopper offset to avoid problems of saturation. For the polarimetry system, the excess noise is reduced to fundamental detector noise levels at moderate chopper amplitudes. Even at abnormally large chopper amplitudes, the detector noise is reduced to a useable level. It is clear that such a system should be applicable to other devices which make use of a chopper.

5-14 Design Performance of the Polarimeter

We can obtain a rough estimate of the capability of the polarimeter when used at Tenerife by using the formula of Eqn.4-1.

At Tenerife, $N \simeq 40\ n\,V\,Hz^{-\frac{1}{2}}$

$A \simeq 1.7 m^2$

$\Delta\nu = 6.2 \times 10^{12} Hz$ (10.25 - 13μ)

$t_r \simeq 0.17$

$R \simeq 0.5 \times 10^{6}$ V/W

With the awkward positioning of the dewar on the telescope, limiting the useable declination range, the maximum telescope time on any one object is roughly 2 hours. Only half the observing time is spent sampling, and further factors of $\frac{1}{\pi}$ must be inserted to allow for sine wave chopping and the analyser rotation. Thus the maximum integration time is $(\frac{1}{2}(\frac{1}{\pi})^2\ 2 \times 60^2)$, i.e. equivalent to only about 6 minutes.

Eqn.4-1 gives a minimum flux on which 1% polarimetry at the 3σ level can be achieved of

$$J = \frac{300 \times (40 \times 10^{-9})}{10^{-26} \times 1.7 \times (6.2 \times 10^{12}) \times 0.17 \times (0.5 \times 10^{6}) \times (\frac{1}{2}(\frac{1}{\pi})^2 2 \times 60^2)^{\frac{1}{2}}} \text{ Jy}$$

$$= 70 \text{ Jy}$$

This is a lower limit, and factors which might increase this include:

1. Guiding error
2. Poor "seeing"
3. Increased detector noise
4. Reduction in possible observing time

if the source is not optimally positioned in the sky, or if allowance is made for setting up on the object etc.

Thus, taking these factors into account, it is reasonable to attempt sources with a flux of (say) > 200 Jy.

In the 10μ catalogue (Hall 1974), there are approximately 110 objects whose flux exceeds 200 Jy. Thus, the sensitivity of the polarimeter should be sufficient to be able to make useful measurements on a reasonable number of objects.

Chapter 6. Data Analysis

6-1 Introduction

This chapter describes the processes by which infrared photons incident on the bolometer are converted to give a computer print-out of the polarization of the infrared source.

Fig.6-1 is a flow diagram of the path of the infrared radiation up to the point that it reaches the bolometer. The various elements in this path have been described in the earlier chapters. Fig.6-2 is a flow diagram showing the Data Analysis Scheme which converts the temperature fluctuations of the bolometer into a print-out of the polarization of the source, and the elements shown are the subject of this chapter. The system that was used for 10μ polarimetry at Tenerife is described in the following sections. The data analysis system for polarimetry at other wavelengths would be broadly similar.

6-2 Signal Amplification

The bolometer signal is first amplified by a pre-amplifier, with a fixed gain of 1000, which is attached by an Amphenol 6-way connector directly to the side of the dewar. This pre-amplifier has a frequency response $\sim$ 0.1 Hz - 300 Hz.

The pre-amplified signal is then passed through the offset bucking system (Section 5-13) which eliminates any large instrumental offset, reduces the noise due to chopper amplitude fluctuations, and filters the 60 Hz component.

This signal is then phase-sensitively detected by an Ithaco Dynatrac Lock-In Amplifier which is referenced by the Bulova chopper. The Ithaco has a variable gain factor of 1 to 10^8 and a variable offset control. These are adjusted to maximise the signal output range during

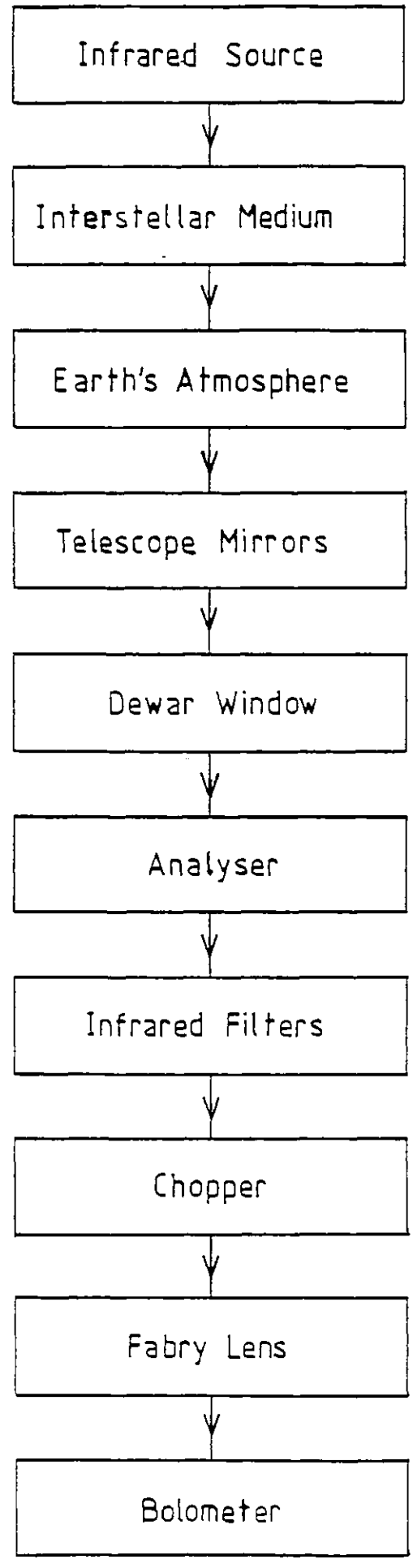

The Path Of The Infrared Radiation

Fig 6-1

Fig 6-2

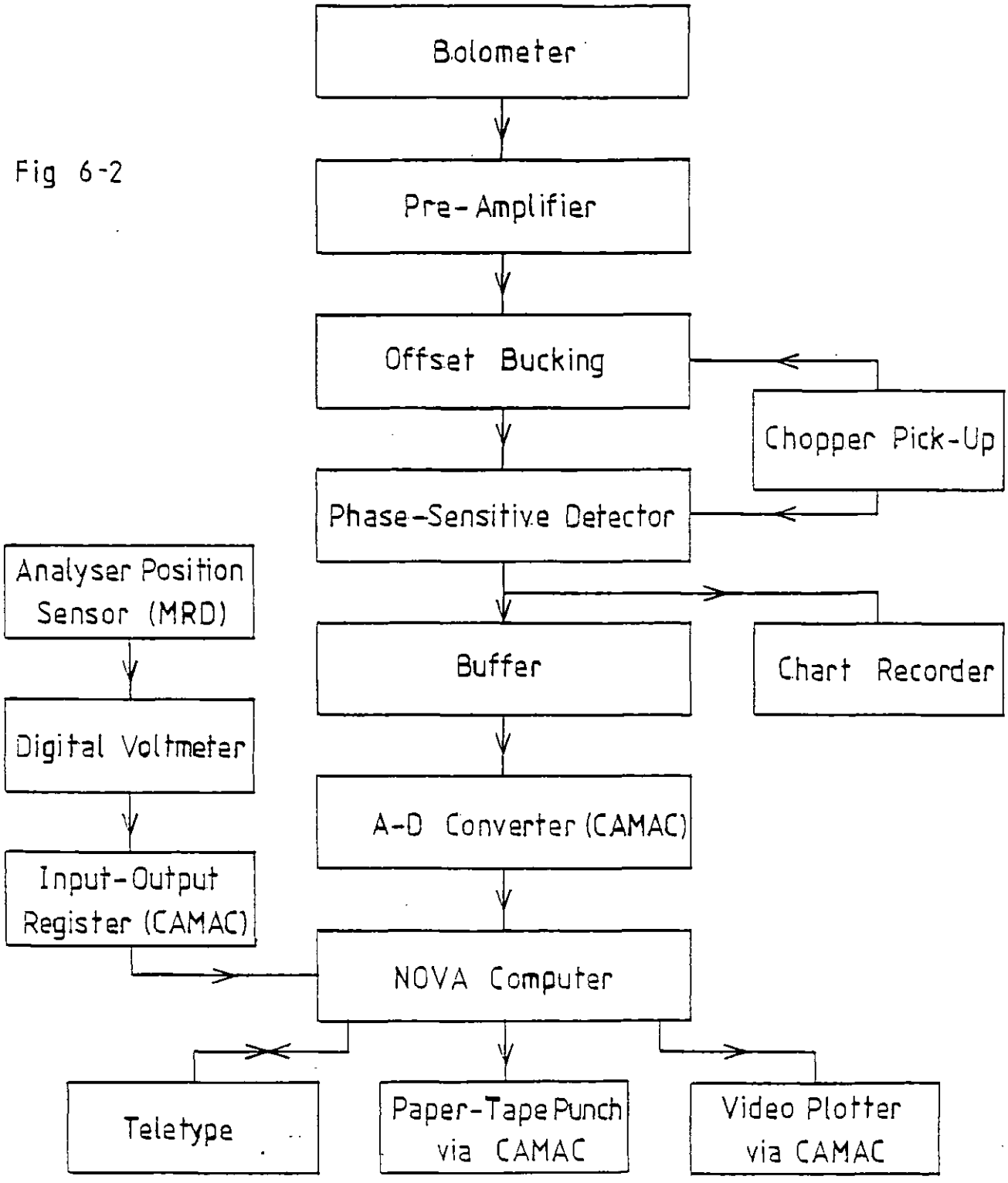

Data Analysis Scheme

each analyser rotation, whilst keeping it within the limits (±1.2V) acceptable to the Camac A-D converter.

The instrumentation described so far is all mounted on the telescope cage itself, and the Ithaco output is taken, by a long screened cable, off the telescope to a 50Ω Buffer and thence to the A-D converter at the Nova computer. The Ithaco output is also monitored on a chart recorder.

6-3 Analyser Reference Signal

The variations in the resistance of the magneto-resistors, as the analyser (and hence the circular magnet) rotates, emerge from the resistance bridge as an almost sinusoidal voltage which is digitised by a Data Precision DP1440 digital volt meter (DVM). This DVM not only provides a visual display, but also a 6-character BCD output to a CAMAC I-O module on the NOVA computer.

6-4 Computer Analysis

The Nova computer at Tenerife was used for data handling. The computer is essential for polarimetry since it is very tedious to derive the degree of polarization and polarization angle from the strip chart records and it would certainly not be possible to do it in "real-time".

The computer at Tenerife is a NOVA 2 with a 24K memory and is connected via a CAMAC interface to a CAMAC crate. A form of extended BASIC is used which includes "CALL" statements to operate the CAMAC modules. For polarimetry, the following input and output devices were used.

INPUT

A-D converter (CAMAC module) - This converts an analogue signal in the range ±1.2V to a 10-bit number (range 0 - 1023). The module has a trigger input as well as the analogue input, and this is used to initiate sampling at the correct time.

Interrupt Register (CAMAC module) - This accepts inputs from eight push buttons which are in the observing dome and enables the observer to control the progress of the sampling.

Input-Output Register (CAMAC module) - This takes a 24-bit input from the digital voltmeter.

Teletype - The observer initiates the observing routine and inputs certain parameters via the teletype.

OUTPUT

Display Driver (CAMAC module) - This drives a Cathode Ray Tube, sited in the dome, which displays the previous set of data and enables the observer to check for large noise spikes or bad data.

Pre-Set Counter (CAMAC module) - This is used merely to provide an output signal from the computer to the Telescope Control box so that the sampling, nodding, and printing of the data remain synchronous.

Fast Paper Tape Punch - This is used to print the raw data onto paper tape so that further data analysis can be carried out if desired. The punch was unfortunately frequently inoperative.

Teletype - The computer prints the raw data onto the teletype and also prints the results of the data analysis whenever requested, and at the end of the observation of each source.

A copy of the computer program written for polarimetry is given in Appendix III, and a flow diagram is shown in Fig.6-3. This program serves the dual purpose of controlling the data acquisition (via CAMAC) and of data analysis. It is written in BASIC, and is based upon a photometry program written by N. Vine of Imperial College when the NOVA was first installed at Tenerife. Once the observer has gone through an initial conversation via the teletype (entering the details of the object, gains etc), data acquisition continues under computer control, until the observer interrupts the sequence using one of the eight push buttons in the dome which connect to the interrupt request register. These buttons had the following functions:

Button 1. INFO. This gives the observer a print-out of the photometry and polarimetry measurements with their signal-to-noise ratios, at the end of the current set of samples.

Button 2. REJECT. By pressing this, the observer can discard the samples from the previous set if they appeared abnormal on the CRT.

Button 3. CONTINUE. This starts the data acquisition, or restarts it after a pause.

Button 4. PAUSE. 'Pause' stops the data acquisition at the end of the current set, permitting the observer to change position, consider whether to reject a previous set etc.

Button 5. Not used.

Button 6. RESTART. This stops the data acquisition at the end of of the current set and goes back to the initial conversation to start the observations again from scratch.

Button 7. STOP. This stops the data acquisition at the end of the current set and calculates the final photometry and polarimetry measure-

A Simplified Flow Diagram For The Polarimetry Computer Program

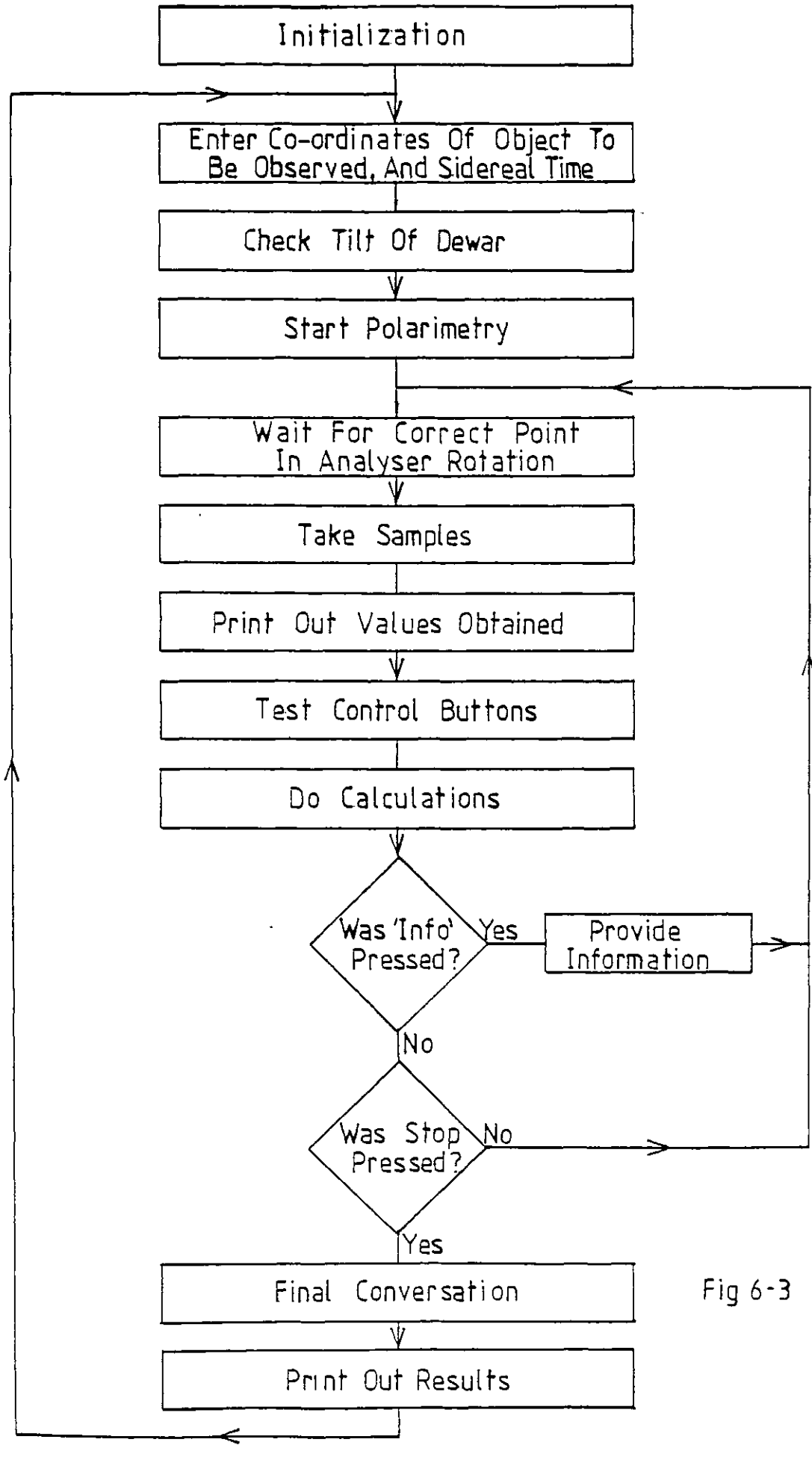

Fig 6-3

ments along with their statistical errors.

Button 8. Not used.

6-5 Determination of Optimum Sampling Rate

The rotation rate of the analyser, the sampling rate, and the PSD time constant are parameters which must be set so as to obtain optimum results in the minimum observation time. There are a number of constraints which need to be taken into consideration.

1. Changes in atmospheric seeing and thermal drifts can be significant on time scales of a few minutes. Hence, the rotation rate of the analyser should be as fast as possible.

2. Stiction in the gearing and ball bearings is reduced with a fast rotation rate.

3. Guiding requires intense concentration and is difficult to do well for long periods. This, too, suggests a fast rotation rate.

4. The chopper operates at $\sim$ 20 Hz. The rotation rate of the analyser must be sufficiently slow:

a) so that the chopper signals and analyser rotation signals do not beat and,

b) so that there is at least one chop period (and therefore a measurement of signal) within each angle resolution element, i.e. if one desires an angular resolution of 5^{o}, the minimum rotation period for 20 Hz chopping is $\frac{360}{5} \times \frac{1}{20}$ secs = 3.6 secs.

5. The integration time on the PSD must be set long enough to filter out noise, yet sufficiently short that the polarization signal is not greatly attenuated. The amplitude of the attenuated polarization signal is given by $A = \frac{A_o}{1+\omega^2\tau^2}$, where ω is the angular frequency of the polarization signal (twice the frequency of the analyser rotation), A_o

is the zero frequency amplitude of the polarization signal and the PSD employs a two-stage low-pass filter (with 12 dB per octave roll-off), each stage having time constant τ. The noise reduction for a two-stage low-pass filter is given by $N_\tau = \frac{N}{\sqrt{8\tau}}$ where N is the noise in a 1 Hz bandwidth. Thus the signal-to-noise ratio SNR is given by

$$SNR = \frac{A_\omega}{N_\tau} = \frac{A_o}{1+\omega^2\tau^2} \frac{\sqrt{8\tau}}{N} \quad .$$

SNR has a maximum value, with respect to τ, when $\tau = \frac{1}{\sqrt{3}\omega}$.
For $\omega = \frac{2\pi}{36}$ radians sec^{-1}, this value of τ is 3.3 secs.

A very long integration time is inconvenient to use as the system will take a long time to settle down after any change. In particular, one must be sure that the signal has risen to nearly full strength after nodding, before sampling recommences. If the time between nodding and sampling starting is t, then if we require the signal to be within 1% of full strength when sampling starts, we need

$$1 - e^{-\frac{t}{\tau}} - \frac{t}{\tau} e^{-\frac{t}{\tau}} > 0.99$$

$$\text{i.e. } t > 6.64\tau$$

6. Sampling should be carried out at a rate of at least twice the bandwidth (Nyquist Sampling Theorem). A slower rate is discarding information (undersampling) whereas a faster rate does not produce any extra information and so the data samples are not independent (over-sampling). The data analysis is carried out using an approximation to integration to measure the $\cos^2$ curve present in the signal if the source is polarized. The quality of this approximation, and in particular, the angle resolution, increases with the number of sample points.
Angle - resolution $\simeq \frac{180^o}{\text{No. of samples}}$, so for an angle resolution of 5^o, $\sim$ 36 samples are necessary. The method used to approximate integration

requires that the number of samples be divisible by four.

7. The parameters are not all freely variable. The sampling rate is set on the Telescope Control Box and can be set to once every $\frac{1}{8}, \frac{1}{4}, \frac{1}{2}, 1, 2, 4$ ... "seconds". (Each Box second was in fact $\sim 1\frac{1}{8}$ seconds long.) The time constant on the PSD can be set for τ = 1.25ms, 4ms, 12.5ms, 40ms... etc. The rotation speed can be freely varied by adjusting the voltage supply to the electric motor.

The following settings for the parameters were chosen to satisfy these constraints as far as possible.

Analyser Rotation Period = 72 seconds.

Sampling Rate = 32 samples per $\frac{1}{2}$ revolution.

PSD time constant for τ = 1.25 seconds.

The sequence of events in one rotation period is then as follows.

0 secs 32 samples are taken

36 secs The Telescope nods

36-52 secs The teletype prints out the values of those samples

52-55 secs The fast paper tape punch prints the values of the samples

36-72 secs The observer guides the telescope into the new nod position

55-72 secs The DVM samples the MRD, and when it falls within the preset range, sampling recommences.

With the analyser rotating once every 72 seconds, the angular frequency of the polarization signal is $\frac{2\pi}{36}$ radians per second and thus the signal-to-noise is maximised if

$$\tau = \frac{1}{\sqrt{3}\,\frac{2\pi}{36}} = 3.3 \text{ seconds.}$$

With τ = 0.4 seconds, the signal-to-noise is only roughly half of the maximum value. However, a longer integration time was found to be too difficult to work with. The integration time for the PSD = 4τ = 1.6 seconds and the bandwidth is $\frac{1}{8\tau}$ = 0.3125 Hz. Thus the Nyquist sampling rate is 2 x 0.3125 Hz = 0.625 Hz, or once per 1.6 seconds. The sampling rate was 32 in 36 seconds, i.e. once per 1.125 seconds - slightly oversampling.

6-6 Data Analysis Mathematics

The object of the data analysis is to compute the linear polarization state and intensity of the source radiation entering the dewar. When photometry is performed, the flux of a source is generally obtained by first calibrating the instrument on a well-known object of known flux. Therefore, it is unnecessary (unless one is trying to remeasure a calibration object) to know the real intensity reaching the instrument. For polarimetry alone, even such calibrations are unnecessary - all that is required is a comparison of the polarized flux with the polarized flux.

In the calculations that follow, the attenuations due to such components as the dewar window, the filters, etc. are not included. However, the various gains/attenuations due to the electronics are included so that the voltage due to the signal at the detector can be calculated. In particular, it is often useful to compare this with the noise voltage.

Suppose the infrared radiation in the filter passband, entering the dewar, has intensity I, and a proportion p is linearly polarized at angle θ (i.e. 100p% linearly polarized radiation). This radiation can be represented by the Stokes vector

$$\begin{bmatrix} I \\ Ipcos2\theta \\ Ipsin2\theta \\ 0 \end{bmatrix}$$

The wire grid analyser with transmissions T_{11} and $T_{\perp}$, parallel and perpendicular to the wires, at an angle ϕ, has the Mueller matrix (Equation 2-12)

$$\frac{1}{2}\begin{bmatrix} T_{\perp}+T_{11} & -(T_{\perp}-T_{11})\cos2\phi & -(T_{\perp}-T_{11})\sin2\phi & 0 \\ -(T_{\perp}-T_{11})\cos2\phi & (\sqrt{T_{\perp}}-\sqrt{T_{11}})^2\cos^2 2\phi+2\sqrt{T_{\perp}T_{11}} & \frac{1}{2}(\sqrt{T_{\perp}}-\sqrt{T_{11}})^2\sin4\phi & 0 \\ -(T_{\perp}-T_{11})\sin2\phi & \frac{1}{2}(\sqrt{T_{\perp}}-\sqrt{T_{11}})^2\sin4\phi & (\sqrt{T_{\perp}}-\sqrt{T_{11}})^2\sin^2 2\phi+2\sqrt{T_{\perp}T_{11}} & 0 \\ 0 & 0 & 0 & 2\sqrt{T_{\perp}T_{11}} \end{bmatrix}$$

Therefore, after passing through the analyser, the radiation has intensity

$$\tfrac{1}{2}(I(T_{\perp}+T_{11}) - Ip(T_{\perp}-T_{11})\cos2\theta\cos2\phi - Ip(T_{\perp}-T_{11})\sin2\theta\sin2\phi)$$

Now with the 10μ grid polarizer used, $T_{11} \ll T_{\perp}$ ($T_{11} \simeq 0.0025$, $T_{\perp} = 0.7$), so the intensity is approximately

$$\tfrac{1}{2}(IT_{\perp} - IpT_{\perp}\cos\{2(\theta-\phi)\}) \qquad \text{(putting } T_{11} = 0\text{)} \qquad (6\text{-}1)$$

This is a sine wave function with a p-p amplitude of $IpT_{\perp}$ plus a constant term $\frac{1}{2}IT_{\perp}$. The radiation is modulated by the tuning-fork chopper, detected by the bolometer and then amplified and phase-sensitively detected.

The tuning-fork chopper is self-resonant and the modulated signal is therefore a sine wave. The PSD may be considered to perform the following operations on the signal, shown pictorially in Figure 6-4. First the signal is rectified by the PSD, which will have been phased-up. The

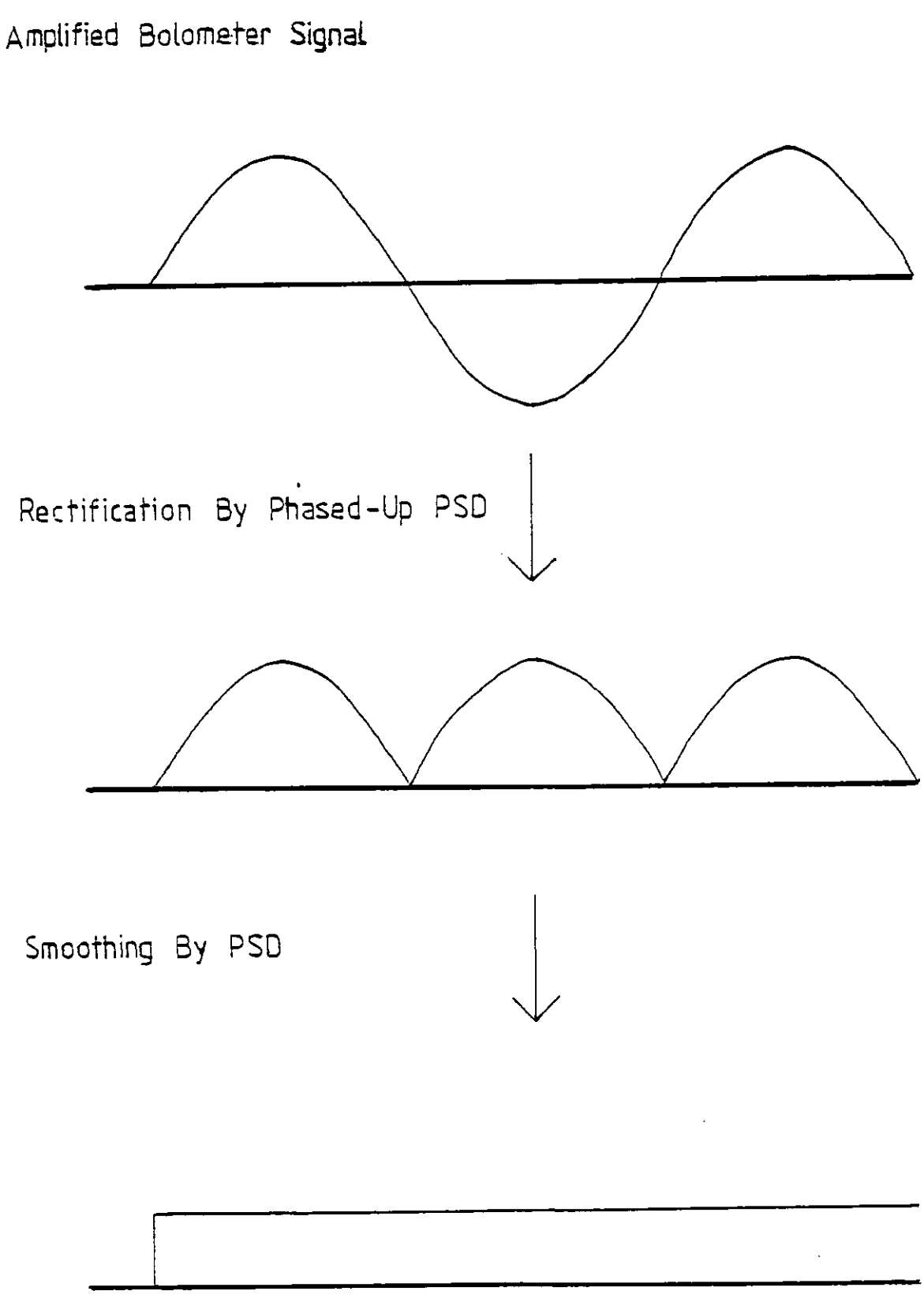

The Effect Of A Phased-Up PSD On A Sine Wave

Fig 6-4

rectified signal is then smoothed to give a constant voltage output provided the phase and amplitude of the signal are not changed.

If the peak-to-peak amplitude of the sine wave is A, the PSD output (assuming a gain of 1) will be

$$\frac{1}{\pi}\int_{o}^{\pi}\frac{A}{2}\sin\theta d\theta = \frac{A}{\pi}\ .$$

The PSD output, when the detector signal is that given by (6-1), will be

$$\frac{1}{2\pi}\ (IT_{\perp}-IpT_{\perp}\cos\{2(\theta-\phi)\})+g(\phi)\text{volts},$$

where $g(\phi)$ is the chopper offset which varies with ϕ, the position of the analyser, and I is now the voltage at the detector arising from the source's flux.

When the telescope nods into the other beam, the PSD output will be

$$-\frac{1}{2\pi}\ (IT_{\perp}-IpT_{\perp}\cos\{2(\theta-\phi)\})\ +g(\phi)\ \text{volts}.$$

So far, we have assumed a pre-amp and PSD gain of unity. Suppose the total gain in the system is G = pre-amp gain x PSD gain x Buffer gain. Then the signal going into the A-D converter is

$$\pm\frac{G}{2\pi}\ \ (IT_{\perp}-IpT_{\perp}\cos\{2(\theta-\phi)\})\ +Gg(\phi)\ \text{volts}.$$

The analysis of this signal is carried out by a computer program. The A-D converter (ADC) samples the buffer output 32 times per half-rotation of the analyser, and converts the analogue signal into a number between 0 and 1023. 0 corresponds to -1.2V whilst 1023 corresponds to +1.2V, so 1 bit is equivalent to roughly 2.25mV.

The numbers output by the ADC are thus

$$\frac{1}{0.00225}\left[\pm\frac{G}{2\pi}\left(IT_{\perp}-IpT_{\perp}\cos\{2(\theta-\phi_i)\}\right)+Gg(\phi_i)\right]$$

$$(1 \leq i \leq 32)$$

where $\phi_i = (i-1)\frac{\pi}{32} + \phi_o$ and ϕ_o is the angle at which sampling commences.

Let these 32 ADC samples be S_{i_1} $(1\leq i\leq 32)$, let the next 32 be S_{i_2} etc. The difference between the signals in the two nod positions is then calculated by subtracting the 32 samples of a set from the mean of the corresponding samples from the adjacent sets. These 32 differences are

$$P_{ij} = \frac{S_{ij} + S_{ij-2}}{2} - S_{ij-1} \quad 1 \leq i \leq 32$$

$$= \frac{1}{0.00225}\,\frac{G}{\pi}\{IT_{\perp}-IpT_{\perp}\cos\{2(\theta-\phi_i)\}\} \qquad (6\text{-}2)$$

$$(1 \leq i \leq 32)$$

This process eliminates the chopper offset. The advantage of using the three sets (S_{ij-2}, S_{ij-1} and S_{ij}) instead of just two (S_{ij-1} and S_{ij}) is that this eliminates the effect of a steady drift, if one were present. No noise has been included in the above analysis, so P_{ij} has no dependence on j.

The problem now is to determine the phase and amplitude of the cosine wave (if any) in the 32 values P_{ij}, and the value of the constant part of the P_{ij}. This is done by a form of digital phase-sensitive detection. The phase is unknown, so one cannot 'phase up' as one might with an electronic PSD. Instead, the phase-sensitive detection is done twice, the second time 90^{o} out of phase with the first. It will be shown that adding the results gives the required value.

Let the continuous function $P(\phi)$ be the ADC output signal (Eqn.(6-2)):

$$P(\phi) \simeq \frac{1}{0.00225}\left[\frac{G}{\pi}\left[IT_{\perp}-IpT_{\perp}\cos\{2(\theta-\phi)\}\right]\right].$$

The first 'phase-sensitive detection' is carried out by summing the first 16 P_{ij} and subtracting the next 16 to give the sum B_1. Therefore

$$B_1 \frac{\pi}{32} \simeq \int_{\phi_o}^{\phi_o+\frac{\pi}{2}} P(\phi)\, d\phi - \int_{\phi_o+\frac{\pi}{2}}^{\phi_o+\pi} P(\phi)\, d\phi$$

$$= -\frac{2GI_pT_{\perp}}{0.00225\pi}\sin\{2(\theta-\phi_o)\}$$

(ϕ_o is the polarizer position angle at the start of the set.)

The second 'phase-sensitive detection' is carried out by summing the first 8 and last 8 P_{ij} and subtracting the middle 16 to give the sum B_2. Therefore

$$B_2 \frac{\pi}{32} \simeq \int_{\phi_o}^{\phi_o+\frac{\pi}{2}} P(\phi)\, d\phi + \int_{\phi_o+\frac{3\pi}{4}}^{\phi_o+\pi} P(\phi)\, d\phi - \int_{\phi_o+\frac{\pi}{4}}^{\phi_o+\frac{3\pi}{4}} P(\phi)\, d\phi$$

$$= -\frac{2GI_pT_{\perp}}{0.00225\pi}\cos\{2(\theta-\phi_o)\}$$

Squaring and adding the results removes the dependence on θ and ϕ_o:

$$\frac{\pi}{32}\sqrt{B_1^{\,2}+B_2^{\,2}} \simeq \frac{2GI_pT_{\perp}}{0.00225\pi},$$

and hence I_p can be determined:

$$I_p \simeq \frac{0.00225\pi\sqrt{B_1^{\,2}+B_2^{\,2}}}{2GT_{\perp}} \times \frac{\pi}{32}.$$

The polarization angle is determined by dividing the two results

$$\frac{B_1}{B_2} \simeq \tan(2(\theta-\phi_o)) \ ,$$

$$\text{so} \quad \theta \simeq \phi_o + \tfrac{1}{2}\tan^{-1}\left[\frac{B_1}{B_2}\right] \ .$$

The value of I is found by averaging P_{ij} over $1 \leq i \leq 32$ to give M, which approximates to integrating $P(\theta)$ between ϕ_o and $\phi_o+\pi$ and dividing by $\frac{\pi}{32}$.

$$\frac{\pi}{32}M \simeq \int_{\phi_o}^{\phi_o+\pi} P(\phi)\, d\phi$$

$$= \frac{G}{0.00225\pi}\left[IT_\perp\phi+\tfrac{1}{2}I_pT_\perp\sin\{2(\theta-\phi)\}\right]_{\phi_o}^{\phi_o+\pi}$$

$$= \frac{G}{0.00225}\ IT_\perp \ .$$

Thus $$I \simeq \frac{0.00225\pi M}{32GT_\perp} \ .$$

The proportion of linearly polarized radiation is therefore

$$p = \frac{I_p}{I} \simeq \frac{\sqrt{B_1^{\,2}+B_2^{\,2}}}{2M} \times \pi \ .$$

The polarization angle ϕ_o can either be calculated from a knowledge of the analyser position, or can be determined by measuring a strongly polarized source with known position angle.

Chapter 7. Observations and Interpretation

7-1 Introduction

The author started his research project in 1975, and at that time the Imperial College 41" balloon-borne far-infrared telescope was under construction. The UK Stabilised Balloon Platform (SBP) was also nearing completion by Marconi for delivery to the Science Research Council's Appleton Laboratory, who were to operate the platform. The SBP was specified and designed to have arc-second pointing accuracy, and the ICST telescope and associated instrumentation were designed to be mounted on the platform. The SBP would thus provide target acquisition and tracking for the astronomical observing programme.

The first flights of the telescope and the SBP were expected to take place in 1976, to be followed by a regular series of flights from then on. The first flights took place from Palestine, Texas in November and December 1976 and are described by Sugden (1976). Details of the telescope are to be found there, as well as in Joseph et al. (1977).

The polarimeter, and a Fabry-Perot interferometer built by M.F. Kessler (1980), were intended for use on the next series of flights. However, the SBP failed to function on the 1976 flights and further flights had to be postponed until the SBP could be made ready. The next flight with the Imperial College telescope did not take place until December 1979, on which occasion the SBP again failed to function.

In the meantime, the polarimeter was under construction and it was decided to modify it for ground-based observations at 10μ wavelength, using the Infrared Flux Collector (IRFC) in Tenerife. This would fulfil the following objectives:

1. To test the performance of the polarimeter.

2. To provide the author with valuable experience of using the

polarimeter, as well as experience of making astronomical observations.

3. To make new polarimetric observations at the shorter infrared wavelength of 10μ. The polarimeter itself was easily adaptable for use at 10μ, since it required merely the replacement of a far-infrared analyser with one designed for the 10μ region, and it incorporated an internal chopper.

7-2 The Tenerife 1.5m Flux Collector

Tenerife is one of the Canary Islands situated off the West Coast of Africa, and is a part of Spain. The observatory at Izaña is sited 2380m above sea level at latitude $+28^{\circ}17'32''$N and longitude $16^{\circ}29'45''$W. The largest telescope at the observatory is the 1.5 metre Infrared Flux Collector (IRFC) which is funded by the UK Science Research Council.

The IRFC is a yoke-mounted telescope with manual slewing. At the f/13.8 Cassegrain focus, the effective focal length is 21.0m, and the plate scale is $10''$ per m.m. Images $\lesssim$ 2 arcsec are obtained under good observing conditions.

Amongst the facilities at the site is a Data General NOVA mini-computer with a CAMAC crate and a range of I/O devices. The computer is intended to be used for data acquisition with a certain amount of real time analysis, control of user instruments (via CAMAC), and preliminary off-line data reduction.

7-3 Tenerife Observing Trips

A total of four observing trips were made to Tenerife to carry out a programme of 10μ polarimetry. Unfortunately, none of them were at the most favourable time of the year (June and July) so bad weather was a continual problem. On the first three trips, the observing time was

shared between the polarimeter and M.F. Kessler's interferometer. The fourth trip was entirely devoted to polarimetry and is analysed in more detail than the other three.

Trip 1 December 2nd - December 16th 1977

This trip was a useful introduction to the IRFC, and to the many difficulties arising from using a telescope that is 2000 miles from base. Problems were encountered with the analyser rotation when the polarimeter was cooled to cryogenic temperature. This was solved by enlarging the bearing holders. Subsequently, the dewar was found to have a leak, but faulty pumping apparatus on site made leak detection difficult. In the two-week period, the weather was only suitable for observations on four nights.

Trip 2 April 28th - May 12th 1978

In addition to work with the polarimeter and the interferometer on this trip, a programme of infrared photometric observations, done simultaneously with observers in other wavelengths and the International Ultraviolet Explorer satellite, was carried out. Problems with a leak round the edges of the dewar window were temporarily cured with vacuum sealant. A probable detection of W Hya was made with the polarimeter. However, high winds and dust in the atmosphere made observing very difficult. It was found that there was a large chopper offset with the polarimeter which tended to saturate the amplifiers and phase-sensitive detector. This time, eight out of the fourteen nights were suitable for observations.

Trip 3 October 13th - October 24th 1978

On the 17th October, signals were recorded when scanning across the moon with the polarimeter which provided the first astronomical confirmation that it was operating properly. The following night α Ori and

Omi Cet were detected. However, the liquid helium supply then ran out when the next consignment, ordered in the usual way, failed to arrive and no 10μ polarimetry could be done thereafter.

One night was spent doing polarimetry at short wavelengths using a nitrogen-cooled photometer. However, the instrumental polarization was about 6% as the system, put together on the spot, included two 45^{o} mirrors. Nevertheless, the BN object was detected and its polarization was measured. These observations are discussed further in Section 7-7.

Trip 4 Februrary 23rd - March 16th 1979

The whole of this observing trip was devoted to polarimetry. However, out of a possible 21 nights, polarimetry was possible only on $4\frac{1}{4}$ of them. An analysis of the three-week period is given in Table 7-1. At this time of year, an average of 64% of the nights are suitable for making observations and this trip was no exception. However, the bad weather included 6" of snow and an electrical storm which put the telescope encoders, the oscilloscope and the telescope out of action.

This trip was plagued by IRFC instrumentation problems, the principal difficulty being a computer failure - the Nova was "down" for half the time. The fundamental reason for this was the absence of technical support for the Nova and its peripherals out in Tenerife. There had been problems with the computer system for several weeks before our arrival at the observatory, and it was only after a considerable amount of inexpert repair work that it was finally in a useable state. For most of the time, the fast paper-tape punch was inoperative and raw data had to be printed onto paper by the teletype. Consequently, several weeks of work were involved back in London, simply typing this data into the computer for re-analysis.

Table 7-1

Analysis of Trip 4 February 23rd-March 16th 1979

	OBSERVING		CAUSES OF FAILURE TO OBSERVE			
Night	Polarimetry	Photometry	Computer Failure	Weather	Lack of Helium	Power Failure
1		½	1			
2			1			
3			1			
4		1	1			
5		1	1			
6		1	1			
7	½		½	½		
8	1					
9	½					½
10					1	
11	¼				¾	
12	1					
13	1					
14			1	1		
15			1	1		
16			1			
17			1	1		
18				1		
19				1		
20				1		
21				1		
TOTALS	4¼	3½	10½	7½	1¾	½

(Figures are number of nights)

Notes

1. On some nights, observations were not possible for more than one reason.

2. It was possible to do photometry and to check the photometric performance of the instrument without the computer. However, the computer was necessary for polarimetric work.

3. The liquid helium failed to arrive on the date for which it was ordered.

4. In general, in the event of a power failure, the on-site generator can be used. However half a night was lost on one occasion when a power failure at the end of the pump-down meant that the pump-down procedure had to be repeated.

5. Numerous other problems such as inoperative vacuum pumps, unroadworthy vehicles, generator seizure etc., took their toll of time and energy but were not directly responsible for lost observing time.

7-4 Observing Procedure At Tenerife

A step-by-step account of the procedure for making polarimetric observations with our instrument at the 1.5m IRFC at Tenerife is given. It is assumed that the dewar is 'warm' to start with. The long cool-down phase makes it more efficient in terms of time and helium usage to maintain the dewar at liquid helium (LHe) temperature, and this was done as far as possible.

1. Pump down dewar, if possible overnight, to about 2×10^{-6} torr.

2. Pre-cool dewar with liquid nitrogen (LN_2) for $\sim$ 2 hours.

3. Fill with LHe. This first fill boils off relatively quickly ($\sim$ 4 hours) due to the comparatively large thermal mass of the polarimeter, some of which is in poor thermal contact (via ball bearings) with the LHe reservoir.

4. Refill with LHe.

5. Pump on the helium vapour with a rotary pump to bring the pressure over the LHe down to $\sim$ 10 torr and the LHe temperature down from its boiling point at 1 atmosphere of $4.2^{o}K$, to $\sim 1.7^{o}K$. This needs to be done reasonably slowly to avoid setting up thermo-acoustic vibrations in the LHe, and generally takes about one hour.

6. Set the telescope encoders by pointing the telescope at the zenith, using Sidereal Time to adjust the Right Ascension and the latitude of the observatory to adjust the Declination.

7. Load the computer programme.

8. Using a 1MΩ resistor across the input to the pre-amp as a calibrated noise source (Johnson noise of 127 $nVHz^{-\frac{1}{2}}$), a check can be made of the data analysis system.

9. Mount the dewar onto the telescope.

10. Focus a star that is bright both in the infrared and the visible on the centre of the dewar window.

11. Align the finder/guider telescope.

12. Focus the telescope back to the Fabry lens in the polarimeter.

13. Scan the telescope until the infrared signal is detected on the chart recorder.

14. The signal can then be "peaked-up" by scanning in RA and Dec, adjusting the focus, and adjusting the dewar position.

15. Check the rotation speed of the analyser.

16. Move the telescope onto the object to be observed and commence polarimetric observations.

Figure 7-1 shows the polarimeter dewar mounted on the IRFC at Tenerife. When observations were being made, the dewar was protected from stray light and air currents by a large metal shield, fastened to the instrument flange.

7-5 Ten-Micron Observations

An observing list of bright ten-micron sources was drawn up for each observing trip. Here, details are given of the 10μ measurements made on the fourth observing trip. Useful observations were made of six sources, all of which are dusty M-type stars.

7-5.1 α Ori

Alpha Orionis (Betelgeuse) is one of the strongest 10μ sources with a flux of 4800 Jy (Hall 1974). It is also very bright in the visible and this makes it a useful object upon which to set up, as it is easy to locate. However, its brightness means that flaring can impede guiding and increase noise. Forbes (1972) and Cox, Hough and McCall (1978)

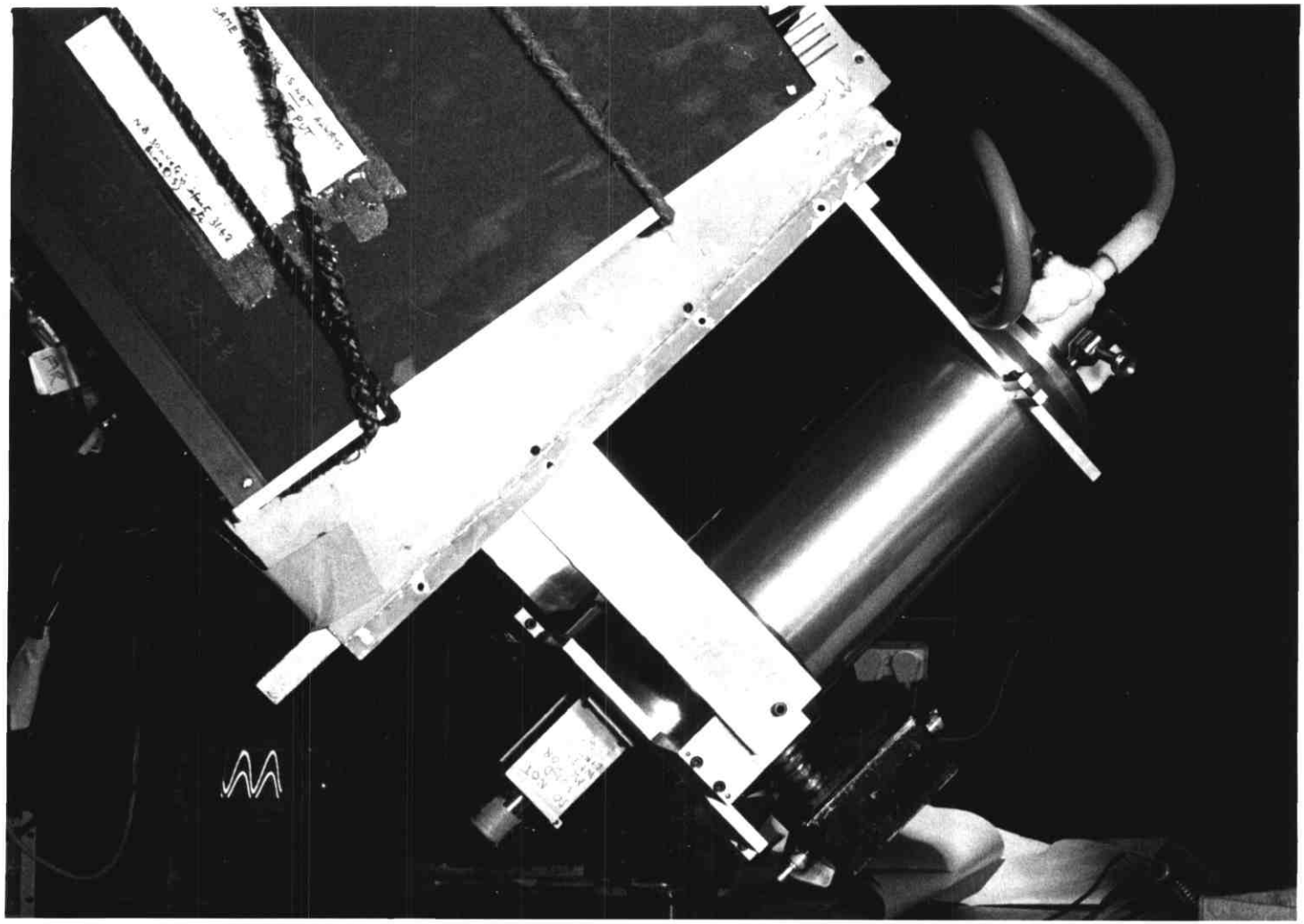

The Polarimeter Dewar At The Cassegrain Focus Of The IRFC

Fig 7-1

found only ± 0.2% polarization at short infrared wavelengths, but Capps and Dyck (1972) measured 10μ polarization of 1.3±0.3% at 12±7°.

In March 1979, we attempted 10μ polarization measurements on three nights. On the 3rd/4th and 4th/5th, power failure and LHe shortage curtailed the observations before significant results could be obtained. However, on the 6th/7th, 4 hours were spent on the object and three long runs were made. The third gave very poor results, probably a result of poor guiding, and the fact that the star was, by then, close to the horizon, and the seeing was degraded.

Table 7-2

Data on α Ori

Date	Run No.	Signal at Detector	S/N	Sets Processed	Sets Discarded	Polarization±1σ	Angle±1σ
3/4 March	1	2.2μV	84	11	1		
4/5 March	1	3.2μV	83	7	0		
6/7 March	1	4.5μV	135	23	11	3.0±0.6%	17±4°
6/7 March	2	4.7μV	203	20	13	2.5±0.9%	1.5±11°
6/7 March	3	3.7μV	72	54	15		

Combining the two measures of polarization we obtain

Polarization = 2.8±0.5%

Angle = 15±4°

7-5.2 α Sco

Alpha Scorpii (Antares) is another source that is bright both at infrared and optical wavelengths. Its 10μ flux is 2850 Jy (Hall 1974). Landau (1974) reports the following polarization measurements: 2.2μ - 6±4% at 50°, 3.5μ - 5±2% at 50°, 4.8μ - 4.5±1% at 60°, 10.6μ - 5±1% at 45°.

This star was observed on three nights and polarimetric data was obtained on the second and third.

Table 7-3

Data on α Sco

Date	Run No.	Signal	S/N	Sets Processed	Sets Discarded	Polarization±1σ	Angle±1σ
3/4 March	1	1.8μV	57	17	4		
3/4 March	2	2.3μV	114	14	15		
5/6 March	1	2.3μV	126	35	3	4.7±1.2%	78±15°
6/7 March	1	2.5μV	231	53	34	2.2±1.2%	36±12°

Combining the two measures of polarization, we obtain

Polarization = 3.45±0.9%

Angle = 52±9°

7-5.3 R Crt

Observations of R Crateris were made only on one night. It has an apparent visible magnitude of 10 and a 10μ flux of 480 Jy (Price and Walker 1976). Therefore it presents a small point image which aids guiding. It was noticeable that the signal-to-noise ratio for the photometry rose uniformly as the root of the integration time.

Table 7-4

Data on R Crt

Date	Signal	S/N	Sets Processed	Sets Discarded	Polarization±1σ	Angle±1σ
7/8 March	0.7μV	178	28	8	4.9±2.1%	10±10°

7-5.4 VY CMa

VY CMa is an irregular variable binary star, associated with a

reflection nebula. It is extremely bright in the infrared (10,300 Jy (Hall 1974)), and the circumstellar envelope is a source of intense OH, H_2O and SiO maser emission (Reid and Muhleman 1978). Shawl (1969) found strong visible polarization which changes from 5.6% at 126° at 0.94μ, to ∿ 22% at 185° at 0.36μ. Near-infrared polarimetry by Hashimoto et al. (1970), Forbes (1971b), Dyck, Forbes and Shawl (1971) and Maihara, Okuda and Sato (1972) all confirm a continued decline in percentage polarization and rotation of position angle with longer wavelength, with the exception of a small increase in polarization to ∿5% around 1.6μ. At 10μ, Capps and Dyck (1972) measured the polarization as 0.5±0.3% at 52±15°, which indicates a continuation of the shorter wavelength trend.

VY CMa was observed on 2 nights, but on the first, the run was too short to give polarimetric information.

Table 7-5

Data on VY CMa

Date	Signal	S/N	Sets Processed	Sets Discarded	Polarization±1σ	Angle±1σ
1/2 March	8.4μV	51	5	2		
2/3 March	6.6μV	73	28	5	0.9±1.2%	87±53°

The poor result can paradoxically be attributed to the extreme infrared brightness of VY CMa. Being only a 7th magnitude object in the visible, it is a little difficult to guide on. However, in the infrared the image will be considerably enlarged due to flaring and hence it is probable that the infrared image was spilling out of the 10" telescope beam, reducing the signal and increasing the noise.

7-5.5 W Hya

W Hya, with a 10μ flux of 3630 Jy (Hall 1974), was observed on two nights but, as for VY CMa, the first run was too short to yield polari-

metric information. On the second, the error on the position angle was very large - as would be expected if there is no detectable polarization.

Table 7-6

Data on W Hya

Date	Signal	S/N	Sets Processed	Sets Discarded	Polarization±1σ	Angle±1σ
1/2 March	2.2μV	71	11	0		
5/6 March	2.2μV	99	59	11	0.4±0.95	

7-5.6 R Hya

This was an easy star to observe, being favourably placed for observation for most of the second half of each night. It is moderately bright in both the visible (5th magnitude) and infrared (1550 Jy (Hall 1974)). Capps and Dyck (1972) observed it, but did not measure significant polarization (0.5±1.9%). A considerable amount of time was spent observing R Hya to try to establish a good upper limit for any instrumental polarization.

Table 7-7

Data on R Hya

Date	Run No.	Signal	S/N	Sets Processed	Sets Discarded	Polarization±1σ	Angle±1σ
2/3 March	1	1.1μV	121	37	3	4.5±1.4%	19±7
2/3 March	2	1.2μV	98	12	1		
3/4 March	1	0.9μV	129	28	12	0.5±2.5%	124±72
6/7 March	1	1.5μV	200	27	10	1.2±1.7%	40±26
6/7 March	2	1.3μV	102	15	8		

The spread of this data implies that it would not be valid to combine the three polarization measurements. Lowest weight should be

attached to the observation on the 3rd/4th March when observing conditions were poor with images flaring to 10 or 15". The large polarization seen on the 2nd/3rd March is a significant result, and it is a pity that it was not positively confirmed on subsequent nights (although it is not contradicted either).

7-5.7 A Note On The Treatment of Errors

In general, neither the percentage polarization nor the position angle have Gaussian probability distributions unless the signal-to-noise ratio is large. For small signal-to-noise ratios, the errors in polarization are one-sided as noise cannot give a negative result. The position angle has values only between 0 and 180° so that standard deviations of about 45° or more imply that the measurement has little meaning. Wardle and Kronberg (1974) show that for a measured polarization $p' \pm \sigma'$, the true value p is given by

$$p \sim p' \left[1 - \left(\frac{\sigma'}{p'} \right)^2 \right]^{\frac{1}{2}} \quad \text{and} \quad \sigma \sim \sigma'$$

when $p/\sigma > 0.5$ (i.e. when $p'/\sigma' > 1.2$). For $p/\sigma < 0.5$, $p'/\sigma' \sim 1$. Thus the measured value of the polarization will be an over-estimate of the true value, and if the measured signal-to-noise ratio is near unity, the statistical error should be regarded as a 1σ upper limit. In table 7-8 the 10μ polarization results have been written in this way. The measured position angle will be an unbiased estimate of the true position angle, although Wardle and Kronberg show that for small signal-to-noise ratios, the statistical error may be an underestimate of the true error.

7-5.8 Summary of 10μ Polarization Results

The 10μ polarization measurements have been corrected using the formulae of section 7-5.7 and are shown in Table 7-8.

The measurement of α Ori (2.8±0.5%) is significant at the 5σ level

and is twice as large as that measured by Capps and Dyck. However the position angle is in agreement with their result. The 4σ measurement of α Sco agrees with Landau's measurement to 1σ. R Crt has not previously been measured polarimetrically in the infrared and further observations would be useful to try to improve the 2σ result. The upper limit of VY CMa is in agreement with other measurements.

Table 7-8

Summary of 10μ Polarization Results*

	P ± σ	θ ± σ
α Ori	2.8±0.5%	15±4°
α Sco	3.3±0.8%	52±9°
R Crt	4.4±2.1%	10±10°
VY CMa	<1.2% (1σ)	-
W Hya	<1% (1σ)	-
R Hya	Inconsistent results	

* cf. Section 7-5.7

7-6 Instrument Performance

Despite the relatively small amount of time during which it was possible to use the polarimeter on the telescope, most of the instrumental parameters were determined. Tests in the laboratory, while useful, are sometimes limited in scope due to the problem of simulating the radiation background from the night sky and a point radiation source.

7-6.1 Detector Noise

The detector noise was measured to be $\sim 40\ n\,V\,Hz^{-\frac{1}{2}}$ with the tuning-fork chopper running, and the detector looking at the night sky.

This was consistent with noise measurements made in the laboratory. When the analyser is rotating, there is a large chopper offset which varies with analyser angle. However, the effects of this are eliminated by use of the offset bucking system (cf. section 5-13). With a responsivity of 0.5×10^{6} V/W, the Noise Equivalent Power (N.E.P.) of the detector is $\frac{\text{Noise}}{\text{Responsivity}} = 8 \times 10^{-14}\ \text{WHz}^{-\frac{1}{2}}$.

7-6.2 Guiding and Seeing Limitations

The tracking and nodding drifts of the IRFC are large enough that constant manual guiding is required. Poor guiding will result in a lower signal-to-noise ratio than would be expected from consideration of detector noise alone. Unlike electronic noise, whose instantaneous fluctuations may increase as well as decrease the signal, guiding errors will only degrade it.

Poor seeing conditions exacerbate the guiding problem. The telescope image in good seeing is $\lesssim$ 2 arcsec, much less than the 10 arcsec beam size we employed for these measurements. However poor seeing will increase the size of the visible (guiding) and infrared (signal) images by factors up to 10x. This not only makes guiding more difficult, it makes it much more critical since the infrared image can now easily spill over the focal plane diaphragm. Flaring and short-term variations on time-scales $\sim$ 30 seconds, the time taken for one measurement cycle, are especially serious since they will introduce signal variations which can be indistinguishable from those due to polarization.

To investigate the possible influence of these effects, the following analysis of the noise present during various polarimetry measurements was made.

Suppose the noise during the run is N volts $\text{Hz}^{-\frac{1}{2}}$ at the detector, the photometric signal at the detector is S volts, and n independent samples are taken (the samples are independent if the sampling interval

$\geq$ 4 RC). Then after n independent samples have been integrated, the signal-to-noise ratio, R, is given by $R = \frac{S\sqrt{n}}{N}$. Alternatively, if R and S are known, a mean value for the noise can be calculated from

$$N = \frac{S\sqrt{n}}{R} .$$

This was used to calculate the noise for the results listed in section 7-5. The value of RC was 0.4 secs, and thus 4 RC = 1.6 secs. Hence in a set of 32 samples, which lasted 36 seconds, there were only 22.5 independent samples. The mean noise values obtained are given in Table 7-9.

Object	Date	Run No.	Signal at Detector	S/N	No.of independent samples.	Mean Noise
α Ori	3/4 March	1	2.2μV	84	247.5	410nVHz$^{-\frac{1}{2}}$
	4/5 March	1	3.2μV	83	157.5	480nVHz$^{-\frac{1}{2}}$
	6/7 March	1	4.5μV	135	517.5	760nVHz$^{-\frac{1}{2}}$
	6/7 March	2	4.7μV	203	450	490nVHz$^{-\frac{1}{2}}$
	6/7 March	3	3.7μV	72	1215	1800nVHz$^{-\frac{1}{2}}$
α Sco	3/4 March	1	1.8μV	57	382.5	620nVHz$^{-\frac{1}{2}}$
	3/4 March	2	2.3μV	114	315	360nVHz$^{-\frac{1}{2}}$
	5/6 March	1	2.3μV	126	787.5	510nVHz$^{-\frac{1}{2}}$
	6/7 March	1	2.5μV	131	1192.5	660nVHz$^{-\frac{1}{2}}$
R Crt	7/8 March	1	0.7μV	178	630	100nVHz$^{-\frac{1}{2}}$
VY CMa	1/2 March	1	8.4μV	51	112.5	175nVHz$^{-\frac{1}{2}}$
	2/3 March	1	6.6μV	73	630	2270nVHz$^{-\frac{1}{2}}$
W Hya	1/2 March	1	2.2μV	71	247.5	490nVHz$^{-\frac{1}{2}}$
	5/6 March	1	2.2μV	99	1327.5	810nVHz$^{-\frac{1}{2}}$
R Hya	2/3 March	1	1.1μV	121	832	260nVHz$^{-\frac{1}{2}}$
	2/3 March	2	1.2μV	98	270	200nVHz$^{-\frac{1}{2}}$
	3/4 March	1	0.9μV	129	630	175nVHz$^{-\frac{1}{2}}$
	6/7 March	1	1.5μV	200	607.5	180nVHz$^{-\frac{1}{2}}$
	6/7 March	2	1.3μV	102	337.5	230nVHz$^{-\frac{1}{2}}$

Table 7-9

Noise during 10μ observations

The large variations seen in Table 7-9 are best explained by guiding and seeing differences. The lowest mean noise was obtained on the 7th/8th March when, for the observations of R Crt, the noise averaged 100 n V $Hz^{-\frac{1}{2}}$. At the other extreme, during polarimetry of the very bright infrared source VY CMa, the mean noise was 2270 n V $Hz^{-\frac{1}{2}}$. Such a large noise was exceptional and is best explained by the problems of guiding on such a bright infrared source which is very faint in the visible (cf. Section 7-5.4).

7-6.3 Boil-Off Rate

For the initial LHe fill, the boil-off rate is very high and 1.7ℓ of helium boils off in ∿ 4 hours. However, the second fill of LHe lasts ∿ 13 hours, which is sufficient for a night's observing. This hold-time is independent of whether the analyser is rotated during that period, and whether the helium vapour is pumped, or left at atmospheric pressure. However, tilting the dewar over to look at high elevation stars did have a significant detrimental effect on hold-time, and it was found to be unwise to tilt the dewar past ∿ 75° from the vertical.

The 13-hour hold-time implies a heat input to the dewar of ∿ 85mW, and this arises from three sources:

1. Thermal conduction along the stainless steel support wire, the constantin wires providing the electrical connections and the dewar neck tube.

2. Thermal radiation (293°K) entering through the dewar window and the hole in the nitrogen shield.

3. Thermal radiation (77°K) from the radiation shield and nitrogen can.

The heat input to the unmodified dewar was only 11mW and thus the extra heat input arises from the modifications made for the polarimeter.

The only extra path for thermal conduction is along the constantin wires which only provide a heat leak of ∿ 1mW each. The principal extra heat input is from source 2 above. The hole in the nitrogen shield is ∿ 1.2cm in diameter, and a black body of this size at 293°K would emit 47mW. We can thus account for about three-quarters of the 85mW heat input.

7-6.4 Instrumental Polarization

Instrumental polarization may arise from features of both the polarimeter and the telescope. It is possible to subtract out its effects (cf. Section 7-7), but this is inconvenient and may limit the instrument's accuracy. This polarimeter was designed to minimise instrumental polarization, and when in use at Tenerife, there are no off-axis reflections.

Measurement of the instrumental polarization is very difficult to do in the laboratory. It requires either an unpolarized infrared source, or a source for which the polarization is accurately determined. With this polarimeter and the integral tuning-fork chopper, measurement of a source which is larger than a few arcseconds is very difficult. If one attempts to use an external chopper, the small vibrations of the tuning-fork chopper will

a) have a natural frequency of 20Hz and may beat with the external chopper

b) be a source of extra detector noise.

The most straightforward method of measuring the instrumental polarization is to carry out polarimetry of an unpolarized star. In the absence of many 10μ polarization measurements, so that guaranteed unpolarized sources may not be available, an alternative strategy is to measure a number of sources that can reasonably be expected to be unpolarized. An average is then taken of the normalised Stokes parameters of the polarization measurements. This should give the instru-

mental polarization, providing account has been taken of any rotation of the instrument for the different sources.

A further, and more classical, method is to rotate the polarimeter. On a telescope with a non-equatorial mount, this will effectively occur during the night.

Unfortunately, the small amount of clear, working telescope time with the polarimeter did not allow sufficient observations to make a good measurement of the instrumental polarization. One would expect that the instrumental polarization should be negligible because of the polarimeter design, and there were no indications to the contrary. Cox, Hough and McCall (1978) give the instrumental polarization of the 1.5m Flux Collector as .08±.04% at 0.9μ, .05±.04% at 1.25μ, .09±.05% at 1.6μ and .03±.03% at 2.2μ. It thus seems likely that at 10μ, the instrumental polarization due to the telescope will be less than 0.1%. Summing the normalised Stokes parameters for the nine recorded 10μ polarization measurements for which a position angle was found, gives a mean of $\sim$ 1.5% at 26^{o}. However, the sample of stars is not large enough to allow much weight to be attached to this result.

7-6.5 Instrument Sensitivity and Transmission

The performance of the polarimeter can be compared with the design performance quoted in 5-14. There, it was estimated that the minimum flux for which 1% polarimetry at the 3σ level can be achieved in 2 hours observing is 70 Jy. If a polarization measurement on a J Jansky source of $p\pm\varepsilon$% is made in t minutes, then this is equivalent to doing 1% polarimetry at the 3σ level in 2 hours on a source of flux

$$J \times \frac{t}{120} \times 3\varepsilon \quad Jy \ .$$

The 'best' of the 10μ measurements by this criterion is the one of

R Crt, the faintest source observed, for which a result of 1600 Jy is obtained applying the above formula. The 'worst' measurement, on VY CMa, gives a result of 19,600 Jy. Clearly a bright source is not necessarily more favourable to observe than a faint one.

The factor of ~ 25 difference between the design performance and the best performance in practice can be attributed to:

1) Greater noise - detector, background, etc.,
2) Non-optimum 'seeing',
3) Guiding error,
4) Lower transmission and responsivity than predicted.

The overall transmission, t_r, of the polarimeter and telescope can be obtained by considering the detector signal, S volts, from a star of known flux. A source of strength J Jansky gives rise to a signal at the detector of $Jx10^{-26}xA\Delta\nu t_r R_{20} x\frac{1}{\pi}$ volts where A m^2 is the area of the primary, $\Delta\nu$ Hz is the passband of the filters, and R_{20} volts/watt is the 20 Hz responsivity of the bolometer. (The factor $\frac{1}{\pi}$ allows for sine-wave chopping.) Thus

$$t_r = \frac{S\pi}{Jx10^{-26}A\Delta\nu R_{20}}$$

Now $R_{20} \simeq 0.5x10^6$ V/W, $\Delta\nu = 6.2x10^{12}$ Hz (10.25μ to 13μ) and $A \simeq 1.7m^2$ at Tenerife. The values for the overall transmission are shown in the table below, where the detector signal used is the largest obtained for that object.

Table 7-10

Estimates of the Overall Transmission

Star	α Ori	α Sco	R Crt	VY CMa	W Hya	R Hya
Flux (Jy)	4800	2850	480	10,300	3630	1550
Detector Signal(μV)	4.7	2.5	0.7	8.4	2.2	1.5
Transmission	0.058	0.052	0.087	0.049	0.036	0.058

Since the R Crt measurement was obtained only on a single night, and its flux is obtained from the AFGL catalogue (unlike the other stars whose flux is quoted in the 10μ catalogue), it is perhaps less reliable than the other measurements. Thus, the overall transmission of the instrument and telescope can be estimated as ~ 0.055. This is a factor of ~ 3 below the figure of 0.17 derived in Section 5.10. The likely reasons for this discrepancy include:

a) Reduced reflectance of the primary and secondary mirrors as a result of deterioration of their surfaces,

b) Less-than-perfect absorption efficiency of the bolometer,

c) Less-than-perfect atmospheric transmission during the observations, and

d) Guiding errors and large seeing discs.

Factors c) and d) probably account for the variations between the calculated values for the transmission, although the 10μ catalogue values are only averages of several measurements and thus are not completely accurate. In addition, the stars may be variables in the infrared as several are known to be visual variables.

The instrumental problems and the weather on the final observing trip meant that only a relatively small number of polarimetric observations could be made. With more time, giving an opportunity to make further observations of such sources as R Crt, it is likely that the measured 'Detection Limit' of 1600 Jy could have been reduced by at least a factor of 2.

7-7 Short Wavelength Measurements

In the absence of liquid helium, the night of the 24th/25th October 1978 was spent attempting to do short-wavelength polarimetry using a nitrogen cooled photometer. Measurements were made in three wavelength

bands - K(2.2μ), L(3.4μ) and M(4.8μ), on 6 sources, the first three of which were expected to be unpolarized.

The instrumental arrangement is shown in Fig.7-2. The infrared beam undergoes two 45° reflections at the mirrors of a two-mirror vibrating chopper (Jorden et al. 1976) and then passes through an iris into the downward-looking dewar. This iris is not normally used for photometry. However, it neatly holds a KRS-5 analyser (Cambridge Physical Sciences IGP22), and by loosening the retaining screws, the iris can be rotated. A scale was fixed to the baseplate, allowing the position of the analyser to be ascertained to ±5°. For each object and for each filter, the analyser was set at a particular position, and a scan through the object was made to determine the relative flux. This was repeated for at least a further two positions of the analyser.

If an object's radiation is partially polarized, one expects the fully polarized part of the flux, measured by the photometer, to be a $\cos^2$ function of analyser angle ϕ. If we suppose the analyser has zero transmittance for radiation polarized parallel to the wires, and transmittance $T_\perp$ for radiation polarized perpendicularly to the wires, then the Mueller matrix for the analyser is

$$\tfrac{1}{2}\begin{bmatrix} T_\perp & -T_\perp\cos 2\phi & -T_\perp\sin 2\phi & 0 \\ -T_\perp\cos 2\phi & T_\perp\cos^2 2\phi & \tfrac{1}{2}T_\perp\sin 4\phi & 0 \\ -T_\perp\sin 2\phi & \tfrac{1}{2}T_\perp\sin 4\phi & T_\perp\sin^2 2\phi & 0 \\ 0 & 0 & 0 & 0 \end{bmatrix} \qquad (2\text{-}12)$$

If the radiation incident on the analyser has Stokes Parameters

$$\begin{bmatrix} I \\ Ip\cos 2\theta \\ Ip\sin 2\theta \\ 0 \end{bmatrix}$$

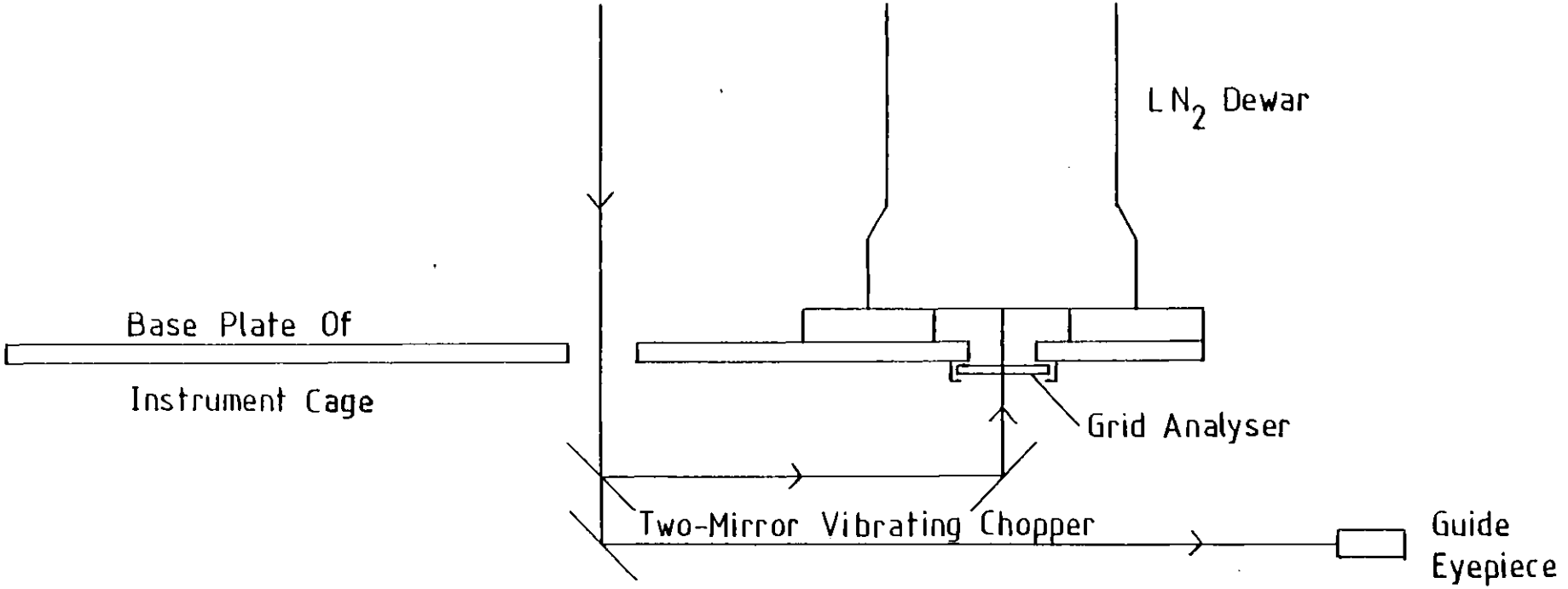

Near-Infrared Polarization Arrangement

Fig 7-2

the emergent flux will have intensity

$$\tfrac{1}{2}IT_{\perp}\left(1 - p\cos[2(\theta-\phi)]\right)$$

$$= \tfrac{1}{2}IT_{\perp}(1-p) + IT_{\perp}p\cos^2(\theta-\phi)$$

There are three unknowns in this expression, and hence they can be determined by making a minimum of 3 observations at three different analyser positions. Let three such positions be ϕ_1, ϕ_2 and ϕ_3, and the fluxes measured at these three positions be F_1, F_2 and F_3.

Then $F_i = a - b\cos\ 2(\theta-\phi_i)$ for $i = 1,2,3$ where $a = \tfrac{1}{2}IT_{\perp}$ and $b = \tfrac{1}{2}IT_{\perp}p$. These three equations can be solved giving

$$\tan 2\theta = \frac{(F_3-F_2)\cos2\phi_1 + (F_1-F_3)\cos2\phi_2 + (F_2-F_1)\cos2\phi_3}{(F_2-F_3)\sin2\phi_1 + (F_3-F_1)\sin2\phi_2 + (F_1-F_2)\sin2\phi_3},$$

$$b = \frac{F_1-F_2}{\cos2(\theta-\phi_2) - \cos2(\theta-\phi_1)},$$

$$\text{and}\quad a = \frac{F_1 + (F_1-F_2)\cos2(\theta-\phi_1)}{\cos2(\theta-\phi_2) - \cos2(\theta-\phi_1)}.$$

$$\text{Hence}\quad I = \frac{2a}{T_{\perp}} \quad \text{and} \quad p = \frac{b}{a}$$

Thus, three measurements are sufficient to derive the polarization. However, estimation of the error is difficult if only this minimum number of measurements is made. Shortage of time allowed extra measurements to be made only on three of the objects. It can be seen from the results below that there is fairly good consistency, and the polarization measurements are probably good to ±1% with the angles good to $\pm5^{\circ}$.

In the results below, numbers in brackets indicate the number of different analyser positions used. If more than three positions were used, several sets of 3 have been used, and an average taken to give the figures shown.

Table 7-11

Short-Wavelength Polarization Data

χ Cet - an FO-type star

K (2.2μ)	6%	at	90°	(3)
L (3.4μ)	3.5%	at	104°	(3)
M (4.8μ)	Insufficient signal			

α Aur - a GO-type star

K (2.2μ)	6%	at	91°	(5)
L (3.4μ)	6.5%	at	89°	(5)
M (4.8μ)	6.7%	at	87°	(5)

α Ori - an MO-type star

K (2.2μ)	No data taken			
L (3.4μ)	4%	at	83°	(3)
M (4.8μ)	6%	at	87°	(3)

BN source (in M42) - a hot object embedded in a dust cloud

K (2.2μ)	16.4%	at	104°	(5)
L (3.4μ)	10.3%	at	99°	(5)
M (4.8μ)	9.8%	at	94°	(5)

NGC 1068 - a Seyfert Sb galaxy

K (2.2μ)	6.5%	at	105°	(5)
L (3.4μ)	Insufficient signal			
M (4.8μ)	Insufficient signal			

Saturn's rings at edge of disk

K (2.2μ)	9.2%	at	102°	(3)

Saturn's rings at centre of disk

K (2.2μ)	4.6%	at	91°	(3)

It is clear from these results that there is a large instrumental polarization - about 6% at 90^{o}. This is not unexpected as there are two 45^{o} reflections in the beam path. The line joining the two mirrors is always North-South, and thus the instrumental polarization will be perpendicular to this because the reflection coefficient for the sine-wave (polarized in this case in an East-West direction) is greater than that for the p-wave (Appendix II). The chopper mirrors are made of glass, but are coated with a thin gold layer to reflect infrared radiation but transmit visible radiation.

Azzam and Bashara (1977) give the visible reflectivities at a gold-air surface at 45^{o} as $R_s = 0.86$, $R_p = 0.76$ for light of wavelength 5461Å. Thus the reflected light will be 6% polarized. We may use the formula derived in Appendix II to make a theoretical estimate of

$$P_r = \sqrt{\frac{\nu}{\sigma}} \left[\frac{1}{\cos i} - \cos i \right],$$

$\nu = 10^{14}$ (at $\lambda = 3\mu$), $i = 45^{o}$, $\sigma = 10^{17}$ (p614 Born and Wolf 1975), so $P_r = 2.2\%$. However, Born and Wolf noted that the value of σ is only reliable for longer wavelengths ($\lambda \gtrsim 10\mu$).

The above discussion shows that the measured value of $\sim$ 3% for each mirror is reasonable. A more detailed discussion would not be worthwhile, as the gold coatings were several years old, and thus results obtained for fresh, clean gold coatings would not necessarily be applicable.

Using the matrix (2-13), and assuming that any birefringence (causing linear to circular conversion) can be neglected, we can construct a Mueller matrix for the chopper.

Putting $T_r = 1$, $i = 0.06$ and $\phi = 90^o$, the Mueller matrix is

$$\begin{bmatrix} 1 & -0.06 & 0 & 0 \\ -0.06 & \frac{1}{2}(1.06 - 0.94)^2 + 1-0.06^2 & 0 & 0 \\ 0 & 0 & 1-0.06^2 & 0 \\ 0 & 0 & 0 & 1-0.06^2 \end{bmatrix}$$

$$= \begin{bmatrix} 1 & -0.06 & 0 & 0 \\ -0.06 & 1 & 0 & 0 \\ 0 & 0 & 0.998 & 0 \\ 0 & 0 & 0 & 0.998 \end{bmatrix} \qquad (7\text{-}1)$$

By writing the Stokes vector for the measured polarization for each of the observed objects at each wavelength, and pre-multiplying by the inverse of the above matrix, the Stokes vector for the radiation from each source is obtained, corrected for instrumental polarization.

The inverse of matrix (7-1) is

$$\begin{bmatrix} 1.0036 & 0.0602 & 0 & 0 \\ 0.0602 & 1.0036 & 0 & 0 \\ 0 & 0 & 1.002 & 0 \\ 0 & 0 & 0 & 1.002 \end{bmatrix} \qquad (7\text{-}2)$$

The Stokes vector of the measured polarization for the BN object at K is

$$\begin{bmatrix} 1 \\ 0.164\cos 208^o \\ 0.164\sin 208^o \\ 0 \end{bmatrix} = \begin{bmatrix} 1 \\ -.1448 \\ -.0770 \\ 0 \end{bmatrix}$$

and pre-multiplying by (7-2), we obtain

$$\begin{bmatrix} 0.995 \\ -0.0851 \\ -0.00771 \\ 0 \end{bmatrix}$$

which corresponds to a polarization of 11.5% at 111°.

Using the same procedure, the results for the BN object, NGC 1068 and Saturn's rings at the edge of the disk are

BN object

K	11.5%	at	111°
L	5%	at	110°
M	4.9%	at	110°

NGC 1068

K	3.3%	at	138°

Saturn's rings at the edge of the disk

K	4.5%	at	119°

It is emphasized that the above data result from a very quick trial experiment conducted on only one night. The small quantity of data makes it difficult to assign error bars to the above values. However, the photometry measurements on a particular object have a 1σ accuracy of $\sim$1% and so, taking into account the uncertainties of subtracting out instrumental polarization, the above polarizations can reasonably be expected to have 1σ error bars of ±2% with error bars on the polarization angle of $\pm 20^{\circ}$.

It is encouraging to note that the above measurements are fairly consistent with those of other observers (Table 7-12). Kemp *et al.*

(1978) found much less polarization of Saturn's rings at K, although they report 2.10±0.28% polarization at L.

Table 7-12

Short-Wavelength Measurements on Three Objects

Object	Observer	Wavelength	Polarization	Position Angle
BN	Rosen	K	11.5%	111°
		L	5%	110°
		M	4.9%	110°
	Breger & Hardorp (1973)	K	14.2±1.3%	115°
	Dyck et al. (1973)	L	7.4±0.6%	117°
		M	4.5±0.8%	63°
NGC 1068	Rosen	K	3.3	138°
	Lebofsky, Rieke & Kemp (1978)	K	3.6±0.3	116±2°
Saturn's rings	Rosen	K	4.5%	119°
	Kemp et al. (1978)	K	0.76±0.08%	

Chapter 8. Discussion and Interpretation of the Observations

8-1 Introduction

The results of the 10μ observations made at the IRFC in March 1979 are summarised in Table 7-8. The measured values have been corrected according to the formula in Section 7-5.7. All six stars are of spectral type M and their infrared emission originates from circumstellar dust. These 10μ observations show that the radiation from α Ori, α Sco and R Crt is polarized. For α Ori, the polarization is 2.8±0.5%, for α Sco it is 3.3±0.8%, and for R Crt it is 4.4±2.1%.

There are two alternative mechanisms which have been proposed to explain such stellar polarization. One is scattering by the dust grains. The circumstellar dust would need to be asymmetrically distributed, but this is quite likely as any stellar rotation would tend to concentrate the dust around the stellar equator. A further necessary condition is that the dust must have an appreciable scattering optical depth, and the value of this will depend on the wavelength as well as the particle size and composition.

Absorption by aligned grains has been suggested as a polarizing mechanism. However, there is no direct evidence for strong magnetic fields around these stars. Without this, conventional alignment mechanisms will not give rise to a sufficiently high degree of alignment to produce significant polarization (Elsässer and Staude 1978). Therefore, it seems preferable to explain polarization with a scattering model.

The most interesting of the six stars is VY CMa, in that there is fairly complete optical and near-infrared polarization data which shows large (22%) polarization at short wavelengths. The data from Dyck, Forbes and Shawl (1971) is shown in Fig.8-1. Clearly the null result is consistent with the previous observations, indicating that the scattering is by sub-micron size particles which become inefficient scatterers at

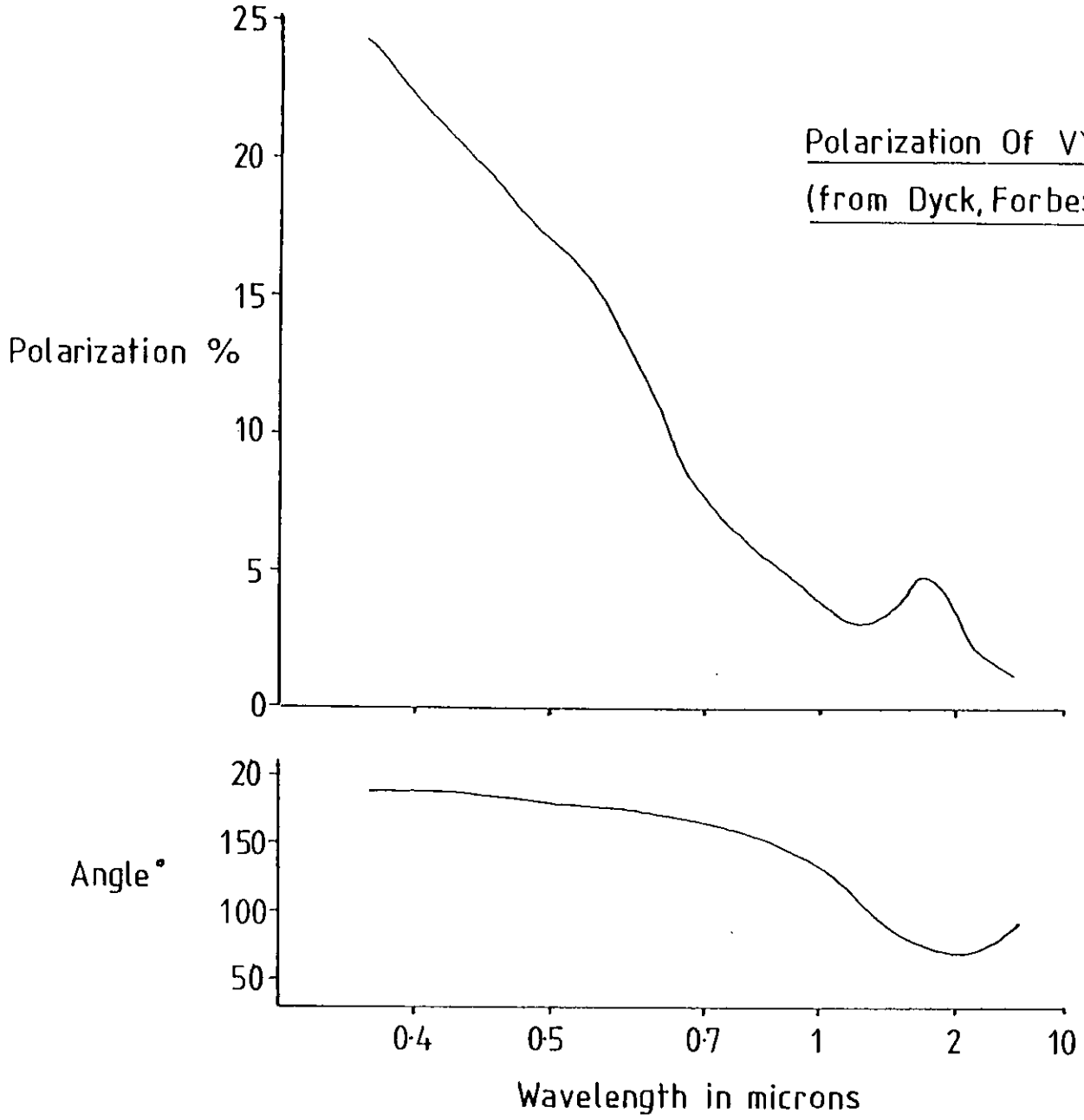
Polarization Of VY CMa
(from Dyck, Forbes and Shawl (1971))
Polarization %
25
20
15
10
5
0
Angle°
20
150
100
50
0·4
0·5
0·7
1
2
10
Wavelength in microns

Fig 8-1

longer wavelengths.

The positive results for α Ori and R Crt indicate that the dust around these objects includes particles of the order of 1μ in size. However, much smaller particles probably also exist around α Ori, as McMillan and Tapia (1978) find up to 6% polarization of blue light around the star.

The upper limit on W Hya is consistent with the optical polarization of 0.9% reported by Dyck et al. (1971). The positive detection for α Sco is in agreement with Landau (1974) who found 5±1% polarization at 45^{o} for 10.6μ.

Section 8-2 investigates how polarization may arise when radiation is scattered from a ring of dust around a star, and in Section 8-3, this is generalized to a star with a circumstellar dust shell. In Section 8-4, the results of 8-3 are compared with the observations to see if they can explain the measured polarizations.

8-2 Scattering Off An Equatorial Dust Ring

The observations of infrared excesses in some stars, and the presence of the 9.7μ silicate feature, indicate that these stars must be surrounded by dust. The short wavelength radiation from the star will be absorbed by the grains, whilst infrared radiation will be scattered by the grains and may thus become polarized.

In an extended scattering source, one would expect to see a variation in the position angle and percentage polarization across the source, because of the change of orientation of the scattering plane as seen by the observer. In a point source, it is necessary for some sort of asymmetric dust distribution to exist, for over a perfectly spherical shell of randomly-oriented grains, the net polarization will be zero.

One particular form of asymmetry that might be expected to exist is

that the dust shell may be oblate. Most stars will be rotating, and thus the dust shell would have some angular velocity which would concentrate the dust around the equator, and reduce the amount at the poles.

As a preliminary to calculating the polarization that might be expected from such an ellipsoid, the polarization that arises from scattering off an equatorial dust ring or disc will be derived. Of course this itself may have some useful applications as dust discs are known to exist round such familiar objects as Saturn and Uranus. It will be assumed that Rayleigh Scattering is operating, which requires $\lambda \geq 20a$ where a is the radius of the dust grain. Since interstellar dust is generally thought to have size $2a \sim 0.3\mu$ (p264 Allen 1973) this requirement is satisfied throughout the infrared.

Suppose the observer is a distance R from the star, n is the index of refraction of the dust grain, and H is the scattering angle. Then the intensity of the scattered light resolved into totally polarized components perpendicular and parallel to the plane of scattering (containing both the incident and the scattered wave) is

$$I_{\perp} = \frac{16\pi^4 a^6}{R^2\lambda^4}\left[\frac{n^2-1}{n^2+2}\right]^2$$

$$I_{\parallel} = \frac{16\pi^4 a^6}{R^2\lambda^4}\left[\frac{n^2-1}{n^2+2}\right]^2 \cos^2 (H)$$

for unit intensity of unpolarized incident radiation (p72 Lang 1974). At a given scattering angle (H), the polarization of the scattered radiation is $\frac{I_{\perp}-I_{\parallel}}{I_{\perp}+I_{\parallel}}$, which reduces to $\frac{\sin^2\theta}{1+\cos^2\theta}$ (equation 3-2).

In Fig.8-2, the point B on the dust ring subtends an angle ϕ at the star S with the projection onto the plane of the ring of the line from the observer O to the star. The dust ring is inclined at an angle θ, i.e. θ is the angle between the plane of the ring and the line OS. Then

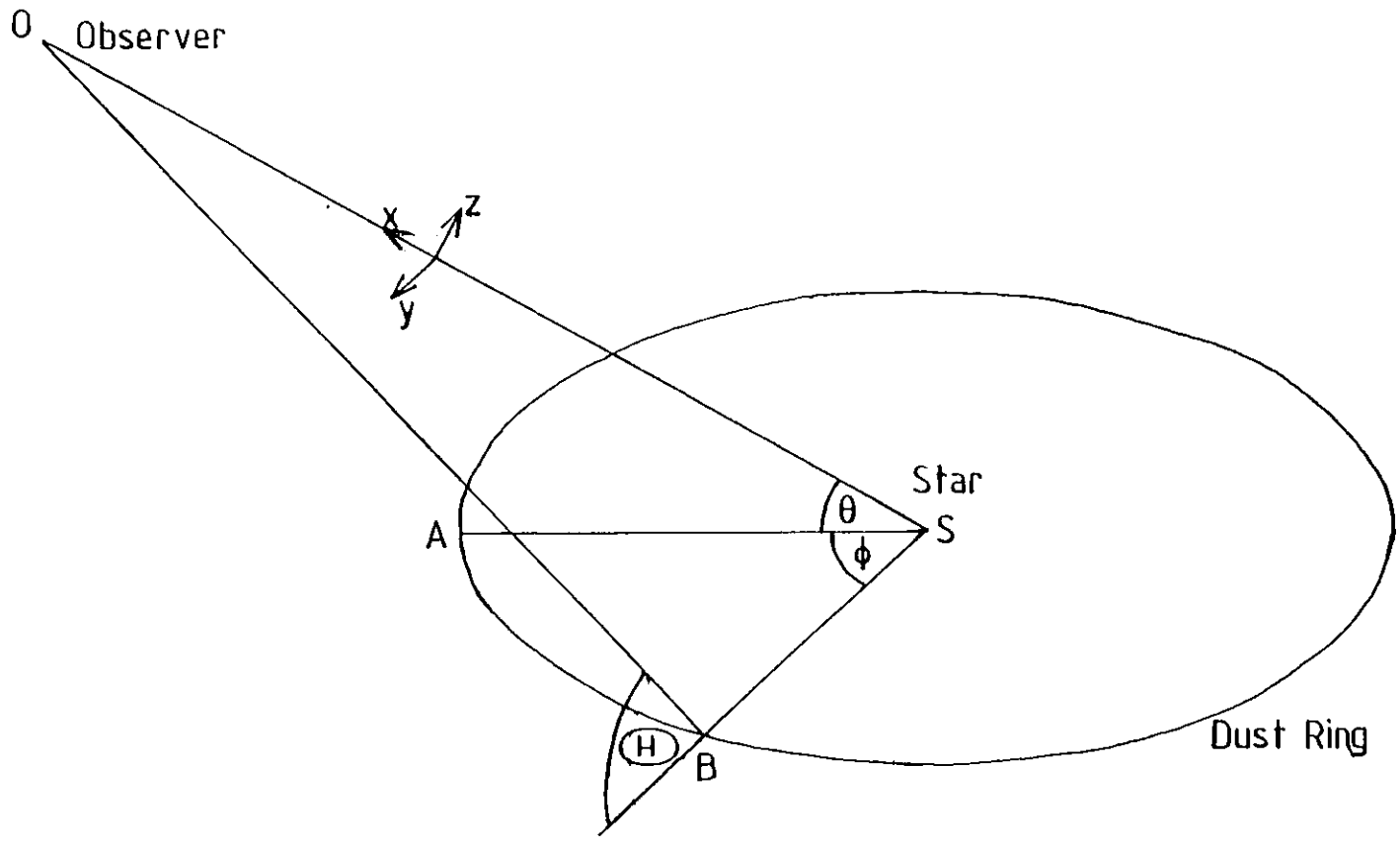

Scattering By A Dust Ring

Fig 8-2

the angle (H) is given by

$$\cos (H) = \cos\theta\cos\phi \ .$$

Defining axes x, y and z, x is along SO and z is in the plane OSA. Let the total radiation scattered off the entire ring towards O have flux I_y polarized in the y direction and I_z polarized in the z direction. Let the angle between the planes BSO and ASO be η.

$$\text{Then } I_y = \int_0^{2\pi} I_{\perp}\cos^2\eta + I_{\parallel}\sin^2\eta \, d\phi$$

$$I_z = \int_0^{2\pi} I_{\perp}\sin^2\eta + I_{\parallel}\cos^2\eta \, d\phi$$

$$\text{Since } \cos\eta = \frac{\cos\phi\sin\theta}{\sqrt{[1-\cos^2\theta\cos^2\phi]}}, \text{ and writing } \frac{16\pi^4 a^6}{R^2\lambda^4}\left[\frac{n^2-1}{n^2+2}\right]^2 \text{ as K,}$$

$$\text{then } I_y = K\int_0^{2\pi}\left[\frac{\cos^2\phi\sin^2\theta}{1-\cos^2\theta\cos^2\phi} + \cos^2\theta\cos^2\phi\left(1-\frac{\cos^2\phi\sin^2\theta}{1-\cos^2\theta\cos^2\phi}\right)\right]d\phi$$

$$= K\pi$$

$$I_z = K\int_0^{2\pi}\left[1-\frac{\cos^2\phi\sin^2\theta}{1-\cos^2\theta\cos^2\phi} + \cos^2\theta\cos^2\phi\,\frac{\cos^2\phi\sin^2\theta}{1-\cos^2\theta\cos^2\phi}\right]d\phi$$

$$= K\int_0^{2\pi}\frac{\sin^2\phi + \cos^4\phi\cos^2\theta\sin^2\theta}{1-\cos^2\theta\cos^2\phi}\, d\phi$$

I_z can be evaluated using Simpson's rule to obtain the results given in Table 8-1.

Table 8-1

Values of $I_z = K\int_0^{2\pi} \frac{\sin^4\phi + \cos^4\phi\cos^2\theta\sin^2\theta}{1-\cos^2\theta\cos^2\phi}\, d\phi$ evaluated using Simpson's rule.

θ	0^o	10^o	20^o	30^o	40^o	50^o	60^o	70^o	80^o	90^o
I_z	$2\pi K$	6.2K	5.9K	5.5K	5.0K	4.4K	3.9K	3.5K	3.2K	πK

The observed polarization at 0, $P_o(\theta)$ is given by $P_o(\theta) = \frac{I_z - I_y}{I_z + I_y}$ and this is tabulated in Table 8-2.

Table 8-2

Polarization of Radiation Scattered by an equatorial dust ring for inclination angles θ.

θ	0^o	10^o	20^o	30^o	40^o	50^o	60^o	70^o	80^o	90^o
$P_o(\theta)$	33%	33%	31%	27%	23%	17%	11%	5.5%	1.5%	0

These values are calculated assuming that all the observed radiation is that scattered off a thin ring with an infrared source at its centre. In practice, the observer may also see unscattered (and hence unpolarized) radiation emitted by the warm dust, as well as radiation direct from the star itself which has not been scattered. This will dilute the polarization and reduce the figures of Table 8-2. In addition, the dust may form a toroid or a complete spheroid. In this case the calculations would have to be extended to sum the radiation from all the dust in the shell.

The results of Table 8-2 can be used to give an estimate of polarization from a toroidal dust ring seen "edge-on" so that it completely obscures the central source. The results show that if the dust ring subtends an angle of up to $\sim 60^o$ at the central star, so that $\theta \leq 30^o$, then

the infrared radiation from the source could have a maximum polarization of $\sim$ 30%.

This analytical result appears to be similar to that obtained by Shawl (1974) who finds that the polarization of scattered light from a disc seen edge-on is 33%. He obtained the result using a computer to sum the polarization over a large number of points around the disc.

8.3 The Polarization From An Ellipsoidal Circumstellar Dust Cloud

Using the results of Section 8-2, we now attempt to determine the polarization that may occur by single scattering off an optically thin circumstellar dust cloud. If the dust cloud is spherically symmetric, there will be no polarization. However, if we assume that there is some equatorial thickening, due perhaps to centrifugal effects, then polarization may arise from scattering off the non-spherical part.

The model dust cloud is shown in Fig.8-3. It consists of a central star with temperature T_*, surrounded by a dust shell which is ellipsoidal in shape. It has a radius at the poles of R, and a radius at the equator of R+X. The thickness of the spherical part of the shell is t and the dust is assumed to be at temperature T_d. The dust particles are assumed to have a mean radius a and a number density n.

Then the observed polarization in the 10μ band, P, will be given by

$$P \simeq \frac{p_{10}}{S_{10}+D_{10}} \qquad (8\text{-}1)$$

where p_{10} is the flux at the earth of totally polarized 10μ radiation scattered off the dust shell, S_{10} is the 10μ (unpolarized) flux at the earth directly from the star, and D_{10} is the 10μ (unpolarized) flux at the earth emitted by the dust.

We first investigate the relative contributions of S_{10} and D_{10} to the unpolarized flux observed at the earth. If the specific intensity

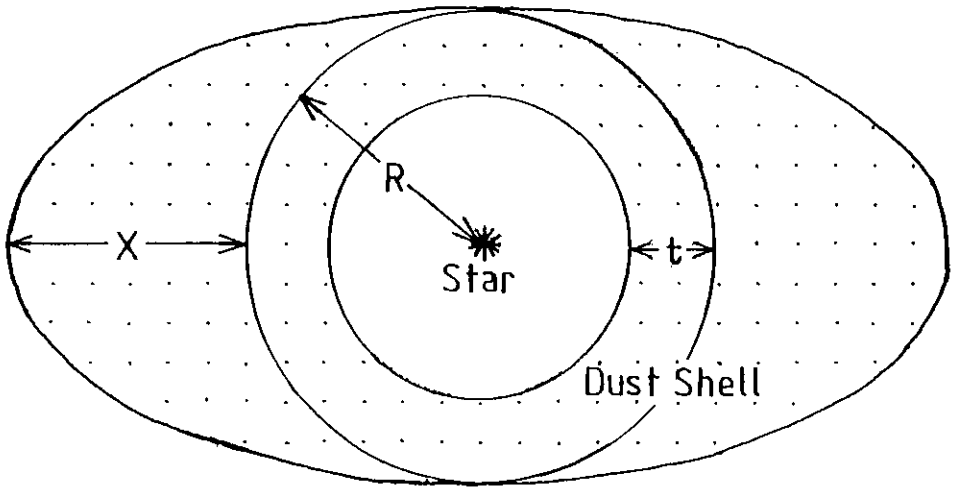

Model Dust Cloud Fig 8-3

at the surface of the star is I_{10} in the 10μ band, and I_{vis} is that in the visible, the flux at the dust shell is $I_{10}\,\pi\,\frac{R_*^2}{R^2}$ where R_* is the stellar radius. Also $S_{10} = I_{10}\,\pi\,\frac{R_*^2}{D^2}$ where D is the distance to earth.

If the grains in the dust shell are in equilibrium, their emitted power is the same as the power they absorb. Since the major part of the stellar emission is in the visible, and dust grains will be reasonably efficient absorbers of radiation with wavelength small compared to their size, we can assume for this calculation that the radiation absorbed by the dust is roughly just the visible radiation incident upon it. Hence

$$D_{10} \sim I_{vis}\,\frac{\pi R_*^2 R^2}{R^2 D^2} = I_{vis}\,\frac{\pi R_*^2}{D^2}$$

Comparing this with the expression for S_{10}, and since $I_{vis} >> I_{10}$ (e.g. if $T_* = 3000K$, $I_{vis}\mu^{-1} \simeq 200 I_{10}\mu^{-1}$), we see that $D_{10} >> S_{10}$. Therefore, equation (8-1) can be written as

$$P \simeq \frac{P_{10}}{D_{10}} \qquad (8\text{-}2)$$

Using the result of Section 8-2, the totally polarized radiation is about 30% of the stellar radiation that is scattered off the non-spherical part of the dust shell. So

$$P_{10} \simeq 0.3 I_{10}\,\frac{\pi R_*^2}{R^2}\,\frac{\sigma_{sca}\,n}{4\pi D^2}\,\left[\frac{4}{3}\pi R(R+X)^2 - \frac{4}{3}\pi R^3\right] \qquad (8\text{-}3)$$

Volume of the non-spherical part of the dust shell

where σ_{sca} is the scattering cross-section of a dust grain for 10μ radiation.

The specific intensity at the surface of the star in the 10μ band, I_{10}, is related to the specific intensity I over all wavelengths by

$$I_{10} = f_{10}(T_*)I \tag{8-4}$$

where $f_{\Delta\lambda}(T)$ is the fraction of T K black-body radiation emitted in the wavelength interval $\Delta\lambda$. We can obtain a relationship between I and the dust temperature T_d using the thermal balance equation for a dust grain:

$$\sigma_{abs} I \frac{\pi R_*^2}{R^2} = \langle Q_{IR} \rangle 4\pi a^2 \sigma T_d^4 \tag{8-5}$$

Absorbed power Emitted power

where σ_{abs} is the absorption cross-section of a dust grain for the total stellar radiation and $\langle Q_{IR} \rangle$ is the Planck mean emission efficiency of a dust grain in the infrared.

Substituting equations 8-4 and 8-5 into 8-3, we obtain

$$p_{10} \approx 0.3 f_{10}(T_*) \langle Q_{IR} \rangle \sigma T_d^4 \frac{\sigma_{sca}}{\sigma_{abs}} \frac{4\pi a^2 n}{4\pi D^2} \left[\frac{4}{3}\pi R(R+X)^2 - \frac{4}{3}\pi R^3 \right] \tag{8-6}$$

Now the 10μ flux at earth, emitted by the dust, is

$$D_{10} \approx 4\pi a^2 \langle Q_{IR} \rangle f_{10}(T_d) \sigma T_d^4 \frac{n}{4\pi D^2} \left[\frac{4}{3}\pi R(R+X)^2 - \frac{4}{3}\pi (R-t)^3 \right] \tag{8-7}$$

Volume of dust shell

Using expressions 8-6 and 8-7 in 8-1, we obtain

$$P \simeq 0.3 \frac{\sigma_{sca}}{\sigma_{abs}} \frac{f_{10}(T_*)}{f_{10}(T_d)} \left[\frac{R(R+X)^2 - R^3}{R(R+X)^2 - (R-t)^3} \right] \qquad (8\text{-}8)$$

The right hand part of this expression is the fraction of dust in the non-spherical part of the shell, compared to the total quantity of dust in the shell. It is tabulated below for a range of values of $\frac{X}{R}$ which gives a measure of the ellipticity of the shell, and for two reasonable values of t : $\frac{R}{3}$ and $\frac{R}{10}$.

Table 8-3

The Fraction of Dust In A Non-Spherical Shell For Two Different Shell Thicknesses

$t = \frac{R}{3}$		$t = \frac{R}{10}$	
$\frac{X}{R}$	$\frac{R(R+X)^2 - R^3}{R(R+X)^2 - (R-t)^3}$	$\frac{X}{R}$	$\frac{R(R+X)^2 - R^3}{R(R+X)^2 - (R-t)^3}$
0	0	0	0
0.2	0.39	0.2	0.62
0.4	0.58	0.4	0.78
0.6	0.69	0.6	0.85
0.8	0.76	0.8	0.89
1.0	0.81	1.0	0.92
1.5	0.88	1.5	0.95
2.0	0.92	2.0	0.97
3.0	0.96	3.0	0.98
4 0	0.97	4.0	0.99

In order to determine the polarization that might be observed from a star surrounded by an ellipsoidal dust cloud, the cross-sections for olivine are used to evaluate expression (8-8). Olivine ($(Mg,Fe)_2SiO_4$) is a common terrestrial and lunar silicate which has been put forward as a possible candidate for circumstellar dust. With a grain radius of 0.5μ,

Gilman (1973) gives σ_{abs}, the Planck mean absorption cross-section for olivine, as $3.9\text{x}10^{-15}\text{m}^2$ for 3000K radiation. Huffmann and Stapp (1973) determine the index of refraction, n, of olivine in the infrared as 1.65 with no complex part. Then the scattering cross-section, σ_{sca}, is found from the equation

$$\sigma_{sca} = \frac{128\pi^5 a^6}{3\lambda^4}\left[\frac{n^2-1}{n^2+2}\right]^2 \qquad \text{(Rayleigh 1871).}$$

For grains radius 0.5μ, and 10μ radiation, this gives

$$\sigma_{sca} = 2.7\text{x}10^{-15}\text{m}^2.$$

An M-type star has a typical temperature of ∿ 3000K, and assuming a value of 1400K for T_d, we obtain $f_{10}(T_*) = 1.9\text{x}10^{-3}$ and $f_{10}(T_d) = 1.41\text{x}10^{-2}$ for the wavelength interval 10-12μ. (The melting point of olivine lies between 1200K and 1800K depending on the ratio of magnesium to iron that it contains.)

Using these figures in expression (8-8), we find that for an ellipsoidal dust cloud seen edge-on, the observed polarization could be roughly

$$P = 0.028\ f\left(\frac{X}{R}\right) \qquad \text{where } f\left(\frac{X}{R}\right) = \frac{R(R+X)^2-R^3}{R(R+X)^2-(R-t)^3}$$

Assuming a fairly large asymmetry so that $\frac{X}{R}$ is near 1, we can see from Table 8-3 that $f\left(\frac{X}{R}\right)$ could be about 0.9 and thus significant polarizations of ∿ 2.5% could arise through single scattering in non-spherical circumstellar dust shells.

8.4 Discussion

In Section 8-3, it was shown that Rayleigh scattering from an optically thin, asymmetric dust shell is adequate for polarizations of a few percent. Higher polarizations could occur with more specialised geometries. The parameters required for the dust shell are easily consistent with those found by Rowan-Robinson and Harris (1982) which best fit the IR spectra of these star types, and in particular the optically-thin models they favour.

There is one major modification to the standard circumstellar dust shell models which our interpretation of the polarimetric data requires: a rather significant asymmetry in the dust distribution, in contrast to the spherical symmetry which is usually used. Table 8-3 shows that for substantial polarization, $\frac{X}{R}$ must be ≥ 0.5, which implies very significant asymmetry in the thickness of the dust shell. In fact, since the three measured polarizations have values of rather more than 2.5%, it may be appropriate to consider the dust distribution as being more disc-like than spheroidal. The exact percentage polarizations expected for particular dust cloud geometries are highly dependent on other variables such as grain temperature, size, and composition, which are not well established at present. Hence, deductions about the precise cloud geometry would probably be premature.

The asymmetry required to account for our polarization measurements is likely to be characteristic of all circumstellar dust shells in M stars, and whether substantial polarization is observed in a particular star would depend on the equatorial inclination angle, θ, it happens to have. Table 8-2 shows that θ must be $\lesssim 45^{\circ}$ for substantial polarization to be seen, and so on average about half the observed stars would be expected to satisfy this. In fact this distribution, with admittedly poor statistics, is just what we have found -- three of the six stars observed have polarization > 1%.

Whilst it has been demonstrated that the results on the six stars are consistent with polarization by scattering, it is not possible at present to rule out absorption by magnetically-aligned elongated grains as an alternative. The alignment mechanism for interstellar grains, which polarizes the light of stars lying near the galactic plane, is still not understood, and thus the apparent absence of strong stellar magnetic fields cannot be taken as conclusive. Further observations to establish the wavelength-dependence of polarization would help resolve this, as polarization due to scattering would be expected to show a λ^{-4} relationship, whereas the polarization from aligned grains would fall off more gradually with wavelength.

Chapter 9. Suggestions For Further Work

9-1 Suggested Improvements To The Polarimeter

9-1.1 An Upward-Looking Dewar

The present dewar with its sideways-looking window is inconvenient for ground-based work. The area of sky available for observation at any one time is limited by the inclination of the dewar - tipping it beyond $\sim 75^{\circ}$ from the vertical causes cryogenic spillage. Thus if the Tenerife telescope is on the meridian, the range of visible declination is limited to $\sim -42^{\circ}$ to $+13^{\circ}$. Larger declinations could feasibly be reached by rotating the instrument flange, but in practice this is inconvenient. The area of sky within $\sim 15^{\circ}$ of the zenith is not accessible in any case, and this is a disadvantage as seeing conditions are likely to be best near the zenith.

For ground-based polarimetry, an upward-looking dewar would be preferable. The Hatfield polarimeter (Cox, Hough and McCall 1978) uses such a nitrogen dewar with a top window.

A new dewar would also be designed to have an increased hold time - the present 13-hour hold time is useable, but it is a great convenience if the hold time is greater than 24 hours, so that a refill can be made at the same time each day during the observing period.

9-1.2 Improved Bearings

Ball bearings are intended for use with proper lubricants and can support large loads. They have proved to be noisy when running degreased, and are subject to sticking at low temperatures due to differential contraction. The problem seems to get worse with bearing size.

Jewelled bearings, as used in clocks and watches, are designed to run smoothly and reliably at a range of speeds. Their load bearing capacity is small, but for this application, it should be no disadvantage.

With careful design, so that differential contractions are allowed for, the use of jewelled bearings could improve the performance of the polarimeter dramatically. There should be less vibration transmitted to the chopper, and it should be possible to ensure that the tube and analyser are held firmly. Thus the detector noise would be reduced as would the instrumental signal which arises from the analyser rotation.

9-1.3 Improved Detectors

The performance of the polarimeter at 10μ could be improved by the use of a cooled photoconductive detector. These have recently become available, and have two principal advantages over bolometers:

1. They can operate at 4.2°K, avoiding the necessity to pump on the liquid helium when making ground-based observations.

2. They do not need to be thermally separated from the helium, so that they can be firmly mounted - unlike a bolometer which is suspended by two thin wires. Thus they are more robust (and much less microphonic) than bolometers.

9-1.4 Data Analysis

The most efficient way to carry out data analysis would be to use a dedicated micro-computer. This would avoid the need to rely on site facilities, which is an advantage if site facilities are unreliable or a number of different observatories are to be used.

9-2 Further Observations

9-2.1 Ground-based Observations

The sources observed at 10μ at Tenerife are only a very small fraction of the number of 10μ sources that are brighter than the theoretical detection limit of the polarimeter. The 10μ catalogue (Hall 1974) lists ∿ 100 sources which are brighter than the 200 Jy limit

obtained in 5-14 , while the AFGL Sky Survey (Price and Walker 1976) lists ∿ 250 sources brighter than 200 Jy at 11μ. Using the 1.5m Flux Collector at Tenerife in June or July one could realistically expect 90% of nights to be useable, and if the site equipment were in working order, many sources could be attempted.

Of course at Hawaii, the 3.8m telescope provides a collecting area ∿ 6 times greater than at Tenerife. In addition, its altitude of 4200m and the facility of a chopping secondary (obviating the need for a tuning-fork chopper) make it an excellent observing site. The effect of the high altitude is not only improved seeing, but also the possibility of making observations through some of the longer wavelength 'windows' that are still closed at lower altitudes.

Observations at a range of wavelengths are important to establish the dependence of polarization on wavelength, which will help to discriminate between the possible polarization mechanisms. Measurements at 10μ are particularly valuable because of the presence of the silicate absorption band.

This band is expected to produce a reduction in the photometric intensity, but an increase in the polarization of a source which has silicon dust grains.

9-2.2 Balloon-Borne Observations

At present the whole field of far-infrared polarimetry is virtually virgin territory, and it would be foolhardy to predict what new discoveries may be made. It is sufficient to note that at far-infrared wavelengths, a number of active galaxies are strong sources and the emission mechanism is still disputed. Polarimetry may be an important tool in discriminating between such processes as synchrotron emission and thermal radiation. Far-infrared polarimetry of galactic sources such as HII regions, the Orion nebula and the galactic centre, will help to

distinguish between scattering models (such as reflection nebulae) and models which invoke absorption or emission by aligned dust grains.

The polarimeter was specifically designed for use with the Imperial College 41" balloon-borne far-infrared telescope. This is an f/7 Cassegrain telescope and has an effective focal length of $\sim$ 7.3m. The plate scale is $\sim 30''mm^{-1}$ and at 100μ the diffraction limit is $\sim 24''$. Above $\sim$ 70μ, the telescope is diffraction-limited.

There are certain modifications which would need to be made to convert the polarimeter used at Tenerife for balloon work. The most important of these are:

a) Optics. For the 1979 flights, a chopping secondary mirror was used and thus the tuning-fork chopper would not be necessary. The field stops and Fabry lens would have to be altered to cater for the f/7 beam and a field of view of 3 arcminutes.

b) Filters and window. The 1976 and 1979 flights used two channels - 40-80μ and 80-350μ. A first flight with the polarimeter would probably use filters giving a 40-80μ passband. A wider passband, while increasing the signal, would have the disadvantage that any polarization that is wavelength-dependent may be smeared out. KRS-5 cuts off at about 40μ and for far-infrared wavelengths, a polythene window is used.

c) Analyser. The IGP225 analyser is mounted on KRS-5 and therefore is not suitable for far-infrared work. Instead, the IGP223, which is useful for the entire wavelength range 20-1000μ, is available. It is mounted on $\frac{1}{2}$mm-thick polythene and the grid has a period of $\sim 4\mu$.

d) Electronics and Data Analysis. The electronics and data analysis would be broadly similar for a balloon experiment to the systems used in Tenerife. However, the polarimeter must be entirely operated by telecommand, and the data is telemetred down to a ground station for recording and analysis.

9-3 The Future of Infrared Polarimetry

There is little doubt that polarimetry will eventually become a standard technique in the infrared, as it is already in the visible and radio regions. However, at present, infrared polarimetry is still a young science and there is enormous scope for interesting work to be carried out. Observations accurate to even a few percent are currently extremely sparse. In the long term a polarization survey, covering all the bright infrared sources at a range of wavelengths, should be attempted.

The advent of telescopes in space will be a significant advance. GIRL, the German Infrared Laboratory, which should be launched on a Spacelab mission in the middle of this decade, includes a polarimeter in its focal plane instrumentation. It is probable that some of the proposed space telescopes such as ISO (Infrared Space Observatory) and SIRTF (Spacelab Infrared Telescope Facility) will carry a polarimeter. Such polarimeters will have to operate at liquid helium temperature.

Compared to satellite experiments, balloon-borne and ground-based work is very cheap, and will continue to have an important rôle to play. The atmospheric absorption that ground or balloon telescopes have to cope with can be compensated by increased collecting area, and at wavelengths for which atmospheric windows exist, the 3.8m telescope at Hawaii will continue to be the most powerful instrument available.

It is not certain that the rotating analyser-type polarimeter will remain the dominant type for infrared work. Very accurate results are reported by Kemp et al. (1977) using photo-elastic modulators at 2.2μ, but their use has not yet been extended to 10μ and far-infrared work. Ekstrom et al. (1981) describe a design for a 10μ polarimeter employing a ZnSe birefringence modulator and a fast photoconductive detector. This detector will have a response time of less than 2 μsec, so that the radiation can be modulated at 37 kHz, and there is no need to beat two such modulators to reduce the frequency. This instrument should be

simpler and the radiation should suffer fewer losses than with Kemp's polarimeter (cf. Section 4-7.6). It is questionable whether such a system could be made to operate at cryogenic temperatures.

As infrared polarimetry becomes more accurate, it will be increasingly important to measure the circular polarization, which is generally about an order of magnitude weaker than the linear polarization.

In conclusion, it can be stated that infrared polarimetry is still a science in its infancy with many new developments to come. I hope that the work described in this thesis will take it a little way along the road to maturity.

Appendix I

The Stokes Parameters

Stokes parameters can be expressed in various ways, the four most common being

$$\begin{aligned} I &= E^2 + \frac{E_{x_o}^2 + E_{y_o}^2}{2} \\ Q &= \tfrac{1}{2}\left[E_{x_o}^2 - E_{y_o}^2\right] \\ U &= E_{x_o}E_{y_o}\cos\delta \\ V &= E_{x_o}E_{y_o}\sin\delta \end{aligned} \qquad \text{(AI-1)}$$

$$\begin{aligned} I &= I \\ Q &= Ip\cos 2\theta \\ U &= Ip\sin 2\theta \\ V &= Iq \end{aligned} \qquad \text{(AI-2)}$$

$$\begin{aligned} I &= I \\ Q &= IP\cos 2\varepsilon\cos 2\theta \\ U &= IP\cos 2\varepsilon\sin 2\theta \\ V &= IP\sin 2\varepsilon \end{aligned} \qquad \text{(AI-3)}$$

$$I = \langle E_{x_i}^2 + E_{y_i}^2 \rangle$$

$$Q = \langle E_{x_i}^2 - E_{y_i}^2 \rangle$$

$$U = \langle 2E_{x_i}E_{y_i}\cos\delta \rangle$$

$$V = \langle 2E_{x_i}E_{y_i}\sin\delta \rangle \qquad \text{(AI-4)}$$

where E is the r.m.s. amplitude of the electric vector of the unpolarized part of the radiation,

E_{x_o} is the amplitude in the x direction of the electric vector of the completely polarized part of the radiation,

E_{y_o} is the amplitude in the y direction of the electric vector of the completely polarized part of the radiation,

δ is the phase difference between the x and y components of the completely polarized part of the radiation,

I is the total intensity of the radiation,

p is the proportion of linearly polarized radiation,

θ is the angle of polarization of the linearly polarized radiation,

q is the proportion of circularly polarized radiation,

P is the proportion of polarized radiation

and ε is defined by the relation $\tan\varepsilon = \frac{b}{a}, \frac{-\pi}{4} \leq \varepsilon \leq \frac{\pi}{4}$

where b and a are the semi-minor and semi-major axes of the polarization ellipse.

x and y are two perpendicular axes such that they make a

right-hand set together with the z axis which is in the direction of propagation of the radiation.

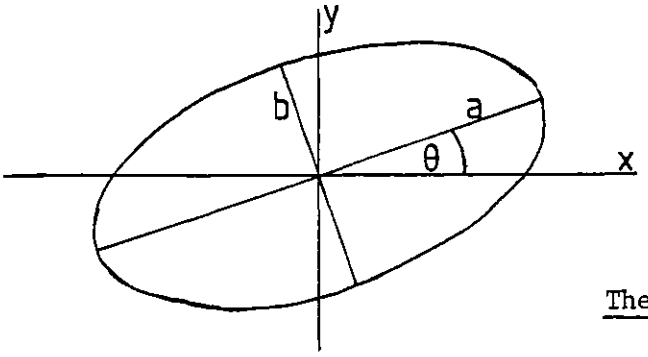

Fig.AI-1

The Polarization Ellipse

$\langle\ \rangle$ denotes time average,

E_{x_i} is the instantaneous r.m.s. amplitude in the x direction of the electric vector of the radiation

and E_{y_i} is the instantaneous r.m.s. amplitude in the y direction of the electric vector of the radiation.

The intensity of the radiation is proportional to the square of the amplitude of the E vector. So we may write

$$I = \frac{E^2}{z} + \text{the intensity of the completely polarized part of the radiation} \qquad \text{(AI-5)}$$

where z is the intrinsic impedance of the medium.

From Eqns.(2-1) and (2-2)

$$E_x = E_{x_o}\cos(\omega t + \delta_x)$$

$$E_y = E_{y_o}\cos(\omega t + \delta_y)$$

where ω is the circular frequency of the radiation.

The amplitude of the E-vector of the completely polarized part of the radiation at time t is $\sqrt{E_x^2+E_y^2}$.

Thus the intensity of the completely polarized part of the radiation

$$= \frac{1}{z}\frac{\omega}{2\pi}\int_o^{\frac{2\pi}{\omega}} E_x^2 + E_y^2\, dt$$

$$= \frac{1}{z}\frac{\omega}{2\pi}\int_o^{\frac{2\pi}{\omega}} E_{x_o}^2\cos^2(\omega t+\delta_x) + E_{y_o}^2\cos^2(\omega t+\delta_y)\, dt$$

$$= \frac{1}{2z}\left[E_{x_o}^2 + E_{y_o}^2\right] \qquad \text{(AI-6)}$$

On combining (AI-5) and (AI-6), we find

$$I = \frac{E^2}{z} + \frac{E_{x_o}^2+E_{y_o}^2}{2z} . \qquad \text{(AI-7)}$$

Suppose we define new axes x' and y' along the major and minor axes of the polarization ellipse - i.e. we rotate the x and y axes through θ.

Then
$$E_x' = E_x\cos\theta + E_y\sin\theta \qquad \text{(AI-8)}$$

$$E_y' = E_y\cos\theta - E_x\sin\theta \qquad \text{(AI-9)}$$

$$E_x' = a\cos(\omega t+\delta_o) \qquad \text{(AI-10)}$$

$$E_y' = b\sin(\omega t+\delta_o) \qquad \text{(AI-11)}$$

because the new axes coincide with the axes of the ellipse. δ_o is the appropriate phase angle which we do not need to express explicitly as it will be eliminated. The x' and y' components are now exactly 90^o out of phase, and b can be positive or negative depending on the direction of

rotation.

Combining equations (AI-8), (AI-9), (AI-10) and (AI-11), and using (2-1) and (2-2), we get

$$a\cos(\omega t+\delta_o) = E_{x_o}\cos(\omega t+\delta_x)\cos\theta + E_{y_o}\cos(\omega t+\delta_y)\sin\theta$$

$$b\sin(\omega t+\delta_o) = E_{y_o}\cos(\omega t+\delta_y)\cos\theta - E_{x_o}\cos(\omega t+\delta_x)\sin\theta$$

Equating coefficients of $\cos\omega t$ and $\sin\omega t$, and writing $\delta = \delta_x - \delta_y$, we obtain

$$a^2 + b^2 = E_{x_o}^2 + E_{y_o}^2 \qquad \text{(AI-12)}$$

$$a^2 - b^2 = (E_{x_o}^2 - E_{y_o}^2)\cos 2\theta + 2E_{x_o}E_{y_o}\sin 2\theta\cos\delta \qquad \text{(AI-13)}$$

$$ab = E_{x_o}E_{y_o}\sin\delta \qquad \text{(AI-14)}$$

and $$(E_{x_o}^2 - E_{y_o}^2)\sin 2\theta = 2E_{x_o}E_{y_o}\cos 2\theta\cos\delta \qquad \text{(AI-15)}$$

From the definition of P and using (AI-6)

$$IP = \frac{E_{x_o}^2 + E_{y_o}^2}{2z} \qquad \text{(AI-16)}$$

$$\text{(AI-15)} \Rightarrow \tan 2\theta = \frac{2E_{x_o}E_{y_o}\cos\delta}{E_{x_o}^2 - E_{y_o}^2} \qquad \text{(AI-17)}$$

Since $\tan\varepsilon = \frac{b}{a}$ $\qquad -\frac{\pi}{4} \leq \varepsilon \leq \frac{\pi}{4}$

$$\sin 2\varepsilon = 2\sin\varepsilon\cos\varepsilon$$

$$= \frac{2\tan\varepsilon}{1+\tan^2\varepsilon}$$

$$= \frac{2\frac{b}{a}}{1+\frac{b^2}{a^2}}$$

$$= \frac{2ab}{a^2+b^2}$$

$$= \frac{2E_{x_o}E_{y_o}\sin\delta}{E_{x_o}^2+E_{y_o}^2} \qquad \text{(AI-18)}$$

using (AI-12) and (AI-14)

$$\cos 2\varepsilon = 2\cos^2\varepsilon - 1$$

$$= \frac{1-\tan^2\varepsilon}{1+\tan^2\varepsilon}$$

$$= \frac{1-\frac{b^2}{a^2}}{1+\frac{b^2}{a^2}}$$

$$= \frac{a^2-b^2}{a^2+b^2}$$

$$= \frac{\left(E_{x_o}^2-E_{y_o}^2\right)\cos 2\theta + 2E_{x_o}E_{y_o}\sin 2\theta\cos\delta}{E_{x_o}^2+E_{y_o}^2} \qquad \text{(AI-19)}$$

using (AI-12) and (AI-13)

Then IP $\cos 2\varepsilon \cos 2\theta$

$$= \frac{E_{x_o}^2+E_{y_o}^2}{2z}\left[\frac{\left(E_{x_o}^2-E_{y_o}^2\right)\cos 2\theta + 2E_{x_o}E_{y_o}\sin 2\theta\cos\delta}{E_{x_o}^2+E_{y_o}^2}\right]\cos 2\theta$$

using (AI-16) and (AI-19)

$$= \frac{\left(E_{x_o}^2-E_{y_o}^2\right)\cos^2 2\theta + 2E_{x_o}E_{y_o}\sin 2\theta\cos 2\theta\cos\delta}{2z}$$

$$= \frac{\left(E_{x_o}^2-E_{y_o}^2\right)\cos^2 2\theta + \left(E_{x_o}^2-E_{y_o}^2\right)\tan 2\theta\sin 2\theta\cos 2\theta}{2z}$$

using (AI-17)

$$= \frac{E_{x_o}^2 - E_{y_o}^2}{2z} \qquad \text{(AI-20)}$$

IP cos 2 ε sin 2 θ

$$= \frac{E_{x_o}^2 + E_{y_o}^2}{2z} \left[\frac{\left(E_{x_o}^2 - E_{y_o}^2\right)\cos 2\theta + 2E_{x_o}E_{y_o}\sin 2\theta\cos\delta}{E_{x_o}^2 + E_{y_o}^2} \right] \sin 2\theta$$

using (AI-16) and (AI-19)

$$= \frac{\left(E_{x_o}^2 - E_{y_o}^2\right)\cos 2\theta \sin 2\theta + 2E_{x_o}E_{y_o}\sin^2 2\theta\cos\delta}{2z}$$

$$= \frac{2E_{x_o}E_{y_o}\cos^2 2\theta\cos\delta + 2E_{x_o}E_{y_o}\sin^2 2\theta\cos\delta}{2z}$$

using (AI-17)

$$= \frac{E_{x_o} E_{y_o} \cos\delta}{z} \qquad \text{(AI-21)}$$

$$\text{IP sin 2 } \varepsilon = \frac{E_{x_o}^2 + E_{y_o}^2}{2z} \quad \frac{2E_{x_o}E_{y_o}\sin\delta}{E_{x_o}^2 + E_{y_o}^2}$$

by (AI-16) and (AI-18)

$$= \frac{E_{x_o}E_{y_o}\sin\delta}{z} \qquad \text{(AI-22)}$$

Equations (AI-7), (AI-20), (AI-21) and (AI-22) demonstrate the equivalence of the expressions (AI-1) and (AI-3) for Stokes parameters.

To measure p, one can place a piece of perfect polaroid in the radiation beam and rotate it. The maximum transmitted intensity is I_{max} and the minimum transmitted intensity is I_{min}.

But $I_{max} = \frac{1}{2}\frac{E^2}{z} + \frac{a^2}{2z}$

and $I_{min} = \frac{1}{2}\frac{E^2}{z} + \frac{b^2}{2z}$

Then $p = \frac{I_{max} - I_{min}}{I_{max} + I_{min}}$

$$= \frac{1}{2}\frac{a^2-b^2}{E^2 + \frac{a^2+b^2}{2}}$$

So $Ip = \frac{1}{2z}(a^2-b^2)$ using (AI-12) and (AI-7)

$$= \frac{1}{2z}\left[\left(E_{x_o}{}^2 - E_{y_o}{}^2\right)\cos 2\theta + 2E_{x_o}E_{y_o}\sin 2\theta\cos\delta\right]$$

using (AI-13)

$$Ipcos2\theta = \frac{1}{2z}\left[\left(E_{x_o}{}^2 - E_{y_o}{}^2\right)\cos^2 2\theta + 2E_{x_o}E_{y_o}\sin 2\theta\cos 2\theta\cos\delta\right]$$

$$= \frac{E_{x_o}{}^2 - E_{y_o}{}^2}{2z} \qquad \text{(AI-23)}$$

and $$Ipsin2\theta = \frac{1}{2z}\left[\left(E_{x_o}{}^2 - E_{y_o}{}^2\right)\cos 2\theta\sin 2\theta + 2E_{x_o}E_{y_o}\sin^2 2\theta\cos\delta\right]$$

$$= \frac{E_{x_o}E_{y_o}\cos\delta}{z} \qquad \text{(AI-24)}$$

using (AI-17)

One can remove the circularly polarized component of the radiation by using a $\frac{1}{4}$ wave retarder to retard the vibration along the minor axis of the polarization ellipse, so that it is exactly out of phase with the vibration along the major axis.

The intensity of the remaining beam is

$$\frac{E^2}{z} + \frac{(a-b)^2}{2z}$$

The intensity of the original beam is

$$\frac{E^2}{z} + \frac{a^2+b^2}{2z}$$

Thus the intensity of the circularly polarized component, which was removed, is

$$Iq = \left(\frac{E^2}{z} + \frac{a^2+b^2}{2z}\right) - \left(\frac{E^2}{z} + \frac{(a-b)^2}{2z}\right)$$

$$= \frac{ab}{z}$$

$$= \frac{E_{x_o} E_{y_o} \sin\delta}{z} \qquad \text{(AI-25)}$$

using (AI-14)

Equations (AI-7)(AI-23),(AI-24) and (AI-25) demonstrate the equivalence of the expressions (AI-1) and (AI-2) for Stokes parameters.

$\frac{1}{z}\langle E_{x_i}{}^2\rangle$ is obtained by placing a perfect polarizer with its transmitting axis along the x-direction. The transmitted power will then be

$$\frac{1}{2}\frac{E^2}{z} + \frac{E_{x_o}^2}{2z}$$

Similarly, $\frac{1}{z}\langle E_{y_i}{}^2\rangle$ is obtained using a perfect polarizer with its transmitting axis along the y-direction, when the transmitted power will be

$$\frac{E^2}{2z} + \frac{E^2_{y_o}}{2z} \quad .$$

$$\text{Thus } \langle E_{x_i}^2 \rangle + \langle E_{y_i}^2 \rangle = E^2 + \frac{E^2_{x_o} + E^2_{y_o}}{2} \qquad \text{(AI-26)}$$

$$\text{Subtracting, } \langle E_{x_i}^2 \rangle - \langle E_{y_i}^2 \rangle = \frac{1}{2}\left(E^2_{x_o} - E^2_{y_o}\right) \qquad \text{(AI-27)}$$

Suppose the transmitted power is first measured with a perfect polarizer placed with its transmitting axis placed at 45^o to the x and y-axes, and then measured with the polarizer rotated through 90^o. Then if these two measurements are denoted I_{45} and I_{135}

$$I_{45} = \frac{E^2}{2z} + \left\langle \frac{1}{2} \frac{(E_x+E_y)^2}{z} \right\rangle$$

$$\text{and} \quad I_{135} = \frac{E^2}{2z} + \left\langle \frac{1}{2} \frac{(E_x-E_y)^2}{z} \right\rangle$$

$$\text{So } I_{45} - I_{135} = \left\langle \frac{2E_xE_y}{z} \right\rangle$$

$$= \frac{2}{z}\frac{\omega}{2\pi} \int_0^{\frac{2\pi}{\omega}} E_{x_o}\cos(\omega t+\delta_x) E_{y_o}\cos(\omega t+\delta_y)\, dt$$

$$= \frac{1}{z} E_{x_o}E_{y_o}\cos\delta$$

The unpolarized components of the radiation are uncorrelated, so their contributions to $\langle E_{x_i}E_{y_i} \rangle$ will cancel out, and its magnitude will depend only on the completely polarized part of the radiation so that $\langle E_{x_i}E_{y_i} \rangle = \frac{1}{2} E_{x_o}E_{y_o}$

$$\text{and } \langle 2\, E_{x_i}E_{y_i}\cos\delta \rangle = E_{x_o}E_{y_o}\cos\delta \qquad \text{(AI-28)}$$

Suppose the transmitted power is measured after a device which accepts right-handed circularly polarized radiation. Such a device would

be a $\frac{1}{4}$-wave plate with its fast axis in the x-direction and its slow axis in the y-direction, followed by a perfect polarizer at 135° to the +x-axis (the +y-axis is $+90^{\circ}$ to the x-axis). Call this power I_R. The transmitted power is then measured, after a device which accepts left-handed circularly polarized radiation. Such a device would be a $\frac{1}{4}$-wave plate with its fast axis in the x-direction and its slow axis in the y-direction, followed by a perfect polarizer at 45° to the +x-axis.

$$\text{Then } I_R = \frac{1}{2}\frac{E^2}{z} + \left\langle \frac{1}{z}\left[-\frac{1}{\sqrt{2}} E_{x_o}\sin(\omega t+\delta_x) - \frac{1}{\sqrt{2}} E_{y_o}\cos(\omega t+\delta_y)\right]^2 \right\rangle$$

$$\text{and } I_L = \frac{1}{2}\frac{E^2}{z} + \left\langle \frac{1}{z}\left[-\frac{1}{\sqrt{2}} E_{x_o}\sin(\omega t+\delta_x) + \frac{1}{\sqrt{2}} E_{y_o}\cos(\omega t+\delta_y)\right]^2 \right\rangle$$

$$I_R - I_L = \frac{\omega}{\pi z}\int_0^{\frac{2\pi}{\omega}} E_{x_o}E_{y_o}\sin(\omega t+\delta_x)\cos(\omega t+\delta_y)\,dt$$

$$= \frac{\omega}{2\pi z} E_{x_o}E_{y_o}\int_0^{\frac{2\pi}{\omega}} \sin(2\omega t+\delta_x+\delta_y)+\sin\delta\,dt$$

$$= \frac{1}{z} E_{x_o}E_{y_o}\sin\delta$$

As before, the unpolarized components of the radiation are uncorrelated, so that

$$\left\langle 2\, E_{x_i}E_{y_i}\sin\delta \right\rangle = E_{x_o}E_{y_o}\sin\delta \qquad \text{(AI-29)}$$

It has been shown how the Stokes parameters are each related to simple physical experiments that can be carried out on a beam of light, and (AI-26), (AI-27), (AI-28) and (AI-29) demonstrate the equivalence of the expressions (AI-1) and (AI-4) for Stokes parameters.

Appendix II

Reflection at a Metal Surface

When unpolarized electromagnetic radiation is incident at an oblique angle to a reflecting surface, the reflected wave will be partially elliptically polarized. This is due to the reduced reflectivity for the p wave compared with that for the s wave, and to some difference in phase delay between the s and p waves. (The s wave is the radiation linearly polarized perpendicularly (or sideways) to the plane of incidence, while the p wave is the radiation linearly polarized parallel to the plane of incidence).

The laws governing the reflection of e.m. radiation are Fresnel's equations, and in the case of a metal reflector, when the refractive index is large, the reflection coefficients for the s and p waves are (p476 Longhurst 1967)

$$R_s = \frac{(n - \cos i)^2 + n^2x^2}{(n + \cos i)^2 + n^2x^2}$$

$$R_p = \frac{(n - 1/\cos i)^2 + n^2x^2}{(n + 1/\cos i)^2 + n^2x^2}$$

where the complex refractive index of the metal is $\underset{\sim}{n} = n(1+ix)$ and i is the angle of incidence.

In general, the reflection coefficients for metals are of the form shown in figure AII-1. Note that R_p never reaches zero, so unlike dielectric reflection, there is no 'Brewster angle' giving pure linearly polarized radiation.

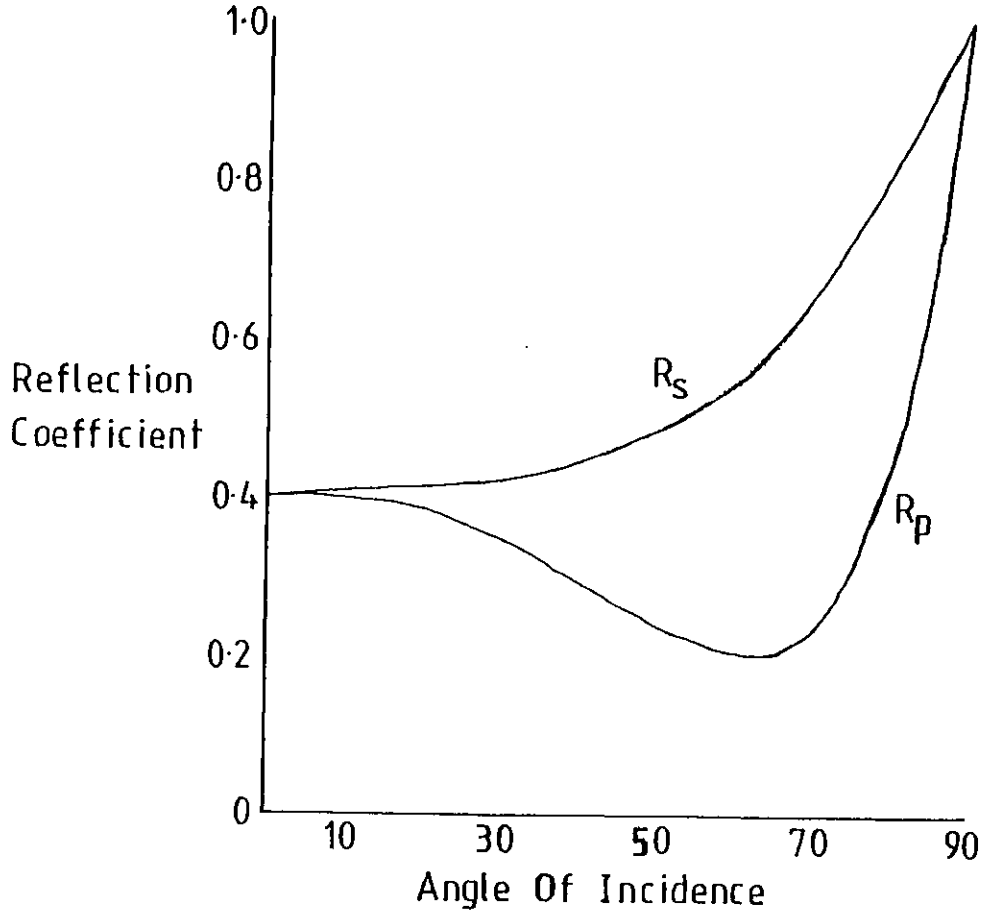

The Reflection Coefficients For Metals

Fig AII-1

The polarization of the reflected beam, P_r is given by

$$P_r = \frac{R_s - R_p}{R_s + R_p}$$

$$= \frac{\left[(n-\cos i)^2+n^2x^2\right]\left[\left(n+\frac{1}{\cos i}\right)^2+n^2x^2\right] - \left[\left(n-\frac{1}{\cos i}\right)^2+n^2x^2\right]\left[(n+\cos i)^2+n^2x^2\right]}{\left[(n-\cos i)^2+n^2x^2\right]\left[\left(n+\frac{1}{\cos i}\right)^2+n^2x^2\right] + \left[\left(n-\frac{1}{\cos i}\right)^2+n^2x^2\right]\left[(n+\cos i)^2+n^2x^2\right]} \qquad \text{(AII-1)}$$

For most metals, the refractive index is large and for long wavelengths ($\gtrsim$ 10μ, p614 Born and Wolf 1975), one can suppose that

$n \sim nx = \sqrt{\frac{\sigma}{\nu}} >> 1$ where σ is the electrical conductivity and ν is the frequency of the radiation.

The denominator of (AII-1) reduces to $\sim 8n^4$ while the numerator is $\sim 8n^3\left(\frac{1}{\cos i} - \cos i\right)$,

so $P_r \simeq \frac{1}{n}\left(\frac{1}{\cos i} - \cos i\right)$

$$\simeq \sqrt{\frac{\nu}{\sigma}}\left(\frac{1}{\cos i} - \cos i\right)$$

The above equation is only valid when it may be assumed that the optical constants can be evaluated from the static conductivity. This is certainly not true for the shorter infrared wavelengths where there are absorption bands. A further factor is that the quality of the surface of the metal (oxidation, dust, etc.) along with the method used to deposit any coatings (e.g. aluminization procedure - p19 Gehrels 1974) can have a large effect on the two reflection coefficients.

In matrix form, the effect of reflection can be represented by the Mueller matrix

$$K\begin{bmatrix} 1 & p & 0 & 0 \\ p & 1 & 0 & 0 \\ 0 & 0 & \cos\phi & \sin\phi \\ 0 & 0 & -\sin\phi & \cos\phi \end{bmatrix} \quad \text{for } p \leq 0.05$$

(Marin 1965)

where K is the reflection coefficient $\frac{R_s+R_p}{2}$, p is the dichroism $\frac{R_s-R_p}{R_s+R_p}$ and ϕ is the birefringence or phase difference introduced between the s and p reflected waves.

Appendix III

The Computer Programme Used For Control And Real-Time Data Analysis Of Polarimetry At The Tenerife IRFC

This programme is written in extended BASIC for use with the NOVA Computer and its associated CAMAC modules at the Tenerife IRFC.

```
2000 REM                    POLARIMETRY PROGRAMME BY D.L.ROSEN
2010 REM                    UPDATED 5/3/79
2020 RESTORE
2030 LET Q=0
2040 LET X=0
2050 LET D=0
2060 LET G=0
2070 LET R8=0
2080 REM                    ASSIGN CAMAC STATION NUMBERS
2090 LET N1=6
2100 LET N2=7
2110 LET N3=4
2120 LET N4=14
2130 DIM R[3,64],P[64],O[23],U[23]
2140 REM                    SET UP INTERNAL VARIABLES FOR READING DVM
2150 LET O[0]=1
2160 LET U[0]=1
2170 LET O1=1
2180 FOR I=1 TO 23
2190 LET O[I]=O[I-1]*2
2200 LET O1=O1+O[I]
2210 READ U[I]
2220 NEXT I
2230 DATA 2,4,8,10,20,40,80,100
2240 DATA 200,400,800,1000,2000
2250 DATA 4000,8000,10000,20000,40000
2260 DATA 80000,100000,0,0,0
2270 REM                    INITIALISE CAMAC MODULES
2280 CALL 1,0
2290 CALL 1,3
2300 CALL 2,N1,0,9
2310 CALL 2,N3,0,26
2320 CALL 3,N2,2,17,1
2330 PRINT 'ANALYSER SHOULD ROTATE CLOCKWISE LOOKING OUT OF DEWAR'
2340 PRINT 'MRD VOLTAGE READ OUT TEST - PRESS STOP TO END'
2350 CALL 4,N1,0,0,D
2360 IF D=64 THEN GOTO 2400
2370 GOSUB 6420
2380 PRINT G;
2390 GOTO 2350
2400 PRINT
2410 REM                    ENTER COORDINATES
2420 PRINT 'OBJECT REF.'
2430 PRINT
2440 PRINT 'R.A.';
2450 INPUT A1,A2
2460 PRINT
2470 PRINT 'DEC ; IF -VE,TYPE -VE MINUTES'
2480 INPUT D1,D2
2490 LET P1=D1
2500 LET P2=D2
2510 PRINT
2520 REM                    RESTART POINT
2530 PRINT 'S.T.';
2540 INPUT H1,H2
2550 REM                    CHECK DEWAR TILT
2560 LET P3=H1
2570 LET P4=H2
2580 IF (D1+D2/60)<0 THEN GOTO 2630
2590 LET D1=90-D1-D2/60
2600 LET H1=12+H1+H2/60
2610 LET H2=0
2620 GOTO 2640
```

```
2630 LET D1=D1+D2/60+90
2640 LET X3=((H1+H2/60)-(A1+A2/60))*ATN(1)/3
2650 LET X1=SIN(D1*ATN(1)/45)*.474
2660 LET X2=COS(D1*ATN(1)/45)*.8805*COS(X3)
2670 LET X4=X1+X2
2680 LET X5=SQR(1-X4*X4)
2690 LET E1=X4
2700 LET E2=X5
2710 LET E9=1
2720 GOSUB 6750
2730 LET X6=90-E5
2740 LET H1=P3
2750 LET H2=P4
2760 LET D1=P1
2770 LET D2=P2
2780 PRINT 'DEWAR TILT = ',X6,'DEGREES'
2790 IF X6<75 THEN GOTO 2820
2800 PRINT 'TILT GREATER THAN 75 DEGREES <7><7>'
2810 REM                    INPUT PARAMETERS
2820 PRINT
2830 PRINT 'N'
2840 INPUT N
2845 PRINT 'CHECK MOTOR SPEED'
2850 PRINT 'RC TIME CONSTANT ON PSD?'
2860 INPUT X8
2870 LET X9=1/(1+ATN(1)*ATN(1)*64/36/36*X8*X8)
2880 PRINT 'CALIBRATION POLARIZATION ANGLE?'
2890 INPUT A9
2900 PRINT
2910 PRINT 'START OF SAMPLING - DVM VALUE ?,  RANGE ? '
2920 INPUT V1,V2
2930 PRINT
2940 PRINT 'RUN REF'
2950 PRINT 'START IN POSITIVE BEAM FOR CONSISTENT RESULTS'
2960 PRINT
2970 REM                    SET CONSTANTS
2980 LET S2=0
2990 LET S3=1
3000 LET T=0
3010 LET T1=0
3020 LET T2=0
3030 LET T3=0
3040 LET T4=0
3050 LET F1=0
3060 LET F4=0
3070 LET M3=0
3080 LET M4=0
3090 LET M5=0
3100 LET F5=-1
3110 LET Z=0
3120 LET F2=0
3130 LET B3=0
3140 LET B4=0
3150 LET S4=2
3160 LET S5=3
3170 LET A3=0
3180 LET A4=0
3190 LET B5=0
3200 LET B6=0
3210 LET K3=0
3220 LET K4=0
3230 LET K5=0
3240 LET K6=0
```

```
3250 REM                        WAIT FOR CONTINUE
3260 CALL 2,N1,0,8
3270 CALL 5,Q,X
3280 IF Q=0 THEN GOTO 3260
3290 CALL 2,N3,0,10
3300 CALL 3,N2,2,17,1
3310 CALL 2,N1,0,9
3320 LET S1=0
3330 IF T=0 THEN GOTO 3350
3340 CALL 100,R[S3,0],N,0
3350 IF S1>0 THEN GOTO 3460
3360 REM                        WAIT FOR MRD VALUE
3370 LET G=100000
3380 GOSUB 6420
3390 IF T=0 THEN GOTO 3410
3400 CALL 100,R[S3,0],N,0
3410 IF G5>G THEN GOTO 3380
3420 IF ABS(V1-G)>V2 THEN GOTO 3380
3430 PRINT
3440 PRINT G
3450 CALL 3,N2,2,17,2
3460 CALL 2,N3,0,8
3470 IF T=0 THEN GOTO 3490
3480 CALL 100,R[S3,0],N,0
3490 CALL 5,Q,X
3500 IF Q=0 THEN GOTO 3460
3510 REM                        READ A-D VALUE
3520 CALL 4,N3,0,0,R[S2,S1]
3530 IF R[S2,S1]=<0 THEN GOTO 3550
3540 IF R[S2,S1]<1023 THEN GOTO 3560
3550 PRINT 'A/D SATURATED'
3560 LET S1=S1+1
3570 FOR Z1=0 TO 80
3580 NEXT Z1
3590 CALL 2,N3,0,10
3600 IF S1<N THEN GOTO 3330
3610 CALL 3,N2,2,17,1
3620 REM                        PRINT OUT A-D VALUES
3630 FOR S1=0 TO N-1
3640 PRINT R[S2,S1];
3650 NEXT S1
3660 LET T=T+1
3670 LET F5=-F5
3680 CALL 4,N1,0,0,D
3690 REM                        TEST STOP
3700 IF D>127 THEN GOTO 3950
3710 IF D<64 THEN GOTO 3770
3720 LET D=D-64
3730 CALL 3,N2,2,17,1
3740 LET F2=1
3750 GOTO 3870
3760 REM                        TEST RESTART
3770 IF D<>32 THEN GOTO 3820
3780 CALL 3,N2,2,17,1
3790 PRINT '*RESTART*'
3800 GOTO 2530
3810 REM                        TEST PAUSE
3820 IF D<>6 THEN GOTO 3870
3830 PRINT '* PAUSE *'
3840 GOSUB 5800
3850 GOTO 3950
3860 REM                        TEST REJECT AND INFO
3870 IF D=0 THEN GOTO 3950
```

```
3880 IF D=2 THEN GOTO 3910
3890 LET F1=1
3900 IF D=1 THEN GOTO 3950
3910 PRINT 'SET';T-1;'REJECTED'
3920 LET Z=1
3930 GOTO 4400
3940 REM                        CALCULATE MEANS
3950 IF T=1 THEN GOTO 4400
3960 IF Z=0 THEN GOTO 3990
3970 LET Z=Z+1
3980 IF Z=4 THEN LET Z=0
3990 LET M3=0
4000 FOR S1=0 TO N-1
4010 LET M3=M3+R[S3,S1]
4020 NEXT S1
4030 LET M3=M3/N
4040 REM                        TEST FOR NOISE
4050 LET Z1=0
4060 LET Z2=0
4070 FOR S1=0 TO N-1
4080 LET Z1=Z1+R[S3,S1]
4090 LET Z2=Z2+R[S3,S1]*R[S3,S1]
4100 NEXT S1
4110 IF Z2-Z1*Z1/N<0 THEN GOTO 4180
4120 LET S=SQR((Z2-(Z1*Z1/N))/(N-1))
4130 FOR S1=0 TO N-1
4140 IF ABS(M3-R[S3,S1])<3*S THEN GOTO 4170
4150 PRINT 'SPIKE<7>'
4160 GOSUB 5800
4170 NEXT S1
4180 IF T=2 THEN GOTO 4400
4190 IF Z=2 THEN GOTO 4400
4200 REM                        TEST FOR DRIFT
4210 IF T1=<1 THEN GOTO 4270
4220 IF ABS((M3+M4)/(2*L))>.8 THEN GOTO 4260
4230 IF ABS((M3+M4)/(2*L))<1.2 THEN GOTO 4260
4240 PRINT 'DRIFT<7>'
4250 GOSUB 5800
4260 REM                        ADD TO RUNNING TOTALS
4270 LET L=(M3+M4)/2
4280 IF T=3 THEN GOTO 4400
4290 IF Z=3 THEN GOTO 4400
4300 IF F2=2 THEN LET F5=-F5
4310 LET C1=F5*(M4-(M3+M5)/2)*.225E-2
4320 LET T1=T1+1
4330 LET T2=T2+C1
4340 LET T3=T3+C1*C1
4350 FOR S1=0 TO N-1
4360 LET P[S1]=(R[S5,S1]+R[S3,S1])/2-R[S4,S1]
4370 LET P[S1]=P[S1]*(-F5)*.225E-2
4380 NEXT S1
4390 GOSUB 6110
4400 LET M5=M4
4410 LET M4=M3
4420 GOTO 4440
4430 REM                        SWOP ARRAYS
4440 LET M1=S5
4450 LET S5=S4
4460 LET S4=S3
4470 LET S3=S2
4480 LET S2=M1
4490 REM                        TEST IF INFO WAS PRESSED
4500 IF F1=0 THEN GOTO 4950
```

```
4505 REM                        INFO CALCULATIONS
4510 LET F1=0
4520 CALL 3,N2,2,17,1
4530 IF T1<2 THEN GOTO 4580
4540 LET M1=SQR((T3-(T2*T2/T1))/(T1*(T1-1)))
4550 LET M2=T2/T1
4560 PRINT 'MEAN =';M2;' S.E. =';M1
4570 PRINT 'S/N';M2/M1
4580 PRINT T;'SETS SAMPLED,';T1;'PROCESSED'
4590 LET C6=SQR((B4-(B3*B3/T1))/(T1*(T1-1)))
4600 LET C6=C6*ATN(1)*4/(.7*N*X9)
4610 LET C7=B3/T1/X9
4620 LET C7=C7*4*ATN(1)/.7/N
4630 LET K7=SQR((K4-(K3*K3/T1))/(T1*(T1-1)))
4640 LET K8=SQR((K6-(K5*K5/T1))/(T1*(T1-1)))
4650 LET K7=K7*T1*45/(ATN(1)*2*B5)
4660 LET K8=K8*T1*45/(ATN(1)*2*B4)
4670 IF ABS(K7)>ABS(K8) THEN GOTO 4700
4680 LET A6=ABS(K8)
4690 GOTO 4710
4700 LET A6=ABS(K7)
4710 LET E1=B5
4720 IF A6=ABS(K7) THEN GOTO 4750
4730 LET Q7=ABS(K7)
4740 GOTO 4760
4750 LET Q7=ABS(K8)
4760 LET E2=B6
4770 LET E9=.5
4780 GOSUB 6750
4790 LET C9=C7/(M2/.35+C7*(1-X9))
4800 PRINT 'POLARIZATION = ',C9*100,' PER CENT '
4810 PRINT 'S/N = ',C7/C6
4820 LET E5=E5-A9
4830 IF E5>-90 THEN GOTO 4860
4840 LET E5=E5+180
4850 GOTO 4880
4860 IF E5<90 THEN GOTO 4880
4870 LET E5=E5-180
4880 IF E5>0 THEN GOTO 4900
4890 LET E5=E5+180
4900 PRINT 'ANGLE= ',E5
4910 PRINT 'STANDARD ERROR  =',A6,'DEGREES'
4920 PRINT '(OR',Q7,')'
4930 PRINT
4940 REM                        TEST IF STOP WAS PRESSED
4950 IF F2=0 THEN GOTO 5040
4960 IF F2=2 THEN GOTO 5090
4970 LET F2=2
4980 FOR Z1=0 TO 600
4990 CALL 100,R[S3,0],N,0
5000 NEXT Z1
5005 LET T=T+1
5010 CALL 4,N1,0,0,D
5020 GOTO 3820
5030 REM                        RETURN FOR NEXT SET OF SAMPLES
5040 CALL 2,N2,0,27
5050 CALL 5,Q,X
5060 IF Q=1 THEN GOTO 3310
5070 GOTO 3290
5080 REM                        FINAL CONVERSATION
5090 PRINT
5100 PRINT 'S,T,';
5110 INPUT H3,H4
```

```
5140 PRINT
5150 IF H1=<H3 THEN GOTO 5180
5160 PRINT 'JUST PASSED THROUGH 0 HOURS OR AN ERROR'
5170 LET H3=H3+24
5180 LET H1=((H1+H3)*7.5+(H2+H4)/8-A1*15-A2/4)*.1745E-1
5190 LET D3=(D1+D2/60)*.1745E-1
5200 LET H2=1/(SIN(D3)*.474+COS(D3)*.881*COS(H1))
5210 PRINT 'MEAN AIR MASS =';H2
5220 PRINT 'TOTAL AMP GAIN'
5230 INPUT H1
5240 PRINT
5250 LET M1=SQR((T3-(T2*T2/T1))/(T1*(T1-1)))/H1
5260 LET M2=T2/(T1*H1)
5270 PRINT 'INTENSITY =';M2;' S.E. =';M1
5280 PRINT 'S/N = ';M2/M1
5290 PRINT T-1,'SETS SAMPLED',T1,'PROCESSED'
5300 PRINT
5310 LET C6=SQR((B4-(B3*B3/T1))/(T1*(T1-1)))/H1
5320 LET C6=C6*ATN(1)*4/(.7*N*X9)
5330 LET C7=B3/(T1*H1*X9)
5340 LET C7=C7*4*ATN(1)/(.7*N)
5350 LET K7=SQR((K4-(K3*K3/T1))/(T1*(T1-1)))
5360 LET K8=SQR((K6-(K5*K5/T1))/(T1*(T1-1)))
5370 LET K7=K7*T1*45/(ATN(1)*2*B5)
5380 LET K8=K8*T1*45/(ATN(1)*2*B4)
5390 IF ABS(K7)>ABS(K8) THEN GOTO 5420
5400 LET A6=ABS(K8)
5410 GOTO 5430
5420 LET A6=ABS(K7)
5430 LET E1=B5
5440 IF A6=ABS(K7) THEN GOTO 5470
5450 LET Q7=ABS(K7)
5460 GOTO 5480
5470 LET Q7=ABS(K8)
5480 LET E2=B6
5490 LET E9=.5
5500 GOSUB 6750
5510 LET C9=C7/(M2/.35+C7*(1-X9))
5520 PRINT 'POLARIZATION= ';C9*100,' PER CENT'
5530 PRINT 'S/N = ',C7/C6
5540 LET E5=E5-A9
5550 IF E5>-90 THEN GOTO 5580
5560 LET E5=E5+180
5570 GOTO 5600
5580 IF E5<90 THEN GOTO 5600
5590 LET E5=E5-180
5600 IF E5>0 THEN GOTO 5620
5610 LET E5=E5+180
5620 PRINT 'ANGLE= ',E5
5630 PRINT 'STANDARD ERROR = ',A6,'DEGREES'
5640 PRINT '(OR',Q7,')'
5650 LET M2=ABS(M2)
5660 PRINT
5670 PRINT '1 FOR NEW OBJECT'
5680 INPUT H1
5690 PRINT
5700 IF H1=1 THEN GOTO 5760
5710 IF H3 24 THEN GOTO 5730
5720 LET H3=H3-24
5730 LET H1=H3
5740 LET H2=H4
5750 GOTO 2930
5760 PRINT
```

```
5770 PRINT 'END OF OBJECT'
5780 PRINT
5790 GOTO 2420
5800 REM                        PAUSE/NOISE DETECTED SUBROUTINE
5820 CALL 3,N2,2,17,1
5830 CALL 2,N1,0,9
5840 CALL 4,N1,0,0,D
5850 IF T<2 THEN GOTO 5870
5860 CALL 100,R[S3,0],N,0
5870 IF F2=2 THEN GOTO 5980
5880 REM                        TEST STOP
5890 IF D>127 THEN GOTO 5840
5900 IF D><64 THEN GOTO 5940
5910 LET F2=1
5920 GOTO 6100
5930 REM                        TEST RESTART
5940 IF D><32 THEN GOTO 5980
5950 PRINT '* RESTART *'
5960 GOTO 2530
5970 REM                        TEST CONTINUE
5980 IF D><4 THEN GOTO 6020
5990 PRINT '* CONTINUE *'
6000 GOTO 6100
6010 REM                        TEST REJECT
6020 IF D><2 THEN GOTO 6070
6030 PRINT 'SET';T-1;'REJECTED'
6040 LET Z=1
6050 GOTO 4400
6060 REM                        TEST INFO
6070 IF D><1 THEN GOTO 5840
6080 LET F1=1
6090 GOTO 5840
6100 RETURN
6110 REM                        PHASE SENSITIVE DETECTION SUBROUTINE
6120 REM
6130 LET B1=0
6140 FOR S1=0 TO N/2-1
6150 LET B1=B1+P[S1]
6160 NEXT S1
6170 FOR S1=N/2 TO N-1
6180 LET B1=B1-P[S1]
6190 NEXT S1
6200 REM
6210 LET B2=0
6220 FOR S1=0 TO N/4-1
6230 LET B2=B2+P[S1]
6240 NEXT S1
6250 FOR S1=N/4 TO 3*N/4-1
6260 LET B2=B2-P[S1]
6270 NEXT S1
6280 FOR S1=3*N/4 TO N-1
6290 LET B2=B2+P[S1]
6300 NEXT S1
6310 REM
6320 LET B5=B5+B1
6330 LET B6=B6+B2
6340 LET B3=SQR(B5*B5+B6*B6)
6350 LET B4=B4+(B1*B1+B2*B2)
6360 LET N3=N3+B1
6370 LET N4=N4+B1*B1
6380 LET N5=N5+B2
6390 LET N6=N6+B2*B2
6400 RETURN
```

```
6410 REM                    SUBROUTINE TO READ DVM
6420 LET Q3=9
6430 LET G5=G
6440 CALL 3,N4,0,16,10
6450 CALL 3,N4,0,16,11
6460 CALL 4,N4,0,1,R8
6470 LET R8=R8+1
6480 LET R8=01-R8
6490 LET R8=R8+1
6500 IF R8<O[23] THEN GOTO 6540
6510 LET R8=R8-O[22]-O[22]
6520 IF R8=>O[22] THEN GOTO 6580
6530 GOTO 6460
6540 IF R8=>O[22] THEN GOTO 6560
6550 GOTO 6460
6560 PRINT 'OVERLOAD'
6570 GOTO 6420
6580 LET X8=-1
6590 LET R8=R8-O[22]
6600 IF R8<O[21] THEN GOTO 6630
6610 LET X8=1
6620 LET R8=R8-O[21]
6630 LET G=0
6640 FOR I=0 TO 20
6650 IF R8<O[20-I] THEN GOTO 6680
6660 LET G=G+U[20-I]
6670 LET R8=R8-O[20-I]
6680 NEXT I
6690 IF R8><1 THEN GOTO 6710
6700 LET G=G+1
6710 LET G=G*X8
6720 LET G5=G5+1
6730 RETURN
6740 REM                    SUBROUTINE TO CALCULATE ARC TAN
6750 IF E1><0 THEN GOTO 6800
6760 IF E2><0 THEN GOTO 6830
6770 PRINT 'POLARIZATION = 0 ???'
6780 LET E5=0
6790 GOTO 6950
6800 IF E2><0 THEN GOTO 6830
6810 IF E1>0 THEN GOTO 6940
6820 GOTO 6920
6830 LET E5=E9*ATN(E1/E2)/ATN(1)*45
6840 IF E2=0 THEN GOTO 6910
6850 IF E2>0 THEN GOTO 6950
6860 IF E1>0 THEN GOTO 6890
6870 LET E5=E5-90
6880 GOTO 6950
6890 LET E5=E5+90
6900 GOTO 6950
6910 IF E1>0 THEN GOTO 6940
6920 LET E5=-45
6930 GOTO 6950
6940 LET E5=45
6950 RETURN
6960 END
```

Appendix IV

Publications

During my time as a research student, I was co-author of the following two publications.

The Imperial College 41-Inch Telescope for Far-Infrared Balloon Astronomy

R. D. Joseph, J. Allen, W. P. S. Meikle, K. C. Sugden,
M. F. Kessler, D. L. Rosen, G. Masson

Astronomy Group
The Blackett Laboratory, Imperial College
London SW7, England

Abstract

We have developed a 41-inch balloon telescope for far-infrared astronomical observations. It is constructed entirely of aluminum alloy, including the optics, and incorporates several novel features. Two composite bolometers, operated at 1.7°K, with adjacent fields of view on the sky, allow us to carry out two-color photometry in the wavelength ranges 40-80 μm and 80-400 μm.

The far-infrared payload flies on a stabilized balloon platform developed in the U.K. as a national facility by the Science Research Council. The maiden flight of both systems was launched in 1976 November. Despite problems with the stabilization system which prevented releasing the telescope from its stow position, we were able to scan a number of far-infrared sources. In-flight calibration, based on detections of both Venus and Saturn, indicates that the far-infrared noise-equivalent flux density* [areance] was ∿ 130 Jy $Hz^{-1/2}$ for the short wavelength channel and ∿ 500 Jy $Hz^{-1/2}$ for the long wavelength channel.

I. Introduction

The opacity of the earth's atmosphere effectively prohibits ground-based astronomical observations throughout the five octaves of the electro-magnetic spectrum that comprise the far infrared (25 μm to 1 mm wavelength). Except for two rather poor transmission windows at ∿ 35 μm and ∿ 350 μm, observations must be made from platforms above most of the atmosphere. Large scientific balloons provide one attractive platform of this kind, and several far-infrared balloon telescopes have been flown, ranging from the pioneering 1" telescope of Woolf *et al.* (1969)[5] to the 40" Smithsonian-Harvard-Arizona telescope described by Fazio *et al.* (1974).[1] At Imperial College (London) we have developed a new 41" balloon telescope, and the associated payload, for far-infrared astronomy. The telescope is designed to fly on a stabilized balloon platform developed in the U.K. by the Science Research Council. In the following we will describe the main features of the infrared astronomy payload, and report on the preliminary analysis of its performance on the first two flights.

II. Instrumentation

Telescope Design

The mechanical configuration of the f/7 Cassegrain telescope is shown in Figure 1. The 41" diameter primary mirror has a spherical figure and a focal ratio of f/2.9. The secondary mirror is also spherical, and has a diameter of 13.6". A flat tertiary mirror behind the primary deflects the beam through 90° into the

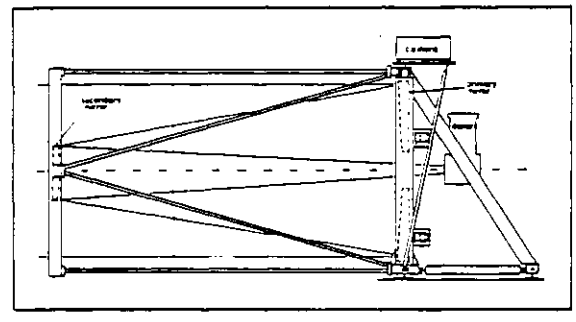

Figure 1. Layout of the 41-inch Cassegrain telescope.

detectors. All three mirrors are made of aluminum alloy and are gold-coated. The secondary and tertiary mirrors were both machined using diamond-turning techniques, whereas the final figuring and polishing of the primary was done by conventional methods after depositing a hard nickel alloy on the machined surface. All the mirrors were optically tested to confirm that they were figured to better than 4 μm.

The telescope is an open structure made of aluminum alloy, and uses conventional Serrurier trusses. The primary mirror cell is constructed of hollow rectangular section tubing. The mirror, which weighs 105 kg, is kinematically mounted inside the cell using orthogonal radial and axial supports. All six supports are shock-mounted and pre-tensioned to prevent movement of the mirror under its own weight as the telescope is tipped to various attitudes. The telescope attaches to the balloon platform by a three-point kinematic mount using commercially-available rod-end bearings. The total weight of the telescope, including the optics, is 215 kg.

The telescope design incorporates several noteworthy features. First, there is negligible thermal focal shift. When the mirrors and telescope structure undergo a temperature change δT, the focal length, F, of the telescope changes by $\delta F = F(\alpha_s - \alpha_m)\delta T$, where α_s and α_m are the thermal expansion coefficients of the structure and mirror materials respectively. For a typical balloon flight, δT is ∿ 80°K, which, with glass optics, would produce a focal shift of ∿ 14 mm. But by using aluminum optics, with thermal coefficient matched to that of the telescope structure, there is no thermal focal shift. This in turn permits mounting the secondary mirror without an active focusing mechanism requiring adjustment by telecommand during flight. This makes the telescope more simple and reliable in operation, and allows a much lighter secondary ring assembly. The trusses supporting the secondary ring can then be lighter and still maintain alignment of the two mirrors as the telescope orientation is

*See explanatory note in Guest Editorial.

IR-102 received June 6, 1977.

altered. Further, the use of aluminum rather than glass optics offers a factor of ∿ 10 more resistance to permanent damage resulting from impact shock after parachute descent. Finally, the factor of 200 in the thermal conductivity of aluminum compared to glass means that thermal gradients across the aluminum mirrors will be much smaller, thereby minimizing thermally-induced aberrations.

Another feature of the telescope is the use of only spherical optics, with attendant figuring economies. The spherical aberration was calculated for a range of telescope parameters, and by the appropriate choice of mirror focal ratios it is possible to keep the spherical aberration less than the diffraction limit in the far infrared, to keep the telescope to a reasonable size, and to achieve a plate scale consistent with both the diffraction limit and the linear size of sensitive helium-cooled bolometers. The telescope is about 2 m in length, is diffraction-limited at ∿ 70 μm, and has a plate scale of 30 arcsec mm^{-1}.

A final point concerns the thermal hygiene of the telescope, the *sine qua non* in achievement of the best far-infrared sensitivity. The entrance pupil of the telescope is fixed by the secondary mirror, which is slightly undersized compared to the aperture of the primary. This ensures that the detector field of view does not extend beyond the rim of the primary at either extreme of the chop cycle. A central hole in the secondary mirror, matching the shadowing of the secondary on the primary, guarantees that the detector does not see radiation emitted by the instrumentation behind the Cassegrain hole in the primary. The four vanes supporting the secondary mirror are very thin, 0.8 mm. Thus the detectors see about as little thermal emission from the telescope as the Cassegrain configuration allows.

Detectors and Infrared Filters

Since the large radiant background from the telescope demands that some form of spatial filtering (chopping) be performed so that faint astronomical sources can be discriminated against this background, observing time is used most efficiently if two detectors are placed in the focal plane with adjacent fields of view on the sky. It is then possible to chop so that the source is viewed by one detector while the other views the adjacent comparison field. Both detectors are composite germanium-silicon bolometers mounted in simple integrating cavities. They are operated at a temperature of 1.7°K by venting the liquid helium (LHe) to the ambient atmosphere. A 1 mm cold stop, just in front of each detector, is at the focus of an f/1 crystal quartz Fabry lens which images the primary mirror onto the cold stop. At the lenses are field stops which restrict the angular field of view on the sky to 3 arcminutes. In front of the field stops are helium-cooled filters which give the detectors effective bandwidths of 40 - 80 μm, and 80 - 400 μm, as shown in Figure 2.

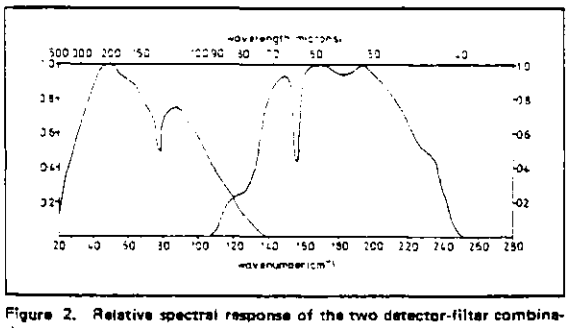

Figure 2. Relative spectral response of the two detector-filter combinations.

Both filters include diamond dust scattering layers on CaF_2 for short-wavelength blocking. The long-wavelength cutoff at 80 μ is provided by a thin 0.3 mm slice of KRS-5, while the cut-on at this wavelength for the other detector is due to KCl. There is additional short wavelength blocking provided by a diamond dust layer on crystal quartz at 77°K. The dewar vacuum window is made of high density polyethylene.

It is important to keep the angular field of view of the detectors as small as possible, consistent with filling the solid angle subtended by the secondary mirror, and this requires that the cold stop in front of each detector be positioned very precisely with respect to the field stop at the Fabry lenses. The mounting for these elements is designed so that the relative positions of the stops are determined to better than 0.05 mm.

The entire detector-filter assembly was enclosed in a LHe-cooled copper shield in order to keep radiation-driven thermal drops and drifts to a minimum. Initial beam-pattern measurements showed that considerable scattered radiation could reach the detectors, but by sand-blasting the inside of the shield and then painting it with a good optical black this stray radiation was greatly reduced. The measured beam pattern was then well-matched to the convergence angle from the secondary mirror.

For reasons both of thermal stability and LHe perdurance we chose to use a LN_2-shielded dewar. Thermal vacuum tests confirm that with Butyl rubber O-rings the dewar vacuum remains intact at the low temperature encountered at balloon float altitudes. Similar tests show a reduction by half in the LHe perdurance when the LN_2 reservoir is vented to the atmosphere, allowing the nitrogen to solidify, despite the fact that the LN_2 reservoir is filled with copper gauze to maintain good thermal contact with the shield when the LN_2 freezes. The dewar was therefore flown with a simple check valve on the LN_2 vent to maintain the vapor pressure over the LN_2 at about one atmosphere.

Chopper

Rather than rocking the comparatively large and heavy secondary mirror, a parallel-motion, focal plane chopper was chosen, in order to reduce problems with microphonic noise, amplitude stability, and drive power required. The chopper is designed to conserve momentum internally as it oscillates, thereby minimizing the generation of microphonic noise which can seriously degrade the noise performance of the detectors. To accomplish this, duplicate mirror carriages are mounted on parallel springs, as shown in Figure 3. The carriages are electromagnetically driven against each other using an amplified and phase-shifted

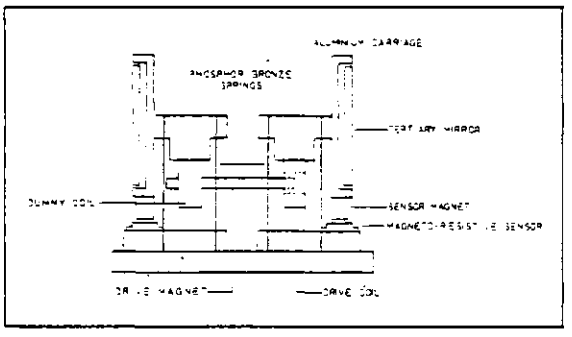

Figure 3. The focal-plane chopper.

signal derived from the motion of one of the carriages. Thus the system is electromechanically resonant, and requires very little drive power. Its amplitude stability, as measured by thermal vacuum tests in the laboratory, was more than adequate, as was its performance in long-term room-temperature runs. Its major disadvantage is the static deflection under its own weight, due to change of attitude, that is a feature of such resonant systems. This results in a small drift of the offset due to chopped instru-

mental radiation as the telescope changes attitude.

Star-Field Camera

For precise post-flight determination of the celestial coordinates of the field observed by the telescope at any time, a 16 mm pulse camera is mounted on the instrument flange of the telescope. It is aligned with the telescope axis, and is capable of taking up to 4000 star-field photographs during the flight. The field-of-view is 1.5° x 2.7°, and the scale is 11.5 mm^{-1}. The camera may be operated in either a manual mode, in which the shutter is both opened and closed by a discrete telecommand from the ground, or in an automatic mode, in which pictures are taken at regular intervals which may be varied from 1 to 16 seconds by the appropriate digital telecommand word. A frame number is written both on each frame of the film and in the main data format, so that there is unambiguous correlation between the star field photographs and the rest of the experimental data. The film we use is Kodak 2475 high-speed recording emulsion. In ground tests, trails of 9^m stars were easily observable.

On-Board Signal Processing

A block diagram of the on-board electronics system is shown in Figure 4. Each signal channel consists of a conventional phase-

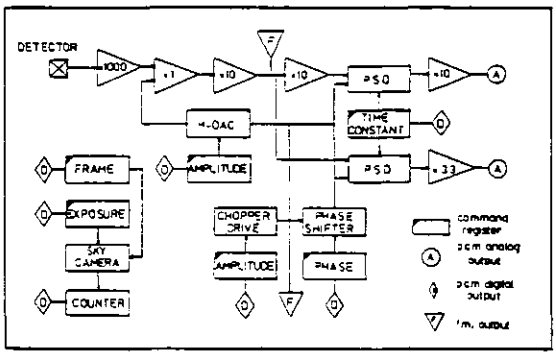

Figure 4. Block diagram of the on-board electronic signal-handling system.

sensitive detector (PSD) with telecommandable phase shifts and integration time constants. Two PSD channels for each detector, with gains differing by a factor of 30, permit linear readout over a dynamic range extending from detector noise to the signal levels expected for planets. One novel feature is the scheme for cancelling the component of signal due to chopped instrumental radiation. This signal can be several orders of magnitude larger than that due to detector noise, and it is virtually impossible to determine its magnitude, or even its phase, before flight. Since we are using a sinusoidal chopping waveform, the detector signals are approximately sinusoidal as well, but shifted somewhat in phase relative to the chopper waveform due to the finite response time of the bolometers. The reference signal derived from the chopper is phase-shifted by telecommand and routed to a multiplying digital-to-analog converter (MDAC), in parallel with the PSDs, and the 10-bit MDAC performs as a digitally-controlled attenuator, adjusted by telecommand from the ground. The attenuated reference signal from the MDAC is then fed to one input of a differential amplifier, while the preamp signal goes to the other input. The MDAC attenuation is commanded from the ground to a value such that the output of the differential amplifier is nearly zero when the telescope is not pointed at a celestial infrared source. By bucking out the instrumental offset signal at this point, extended dynamic range is achieved for the downstream electronics.

Battery power is provided by a rechargeable pack of sealed Ni-Cd batteries with 300 W-hr capacity. There is no active heating for the electronics box; all circuits are designed to operate to specification below $-20^\circ C$, and are kept above this temperature by 1 kW-hr of energy released by 10 kg of water stored inside the insulated electronics box.

Telemetry of scientific and payload housekeeping data is done using the PCM system provided by the National Scientific Balloon Facility (NSBF). Nine digital and fourteen analog data words are telemetered at a rate of 10 kbits sec^{-1}. To provide a measure of redundancy in case of disaster, the analog detector and chopper signals are also telemetered directly to ground via the FM/FM telemetry system. Telecommand requirements include seven discrete and eleven digital functions, and the telecommand equipment used is also that provided by NSBF.

Stabilized Balloon Platform

The Imperial College payload is flown on a stabilized balloon platform designed and built by GEC Marconi Electronics Ltd. for the U.K. Science Research Council, and operated by a team from the SRC's Appleton Laboratory. A preliminary description of the overall design concept and performance specifications of the platform has been given by J. How (1974),[3] and the prototype platform differs from this design only in one or two respects. The approach taken is to stabilize the entire gondola in three axes – azimuth, elevation, and roll – about a central gimbal-torque-motor cluster which is suspended from the balloon. The reaction mass against which the platform is driven in azimuth is the balloon itself.

There are two guidance modes. In the degree mode, position information is derived from magnetometers for the azimuth loop and from accelerometers for the roll and elevation loops. In the arcminute mode, position information comes from a star-sensor which has a stellar magnitude limit of $+5^m$. In both modes rate information is derived from a three-axis gyro package. The star-sensor can be offset $\pm 5^\circ$ both in elevation and in cross-elevation to permit acquisition and tracking by the telescope of fields which have no suitable guide stars. A TV camera which gives a 10° star field picture is also provided to aid acquisition of the desired guide star.

In pre-flight ground tests, the platform pointing and stability were generally up to the design specifications:

Degree Mode

Roll and Elevation:	Offset	<	40 arcmin
	Drift	<	6 arcmin hr^{-1}
	Noise	<	1 arcmin RMS
Azimuth:	Offset	<	1.6°
	Noise	<	1 arcmin RMS

Arcminute Mode

Lateral Axis:	Offset	<	20 arcsec
	Drift	<	1 arcmin hr^{-1}
	Noise	<	10 arcsec RMS
Twist Axis:	Offset	<	62 arcmin
	Drift	<	15 arcmin hr^{-1}
	Noise	<	5.5 arcmin RMS

A major modification to the design described by How (1974)[3] is the scheme for handling out-of-balance torques. An auto-balancing system was devised which pumps fluid between tanks located at the ends of the roll and elevations axes, and this replaces the cross-slide mechanism which How described. The system pumps fluid to readjust the weight distribution about the roll and elevation axes whenever the torque demand exceeds about 2 Nt-m. The gondola is stowed for launch and parachute descent by pumping extra fluid into the forward and right-hand tanks, thereby parking the platform against the stops, normally at -5° in elevation and $+5^\circ$ in roll.

Total payload weight below the parachute is about 2800

pounds. Its dimensions are 10 ft x 15 ft x 9 ft high. Figure 5 shows a picture of the gondola on the launch pad just before the second flight.

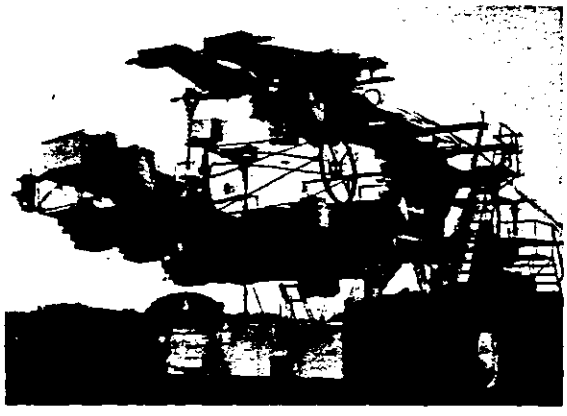

Figure 5. Gondola suspended from the launch truck just before the second flight.

III. Flight Performance

The first flight of this payload was launched on 29 November 1976. With a 4.3 Mft^3 balloon the telescope reached an altitude of 100,000 ft. Unfortunately, we were unable to unstow the payload in roll due to a problem with the auto-balancing system. However, despite a large frictional force against the roll stop we were able to point the telescope at elevations above -5°, and scan it in azimuth in an attempt to detect bright sources. Although the scan was at the rather fast degree mode slew rate of about $1^\circ\ sec^{-1}$, we detected Saturn easily, and the data indicate that the infrared system was working well. Parachute impact was near Selma, Alabama in a pine forest, and in spite of the fact that the gondola did not land on the crush pads, the infrared system suffered almost no damage. Only two vanes of the secondary mirror spider were broken, and the entire infrared telescope system was checked out and ready for reflight within five days. The stabilization system experienced somewhat more damage, and in particular the elevation axis gimbal was slightly sprung. However, the entire payload was repaired and tracking stars from the suspension on the ground within about 10 days after the recovery.

The second flight was launched on 16 December 1976, but we were unable to unstow the gondola from its park position on the forward elevation stop. However, following the first flight the stop had been rebuilt at +5°, so it was possible to attempt to observe sources rising or setting at +5° elevation. To do this, we carried out a raster scan using the sidereal motion of the sky, by scanning the telescope in azimuth about the position in which the putative source would be rising or setting. In this way we were able to detect both Venus and Saturn, and thereby calibrate the far-infrared sensitivity.

Parachute impact on this flight was in open ground, and the payload suffered very little damage, aside from slightly bent telescope trusses and some breaks in the protective structure underneath the telescope. In particular, the telescope, optics, LHe dewar, chopper, star-field camera, and electronics were all undamaged and ready for reflight.

Far-Infrared System Performance

Analysis of the flight data is still under way, but preliminary assessment of the overall performance of the payload indicates that there were no failures in the infrared system during either flight. We have calibrated the in-flight optical efficiency of the entire infrared detection system using the observations of Saturn and Venus. The adopted temperature of Venus was 240°K (Wright, 1976),[6] and that of Saturn plus its projected rings (taken to be optically thick) was 88°K (Rieke, 1975;[4] Fazio *et al.*, 1976 (flight 2);[5] Wright, 1976).[6] These give peak-to-peak signals at the detectors, per Jansky of source flux density at the telescope, of 0.8 nV Jy^{-1} in the 40-80 μm band, and 0.2 nV Jy^{-1} in the 80-400 μm band.

For both detectors the minimum noise during the flights was within 20% of the levels measured in the laboratory under simulated flight conditions, *viz.* ∿ 40 nV (RMS) $Hz^{-1/2}$, although this value was exceeded by several times when the platform underwent oscillation due to problems with the stabilization system. The source flux density that results in an RMS detector signal equal to the RMS detector noise is the noise-equivalent flux density (NEFD), and it can be found by substituting the flight data given above in the expression

$$\text{NEFD} \simeq \frac{1}{D} \frac{\text{detector noise (Volts RMS Hz}^{-1/2})}{\text{detector response (Volts P-P/Jy)}}$$

The duty factor, D, is ½ for a square-wave modulated signal; in our case D ≃ 0.4. (It is not always clear in the literature whether this factor has been included in the measured (or calculated) NEFD reported for infrared astronomical observations.) From the data for these flights we find:

$$\text{NEFD (40-80 } \mu\text{m)} \simeq 130 \text{ Jy Hz}^{-1/2}$$
$$\text{NEFD (80-400 } \mu\text{m)} \simeq 500 \text{ Jy Hz}^{-1/2}.$$

The offset signal produced by chopped instrumental radiation is always a problem besetting infrared observations, not only because it can saturate the signal processing chain at some crucial point, but also because small fluctuations in its amplitude can easily become the dominant noise source that limits sensitivity. In flight the offset signal was about 350 times the RMS noise (in a 1 Hz bandwidth) for the short wavelength detector and about 90 times the RMS noise for the long wavelength detector. To cancel out this signal required less than 10% of the dynamic range available in the electronic compensation scheme described above. The amplitude stability of the chopper was sufficiently good that we did not experience noise due to fluctuations in the radiant background on the detectors from variations in the amplitude of the chopper throw, except for periods when the gondola suffered severe suspension train oscillations.

Star-field photographs were taken mostly with 3 sec and 6 sec exposures throughout the flights, and despite the rather fast angular scan rates we had to employ, traces for 8^m stars are identified on these pictures without difficulty.

During the second flight we were able to scan several possible far-infrared sources in our observing list when they were rising or setting at +5° elevation, and between these times we scanned the galactic plane. Analysis of this data is still under way.

In addition to two-color photometry, future flights of this payload will include far-infrared polarimetry and emission-line observations with a Fabry-Perot interferometer.

Acknowledgments

We are grateful for the support we have received from many sources in developing and flying this payload. Chris Chaloner, Neil Urquhart, and Graham Luscombe of the SRC Appleton Laboratory, and Paul Cope, from GEC Marconi Electronics Ltd., expended really heroic efforts in preparing the SRC stabilized platform for its first flights. Among our colleagues at Imperial College, John Long, Bill Stannard, Roy Barr, and Jack Crabtree were especially helpful with the solution of various mechanical problems, Charles Wynne gave expert advice on the optical calculations, Dick Chater of the Analytical Services Laboratory

provided efficient assistance with the spectral calibration of the detectors and filters, and we would like to thank Jim Ring for his interest and encouragement in the I.C. balloon astronomy program. It is always a pleasure to acknowledge the superb ballooning support, and hospitality, provided by the National Scientific Balloon Facility in Palestine, Texas. And finally, we wish to thank the U.K. Science Research Council for its continuing financial support of this entire project. J.A. and W.P.S.M. are SRC Research Assistants, and M.F.K., D.L.R. and K.C.S. hold SRC Research Studentships.

References

1. Fazio, G. G., Kleinmann, D. E., Noyes, R. W., Wright, E. L., and Low, F. J. 1974, *Proc. Symposium on Telescope Systems for Balloon-Borne Research*, NASA Ames Research Center, California, NASA TM-X-62,397, p. 38.
2. Fazio, G. G., Traub, W. A., Wright, E. L., Low, F. J., and Trafton, L. 1976, Ap.J., *209*, 633.
3. How, J. 1974, *Proc. Symposium on Telescope Systems for Balloon-Borne Research*, NASA Ames Research Center, California, NASA TM-X-62,397, p. 284.
4. Rieke, G. H. 1975, Icarus, *26*, 37.
5. Woolf, N. J., Hoffmann, W. F., Frederick, C. L., and Low, F. J. 1969, Phil. Tran. Roy. Soc., *264*, 263.
6. Wright, E. L. 1976, Ap.J., *210*, 250.

Infrared Physics, Vol. 18, pp. 629–630
© Pergamon Press Ltd 1978. Printed in Great Britain
0020-0891/78/1201-0629$02.00/0

A FAR-INFRARED POLARIMETER FOR BALLOON ASTRONOMY

D. L. ROSEN and R. D. JOSEPH
Astronomy Group, Blackett Laboratory, Imperial College,
London SW7 2BZ, U.K.

Abstract—We have developed a liquid helium cooled far-infrared polarimeter, designed for astronomical observations with the Imperial College 41 in. balloon telescope.

Polarization studies of far-infrared astronomical sources are expected to yield critical information about the emission mechanisms in these sources. To carry out a new programme of far-infrared astronomical polarimetry, we have developed a liquid helium cooled polarimeter, designed for use with the Imperial College 41 in. balloon telescope. The polarimeter assembly is shown in Fig. 1.

The far-infrared detector is a gallium-doped germanium bolometer which runs at 1.7 K. The analyser is a 1 in. diameter wire grid deposited on a polyethylene substrate, and is commercially available. It rotates at a slow speed, ~1 revolution per minute, and modulates the signal at twice this frequency if the far-infrared radiation is polarized. In order to minimize the background on the detector, particularly background which may vary in phase with the analyser rotation, the polarimeter assembly is located inside the helium dewar, as shown in Fig. 1. Chopping is performed at 20 Hz in the focal plane by a Bulova vibrating chopper, which is also at liquid helium temperature.

A magnetic coupling across the dewar wall is used to provide the drive for the rotating analyser. This eliminates the problems connected with a drive shaft passing through the dewar wall—such as heat leak and maintaining a vacuum. A small motor, clamped to the bottom of the dewar, rotates a large magnet at ~4 rpm. A smaller magnet inside the dewar follows the external magnet, and is supported on a shaft passing through standard $\frac{1}{8}$ in. bore ball bearings. Ratio bevel gears turn the drive through a right angle and reduce the rotation speed to ~1 rpm. The analyser is mounted on

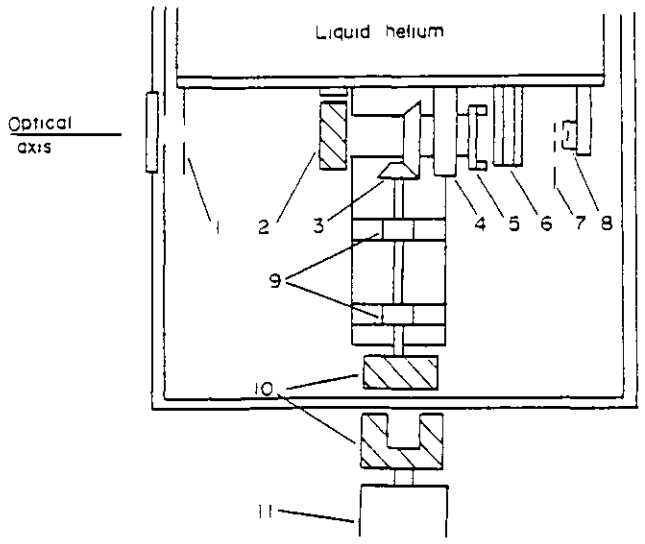

Fig. 1. Far-infrared polarimeter. (1) Cold aperture stop. (2) Circular magnet below magnetoresistive sensor. (3) Ratio bevel gears. (4) Bearing. (5) Wire grid analyser. (6) Infrared filters. (7) Chopper. (8) Detector. (9) Bearings. (10) Magnets. (11) Motor.

a $\frac{1}{2}$ in. bore ball bearing, through which the optical axis passes. The bearings are run dry, and work quite smoothly at helium temperatures, although careful design of the bearing holders is necessary to prevent differential contractions causing the bearings to seize. The reference signal indicating the position of the analyser is provided by a magneto resistive pick-up. This senses the position of a diametrically magnetised circular magnet which rotates with the analyser. The position of the grid at any time is known to an accuracy of better than 5°.

The polarimeter is designed to be used with the Imperial College 41 in. balloon-borne far-infrared telescope.[1] The Cassegrain telescope, and the focal plane chopper, along with the side looking dewar, permit the beam to pass straight through the centre of the primary mirror into the dewar. Thus off-axis reflections are avoided and cylindrical symmetry is maintained, reducing instrumental polarization of source and background radiation to a minimum. After phase-sensitive detection of the bolometer output, referenced by the chopper, the signal is digitised, along with the magneto resistive device output, so that further demodulation can be performed with a mini-computer.

The simple replacement of the analyser by a more finely spaced wire grid, and a different filter, permit use of the polarimeter in the 10 μm atmospheric window for ground based observations.

Our initial aim is to make polarization measurements accurate to 1%, with a position angle accuracy of 5°. Such measurements will yield important information about the brighter far-infrared astronomical sources.

Acknowledgements—The balloon astronomy programme at Imperial College is supported by the UK Science Research Council. DLR holds an SRC Research Studentship.

REFERENCE

1. JOSEPH, R. D., J. ALLEN, W. P. S. MEIKLE, K. C. SUGDEN, M. F. KESSLER, D. L. ROSEN & G. MASSON, *Opt. Eng.* **16**, 558 (1977).

References

Aannestad, P.A. & Purcell, E.M., 1973. Ann.Rev.Astron.Astrophys., 11, 309.

Adams, D.J. & Hough, J.H., 1977. M.N.R.A.S., 179, 73P.

Allen, C.W., 1973. Astrophysical Quantities, 3rd Edition, The Athlone Press.

Anile, A.M. & Breuer, R.A., 1977. Ap.J., 217, 353.

Auton, J.P., 1967. Appl.Opt., 6, 1023.

Auton, J.P. & Hutley, M.C., 1972. IR.Phys., 12, 95.

Azzam, R.M.A. & Bashara, N.M., 1977. Ellipsometry and Polarized Light, North Holland.

Becklin, E.E. & Neugebauer, G., 1968. Ap.J., 151, 145.

Becklin, E.E. & Neugebauer, G., 1967. Ap.J., 147, 799.

Becklin, E.E. & Neugebauer, G., 1975. Ap.J., 200, L71.

Beckman, J.E. & Moorwood, A.F.M., 1979. Rep.Prog.Phys., 42, 87.

Born, M. & Wolf, E., 1975. Principles of Optics, 5th Edition, Pergamon Press.

Breger, M. & Hardorp, J., 1973. Ap.J., 183, L77.

Caderni, N., Fabbri, R., Melchiorri, B., Melchiorri, F. & Natale, V., 1978a. Phys.Rev.D., 16, 1901.

Caderni, N., Fabbri, R., Melchiorri, B., Melchiorri, F. & Natale, V., 1978b. Phys.Rev.D., 17, 1908.

Capps, R.W. & Dyck, H.M., 1972. The Measurement of Polarized 10-Micron Radiation From Cool Stars With Circumstellar Shells. Ap.J., 175, 693.

Capps, R.W., Gillett, F.C. & Knacke, R.F., 1978. Ap.J., 226, 863.

Capps, R.W. & Knacke, R.F., 1976a. Publ.Astr.Soc.Pac., 88, 224.

Capps, R.W. & Knacke, R.F., 1976b. Ap.J., 210, 76.

Capps, R.W. & Knacke, R.F., 1978. Astrophysical Letters, 19, 113.

Cox, L.J., 1976. M.N.R.A.S., 176, 525.

Cox, L.J., Hough, J.H., Adams, D.J. & Jameson, R.F., 1976. M.N.R.A.S., 176, 131.

Cox, L.J., Hough, J.H. & McCall, A., 1978. M.N.R.A.S., 185, 199.

Crawford, F.S., 1968. Waves. Vol.3-Berkeley Physics Course.

Dall'Oglio, G., Melchiorri, B., Melchiorri, F., Natale, V., Aiello, S., & Mencaraglia, F., 1974. in Planets Stars & Nebulae Studied with Photopolarimetry, ed. T. Gehrels, The University of Arizona Press.

Davis, L. & Greenstein, J.L., 1951. Ap.J., 114, 206.

Dennison, B., 1977. Ap.J., 215, 529.

Dennison, B., Ward, D.B., Gull, G.E. & Harwit, M., 1977. A.J., 82, 39.

Duverney, R. & Vergnoux, A.M., 1957. Le Journal de Physique et Le Radium, 18, 527.

Dyck, H.M. & Beichman, C.A., 1974. Ap.J., 194, 57.

Dyck, H.M. & Capps, R.W., 1978. Ap.J., 220, L49.

Dyck, H.M., Capps, R.W. & Beichman, C.A., 1974. Ap.J., 188, L103.

Dyck, H.M., Capps, R.W., Forrest, W.J. & Gillett, F.C., 1973. Ap.J., 183, L99.

Dyck, H.M., Forbes, F.F. & Shawl, S.J., 1971. Astron.J., 76, 901.

Dyck, H.M., Forrest, W.J., Gillett, F.C., Stein, W.A., Gehrz, R.D., Woolf, N.J. & Shawl, S.J., 1971. Ap.J., 165, 57.

Dyck, H.M. & Jones, T.J., 1978. Astron.J., 83, 594.

Ekstrom, P.A., Stokes, R.A., Stokes, G.M. & Hackwell, J.A., 1981. Opt. Eng., 20, 19.

Elsässer, H. & Staude, H.J., 1978. Astron.Astrophys., 70, L3.

Forbes, F.F., 1967. Ap.J., 147, L1226.

Forbes, F.F., 1971a. Ap.J., 165, L21.

Forbes, F.F., 1971b. Ap.J., 165, L83.

Forbes, F.F., 1972. Mémoires Société Royale des Sciences de Liège, III, 217.

Gehrels, T., 1974. Planets Stars and Nebulae Studied with Photopolarimetry. University of Arizona Press.

Gilman, R.C., 1973. Ap.J.Supp., 28, 397.

Ginzberg, V.L. & Syrovatskii, S.I., 1965. Ann.Rev.Astron.Astrophys., 3, 297.

Ginzberg, V.L. & Syrovatskii, S.I., 1969. Ann.Rev.Astron.Astrophys., 7, 375.

Gull, G.E., Houck, J.R., McCarthy, J.F., Forrest, W.J. & Harwit, M., 1978. Astron.J., 83, 1440.

Gull, G.E., Russell, R.W., Melnick, G. & Harwit, M., 1980. Astron.J., 85, 1379.

Hall, J.S., 1949. Science, 109, 166.

Hall, J.S. & Serkowski, K., 1962. Stars and Stellar Systems, ed. Kuiper, G.P., Vol.III. University of Chicago Press.

Hall, R.T., 1974. A Catalog of 10-μm Celestial Objects SAMSO-TR-74-212. Space and Missile Systems Organization, Air Force System Command, Los Angeles.

Harwit, M., 1973. Astrophysical Concepts. J. Wiley & Sons.

Harwit, M., 1974. HII Regions and the Galactic Centre, Proc. Eighth ESLAB Symposium, ed. Moorwood, A.F.M.

Hashimoto, J., Maihara, T., Okuda, H. & Sato, S., 1970. Publ.Astr.Soc. Japan, 22, 335.

Hiltner, W.A., 1949. Science, 109, 165.

Hough, J.H., McCall, A., Adams, D.J. & Jameson, R.F., 1978. Astron. Astrophys., 69, 431.

Huffman, D.R. & Stapp, J.L., 1973. Interstellar Dust & Related Topics, IAU Symposium No.52, D. Reidel Publishing Company, Dordrecht, Holland.

Jones, R.C., 1941. J.Opt.Soc.Am., 31, 488.

Jones, T.J., 1979. Ap.J., 228, 787.

Jones, T.J., & Dyck, H.M., 1978. Ap.J., 220, 159.

Jorden, P.R., Long, J.F., MacGregor, A.D. & Selby, M.J., 1976. Astron. Astrophys., 49, 421.

Joseph, R.D., Allen, J., Meikle, W.P.S., Sugden, K.C., Kessler, M.F., Rosen, D.L. & Masson, G., 1977. Opt.Eng., 16, 558.

Kemp, J.C., Rieke, G.H., Lebofsky, M.J. & Coyne, G.V., 1977. Ap.J., 215, L107.

Kemp, J.C., Rudy, R.J., Lebofsky, M.C. & Rieke, G.H., 1978. Icarus, 35, 263.

Kessler, M.F., 1981. Ph.D Thesis, University of London.

Kleinmann, D.E. & Low, F.J., 1967. Ap.J., 149, L1.

Knacke, R.F. & Capps, R.W., 1974. Ap.J., 192, L19.

Knacke, R.F. & Capps, R.W., 1977. Ap.J., 216, 271.

Knacke, R.F. & Capps, R.W., 1979. Astron.J., 84, 1705.

Knacke, R.F., Capps, R.W. & Johns, M., 1976. Ap.J., 210, L69.

Knacke, R.F., Capps, R.W. & Johns, M., 1979. Nature, 280, 215.

Kobayashi, Y., Kawara, K., Maihara, T., Okuda, H., Sato, S. & Noguchi, K., 1978. Pub.Astr.Soc.Japan., 30, 377.

Landau, R., 1974. Planets, Stars and Nebulae Studied With Photopolarimetry, Gehrels, T. (Ed), University of Arizona Press.

Lang, K.R., 1974. Astrophysical Formulae, Springer-Verlag.

Lebofsky, M.J., Rieke, G.H. & Kemp, J.C., 1978. Ap.J., 222, 95.

Loer, S.J., Allen, D.A. & Dyck, H.M., 1973. Ap.J., 183, L97.

Longhurst, R.S., 1967. Geometrical and Physical Optics (2nd Ed), Longmans, Green and Co. Ltd., London.

Lonsdale, C.J., Dyck, H.M., Capps, R.W. & Wolstencroft, R.D., 1980. Ap.J., 238, L31.

Low, F.J., 1961. J.Opt.Soc.Am., 51, 1300.

Low, F.J., Kleinmann, D.E., Forbes, F.F. & Aumann, H.H., 1969. Ap.J., 157, L97.

McMillan, R.S. & Tapia, S., 1978. Ap.J., 226, L87.

Maihara, T., Noguchi, K., Okuda, H. & Sato, S., 1977. Publ.Astron.Soc. Japan, 29, 415.

Maihara, T., Okuda, H. & Sato, S., 1972. Mémoires Societé Royale des Sciences de Liège, III, 417.

Marin, M., 1965. Revue D'Optique, 44, 115.

Martin, P.G., 1978. Cosmic Dust, Oxford University Press.

Mathewson, D.S. & Ford, V.L., 1970. Memoirs of the R.A.S., 74, 139.

Michalsky, J., Stokes, R. & Ekstrom, P., 1976. Ap.J., 203, L43.

Mitsuishi, A., Yamada, Y., Fujita, S. & Yoshinaga, H., 1960. J.Opt.Soc. Am., 50, 433.

Neugebauer, G. & Leighton, R.B., 1969. Two Micron Sky Survey. NASA SP-3047.

Ney, E.P., Merrill, K.M., Becklin, E.E., Neugebauer, G. & Wynn-Williams, C.G., 1975. Ap.J., 198, L129.

Nyquist, H., 1928. Phys.Rev., 32, 110.

Price, S.D. & Walker, R.G., 1976. The AFGL Four Color Infrared Sky Survey: Catalog of Observations at 4.2, 11.0, 19.8 & 27.4μm. AFGL-TR-76-0208.

Puschell, J.J. & Stein, W.A., 1980. Ap.J., 237, 331.

Rayleigh, Lord, 1871. Phil.Mag., 41, 107, 274.

Rees, M.J., 1968. Ap.J., 153, L1.

Reid, M.J. & Muhleman, D.O., 1978. Ap.J., 220, 229.

Rieke, G.H. & Lebofsky, M.J., 1979. Ann.Rev.Astron.Astrophys., 17, 477.

Rieke, G.H., Lebofsky, M.J., Kemp, J.C., Coyne, G.W. & Tapia, S., 1977. Ap.J., 218, L37.

Rieke, G.H., Lebofsky, M.J., Thompson, R.I., Low, F.J. & Tokunaga, A.T.,

1980. Ap.J., 238, 24.

Rieke, G.H., Low, F.J. & Kleinmann, D.E., 1973. Ap.J., 186, L7.

Robson, E.I., 1973. Ph.D Thesis, University of London.

Rowan-Robinson, M. & Harris, S., 1982. M.N.R.A.S., 200, 197.

Rupprecht, G., Ginsberg, D.M. & Leslie, J.D., 1962. J.Opt.Soc.Am., 52, 665.

Savage, B.D. & Mathis, J.S., 1979. Ann.Rev.Astron.Astrophys., 17, 73.

Serkowski, K. & Rieke, G.H., 1973. Ap.J., 183, L103.

Serkowski, K., Mathewson, D.S. & Ford, V.L., 1975. Ap.J., 196, 261.

Shawl, S.J., 1969. Ap.J., 157, L57.

Shawl, S.J., 1974. Planets, Stars and Nebulae Studied With Photopolarimetry, Gehrels, T., (Ed), University of Arizona Press.

Shawl, S.J. & Terenghi, M., 1976. Ap.J., 204, L25.

Smith, R.A., Jones, F.E. & Chasmar, R.P., 1968. The Detection and Measurement of Infra-red Radiation (2nd Ed), Oxford University Press.

Spitzer, L.Jr., 1978. Physical Processes in the Interstellar Medium, John Wiley & Sons.

Stokes, G.G., 1852. Trans.Cambr.Phil.Soc., 9, 399.

Sugden, K.C., 1978. Ph.D Thesis, University of London.

Telesco, C.M. & Harper, D.A., 1980. Ap.J., 235, 392.

Walker, M.J., 1954. Amer.J.Phys., 22, 170.

Walker, R.G. & Price, S.D., 1975. AFCRL Infrared Sky Survey. Volume 1. Catalog of Observations at 4, 11 and 20 Microns. AFCRL-TR-75-0373.

Ward, D.B., Dennison, B., Gull, G. & Harwit, M., 1975. Ap.J., 202, L31.

Wardle, J.F.C. & Kronberg, P.P., 1974. Ap.J., 194, 249.

Werner, M.W., Gatley, I., Harper, D.A., Becklin, E.E., Loewenstein, R.F., Telesco, C.M. & Thronson, H.A., 1976. Ap.J., 204, 420.

Young, J.B., Graham, H.A. & Peterson, E.W., 1965. Appl.Opt., 4, 1023.

Zellner, B. & Serkowski, K., 1972. Publ.Astr.Soc.Jap., 84, 619.